TECHNICAL REPORT STANDARD PAGE

1. Report No. **FHWA/LA.07/423**	2. Government Accession No.	3. Recipient's Catalog No.
4. Title and Subtitle **Use of Reinforced Soil Foundation (RSF) to Support Shallow Foundation**	5. Report Date **November 2008**	
	6. Performing Organization Code **LTRC Number: 04-2GT** **State Project Number: 736-99-1242**	
7. Author(s) **Murad Y. Abu-Farsakh, Ph.D., P.E.; Qiming Chen, Ph.D.; and Sungmin Yoon, Ph.D., P.E.**	8. Performing Organization Report No. **423**	
9. Performing Organization Name and Address **Louisiana Transportation Research Center** **4101 Gourrier Avenue** **Baton Rouge, LA 70808**	10. Work Unit No.	
	11. Contract or Grant No. **04-2GT**	
12. Sponsoring Agency Name and Address **Louisiana Transportation Research Center** **4101 Gourrier Avenue** **Baton Rouge, LA 70808**	13. Type of Report and Period Covered **Final Report** **March 2004 – December 2007**	
	14. Sponsoring Agency Code	

15. Supplementary Notes
Conducted in Cooperation with the U.S. Department of Transportation, Federal Highway Administration

16. Abstract

This research study aims at investigating the potential benefits of using reinforced soil foundations to improve the bearing capacity and reduce the settlement of shallow foundations on soils. To implement this objective, a total of 117 tests, including 38 laboratory model tests on silty clay embankment soil, 51 laboratory model tests on sand, 22 laboratory model tests on Kentucky crushed limestone, and 6 large scale field tests on silty clay embankment soil, were performed at the Louisiana Transportation Research Center to study the behavior of reinforced soil foundations. The influences of different variables and parameters contributing to the improved performance of reinforced soil foundation were examined in these tests. In addition, an instrumentation program with pressure cells and strain gauges was designed to investigate the stress distribution in soil mass with and without reinforcement and the strain distribution along the reinforcement. The test results showed that the inclusion of reinforcement can significantly improve the soil's bearing capacity and reduce the footing settlement. The geogrids with higher tensile modulus performed better than geogrids with lower tensile modulus. The strain developed along the reinforcement is directly related to the settlement, and therefore higher tension would be developed for geogrid with higher modulus under the same footing settlement. The test results also showed that the inclusion of reinforcement will redistribute the applied load to a wider area, thus minimizing stress concentration and achieving a more uniform stress distribution. The redistribution of stresses below the reinforced zone will result in reducing the consolidation settlement of the underlying weak clayey soil, which is directly related to the induced stress. Insignificant strain measured in the geogrid beyond its effective length of 4.0~6.0B indicated that the geogrid beyond this length provides a negligible extra reinforcement effect.

Additionally, finite element analyses were conducted to assess the benefits of reinforcing embankment soil of low to medium plasticity and crushed limestone with geogrids beneath a strip footing from the perspective of the ultimate bearing capacity and footing settlement. Based on the numerical study, several geogrid-reinforcement design parameters were investigated.

17. Key Words **Reinforced soil foundation, Geosynthetics, Laboratory model test, Large-scale test, Soil, Bearing capacity ratio, Settlement reduction factor, Instrumentation, Vertical stress, Strain**	18. Distribution Statement **Unrestricted. This document is available through the National Technical Information Service, Springfield, VA 21161.**	
19. Security Classif. (of this report) **Unclassified**	20. Security Classif. (of this page) **Unclassified**	21. No. of Pages **218**

Project Review Committee

Each research project will have an advisory committee appointed by the LTRC director. The Project Review Committee is responsible for assisting the LTRC administrator or manager in the development of acceptable research problem statements, requests for proposals, review of research proposals, oversight of approved research projects, and implementation of findings.

The dedication and work effort of the following Project Review Committee members to guide this research study to fruition are acknowledged and appreciated.

LTRC Administrator/ Manager
Zhongjie "Doc" Zhang, Ph.D., P.E.
Pavement and Geotechnical Research Administrator

Members
Art Aquirre, FHWA
Steve Meunier, DOTD
Gavin Gautreau, LTRC
Kim Garlington, DOTD
Keith Angellette, DOTD
Ching Tsai, Ph.D., DOTD

Directorate Implementation Sponsor
William Temple
DOTD Chief Engineer

Use of Reinforced Soil Foundation (RSF) to Support Shallow Foundation

by

Murad Y. Abu-Farsakh, Ph.D., P.E.

Qiming Chen, Ph.D.

Sungmin Yoon, Ph.D., P.E.

Louisiana Transportation Research Center
4101 Gourrier Avenue
Baton Rouge, LA 70808

LTRC Project No. 04-02GT

State Project No. 736-99-1242

conducted for

Louisiana Department of Transportation and Development
Louisiana Transportation Research Center

November 2008

ABSTRACT

This research study aims at investigating the potential benefits of using the reinforced soil foundations to improve the bearing capacity and reduce the settlement of shallow foundations on soils. To implement this objective, a total of 117 tests, including 38 laboratory model tests on silty clay embankment soil, 51 laboratory model tests on sand, 22 laboratory model tests on Kentucky crushed limestone, and 6 large scale field tests on silty clay embankment soil, were performed at the Louisiana Transportation Research Center to study the behavior of reinforced soil foundations. The influences of different variables and parameters contributing to the improved performance of reinforced soil foundation were examined in these tests. In addition, an instrumentation program with pressure cells and strain gauges was designed to investigate the stress distribution in soil mass with and without reinforcement and the strain distribution along the reinforcement. The test results showed that the inclusion of reinforcement can significantly improve the soil's bearing capacity and reduce the footing immediate settlement. The geogrids with higher tensile modulus performed better than geogrids with lower tensile modulus. The strain developed along the reinforcement is directly related to the settlement, and therefore higher tension would be developed for geogrid with higher modulus under the same footing settlement. The test results also showed that the inclusion of reinforcement will redistribute the applied load to a wider area, thus minimizing stress concentration and achieving a more uniform stress distribution. The redistribution of stresses below the reinforced zone will result in reducing the consolidation settlement of the underlying weak clayey soil, which is directly related to the induced stress. Insignificant strain measured in the geogrid beyond its effective length of 4.0~6.0B indicated that the geogrid beyond this length provides a negligible extra reinforcement effect.

Additionally, finite element analyses were conducted to assess the benefits of reinforcing embankment soil of low to medium plasticity and crushed limestone with geogrids beneath a strip footing, from the perspective of the ultimate bearing capacity and footing settlement. Based on the numerical study, several geogrid-reinforcement design parameters were investigated.

ACKNOWLEDGMENTS

IMPLEMENTATION STATEMENT

An experimental testing program including four series of small-scale and large-scale model footing tests was conducted to investigate the benefits of reinforcing soil foundation (RSF), and to study the influence of different design parameters on the improved performance of reinforced soil foundation. The test results clearly demonstrated that the use of reinforcements can significantly increase the bearing capacity of soil foundations and reduce footing settlement.

Analyses of the test results enabled us to derive/modify analytical design procedures for reinforced soil foundations that include the effects of different design variables needed for implementation. The authors recommended a step-by-step procedure for designing RSF. The RSF can be implemented in many geotechnical engineering applications, such as foundations for earth-retaining structures, working platforms for embankment construction, working platforms over soft subgrades for pavement applications, reinforced-soil pile-support caps, reinforced-soil abutments, and foundations for residential and commercial buildings.

One potential implementation is the use of RSF in the design of approach slab for highway engineering applications to minimize the resulting differential settlements. Since the state of Louisiana is renowned for its weak, natural soil formations, the common result of excessive differential settlement of the concrete approach slab currently creates one of the major highway maintenance problems. To solve this problem, the Louisiana Quality Initiative (LQI) study recommended changing the design of approach slabs by increasing its rigidity. As a result, the slab and traffic loads will be carried by the two ends of the slab rather than distributed over the length of the slab. Accordingly, a strip footing will be needed at the far end of the approach slab away from the bridge. To increase the soil's bearing capacity and minimize settlement due to concentration load, the soil underneath the strip footing will be reinforced. Implementation of this research project can lead to a better design of approach slabs with improved performance and significant savings due to expected reduced maintenance and better rideability.

TABLE OF CONTENTS

LIST OF TABLES

LIST OF FIGURES

xviii

INTRODUCTION

Background

The presence of a weak soil (clay) supporting structural foundations (footings) results in low load bearing capacity and excessive settlements. Such can cause structural damage, reduction in the durability, and/or deterioration in the performance level. Conventional treatment methods involved replacing part of the weak cohesive soil with an adequately thick layer of stronger granular fill, increasing the dimensions of the footing, or a combination of both methods. However, an alternative and more economical solution is the use of geosynthetics to reinforce soils. This can be done by either reinforcing cohesive soil directly or replacing the poor soils with stronger granular fill, in combination with the inclusion of geosynthetics. The resulting composite zone (reinforced soil mass) will improve the load carrying capacity of the footing and provide better pressure distribution on top of the underlying weak soils, hence reducing the associated settlements.

One potential application is the use of reinforced soil foundations (RSF) in the design of approach slabs for highway engineering applications to minimize the resulting differential settlements. Excessive differential settlement of the concrete approach slab currently causes the significant bridge "bump" problem, which results in uncomfortable rides, dangerous driving conditions, and frequent repairs. Past solutions for preventing the bump from developing involved: the improvement of the natural soil under the embankment, the use of selected embankments, and the use of piles with decreasing lengths supporting the concrete (approach) slab. Pile supported approach slabs have not performed well, in that they have not significantly reduced the amount of differential settlements. The minimization of excessive settlements and the resulting rideability discomfort in the design of approach slabs continue to be investigated nationwide. Figure 1 schematically illustrates the problem, wherein the difference in settlement, δ, is primarily caused by the settlement of the underlying soft soil. One proposed solution is to use rigid approach slab and transfer the traffic loads to the two ends of the slab (figure 2a). Accordingly, a shallow foundation is needed at the end of the approach slab far from the bridge to carry that part of the load (figure 2b). To achieve better bearing capacity and/or to prevent excessive settlement, the soil underneath the footing needs to be reinforced (figure 3).

The benefits of the inclusion of reinforcements within soil mass to increase the bearing capacity and reduce the settlement of soil foundation have been widely recognized. Many hypotheses have been postulated about the failure mode of RSF. However, the mechanism of

reinforcement is still not fully understood in RSF. As compared to other reinforced soil applications, the development of design method and theory for RSF is relatively slow. These restrictions, on the other hand, inhibit the further development of reinforcement technology. Therefore, it is important to investigate the reinforcement mechanism of reinforcing soils for foundation applications.
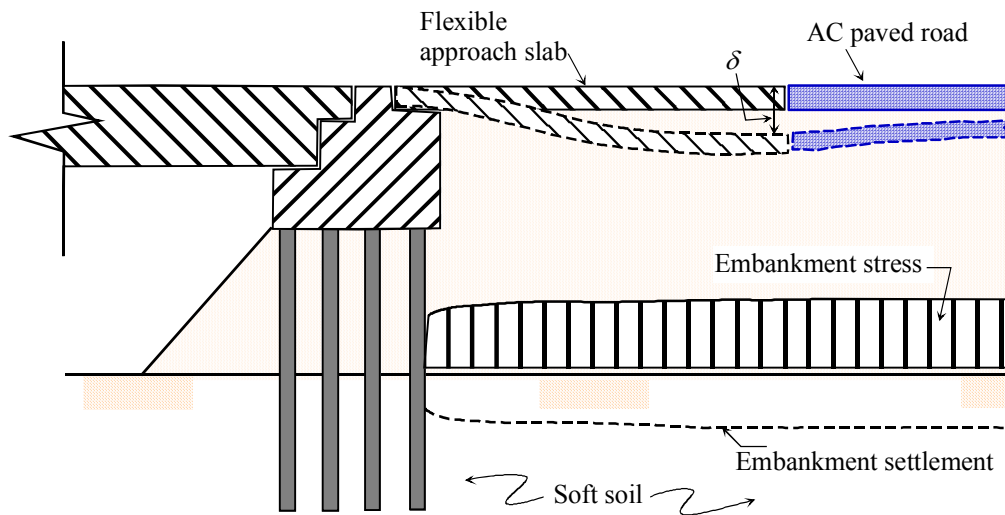
Figure 1
Descriptive schematics of approach slab problem

(a)   **(b)**
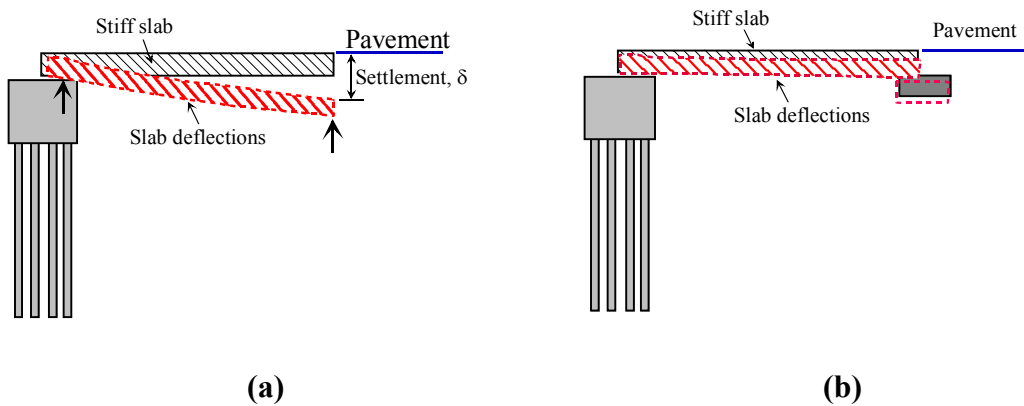
Figure 2
Anticipated deflections in the proposed rigid slab design
(a) without shallow foundation and (b) with shallow foundation.
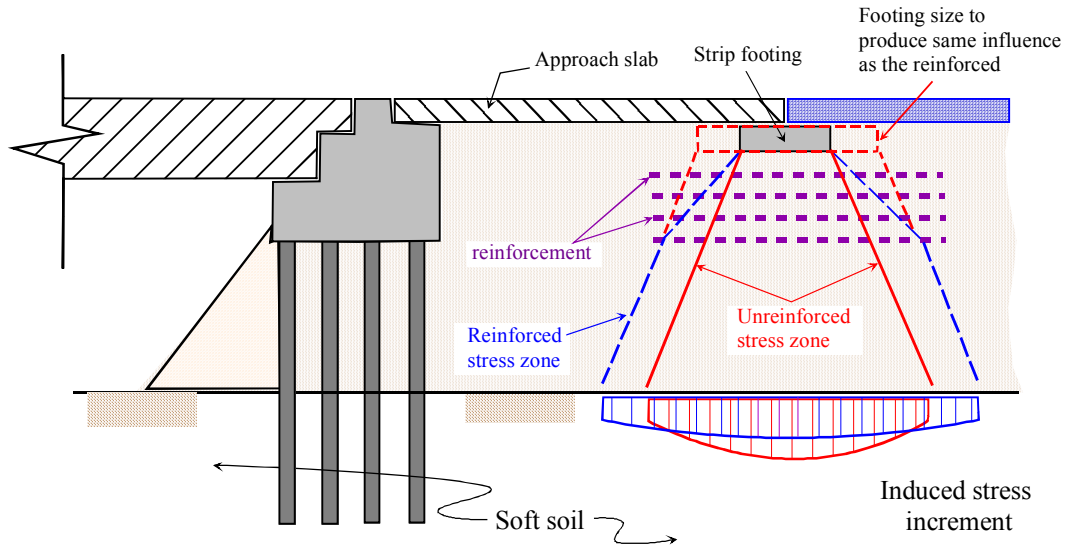
Figure 3
Reinforced soil foundation applied to approach slab and the resulting stress increment

Literature Review

The work done by different researchers and research agencies in the past four decades indicated that the bearing capacity can be significantly improved by reinforcing the soil foundation. Out of the earliest and most pronounced contributions was the work done by Binquet and Lee [1], [2], who demonstrated the benefits of reinforcing the soil foundation in their small-scale experimental study and presented a new method for the prediction of the bearing capacity ratio, *BCR*, defined as the ratio of the bearing capacity of the reinforced soil foundation to that of the unreinforced. Different researchers thereafter attempted to evaluate the benefits of using reinforced soil foundations as indicated by the bearing capacity ratio. They aimed at investigating the parameters and variables that would dominate the *BCR* value and built a background that would enable the development of a reasonably accurate design/evaluation method.

Experimental Study
The results of experimental studies available in the literature indicated that better improvements are obtained when the reinforcement is placed within certain limits, beyond which no significant improvements will occur [2], [3], [4], [5], [6], [7], [8], [9], [10], [11], [12], [13]. They also presented ranges for the optimal reinforcement depth, first layer depth, and number of reinforcement layers. Different studies resulted in somewhat different specifications for reinforcement layouts. Combining some the results from literature showed

that: (i) The first reinforcement layer should be located close to the bottom of the footing at an optimum depth, u, of $0.25B$ to $0.35B$ (B is the width of footing). Placing the first layer at a distance deeper than the footing width, B, below the bottom of the footing, will result in no improvement. (ii) The maximum vertical depth, d, of the reinforcement varied from $1.3B$ to $2B$. (iii) The horizontal extent, b, of the reinforcement was found to vary from $3B$ to $8B$. (iv) Increasing the number of reinforcement layers beyond a specific number (three to five layers) was found to produce no significant improvement. (v) BCR values become more significant at higher settlement values, and (vi) the less the strength of the subgrade (soil foundation), the greater the BCR values, suggesting that the reinforced soil foundations are recommended for use only with weak (soft) subgrades.

The improvement in the bearing capacity is a function of the unreinforced bearing capacity of the foundation and the reinforcement properties (stiffness and rupture strength), reinforcement shape (apertures and rib thickness), and the layouts (depth, spacing, and extent) of the reinforcement. The unreinforced bearing capacity sums up parameters pertaining to the soil and the footing, such as: the shear strength parameters, embedment depth, footing type and shape, and layering of soil foundations. As shown by previous investigators, the higher the bearing capacity of an unreinforced foundation, the less the need will be for soil reinforcement [2], [3], [4], [5], [6]. The experimental results indicated that better improvements, as indicated by higher BCR values, were obtained when a weak soil layer was encountered close to the bottom of the footings. However, this conclusion was based only on specific reinforcement material with a limited range of reinforcement stiffnesses.

The BCR values have been generally based on the magnitudes of the ultimate bearing capacity of the unreinforced and reinforced soil foundations, ignoring the influence of the foundation settlement. A study by Khing, et al. [10] indicated that determination of the BCR should be based on the foundation settlement and not the ultimate bearing capacity. The use of the BCR based on the ultimate bearing capacity alone could be misleading because most foundations are constructed on the basis of limited settlement.

Analytical Study

Compared to the number of experimental studies, theoretical analysis of bearing capacity of footings on reinforced soil is relatively scarce. The proposed reinforcement mechanisms in the literature can be categorized as follows:

(1) Rigid boundary (figure 4a): If the depth of the first layer of reinforcement (u) was greater than a specific value, the reinforcement would act as a rigid boundary, and the failure would occur above the reinforcement. Binquet and Lee [2] were the first to report this finding. Subsequent experimental studies conducted by several other researchers confirmed this fact [3], [9], [10], [14], [15].

(2) Membrane effect (figure 4b): With the applied load, the footing and soil beneath the footing move downward, causing the reinforcement to be deformed and tensioned. Due to its stiffness, the curved reinforcement develops an upward force to support the applied load. A certain amount of settlement is needed to mobilize tensioned membrane effect, and the reinforcement should have enough length and stiffness to prevent it from failing by pull-out and tension. Binquet and Lee [2] were perhaps the first who applied this reinforcement mechanism to develop a design method for a strip footing on reinforced sand with the simple assumption made for the shape of reinforcement after deformation. Kumar and Saran [16] extended this method to a rectangular footing on reinforced sand.

(3) Confinement effect (lateral restraint effect) (figure 4c): Due to relative displacement between soil and reinforcement, the friction force is induced at the soil-reinforcement interface. Furthermore, the interlocking can be developed by the interaction of soil and geogrid. Consequently, lateral deformation or potential tensile strain of the reinforced soil is restrained. As a result, vertical deformation of soil is reduced. As most soils are stress-dependent materials, improved lateral confinement can increase the modulus/compressive strength of soil and thus improve the bearing capacity. Huang and Tatsuoka [17] substantiated this mechanism by successfully using short reinforcement having a length (L) equal to the footing width (B) to reinforce sand in their experimental study.

(a) Rigid boundary

- - - - before deformation
——— after deformation
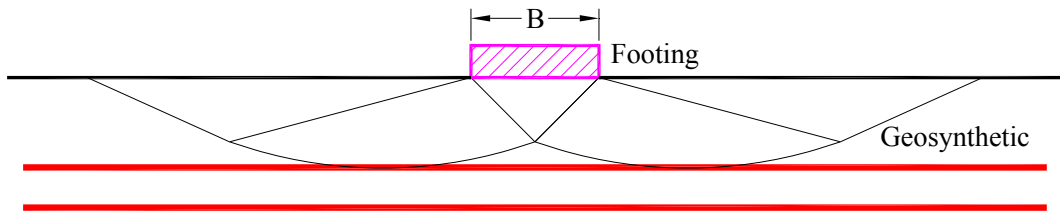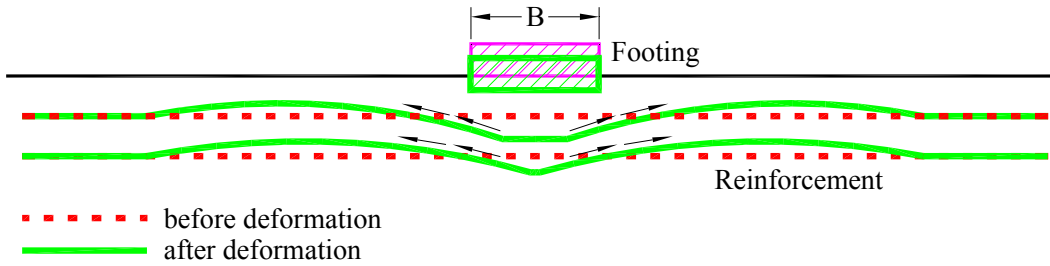
(b) Membrane effect
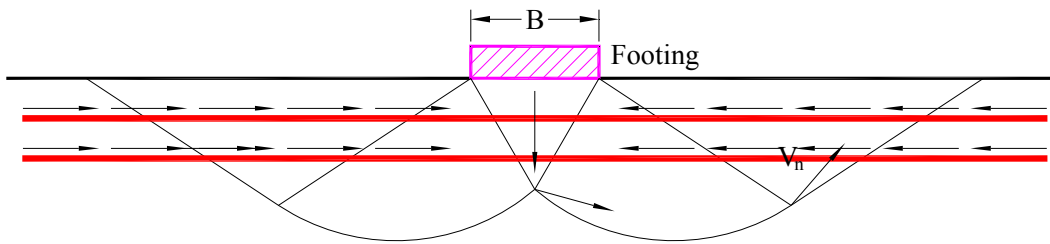
(c) Confinement effect

Figure 4
Reinforcement mechanisms

Table 1 summarizes some analytical solutions for RSF suggested by several researchers.

Table 1
Analytical solutions for RSF

Author	Analytical Solution	Reference
Binquet and Lee [1, 2]	$$T_t(z,N) = \frac{1}{N}\left[J\left(\frac{z}{B}\right)B - I\left(\frac{z}{B}\right)h \right]q_0\left(\frac{q_r}{q_0}-1\right)$$ $$J\left(\frac{z}{B}\right) = \frac{\int_0^{X_0}\sigma_z\left(\frac{z}{B}\right)dx}{q_r B}, \qquad I\left(\frac{z}{B}\right) = \frac{\tau_{xz\max}\left(\frac{z}{B}\right)}{q_r}$$	T_t is force developed in the reinforcement; z is the depth of reinforcement; N is the number of reinforcement layers; h is the vertical spacing between layers; B is the width of footing; q_0 is the footing bearing pressure of unreinforced soil foundation; q_r is the footing bearing pressure of reinforced soil foundation; and I and J are dimensionless force; X_0 is the distance of the point at which τ_{xz} is a maximum. σ_z is the vertical stress at the depth z; τ_{xzmax} is the maximum shear stress at the depth z.
Huang and Tatsuoka [17]	$$\Delta q = K_p{}^2\gamma_d\left[\frac{2d+b+2s_2}{2} - \frac{c+s_1}{2}\right] + \frac{2\left[\sum_{i=1}^{N}T_{t,i}\cdot\tan\phi\cdot N_i\right]}{B}$$ (Failure Model 1) $$\Delta q = K_p\frac{\left[\sum_{i=1}^{N}T_{tav,i}\cdot N_i\right]}{d} \quad \text{(Failure Model 2)}$$	Δq is the bearing capacity increase of strip footings in reinforced san;. $K_p = tan^2(45^o+\phi/2)$; ϕ is the internal friction angle of sand in the corresponding plane strain compression (PSC) test at $\delta = 90^o$ (δ is the angle between major stress (σ_1) direction and the bedding plane), γ_d is the dry unit weight of sand; d is the total depth of reinforcement, b and s_2 are the height of block B beneath the reinforced zone and the settlement of footing at failure for reinforced sand, c and s_1 are the height of block beneath the footing and the settlement of footing at failure for unreinforced sand, N is the number of reinforcement layers, $T_{t,i}$ is the tensile force in each in strip in the layer i at the lateral face of the block A, N_i is the number of reinforcements per unit length in the layer i, and $T_{tav,i}$ is the average tensile force at the layer i in the block A.

(Continued)

Huang and Menq [18]	$q_{u(R)} = q_{u(unreinforced,D_f=d)} = \eta \times \gamma \times (B + \Delta B) \times N_\gamma + \gamma \times d \times N_q$ $\tan\alpha = 0.680 - 2.071h/B + 0.743CR + 0.03l/B + 0.076N$	η is an coefficient depending on footing shape; ΔB is the increase of footing width due to the inclusion of reinforcement, $= (2 \times d)\tan\alpha$; α is the stress distribution angle due to the wide-slab effect; h is the vertical spacing between reinforcement layers; CR is the covering ratio of reinforcement = the area of reinforcement divided by the area of soil covered by reinforcement; l is the length of reinforcement; N is the total number of reinforcement layers.
Wayne et al. [19]	$q_{u(R)} = q_b + 2c_t(B+L)\dfrac{d}{BL} + \gamma_t H^2 \left[1 + 2\dfrac{D_f}{d}\right] K_s(B+L)\dfrac{\tan\phi_t}{BL} + 2(B+L)\dfrac{T}{BL} - \gamma_t d$	q_b is the ultimate bearing capacity of the foundation below the reinforced zone; c_t is the cohesion of the upper layer; γ_t is the unit weight of the upper layer; d is the thickness of the upper layer; ϕ_t is the friction angle of the upper layer; K_s is the punching shear coefficient for upper layer, which is the function of the friction angle and dependent on the ultimate bearing capacities of surface footing on upper and lower soil layers; T is the uplift or restraining force of the reinforcements.

OBJECTIVE

The main objective of this research study is to investigate the potential benefits of using the reinforced soil foundations to improve the bearing capacity and reduce the settlement of shallow foundations on soils. These include (1) examining the influences of different variables and parameters contributing to the improved performance of RSF, (2) investigating the stress distribution in soil mass with and without reinforcement and the strain distribution along reinforcements, (3) understanding the failure mechanism of reinforced soil, (4) developing regression models to estimate the bearing capacity of RSFs, and (5) conducting the stability analysis of reinforced soil foundations and developing a step-by-step procedure for the design of reinforced soil foundations.

SCOPE

Four series of tests were conducted, including: 1) small-scale laboratory tests on silty clay soil; 2) small-scale laboratory tests on sandy soil; 3) small-scale laboratory tests on crushed limestone; 4) and large-scale field tests on silty clay soil. The model footings used in the laboratory model tests were 1 in. thick steel plates with dimensions of 6 in. × 6 in. and 6 in. × 10 in. The model footing used in the field tests was 8 in. thick, steel-reinforced precast concrete block with dimensions of 1.5 ft. × 1.5 ft. The parameters investigated in these tests include: (1) top layer spacing (u), (2) number of reinforcement layers (N), (3) total depth of reinforcement (d), (4) vertical spacing between reinforcement layers (h), (5) the type and stiffness of reinforcement, (6) the embedment of the footing (D_f), (7) the shape of the footing, and (8) the type of soil. The experimental study also includes the investigation of the stress distribution in the soil mass with and without reinforcement and the strain distribution along reinforcement. Based on the results of this study, existing analytical solutions were examined, and new methods based on limit equilibrium analysis were proposed to calculate the bearing capacity of RSF for different soil types. Typical reinforcement configuration parameters for soil foundations are recommended for design purposes. Additionally, numerical simulation was performed to investigate the influence of different parameters involved in RSF design. Based on the numerical analysis results, statistical analyses were performed to develop regression models to predict the bearing capacity of reinforced soil.

METHODOLOGY

Laboratory and Field Tests

Two series of tests, small-scale laboratory tests and large-scale field model tests, were conducted to investigate the influence of different parameters involved in the design of RSF. The experimental study also includes the investigation of the stress distribution in the soil mass with and without the inclusion of reinforcement and the strain distribution along the reinforcement.

Testing Materials Properties

Soils

LADOTD standard specifications require that the natural soils in road construction should have a maximum plastic index (PI) of 25 and a maximum organic content of 5%. Soils with a silt content of 50% or greater and a PI of 10 or less are not allowed in road construction. Nonplastic embankment materials can be an approved sand and stone (Section 203.06). In accordance with these specifications, three different types of geomaterial (sand, silty clay, and Kentucky crushed limestone soils) were used in the present study. The sand used in this study has an effective particle size (D_{10}) of 0.0089 in., a mean particle size (D_{50}) of 0.0177 in., a uniformity coefficient (C_u) of 2.07, and a coefficient of curvature (C_c) of 1.25. The maximum dry density of the soil was 101 lb/ft^3 with an optimum moisture content of 4.8% as determined by the Standard Proctor test, and the grain-size distribution curve of sand is shown in figure 5. Based on Unified Soil Classification System (USCS) and American Association of State Highway and Transportation Officials (AASHTO) classification system, this sand is classified as SP and A-1-b, respectively. Large scale (12 in. × 12 in. × 5.2 in.) direct shear tests on this sand at densities of 105 to 110 lb/ft^3 revealed internal friction angles of 44° to 48°.

The silty clay soil used in the present study was a marginal embankment soil with low to medium plasticity that is often encountered in embankments in southern Louisiana. The silty clay has a liquid limit and PI equal to 31 and 15, respectively. The soil has a maximum dry density of 104 lb/ft^3 and an optimum moisture content of 18.75%, as determined by Standard Proctor test. From the Atterberg limit test, the silty clay is classified as CL according to the USCS, and A-6 according to the AASHTO classification system. Large scale direct shear tests on this silty clay at densities ranging from 95 lb/ft^3 to 110 lb/ft^3 revealed internal friction angles between 25.96^o and 24.13^o and cohesion intercept between 0.73 psi and 3.57 psi.

Figure 5 depicts the grain-size distribution curve of Kentucky crushed limestone. The crushed limestone has an effective particle size (D_{10}) of 0.0183 in., a mean particle size (D_{50}) of 0.2189 in., a uniformity coefficient (C_u) of 20.26, and a coefficient of curvature (C_c) of 1.37. The maximum dry density of the soil was 142 lb/ft^3 with an optimum moisture content of 7.5% as determined by the Standard Proctor test. The shear strength parameter obtained from large scale direct shear test at optimum moisture content of 7.5% and maximum dry density of 142 lb/ft^3, as determined by standard proctor test, is $\varphi = 53°$ and c = 0 psi. This crushed limestone is classified as GW and A-1-a according to USCS and AASHTO classification system, respectively.
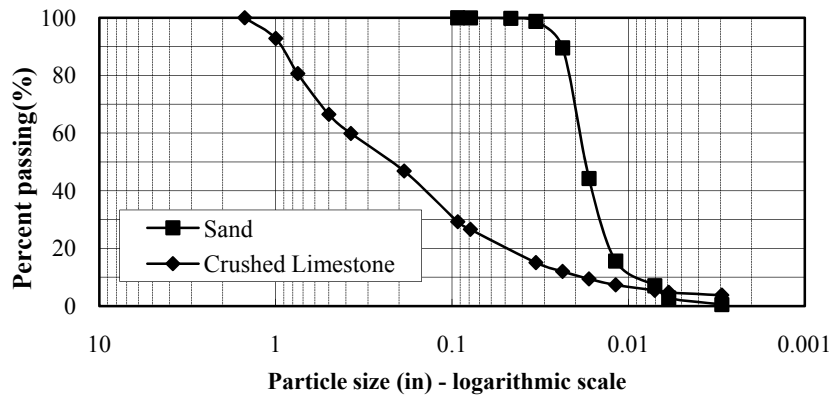
Figure 5
Grain-size distribution curve of sand and limestone

Reinforcement

Nine types of geosynthetics (eight geogrid types and one geotextile type), one type of steel wire mesh and one type of steel bar mesh were used in the present study. The physical and mechanical properties of these reinforcements as provided by the manufacturers are summarized in table 2.

Testing Program and Sample Preparation Techniques

Small-Scale Laboratory Tests

The model tests were conducted inside a steel box with dimensions of 5ft. (1.5 m) (length) × 3 ft. (0.91 m) (width) × 3 ft. (0.91 m) (height). The model footings used in the tests were 1 in. thick steel plates with dimensions of 6 in. × 6 in. and 6 in. × 10 in. The footings were loaded with a hydraulic jack against a reaction steel frame (figure 6). The testing procedure was performed according to the ASTM D 1196-93 [20], where the load increments were applied and maintained until the rate of settlement was less than 0.001 in./min (0.03 mm/min) for three consecutive minutes. The load and the corresponding footing immediate settlement were measured using a ring load cell and two dial gauges, respectively.

14

Table 2
Properties of reinforcement

Type	Reinforcement	Polymer Type	T^a, lb/ft		J^b, lb/ft		T^c, lb/ft		J^d, lb/ft		Aperture
			MD^e	CD^f	MD^e	CD^f	MD^e	CD^f	MD^e	CD^f	Size, in.
GG1	Mirafi BasXgrid11 geogrid	Polyester	500	500	25000	25000	920	920	18400	18400	1.0×1.0
GG2	Tensar BX6100 geogrid	Polypropylene	250	350	12500	17500	…	…	…	…	1.3×1.3
GG3	Tensar BX6200 geogrid	Polypropylene	375	510	18750	25500	…	…	…	…	1.3×1.3
GG4	Tensar BX1100 geogrid	Polypropylene	280	450	14000	22500	580	920	11600	18400	1.0×1.3
GG5	Tensar BX1200 geogrid	Polypropylene	410	620	20500	31000	810	1340	16200	26800	1.0×1.3
GG6	Tensar BX1500 geogrid	Polypropylene	580	690	29000	34500	1200	1370	24000	27400	1.0×1.2
GG7	Tenax MS330 Geogrid	Polypropylene	418	616	20900	30800	925	1340	18500	26850	1.65×1.96[*]
GG8	Mirafi Miragrid 8XT geogrid	Polyester	1095	5480	54750	274000	2520	2520	50400	50400	0.875×1.0
GT1	Mirafi HP570 geotextile	Polypropylene	960	1320	48000	66000	2400	2400	48000	48000	≈ 0
SWM	Steel Wire Mesh	Stainless Steel	16170	30630	808500	1531500	40425	76575	808500	1531500	1.0×2.0
SBM	Steel Bar Mesh	Steel	66470	66470	3323500	3323500	166175	166175	3323500	3323500	3.0×3.0

[a]Tensile Strength (at 2% strain), [b] Tensile Modulus (at 2% strain), [c]Tensile Strength (at 5% strain), [d]Tensile Modulus (at 5% strain), [e]Machine Direction, [f]Cross Machine Direction, [*]Single Layer Dimension

The soil was placed and compacted in lifts inside the steel box. The thickness of each lift varied from 1 in. to 4 in. depending on reinforcement spacing. The amount of soil needed for each lift was calculated first. The test samples were prepared by hand mixing pre-weighted soil and water. Then, the soil was placed into the box, leveled, and compacted using an 8 in. (203 mm) × 8 in. (203 mm) plate adapted to a vibratory jack hammer to the predetermined height. The jackhammer delivers compaction energy of 43 ft·lb and blows at a rate of 1400 per minute. The compaction started on one side and proceeded to the other side.

The quality control of compaction and repeatability of test sections were a major source of discrepancy for such material. Accordingly, the compaction-quality control processes to achieve the required soil densities were accomplished by conducting three passes of vibrating compaction: the compaction effort was applied through the plate for approximately eight seconds in the first pass, three seconds in the second pass, and one second in the third pass at each location. The nuclear density gauge and the geogauge stiffness device were used to measure the density and stiffness modulus for each lift.
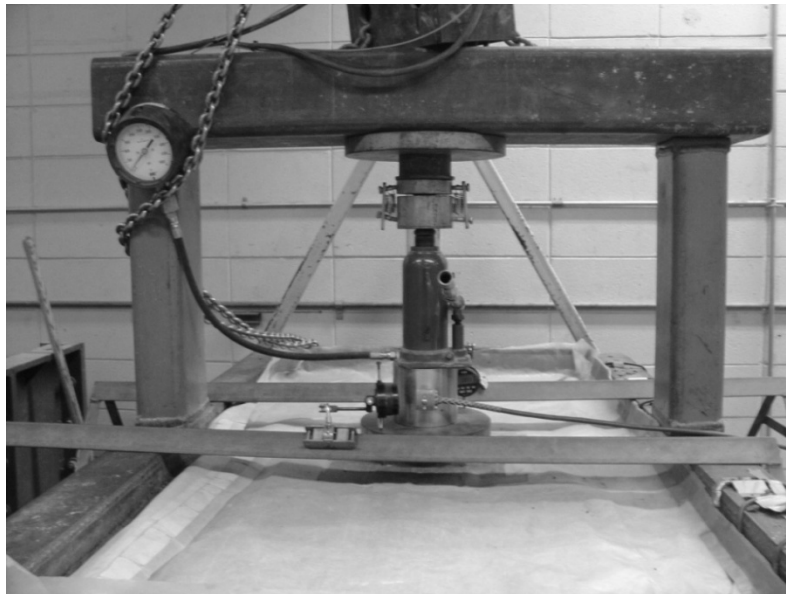
Figure 6
Laboratory test setup, loading, and reaction system

As indicated in literature review, several parameters are crucial for design of reinforced soil foundation (RSF). The purpose of these model tests was to examine the influences of the following parameters on the benefit of RSF:

i) Depth (u) to the first reinforcement layer,

ii) Number of reinforcement layers (N),

iii) Vertical spacing between reinforcement layers (h),

iv) Type and tensile modulus of reinforcement,

v) Embedment of the footing (D_f),

vi) Shape of footing, and

vii) Type of soil.

Tables A.1 through A.3 in Appendix A present the detailed test factorial of laboratory model tests used in this research study. The laboratory experimental study also included the investigation of the stress distribution in soil with and without reinforcement and the strain distribution along the reinforcement. The vertical stress distribution in the soil was measured by Model 4800 VW earth pressure cells (4 in. diameter) from Geokon Inc. installed within the soil mass. The strain distribution along the reinforcement was measured using electrical resistance strain gauges (EP-08-250BG) from Vishay Micro – Measurements that were instrumented at different locations along the reinforcements. Figures 7 and 8 depict typical layouts of instrumentation (pressure cells and strain gauges) used for laboratory model tests on silty clay and sand soils, respectively; while the corresponding plane layouts of pressure cells are shown in figures 9 and 10, respectively.

The pressure cells and strain gauges were connected to the terminal board of Geokon model 8032 16/32 channels multiplexer. The channels are protected against voltage surges with tripolar plasma surge arrestors and bipolar surge arrestors. The Geokon Model 8020 MICRO-10 Datalogger was connected to multiplexers to read the sensors. Multilogger software package from Canary Systems Inc. was used to manage the data acquisition hardware (Datalogger) which was connected directly to a PC. Figure 11 depicts the whole instrumentation system set-up.

Large-Scale Field Tests

The large-scale model tests were performed on an outdoor test embankment, constructed next to the LTRC building. The test embankment has a dimension of 12 ft. (3.658 m) (length) × 12 ft. (3.658 m) (width) × 6 ft. (1.829 m) (height). The test embankment was built using the silty clay soil and had a slope of 1:1, as shown in figure 12. Reaction steel piles were

installed on each side of the test foundation and connected with a steel beam. A hydraulic jack against the steel beam provided downward load. A load cell was placed between the jack and the foundation to measure the applied load. The immediate settlement was measured using dial gauges mounted on reference beams, as shown in figure 13. The model footing used in the field tests was an 8 in. (203 mm) thick, steel-reinforced, precast concrete block with dimensions of 1.5 ft. (457 mm) × 1.5 ft. (457 mm). Silty clay soil was selected for the large-scale model tests. Figures 13 and 14 show the front and side view of the test setup. The large-scale tests were performed according to the ASTM D 1196-93 [20]. A total of six large-scale field tests were conducted. Table A.4 presents the test factorial for this research study.

The soil was placed and compacted in lifts. First, the amount of soil needed for each lift was calculated. The test samples were prepared by using a tiller to mix the pre-weighted soil and water. Then, the soil was placed into the test embankment, raked level, and compacted using a MultiQuip plate compactor and a Wacker-Packer tamper to the predetermined height to achieve the desired densities. The MultiQuip plate compactor having a 19.7 in. × 20.7 in. (500 mm × 526 mm) plate, delivers 3,450 pounds (1,565 kg) of compaction force. The Wacker-Packer tamper's 10 in. × 12 in. (254 mm× 305 mm) plate delivers compaction force of 3,300 lb (1,497 kg) and blows at a rate of 700 per minute.

The compaction-quality control processes were accomplished by conducting three passes with the MultiQuip plate compactor, followed by six passes with the Wacker-Packer tamper. As done in earlier laboratory test, the nuclear density gauge and the geogauge stiffness device were used to measure the density and stiffness modulus for each lift.

The purpose of these large-scale tests was to study the behavior of reinforced soil foundation under field conditions and validate the results of laboratory model results. The stress distribution in the soil, with and without reinforcement, and the strain distribution along the reinforcement were also evaluated in this series of field tests. Figure 15 depicts typical layout of instrumentations (pressure cells and strain gauges) used for large-scale field tests.
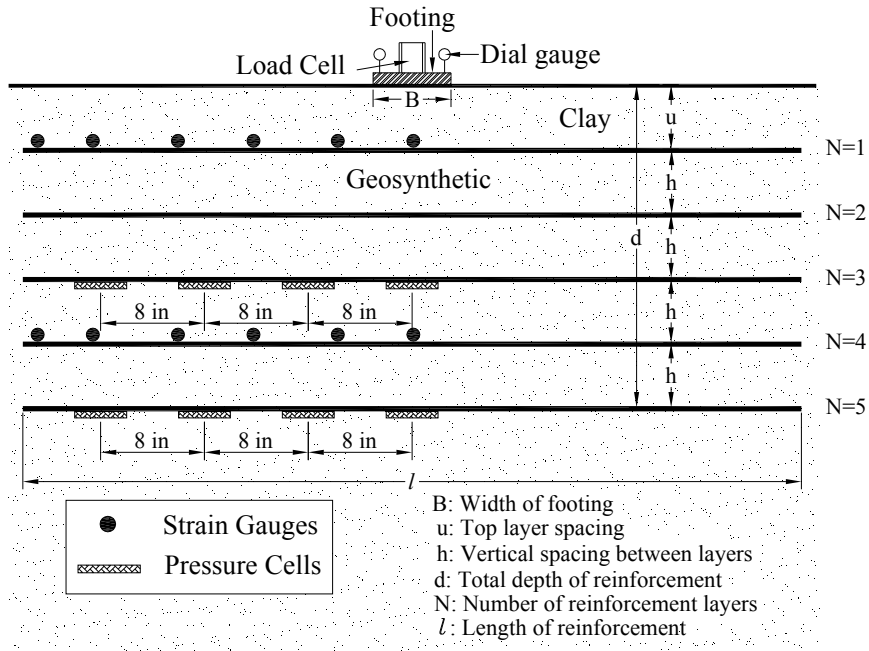
Figure 7
Typical layout of instrumentation for laboratory model tests on silty clay soil
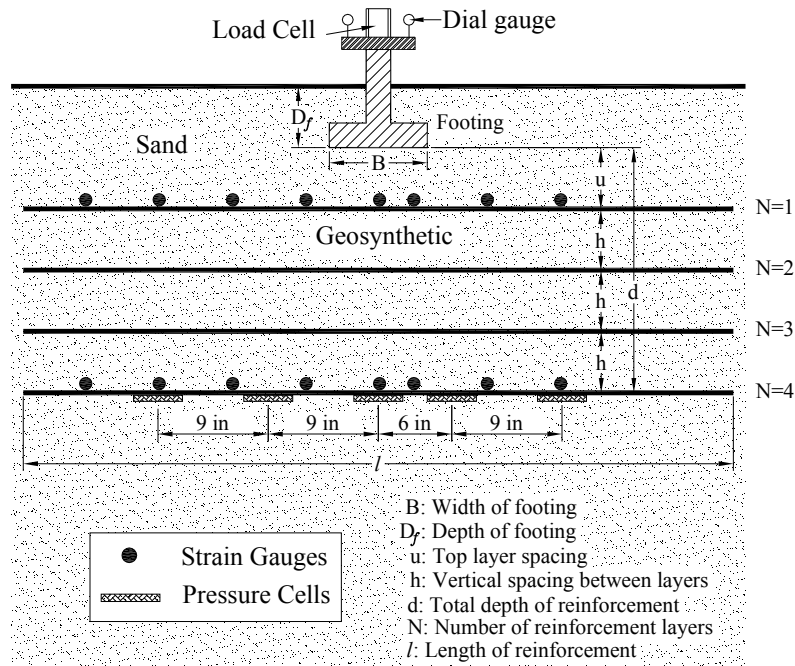
Figure 8
Typical layout of instrumentation for laboratory model tests on sand soil
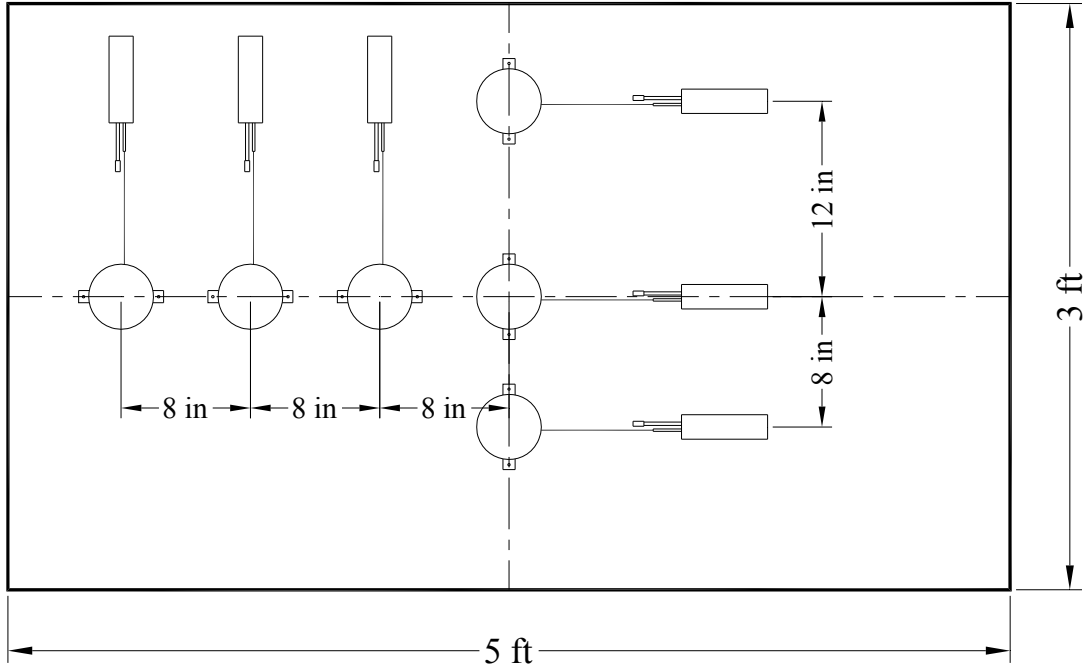
Figure 9
Plane layout of pressure cells for laboratory model tests on silty clay soil
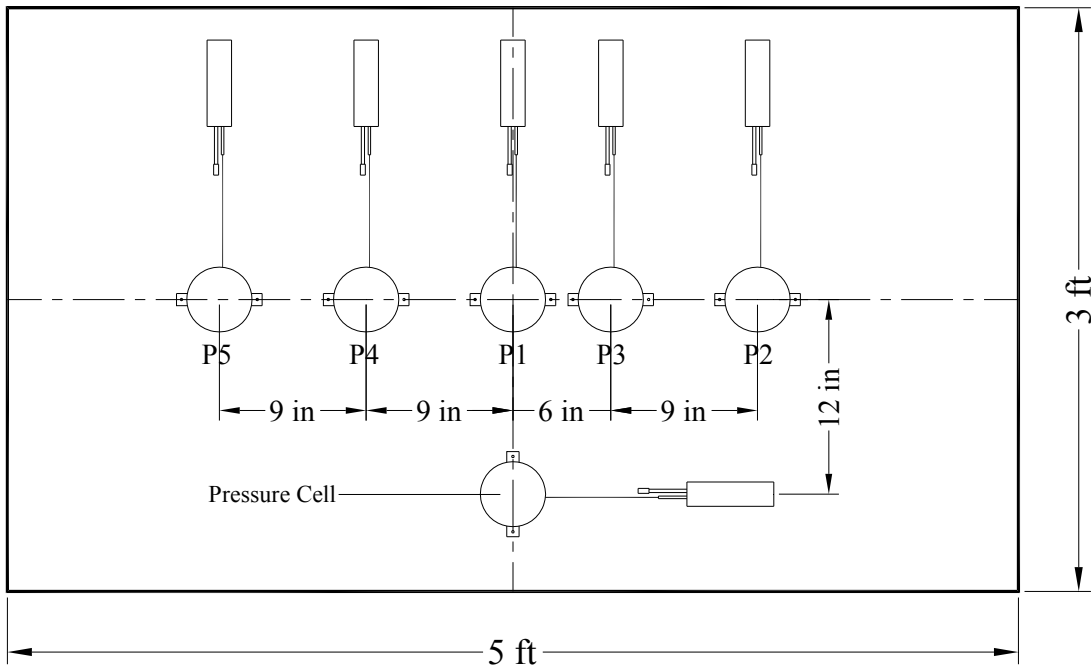
Figure 10
Plane layout of pressure cells for laboratory model tests on sand soil
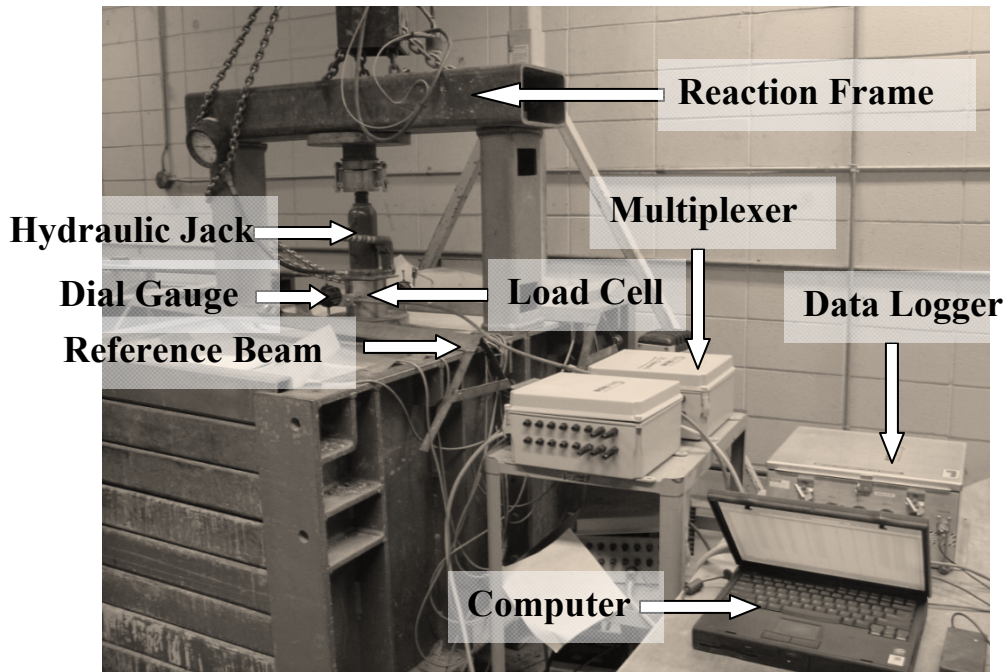
Figure 11
Instrumentation system
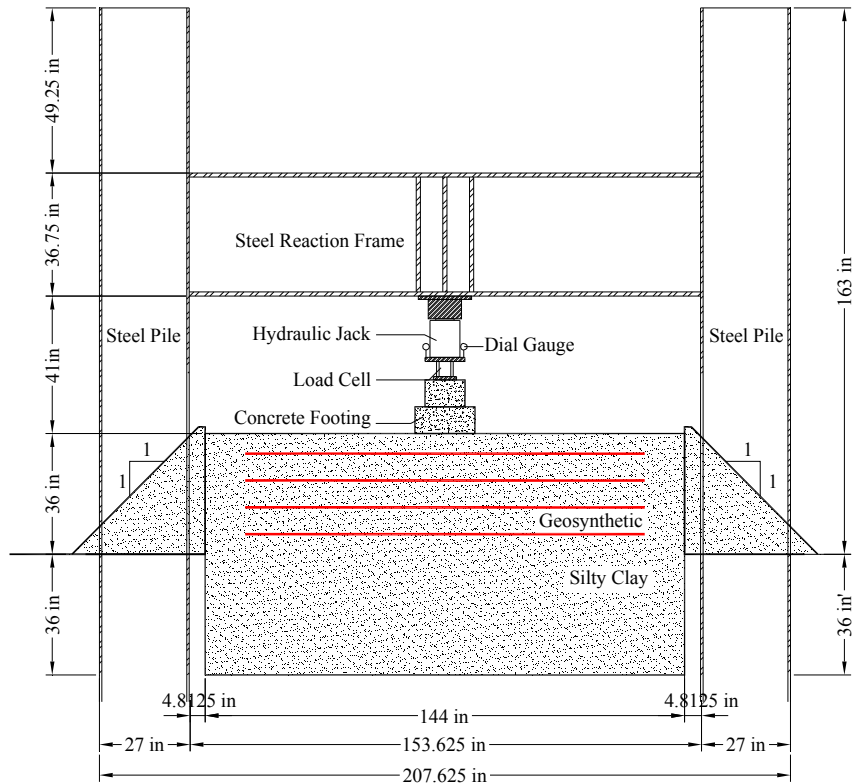
Figure 12
Field test setup, loading, and reaction system
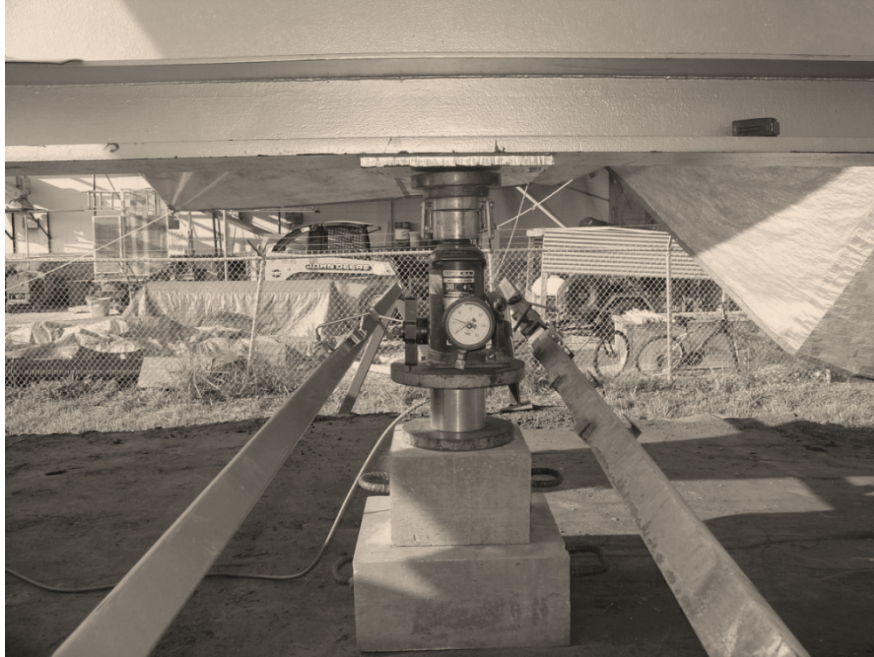
Figure 13
Field test setup — front view
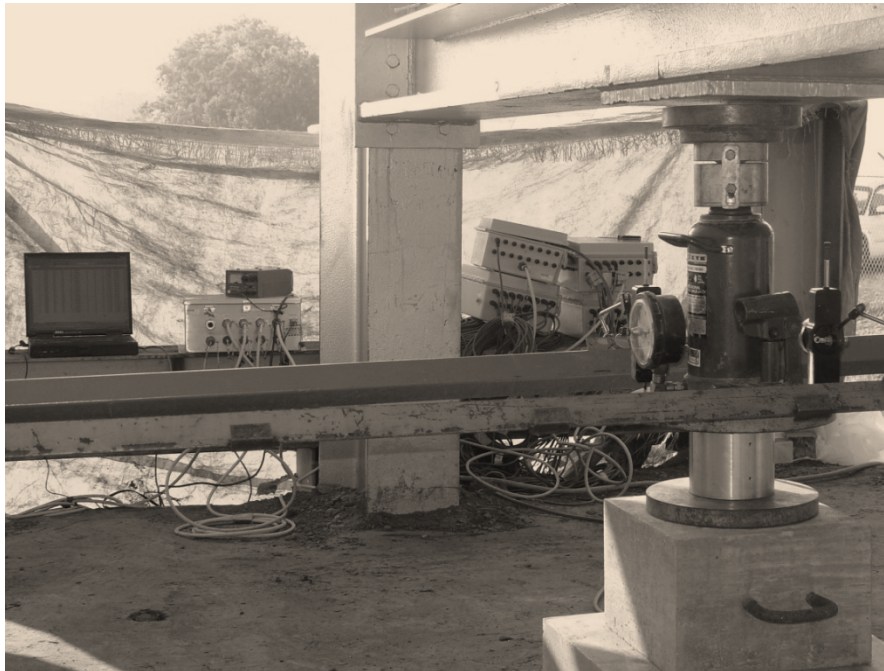
Figure 14
Field test setup — side view
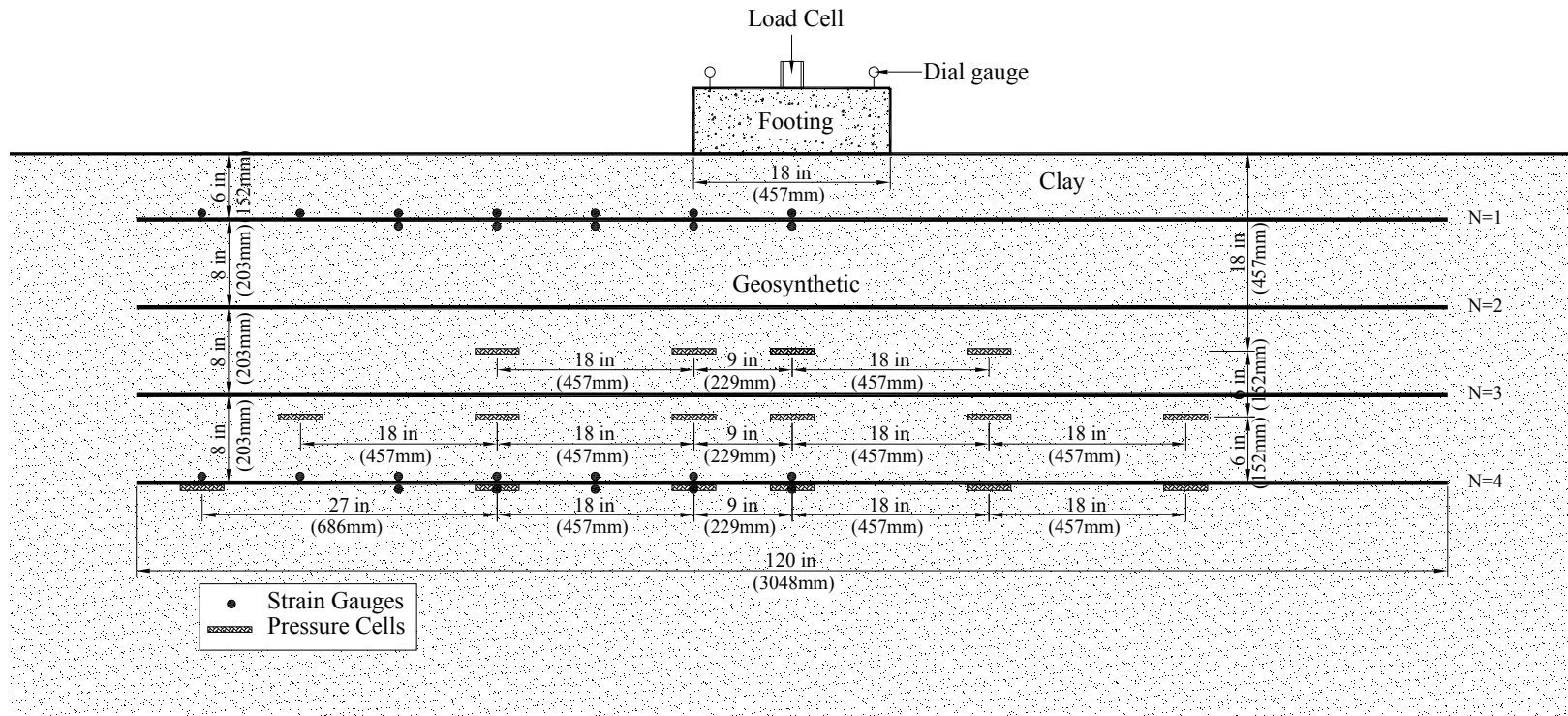
Figure 15
Typical layout of instrumentation for field tests on silty clay

Numerical Study

Over the years, the finite element method has been proven to be the most effective technique to conduct complex numerical analysis of many geotechnical problems. As many previous researchers have found, the realization of potential benefits of a footing on reinforced soil will depend on multiple factors; so does a rational design methodology to fully exploit these benefits. Subsequently, it is a logical step to seek optimum design parameters through a finite element parametric study on the influence of various factors on the bearing capacity and the settlement of strip foundations. Existing design procedures for reinforced soils do not include the influence of many design factors that are examined in this study on the performance of footings on reinforced soils. The findings from this extensive Finite Element Model (FEM) analysis will provide some guidelines to geotechnical practitioners in selecting appropriate values for these design parameters.

Properties of Materials

There are two kinds of material being studied. One is embankment soil and the other is crushed lime stone. Eight different uniaxial geogrids are used to reinforce the embankment soil in this study, designated as Type I to VIII, which are commercially available and widely used in geotechnical engineering applications. Steel wire and steel bar were also used to reinforce the crushed limestone in the lab test. The properties of studied soils and reinforcement are summarized in table 3.

Finite Element Model (FEM)

The commercial FEM program, ABAQUS, was used in this study [21]. The two-dimensional plane strain model was adopted to simulate the strip footing above a reinforced soil. Because of symmetry, only half of the footing was simulated. The soil was discretized using four-node isoparametric elements while the reinforcements were modeled with two-nodded isoparametric truss elements. The interaction between the embankment soil and the geogrid was simulated by two contact surface pairs above and below the geogrid layer, with the master and the slave surfaces for the top and bottom contact surfaces of the geogrid, respectively [22]. The interaction between the crushed lime stone and its reinforcement was simulated by two fully bonded contact surfaces.

The boundary dimensions for the finite element model were determined by conducting several analyses on different mesh sizes to select the dimension of the mesh in which the footing's bearing capacity is not affected by the boundary conditions. Sensitivity analysis was also conducted to find the appropriate mesh size to minimize mesh-dependent effects.

Table 3
Material properties

Material	Friction Angle	Cohesion(psi /kPa)	Elastic Modulus[*] (psi/kPa)	Poisson ratio
Embankment soil	30	11.6/80.0	37700/259932	0.3
Crushed lime stone	48	-	17420/120000	0.35
Geogrid I	-	-	10380/71568	0.3
Geogrid II	-	-	21760/150030	0.3
Geogrid III	-	-	43580/300474	0.3
Geogrid IV	-	-	47440/327087	0.3
Geogrid V	-	-	54620/376592	0.3
Geogrid VI	-	-	91280/629353	0.3
Geogrid VII	-	-	102100/703955	0.3
Geogrid VIII	-	-	131800/908729	0.3
Steel Wire	-	-	171000/1178000	0.3
Steel Bar	-	-	204200/1407000	0.3

[*] *Provided by the manufactures*

A number of finite element meshes with different degrees of refinement were tried first in order to obtain the appropriate mesh for the analysis of a strip footing on reinforced soil that converges to a unique solution. Figure 16 illustrates the final adopted finite element model, which has the dimensions of 7.5B × 7.5B and includes 16,500 elements. In the figure, the width of the footing, depth of the first reinforcement layer (also called top layer spacing), depth of last reinforcement layer, and the vertical spacing between reinforcement layers is designated as B, u, D, and h, respectively. Because the footing is regarded as rigid, applying a load on the footing is equal to applying uniform, vertical, downward displacements at the nodes immediately underneath the footing [23]. Horizontal displacements at the interface between the footing and the soil were restrained to zero, assuming perfect roughness of the interface and symmetry of the footing. The vertical displacement was applied in 1000 increments to achieve a smooth response curve. In the loading process, a footing pressure producing a footing settlement of 10% of the footing width (s/B = 0.1, here s is the footing settlement) at the footing center was taken as the ultimate bearing stress [24]. The embedment of a footing was simulated by applying a uniform pressure ($\sigma = \gamma_s . D_f$, with γ_s is the soil's unit weight, and D_f is the embedment depth of footing) at the bottom level of the footing. The initial geostatic stress condition of the reinforced soil was established by applying the gravity force due to soil in steps with the reinforcement in place.
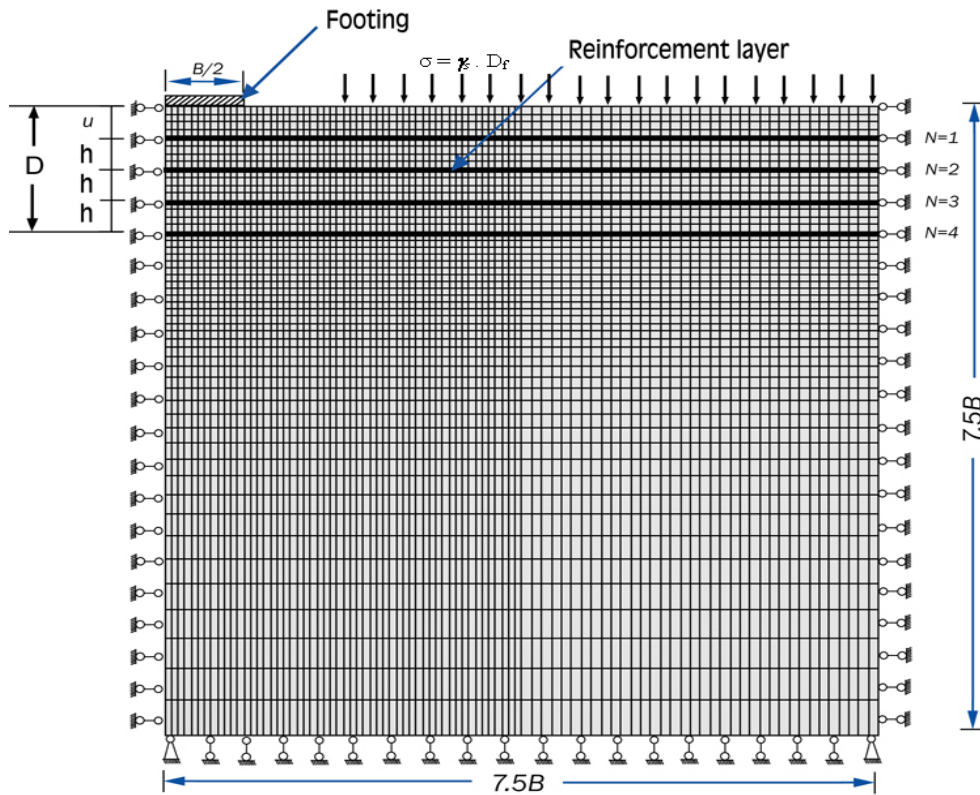
Figure 16
Finite element model of the strip footing on geosynthetic-reinforced soil

Material Model and Parameters

The soil was modeled as an isotropic elasto-plastic continuum described by the extended Drucker-Prager model. Reinforcements were modeled as linear elastic material. The material properties of the soil and reinforcements were presented earlier in table 3.

Normal interaction between soil and reinforcement is simulated by a "hard" contact while shear interaction between them was modeled with two contact surface pairs above and below the reinforcement. Master/slave surface definitions were used for the top and bottom contact surfaces of the reinforcement. The Coulomb friction model is used for the shear interaction, which relates the maximum allowable frictional (shear) stress across an interface to the contact pressure between the contacting bodies. Two contacting surfaces can carry shear stresses up to a certain magnitude across their interface before they start sliding relative to one another. Finite element analyses were first checked against the results from laboratory model tests for a square footing on the reinforced soil, with a reasonable agreement between the finite element analyses with model test results.

DISCUSSION OF RESULTS

Two terms are used in the present study to evaluate the benefits of using RSF. The bearing capacity ratio (BCR) is defined as the ratio of the bearing capacity of the RSF to that of the unreinforced; the settlement reduction factor (SRF) is defined as the ratio of the immediate settlement of the RSF to that of the unreinforced.

Two different types of load-settlement behavior were observed in the model footing tests. For the first type of load-settlement curve as shown in figure 17a, the failure point is not well defined. The benefits of using RSF are then evaluated in terms of BCR at a specific settlement (BCR_s) and SRF at a specific surface pressure. Figure 17b depicts the second type of load-settlement curve, which has a well-defined failure point. For this type of load-settlement behavior, BCR at a specific settlement (BCR_s), BCR at the ultimate bearing capacity (BCR_u), and SRF at a specific surface pressure are used to evaluate the improved performance of RSF.

The optimal values for reinforcement layout and the effect of types of reinforcement and soil are determined based on BCR and SRF in this study. This analytical discussion also includes the characterization of RSF, stress distribution in soil with and without reinforcement, and strain distribution along the reinforcement. The results of this experimental study are also compared with results of previous studies by different researchers.

Figure 17
Definition of BCR and SRF

Small-Scale Laboratory Tests on Reinforced Silty Clay Embankment Soil

The main objective of this study was to investigate the potential benefits of using the RSFs to improve the bearing capacity and reduce the settlement of shallow foundations on cohesive soils of low to medium plasticity. For this purpose, extensive laboratory model tests were conducted on geosynthetic reinforced clayey soils. The parameters investigated in the model tests included: the top layer spacing (u), the number of reinforcement layers (N), the vertical spacing between reinforcement layers (h), the tensile modulus and type of reinforcement, and shape of footing. The experimental study also includes investigating the stress distribution in clay and the strain distribution along the reinforcement.

Three types of geogrids, BasXgrid11, BX6100, and BX6200, and one type of geotextile, HP570, were used as reinforcement in the tests. The physical and mechanical properties of these reinforcements are presented earlier in table 2. The dry densities measured by nuclear density gauge varied from 102 to 107 lb/ft^3 (1,640 to 1,709 kg/m^3) for geogrid reinforced silty clay embankment soil and from 100 to 103 lb/ft^3 (1,601 to 1,644 kg/m^3) for geotextile reinforced silty clay embankment soil. Both had moisture contents ranging from 18 to 18.5%. The corresponding geogauge stiffness moduli were in the range of 14,504 to 17,405 psi (100 to 120 MPa) for silty clay embankment soil in all tests with/without reinforcement inclusion.

The results of the laboratory model tests for silty clay embankment soil are summarized in table 4. This table presents the BCRs obtained at settlement ratios (s/B) of 3%, 10%, and 16%. The settlement ratio (s/B) is defined as the ratio of footing settlement (s) to footing width (B). The results of the model footing tests are also graphically presented in figure 18 and figures B.1 through B.6 in Appendix B. Figure B.1 presents the pressure-settlement curves measured for model footing tests with single layer of BasXgrid11 placed at different top layer spacing. The measured pressure-settlement curves for model footing tests with different numbers of reinforcing layers are presented in figure 18 and figures B.2 through B.5. Figure B.6 depicts the pressure-settlement curves obtained for the model footing tests using three layers of BX6200 placed at different vertical spacing. Investigating the pressure-settlement curves, one can see that as the pressure increases, so does the settlement for both unreinforced and reinforced silty clay. This settlement pattern resembles a typical punching-shear failure. Since the failure point is not well-defined, the bearing capacity is obtained at different settlement ratios and used to calculate the corresponding BCRs.

Table 4
Summary of laboratory model tests for silty clay embankment soil

Test No.	Reinforcement configuration	u in.	h in.	s/B = 3%		s/B = 10%		s/B = 16%.	
				q, psi	BCR	q, psi	BCR	q, psi	BCR
CNR*	Unreinforced	…	…	51.9	...	82.7	...	99.6	…
CGG11-1		1	…	52.1	1.00	85.1	1.03	105.7	1.06
CGG11-2		2	…	52.9	1.02	88.3	1.07	111.7	1.12
CGG11-3		3	…	51.6	0.99	86.9	1.05	109.9	1.10
CGG11-4	N=1, BasXgrid11	4	…	51.9	1.00	85.0	1.03	106.9	1.07
CGG11-5		5	…	51.2	0.99	83.5	1.01	105.0	1.05
CGG11-6		6	…	51.3	0.99	83.7	1.01	105.1	1.06
CGG11-7		8	…	51.0	0.98	82.8	1.00	103.7	1.04
CGG12	N=2, BasXgrid11	2	2	65.3	1.26	106.7	1.29	134.9	1.35
CGG13	N=3, BasXgrid11	2	2	73.2	1.41	117.9	1.43	152.4	1.53
CGG14	N=4, BasXgrid11	2	2	77.3	1.49	132.5	1.60	174.7	1.75
CGG15*	N=5, BasXgrid11	2	2	77.4	1.49	138.9	1.68	182.4	1.83
CGG21	N=1, BX6100	2	...	61.8	1.19	88.7	1.07	107.9	1.08
CGG22	N=2, BX6100	2	2	62.1	1.20	105.7	1.28	138.8	1.39
CGG23	N=3, BX6100	2	2	75.1	1.45	124.8	1.51	158.3	1.59
CGG24#	N=4, BX6100	2	2	75.5	1.46	128.0	1.55	164.9	1.66
CGG25*	N=5, BX6100	2	2	77.3	1.49	133.4	1.61	174.6	1.75
CGG31	N=1, BX6200	2	...	62.8	1.21	100.2	1.21	127.2	1.28
CGG32	N=2, BX6200	2	2	63.1	1.22	108.2	1.31	143.6	1.44
CGG33-1*	N=3, BX6200	2	1	80.0	1.54	141.8	1.72	177.9	1.79
CGG33-2*	N=3, BX6200	2	2	75.1	1.45	125.9	1.52	160.1	1.61
CGG33-3*	N=3, BX6200	2	3	69.9	1.35	117.2	1.42	158.3	1.59
CGG33-4*	N=3, BX6200	2	4	68.2	1.31	111.4	1.35	145.1	1.46
CGG34*	N=4, BX6200	2	2	75.4	1.45	134.4	1.63	178.8	1.79
CGG35*	N=5, BX6200	2	2	78.0	1.50	135.0	1.63	180.7	1.81
CGT11	N=1, HP570	2	...	58.1	1.12	90.9	1.10	112.4	1.13
CGT12	N=2, HP570	2	2	59.6	1.15	115.0	1.39	151.7	1.52
CGT13	N=3, HP570	2	2	63.8	1.23	119.3	1.44	163.4	1.64
CGT14	N=4, HP570	2	2	69.7	1.34	120.6	1.46	170.1	1.71
CGT15*	N=5, HP570	2	2	70.6	1.36	123.0	1.49	174.0	1.75
CFNR	Unreinforced	…	…	48.0	…	79.3	…	96.3	…
CFGG15*	N=5, BasXgrid11	2	2	71.3	1.49	127.3	1.61	161.2	1.67

Table 4
(continued)

CFGG21	N=1, BX6100	2	…	58.9	1.23	85.8	1.08	104.7	1.09
CFGG22	N=2, BX6100	2	2	69.0	1.44	115.0	1.45	142.8	1.48
CFGG23*	N=3, BX6100	2	2	71.5	1.49	116.4	1.47	148.0	1.54
CFGG24*#	N=4, BX6100	2	2	70.5	1.47	124.4	1.57	157.3	1.63
CFGG25*	N=5, BX6100	2	2	70.8	1.47	126.6	1.60	157.8	1.64
CFGT15*	N=5, HP570	2	2	55.8	1.16	110.5	1.39	156.0	1.62

Instrumented with pressure cell
 # Instrumented with strain gauge
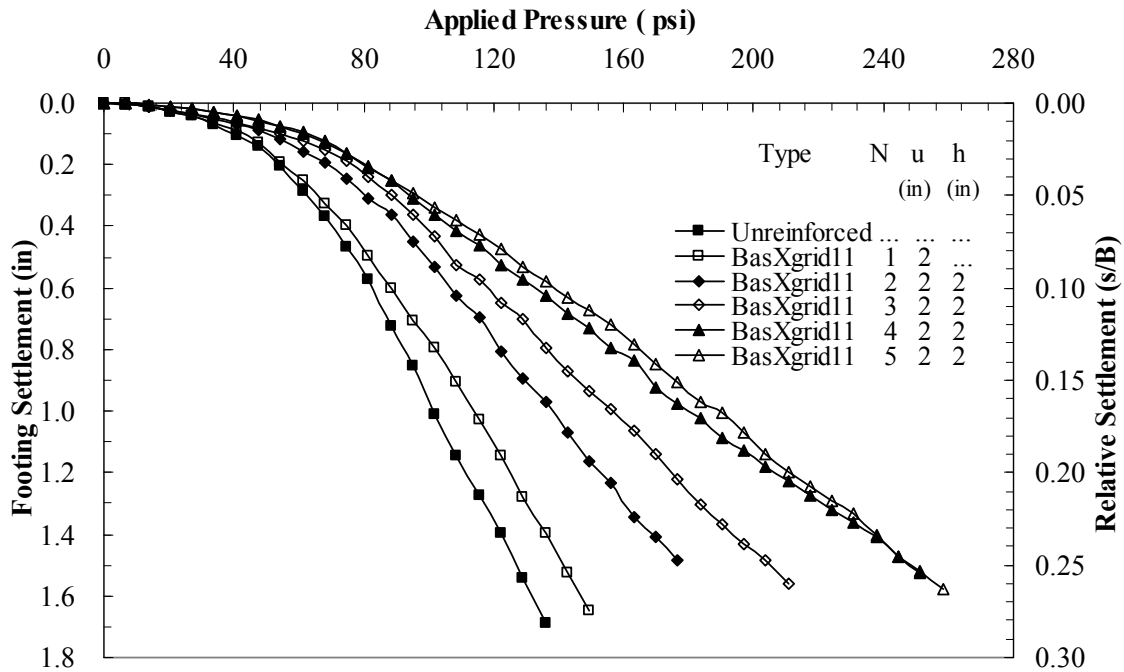
Figure 18
Pressure-settlement curves for model footing tests with different number of layers of BasXgrid11 geogrid in silty clay (B × L: 6 in. × 6 in.)

Effect of Reinforcement Top Spacing

The optimum location of the first reinforcement layer was investigated using a six inch wide square footing with BasXgrid11 geogrid reinforcement. Figure 19 shows that the BCRs at settlement ratios s/B=3%, 10%, and 16% increase with increasing the top layer spacing ratios (u/B) up to a maximum value at u/B = 0.33, after which it decreases. The top layer spacing ratio (u/B) is defined as the ratio of top layer spacing (u) to footing width (B). The optimum location of the top layer is then estimated to be about two inches, which is equivalent to 0.33B.

Effect of Number of Reinforcement Layers

A series of laboratory model footing tests were conducted on the silty clay embankment soil reinforced with multiple layers of four different types of geosynthetics placed at a spacing of
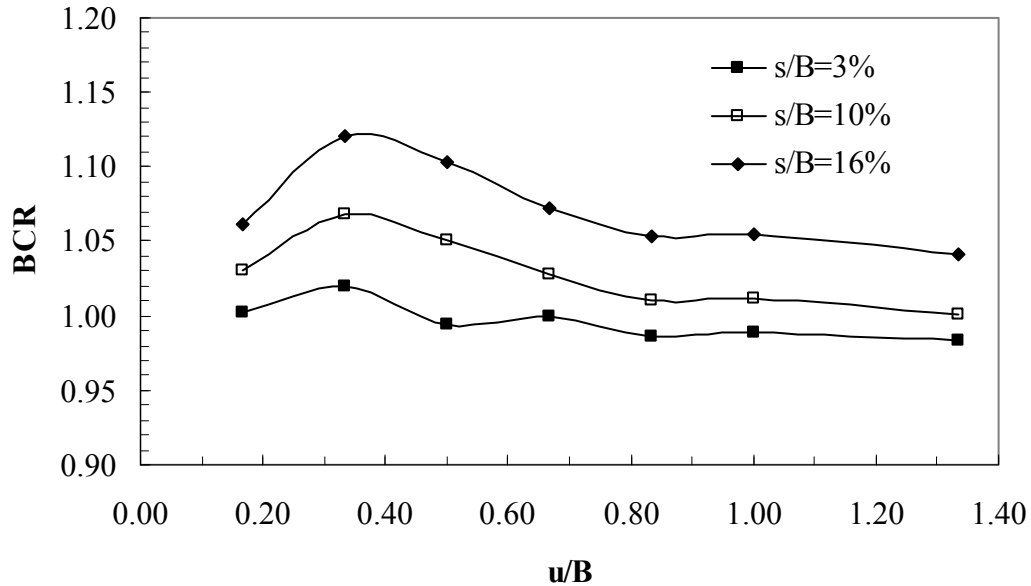
Figure 19
BCR versus *u/B* for one layer of BasXgrid11 at different settlement ratios (s/B) in silty clay soil (B × L: 6 in. × 6 in.)

two inches figures 18 and B.2 through B.5 present the pressure-settlement curves of these model tests. As expected, the bearing capacity increased with increasing number of reinforcement layers. However, the significance of an additional reinforcement layer decreases with the increase in number of layers. This effect becomes negligible below the influence depth. The influence depth is the total depth of reinforcement below which the rate of increase in BCR is negligible with an additional reinforcement layer. The variations of BCRs obtained at settlement ratios of s/B=3%, 10%, and 16% for different numbers of reinforcement layers (N) and reinforcement depth ratios (d/B) are shown in figure 20 for 6 inch-wide square footing, and figure 21 for 6 in. × 10 in. rectangular footing. The reinforcement depth ratio is defined as the ratio of the total depth of reinforcement (d) to footing width (B). It can be seen from these figures that the BCRs increase with N and d/B, and appear to become almost constant after N=4 (d/B=1.33) for geogrid reinforced silty clay and N=3 (d/B=1.0) for geotextile reinforced silty clay, respectively. Accordingly, the influence depth can be estimated to be 1.5B for geogrid reinforced clay and 1.25 B for geotextile reinforced clay. The influence depth seems to be independent of the footing shape based on the test results of this study.

Effect of Vertical Spacing of Reinforcement Layers

The effect of vertical spacing of reinforcement layers was investigated using 6 inch-wide footing and three layers of BX6200 geogrid reinforcement with a top layer spacing of 2 in. (0.33B). The vertical spacing of reinforcement varied from 0.167B to 0.667B. Figure 22 depicts the variation in the BCR values of the loads corresponding to settlement ratios of s/B=3%, 10%, and 16% as a function of the vertical spacing ratio (h/B), which is defined as the ratio of the vertical spacing of reinforcement layers (h) to the footing width (B). It is obvious that the BCR values decrease with increasing vertical spacing of reinforcement layers, with the maximum BCR at $h = 0.167B$ in the present study. No optimum vertical spacing was obtained for the BX6200 geogrid reinforced silty clay tested. As stated before, there is an influence depth for placing geogrid. The effect of vertical spacing is not independent. Instead, it is a function of top layer spacing (u) and number of layers (N), and may also be a function of reinforcement modulus and size. However, for the silty clay and geogrid reinforcement tested in this study, one can assume that the smaller the spacing, the higher the BCR. In design, engineers must find the balance between using smaller spacing and using higher modulus geogrid. The effect of geogrid modulus will be discussed later. The author believes a value of $h/B = 0.33$ can be a reasonable value for use in the design of reinforced silty clay.

Effect of Footing Shape

The effect of footing shape on the BCR of reinforced soils was investigated by conducting two sets of model tests, one with a 6 in. wide square footing, and one with a 6 in. ✕ 10 in. rectangular footing. The test results show that the bearing capacity of unreinforced silty clay for 6 inch-wide square footing is greater than that for 6 in. ✕ 10 in. rectangular footing (table 4), which is consistent with the theoretical analysis by using bearing capacity formula suggested by Vesic [29]. A similar trend was also found in reinforced silty clay. The comparison of BCRs obtained for these two different shape footings is shown in figure 23. From this figure, it is clear to see that the BCRs for 6 inch-wide square footing are generally greater than those obtained for 6 in. ✕ 10 in. rectangular footing.

Effect of Tensile Modulus and Type of Reinforcement

Four different types of reinforcement with different strength/modulus were used in the model footing tests. These included BasXgrid11 geogrid, BX6100 geogrid, BX6200 geogrid, and HP570 geotextile, all of whose properties were presented in table 2. Figures B.7 through B.12 in Appendix B rearrange the pressure-settlement curves obtained for different types of reinforcements to compare the results of model tests with the same reinforcement configuration. The BX6100 and BX6200 geogrids are made of the same material and have

similar aperture size, but BX6200 has higher tensile strength/modulus than BX6100. As seen in figures B.7 through B.12, the silty clay reinforced by BX6200 geogrid performed better than that reinforced by BX6100 geogrid.
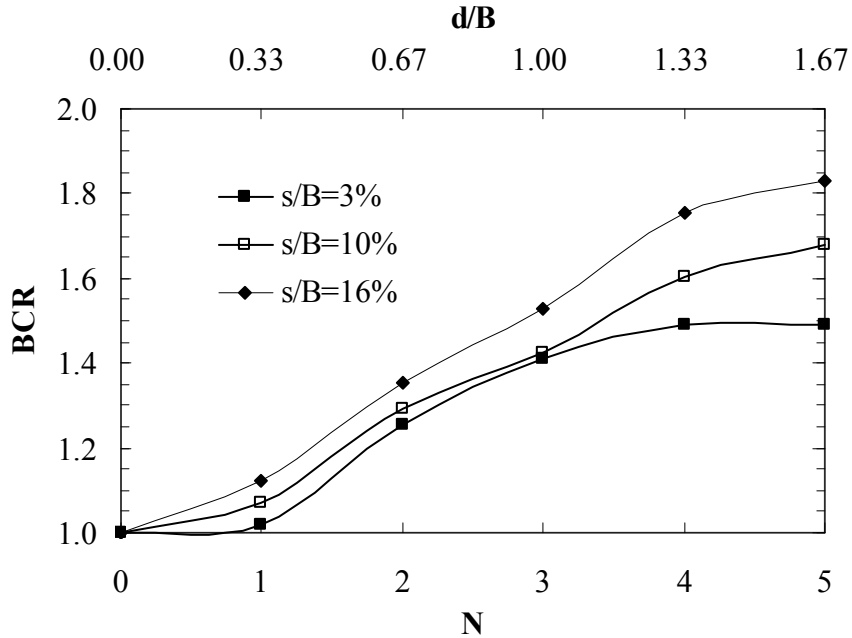
(a) BasXgrid11 geogrid
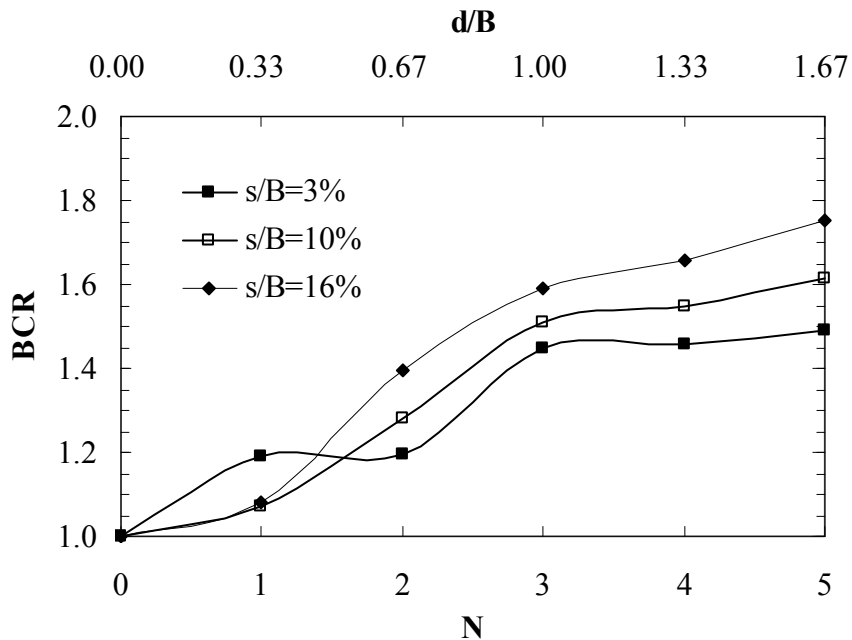
(b) BX6100 geogrid

Figure 20
BCR versus *N* and *d/B* at different settlement ratios (s/B) for silty clay embankment soil
(B × L: 6 in. × 6 in.)
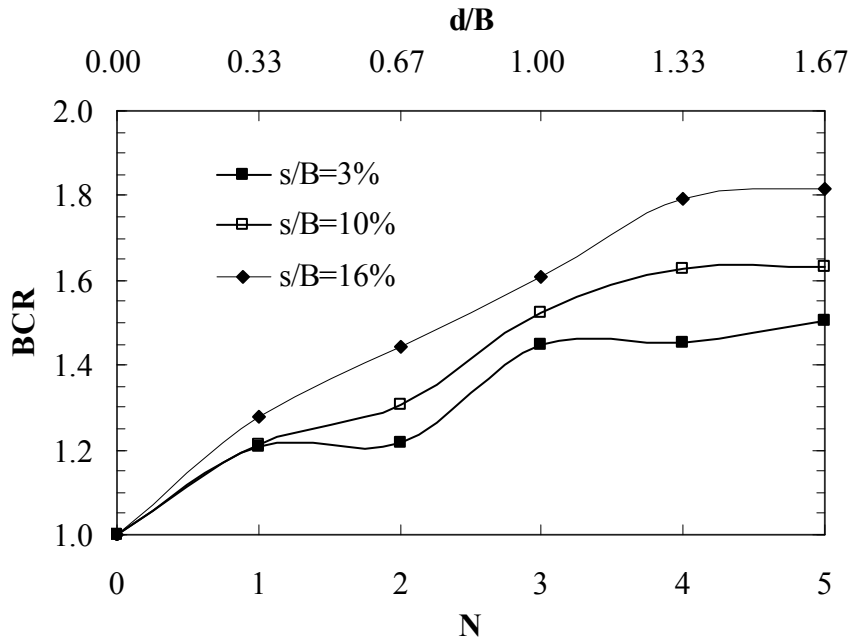
(c) BX6200 geogrid
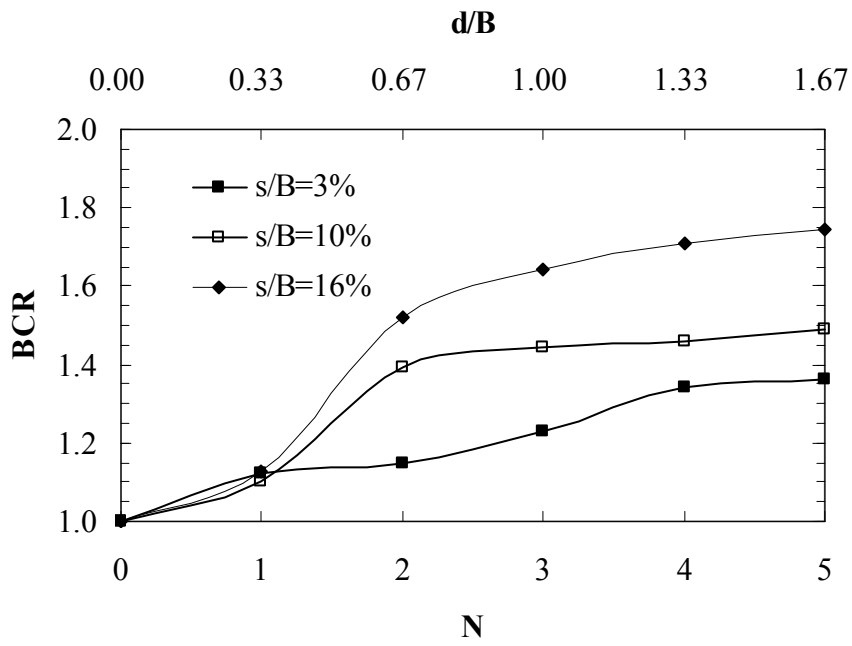
(d) HP570 Geotextile

Figure 20
(continued)

34
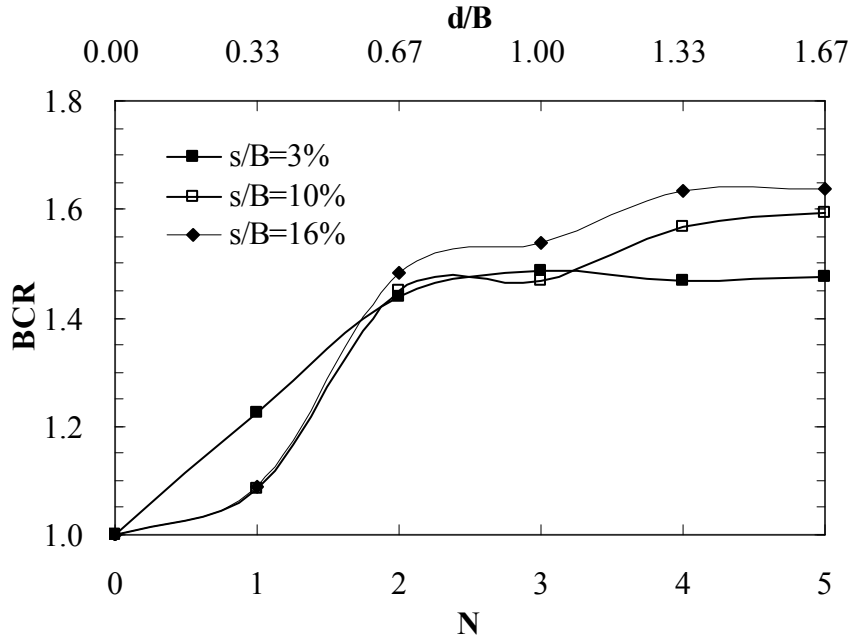
Figure 21
BCR versus *N* and *d/B* at different settlement ratio (s/B) for BX6100 geogrid in silty clay embankment soil (B × L: 6 in. × 10 in.)
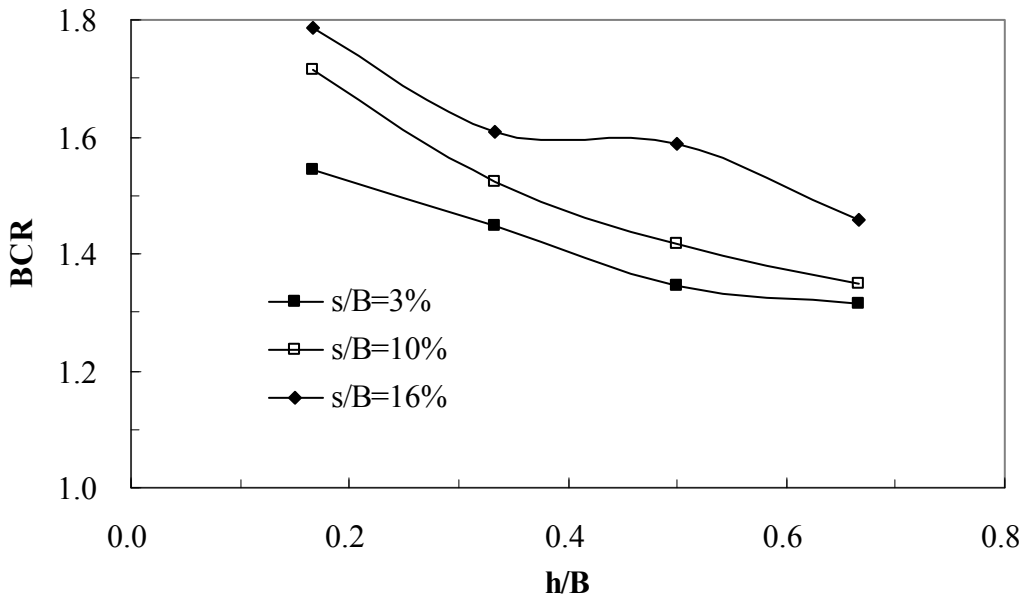
Figure 22
BCR versus *h/B* for three layers of BX6200 in silty clay embankment soil at different settlement ratio (s/B) (B × L: 6 in. × 6 in.)
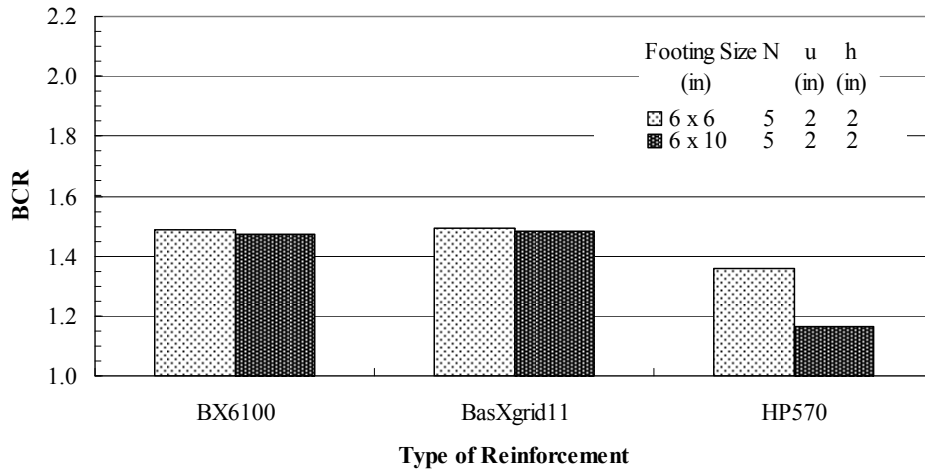
(a) s/B = 3%
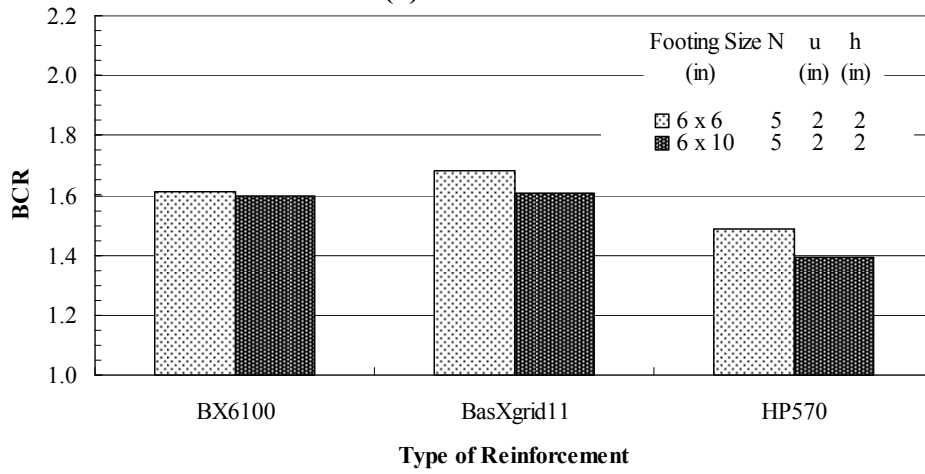
(b) s/B = 10%
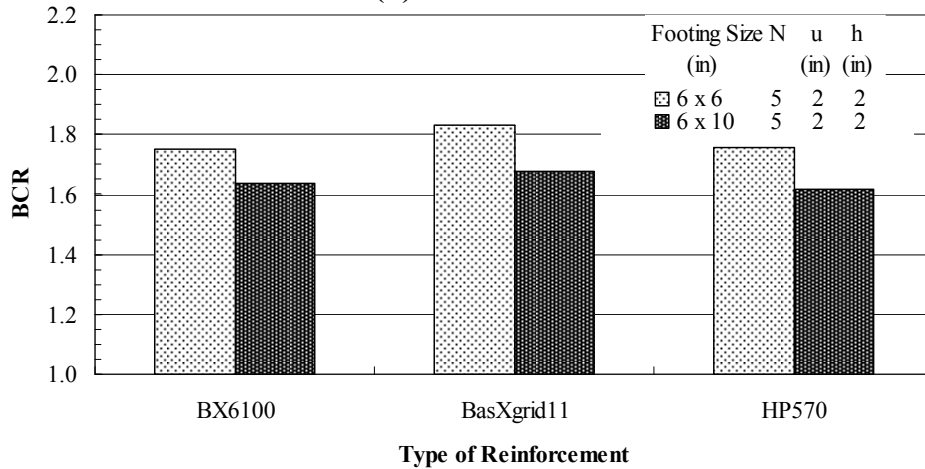
(c) s/B = 16%

Figure 23
BCR versus type of reinforcement for two different size footings

The authors also noted that the behavior of these two geogrids is very similar until a certain amount of settlement is reached in order to mobilize the geogrid. The figures also show that BasXgrid11 geogrid, which has the highest tensile modulus and smallest aperture size of the study's the three types of geogrid, has the best performance. As shown in figure 24, this study demonstrates that the performance of reinforced silty clayey soil improves with increasing geogrid tensile modulus. However, the effect of the tensile modulus seems to be a function of settlement. In support of this finding, lower stresses were measured for higher tensile modulus geogrids at the same depth under the center of the footing, as will be discussed later in the study.

The BCRs at different settlement ratios (s/B) for model tests, with multiple layers of different types of reinforcement, are presented in figures 25a to 25d. It can be seen that the BCR generally increases with the increase of settlement ratio (s/B). At a relatively low settlement ratio (s/B), the increase of the bearing capacity of silty clay soil reinforced with geogrids is more significant than those with HP570 geotextile of higher tensile modulus. However, with the increase of settlement ratio (s/B), the BCRs of HP570 geotextile reinforced silty clay increased more quickly than those of geogrid reinforced silty clay. Figures B.7 through B.12 also show that the silty clay, reinforced by geogrids, performs better than that reinforced by HP570 geotextile at relatively low settlement. However, the response of HP570 geotextile reinforced silty clay is stiffer than geogrid reinforced silty clay after reaching a certain amount of settlement, depending on the number of reinforcement layers. This behavior can be attributed to the slack of woven geotextile. The slack of woven geotextile can be caused by stretching of the woven geotextile, the test setup, or both. At a low settlement level, the friction and adhesion developed at the silty clay-geotextile interface started to stretch the geotextile. With the increase of settlement, the slack of woven geotextile was removed gradually; and finally, the geotextile was fully stretched. Because the geotextile has the highest stiffness of all four types of reinforcement used, the reinforcing effect of geotextile would be more appreciably mobilized after reaching a certain amount of settlement. The authors note here that the change of stresses in HP570 geotextile reinforced silty clay and geogrid reinforced silty clay with the increase of footing pressure show the same trend.

Because of a serviceability requirement, foundations are always designed at a limited settlement level. From an engineering practice point of view, geogrid reinforcement is considered to perform better for a silt clay foundation than for geotextile. But just as Guido, et al. [25] stated, the selection of type of reinforcement is a project dependent issue. For example, some projects require that geosynthetics only function as reinforcement, while

other projects require geosynthetics to function as both reinforcement and separator or filter in which relatively poor reinforcement is also acceptable.

The settlement reduction factors (SRF) at different footing pressure (q) for the model tests with multiple layers of different types of reinforcements are presented in figures 26a through 26d. It is obvious that the inclusion of reinforcement would reduce the immediate settlement significantly. With three or more layers of reinforcement, the immediate settlement can even be reduced by 50% at a relatively medium footing pressure (58 psi). The higher tensile modulus geogrids provided better reduction in immediate settlement than the lower tensile modulus geogrids. The SRF values of geotextile reinforced silty clay were generally lower than those of geogrid reinforced silty clay. The SRF values associated with geotextile at low stresses with N equal to/less than 3 was even greater than 1.0. This behavior may be attributed to the slack effect of the woven geotextile. The rate of decrease of SRF with the increase of footing pressure for geotextile reinforced silty clay was higher compared to that for geogrid reinforced silty clay. In all cases, the SRFs became stabilized at a footing pressure of 72.5 psi (500 kPa) and higher.

Stress Distribution in Silty Clay Embankment Soil
Several laboratory model tests were conducted to evaluate the stress distributions in the silty clayey soil with and without reinforcement inclusion induced by footing load. Pressure cells were placed at specified locations/depth for this purpose. The induced vertical stress distributions along the center line of the footing at the depth of 10 in. (1.67B) are shown in figure 27 for a 6 inch-wide footing with different number of layers of BX6200 geogrid. Figure 28 presents the induced vertical stress distributions at depths of 10 in. (1.67B) for a 6 inch-wide footing with three layers of BX6200 geogrid placed at different vertical spacing. The induced vertical stress distributions at a depth of 10 in. (1.67B) for a 6 inch-wide footing and a 6 in. × 10 in. rectangular footing with five layers of different types of reinforcement are presented in figures 29 and 30. The profiles of induced vertical stress with depth below the center of the footing are shown in figure 31 for a 6 inch-wide footing with three layers of BX6200 geogrid placed at different vertical spacing. Here, the vertical stress distributions are only presented for two footing pressure levels, the vertical stress distributions at the other applied footing pressures can be found in Chen [26]. It is noted that the stresses measured here by the pressure cells are the total vertical stresses induced by the applied footing load, while the stresses induced by the weight of soil are not included.

As can be seen from these figures, the induced maximum stresses beneath the center of the footing in reinforced silty clay are appreciably reduced, compared to those in unreinforced silty clay.
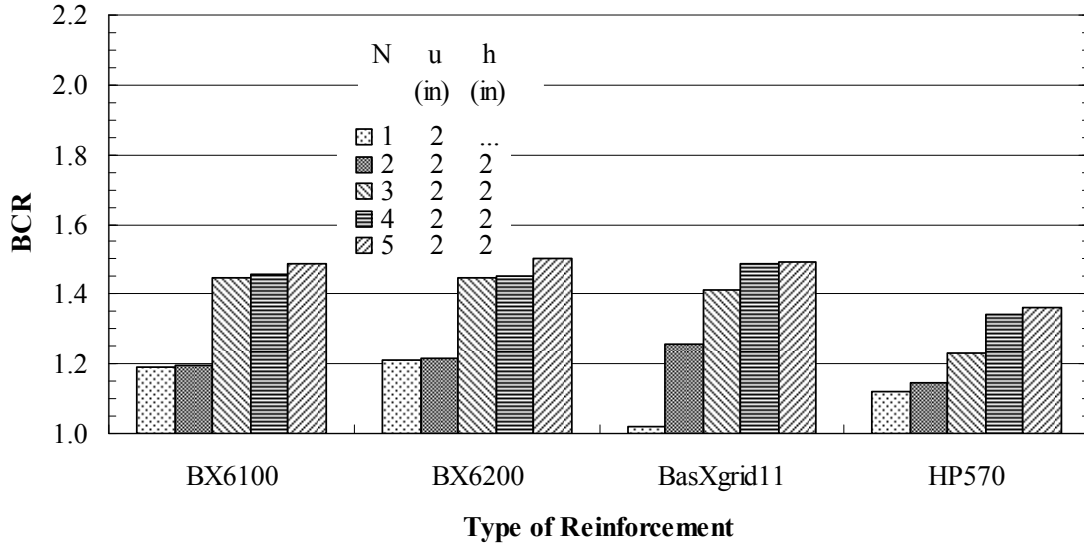
(a) s/B=3%
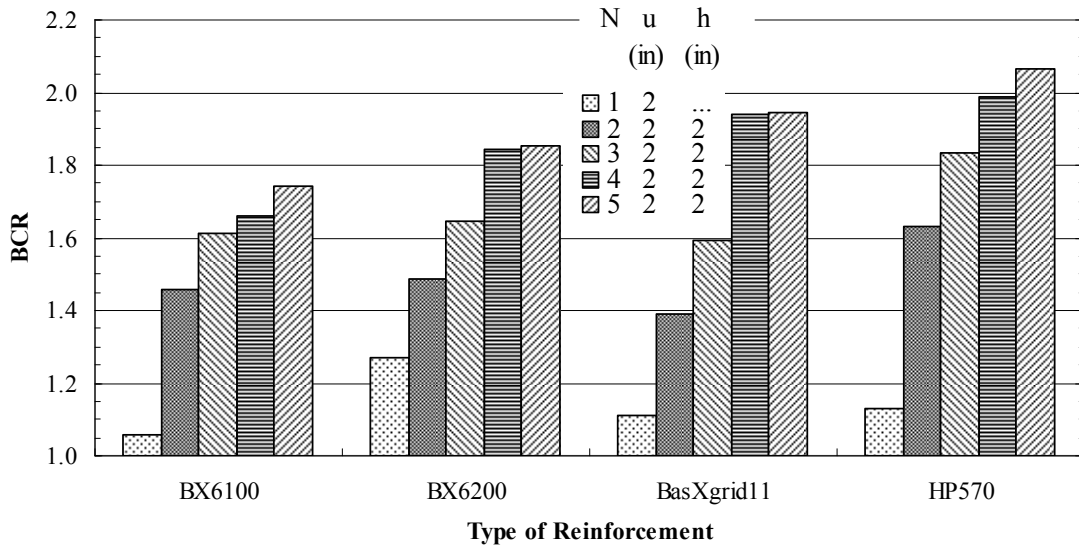
(b) s/B=24%

Figure 24
BCR versus type of reinforcement for silty clay
(B × L: 6 in. × 6 in.)
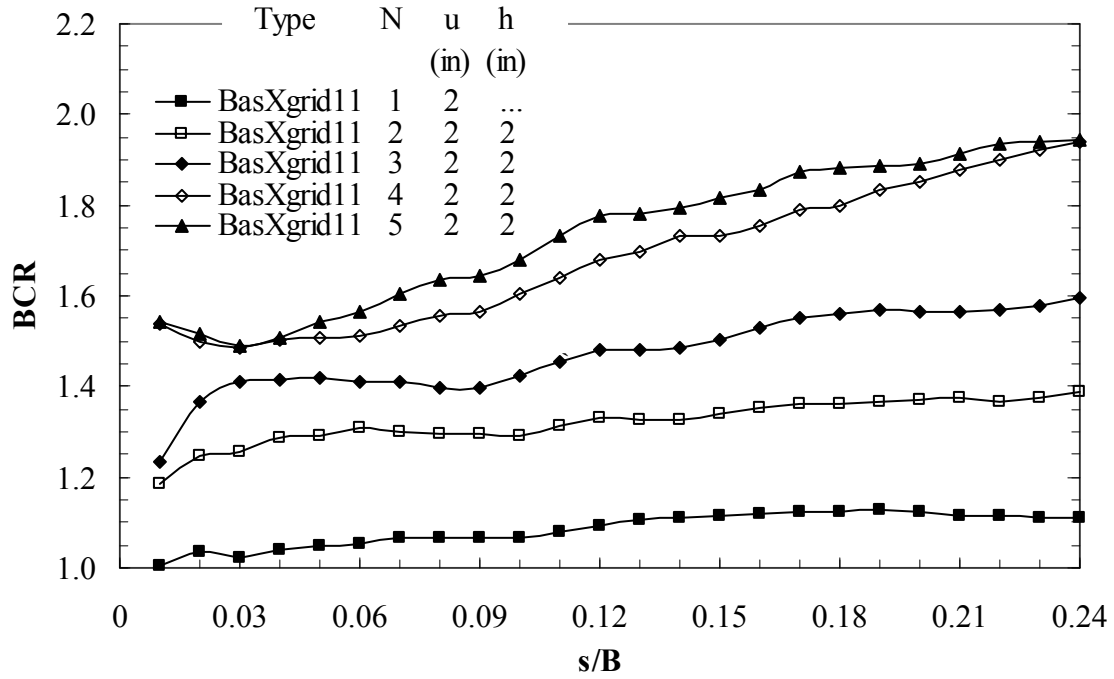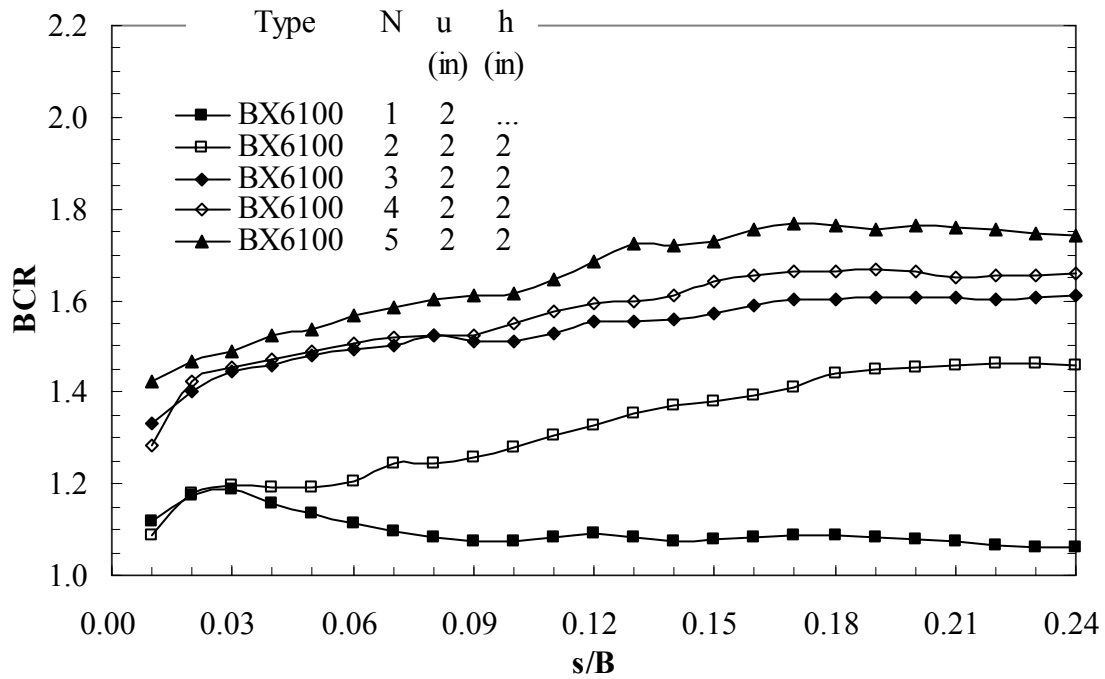
Figure 25
BCR versus settlement ratio (s/B)
(B × L: 6 in. × 6 in.)
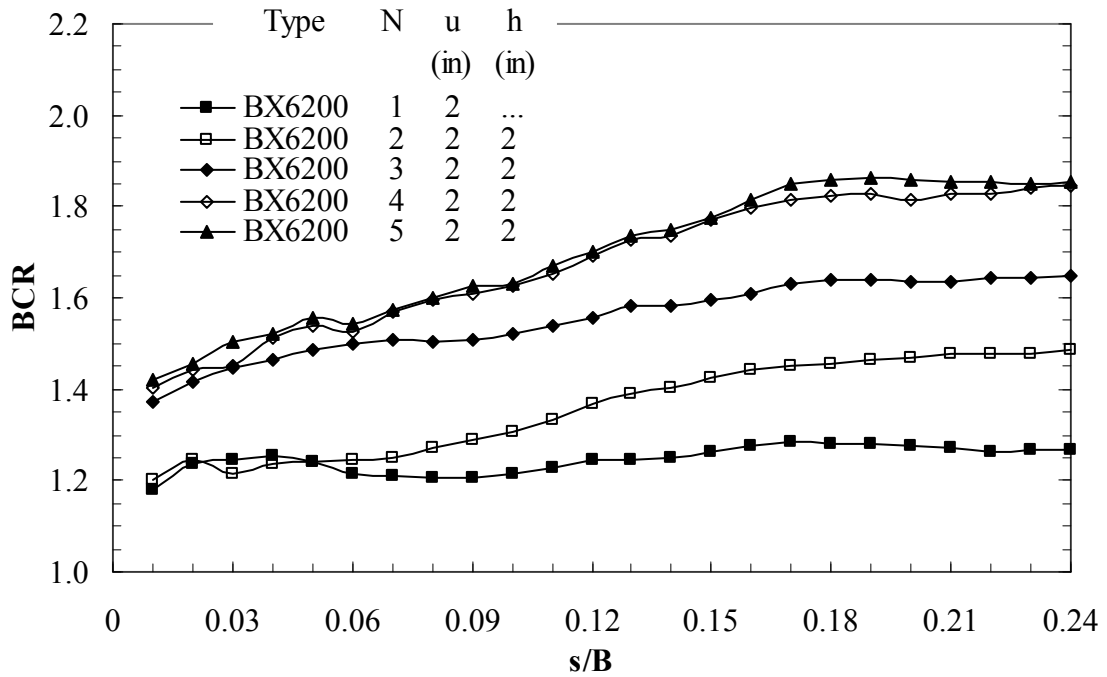
(c)
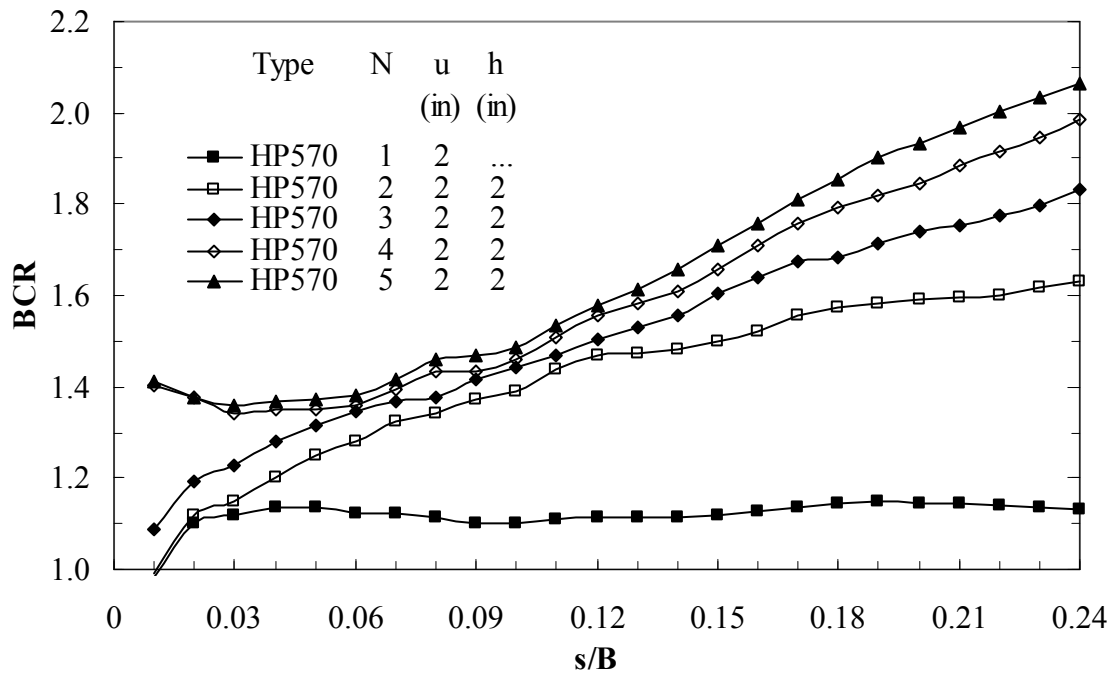
(d)

Figure 25
(continued)
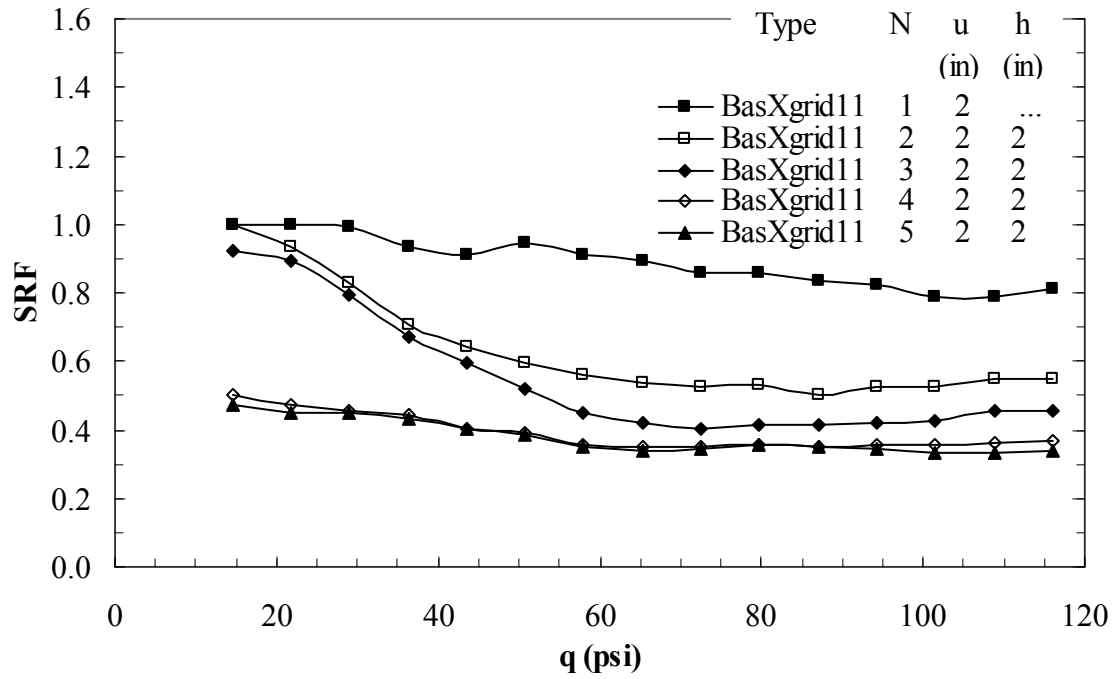
(a)
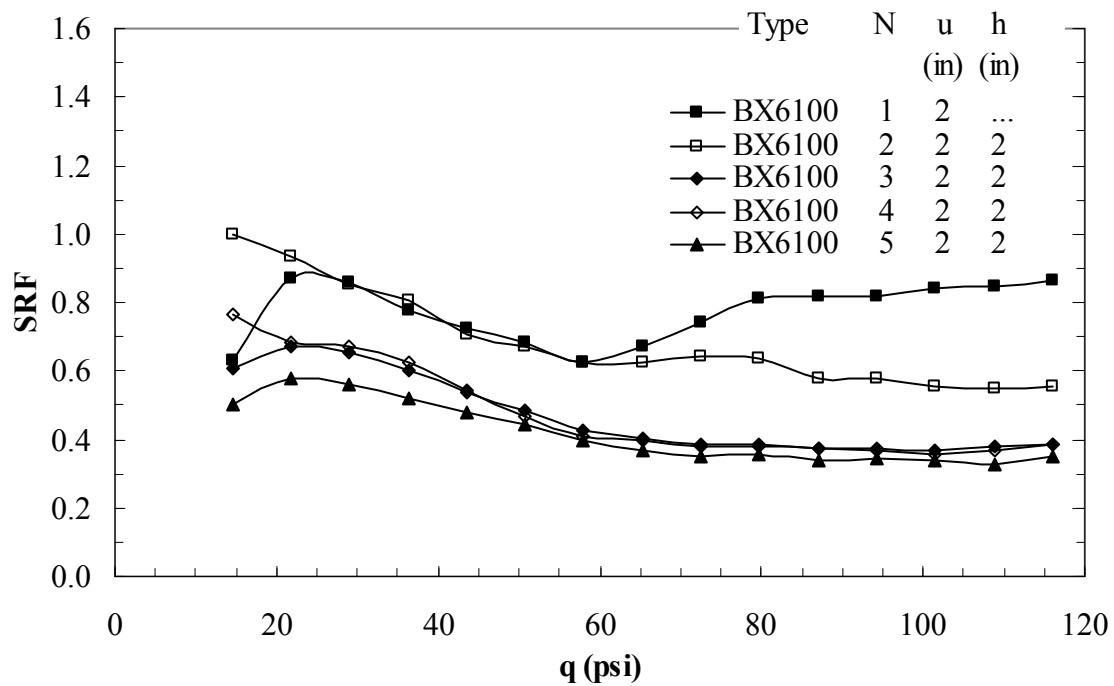
(b)

Figure 26
SRF versus applied footing pressure (q)
(B × L: 6 in. × 6 in.)
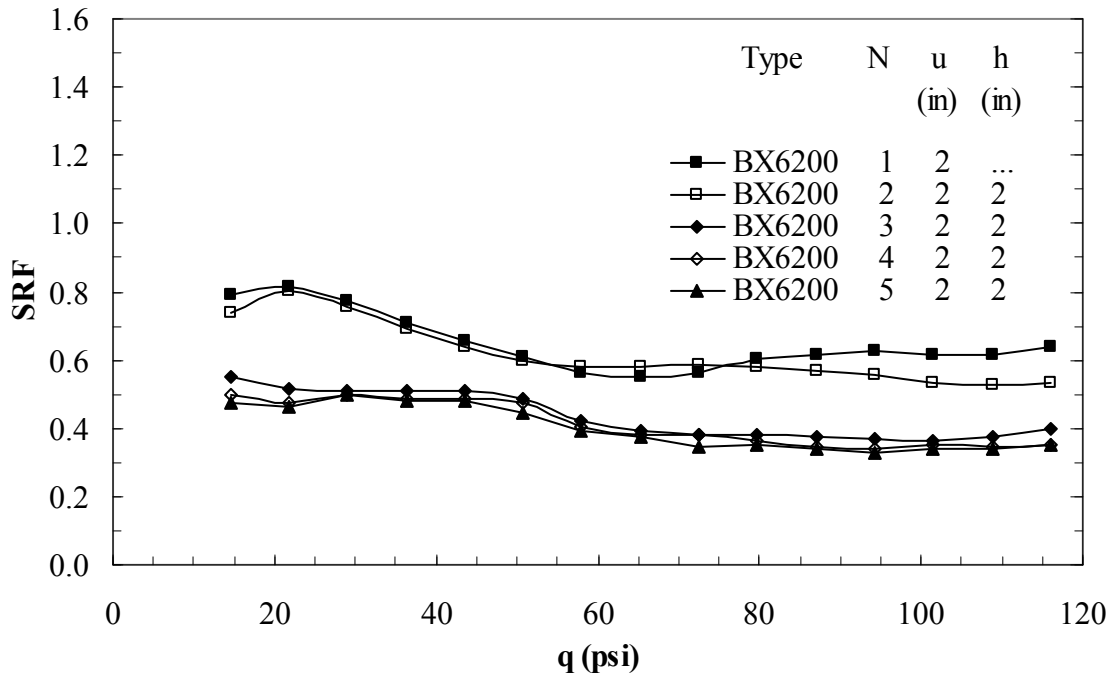
(c)
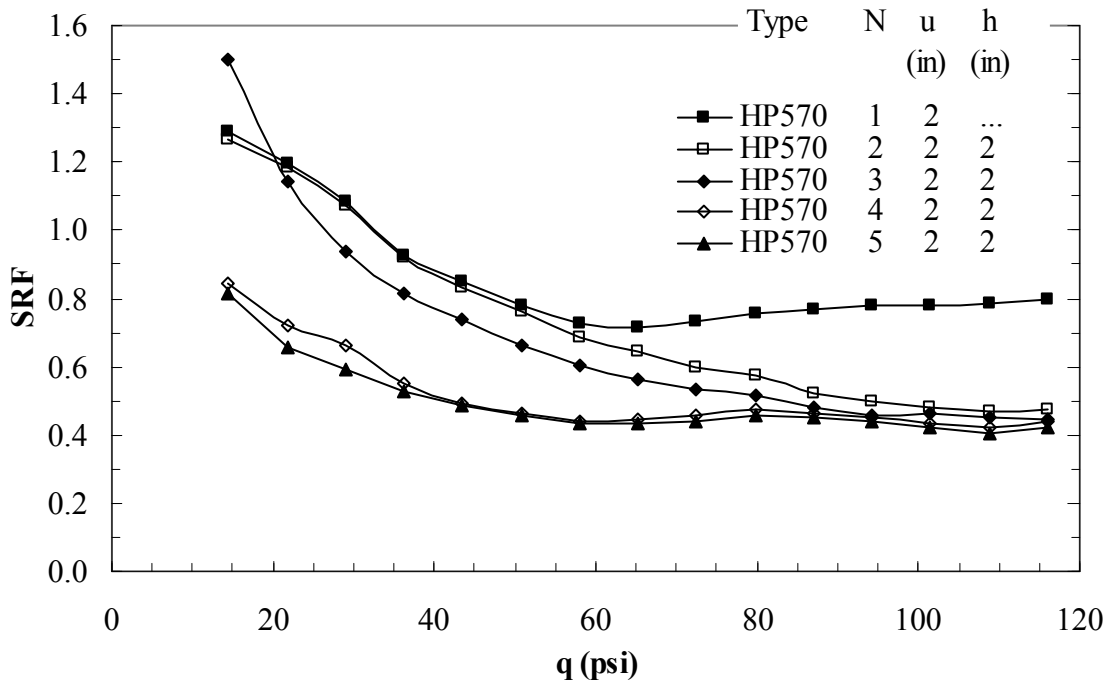
(d)

Figure 26
(continued)

For three layers of BX6200 geogrid at different vertical spacing, the stress at a depth of 6 in. (1.0 B) can be reduced up to 49% and up to 19% at a surface pressure of 6.8 psi and 67.9 psi (47 kPa and 468 kPa), respectively. For a 6 inch-wide square footing with five layers of different types of reinforcement, the reduction in stress at a depth of 10 in. (1.67B) ranges from 18% to 69% and from 18% to 36% at a surface pressure of 6.8 psi and 67.9 psi (47 kPa and 468 kPa), respectively. The reduction in stress at the same depth for a 6 in. × 10 in. rectangular footing varies from 5% to 35% and from 15% to 26% at a surface pressure of 4.1 psi and 61.2 psi (28 kPa and 422 kPa), respectively. For a 6 inch-wide square footing, due to the pressure cell next to the center of footing having a distance of 1.33B from the center of footing, this redistribution of load was not shown from the measurement data, but it is believed to exist. This point was confirmed in the field tests. The reduction in stress distribution at the center will result in reducing the consolidation settlement of silty clay which is directly related to the induced stress. Generally, for the same applied footing pressure, the vertical stresses under the center decrease with an increasing number of layers (figure 27) and decreasing vertical spacing of reinforcement layers (figures 28 and 31).

For geogrids with the same material and aperture size, the higher modulus geogrid (BX6200) results in more significant reduction of center stresses than the lower modulus geogrid (BX6100) does. BasXgrid11, which has the highest modulus and smallest aperture size among the three geogrids, provided the best attenuation of the stresses under the center of footing, while HP570 geotextile, which has higher modulus than all of three geogrids, showed better attenuation of the center stresses than geogrids. It appears that the improvement of stress distribution in reinforced silty clay is related to the modulus of reinforcement. It is also noted that the improved performance of reinforced soil is not always compatible with the improved stress distribution. As shown earlier, at relatively low footing pressure, geogrid reinforced silty clay performs better than geotextile reinforced silty clay, but the induced stresses under the center of the footing in geogrid reinforced silty clay are higher than those in geotextile reinforced silty clay, even at relative low footing pressure.

Interestingly, negative stresses (stresses less than the self weight of the soil) are measured in unreinforced silty clay at approximately 3.5B for a 6 inch-wide square footing and at 2.0L for 6 in. × 10 in. rectangular footing as measured from the center of footing. This result indicates that the soil is pushed upward at 3.5B (2.0L) from the center of footing. By contrast, the similar behavior is only observed in reinforced silty clay with three layers of reinforcement placed at a spacing of 3 in. and 4 in., but the values of measured negative stresses are much smaller than those in unreinforced silty clay. Apparently, the stresses at the same locations

for reinforced silty clay with appropriate reinforcement configuration are positive, which means an increase in vertical earth pressure. This increase in vertical earth pressure due to the inclusion of reinforcement can prevent soil from moving upward at locations far away from the footing, thus improving the bearing capacity of silty clay. This phenomenon is known as "surcharge effect," since this effect is equivalent to adding a surcharge load.

Figures 32 through 35 depict the variation of the stress influence factor (I) at a depth of 10 in. below the center of the footing with applied footing pressures. The stress influence factor (I) is defined here as the ratio of the induced stress at a certain location/depth in the soil to the footing pressure. As shown in the figures, under the same footing pressure, the stress influence factor (I) decreases with the increase of the number of reinforcement layers. For example, under the footing pressure of 135.9 psi (937 kPa), the stress influence factor in BX6200 geogrid reinforced silty clay with a 6 inch-wide square footing is reduced from 0.36 to 0.32 as the number of reinforcement layers increases from three to five. However, the decrease is not significant for BX6200 geogrid reinforced silty clay between four and five layers of reinforcement. In general, the stress influence factor (I), as shown in figure 33, increases with the increase in the vertical spacing of reinforcement layers. Figures 32 through 35 show that the stress influence factors (I) increase with the increase of the footing pressures; therefore the stress influence factor (I) appears to be a load-dependent value instead of a constant value as indicated by the elastic solutions such as the Boussinesq solution.

Strain Distribution Along Reinforcement
Two laboratory model tests were conducted to evaluate the strain distribution along the reinforcements. One model test was for square footing with dimensions of 6 in. × 6 in. (B×L), while the other model test was for rectangular footing with dimensions of 6 in. × 10 in. (B×L). Four layers of BX6100 geogrid placed at a spacing of 2 in. apart were used in both tests. The geogrids with instrumentation were placed at the top and bottom layers (at depths of 2 in. and 8 in., respectively). The distributions of strains along the centerline of the BX6100 geogrid measured at different settlement ratios (s/B) are presented in figures 36 through 38. The maximum tensile strain was measured at the point beneath the center of the footing and becomes almost negligible at about 2.5~3.0B from the center of footing. This indicates that the geogrid beyond the effective length (5.0 ~ 6.0B) results in insignificant mobilized tensile strength, and thus provides negligible effects on the improved performance of reinforced silty clayey soil foundation.

It is interesting to mention here that compressive strains were measured in the geogrid beyond 1.0~2.0B (L) from the center of footing. This means that the geogrid past this length cannot restrain lateral soil shear flow and works as an anchorage unit to prevent geogrid from failing by pull out.
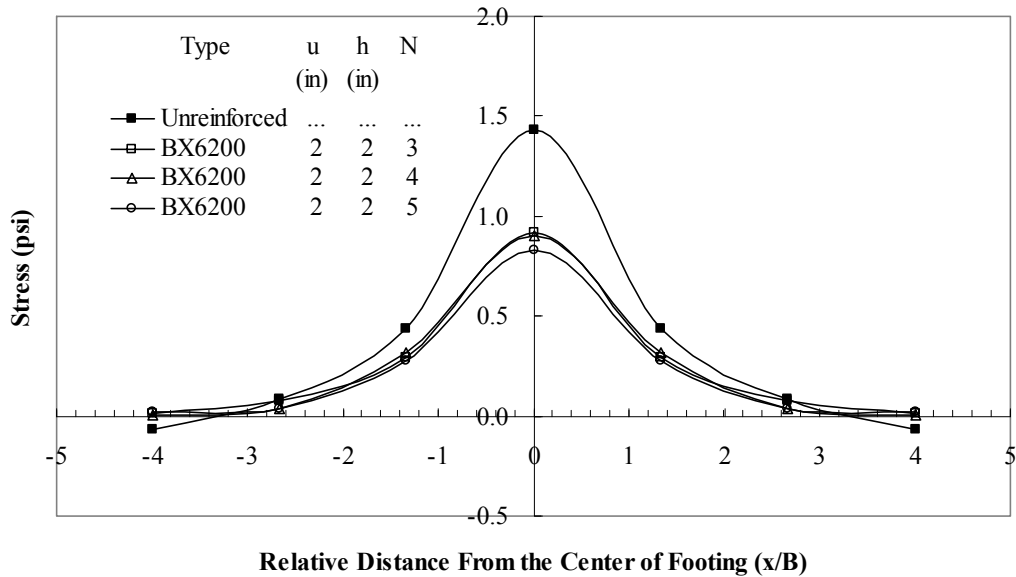
(a) Applied footing pressure q=6.8 psi
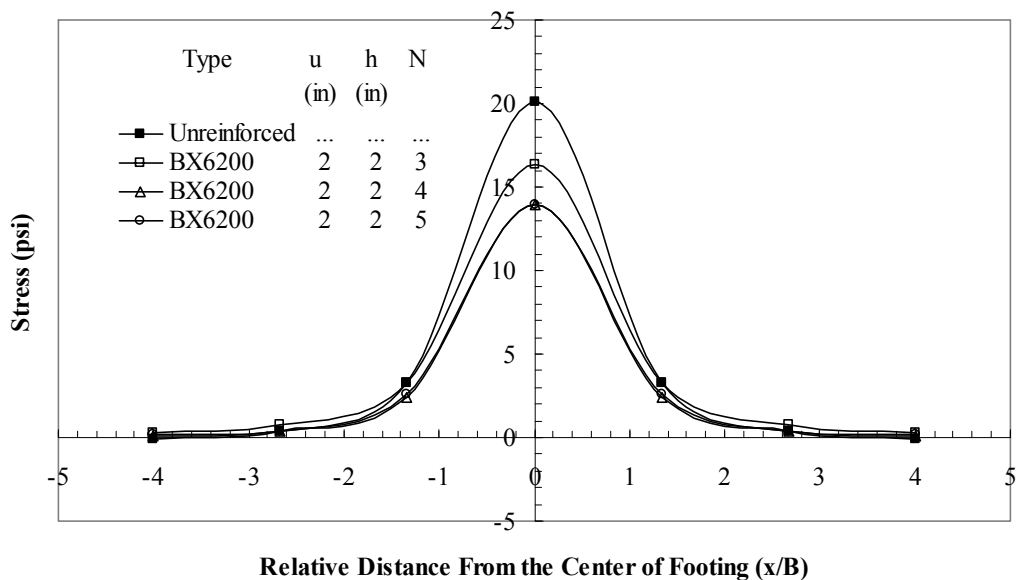
(b) Applied footing pressure q=67.9 psi

Figure 27
Vertical stress distribution along the center line of footing at a depth of 10 in. for multilayer of BX6200 geogrid reinforced section (B × L: 6 in. × 6 in.)
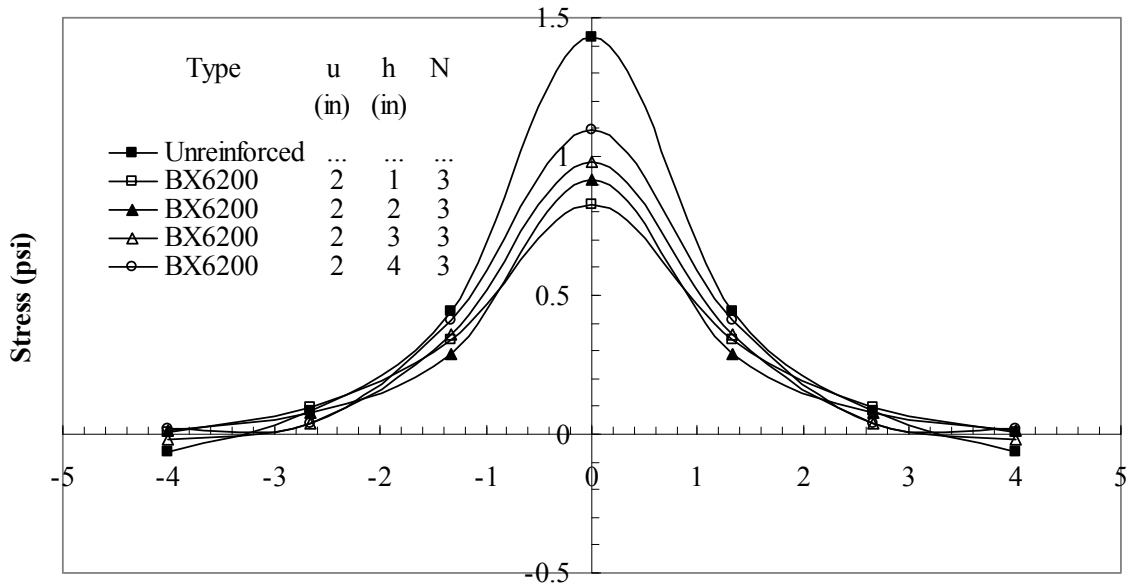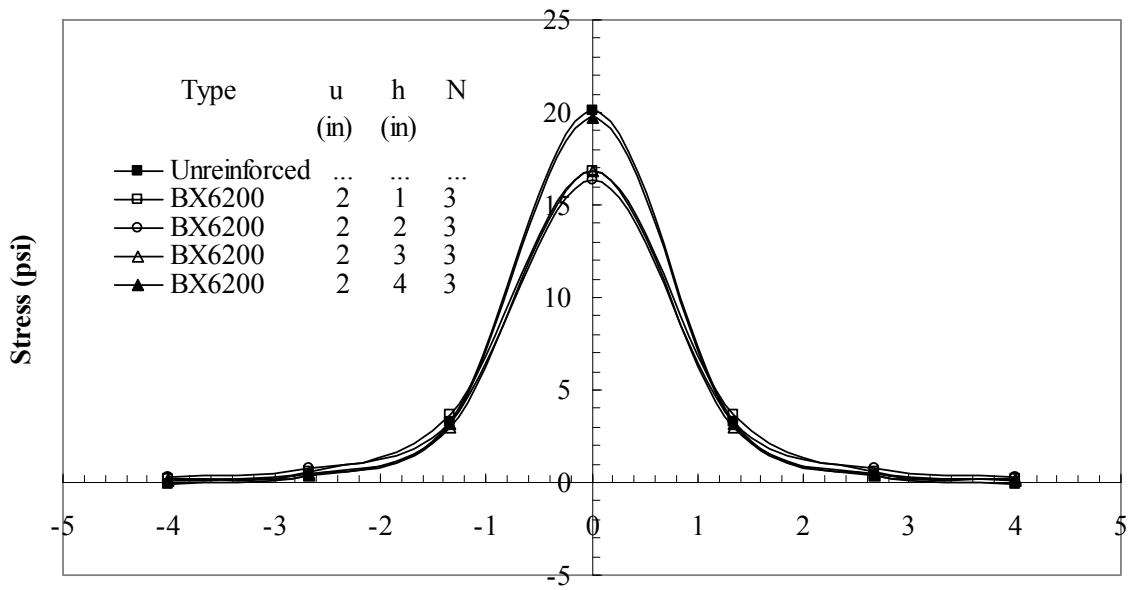
(a) Applied footing pressure q=6.8 psi

(b) Applied footing pressure q=67.9 psi

Figure 28
Vertical stress distribution along the center line of footing at a depth of 10 in. for three layers of BX6200 geogrid at different vertical spacing (B × L: 6 in. × 6 in.)
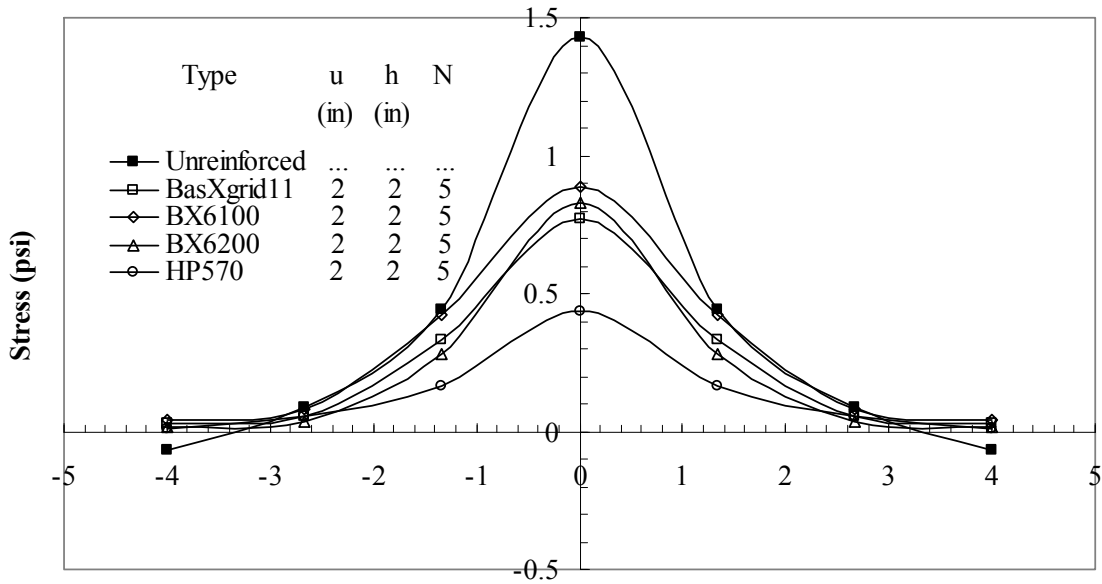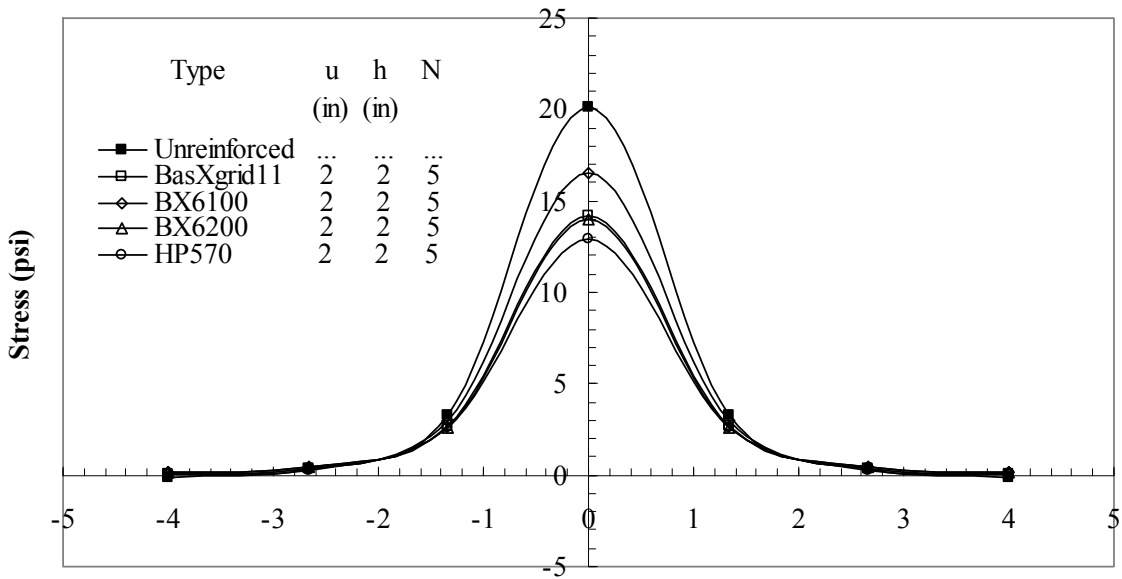
(a) Applied footing pressure q=6.8 psi

(b) Applied footing pressure q=67.9 psi

Figure 29
Vertical stress distribution along the center line of footing at a depth of 10 in. for five layers of different types of reinforcement (B × L: 6 in. × 6 in.)
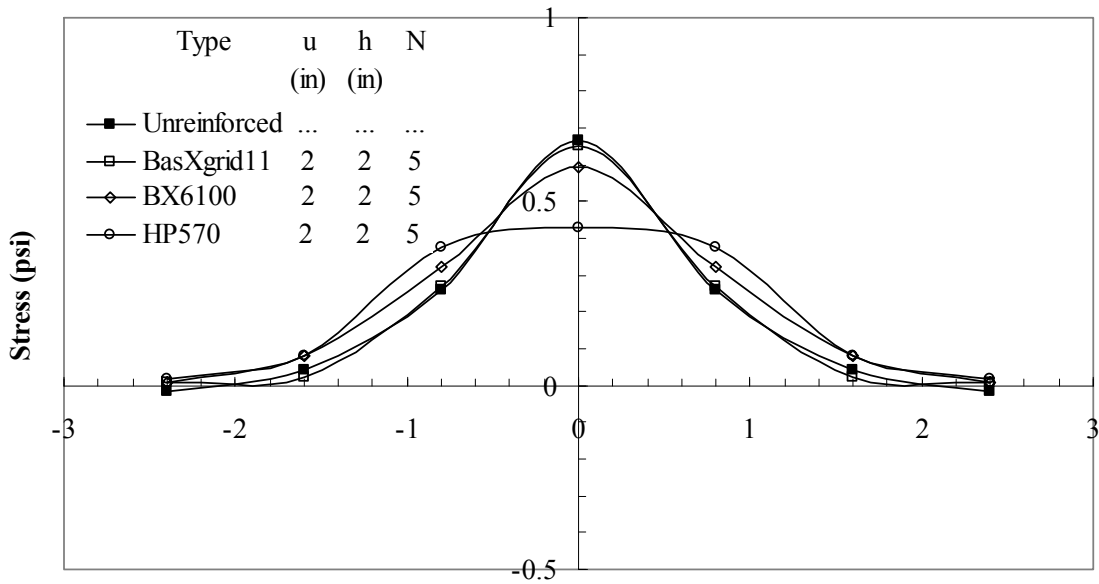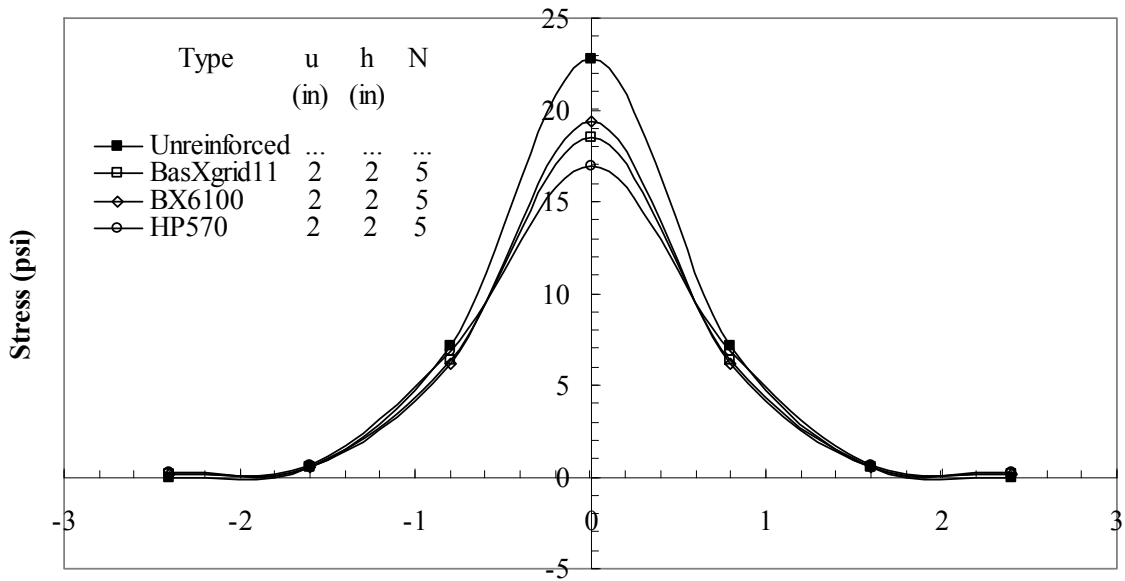
(a) Applied footing pressure q=4.1 psi

(b) Applied footing pressure q=61.2 psi

Figure 30
Vertical stress distribution along the center line of footing at a depth of 10 in. for five layers of different types of reinforcement (B × L: 6 in. × 10 in.)
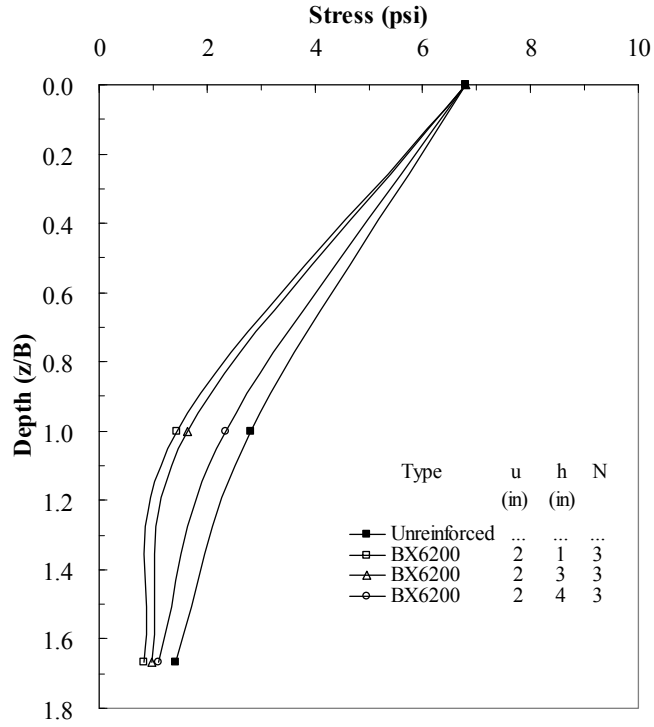
(a) Applied footing pressure q=6.8 psi
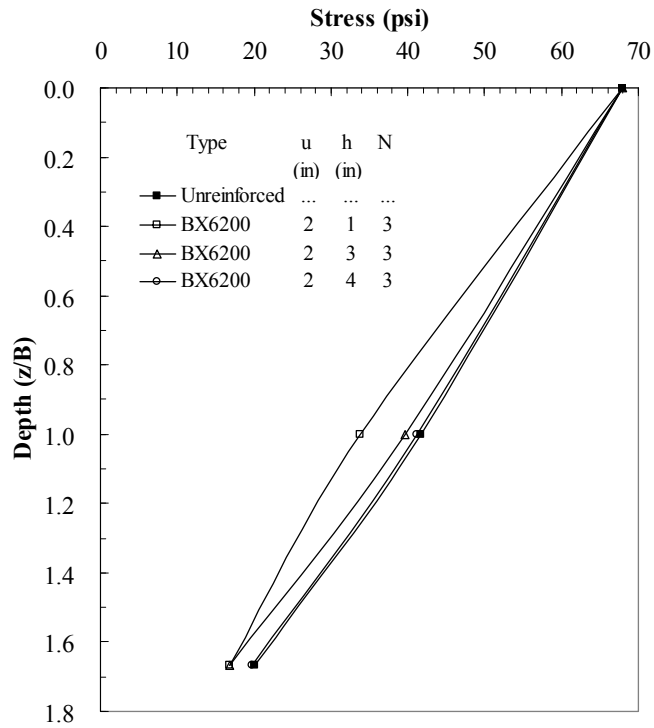
(b) Applied footing pressure q=67.9 psi

Figure 31
Profiles of vertical stress with the depth below the center of footing
(B × L: 6 in. × 6 in.)
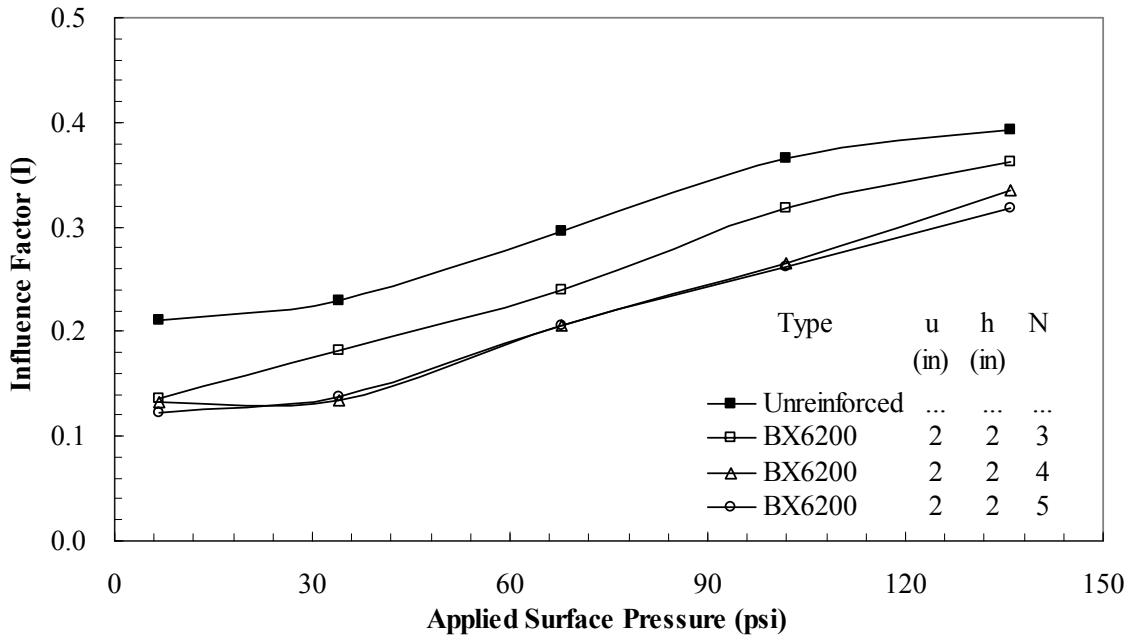
Figure 32
Stress influence factor (I) at a depth of 10 in. (1.67B) below the center of footing versus applied footing pressure for multilayer of BX6200 geogrid
(B × L: 6 in. × 6 in.)
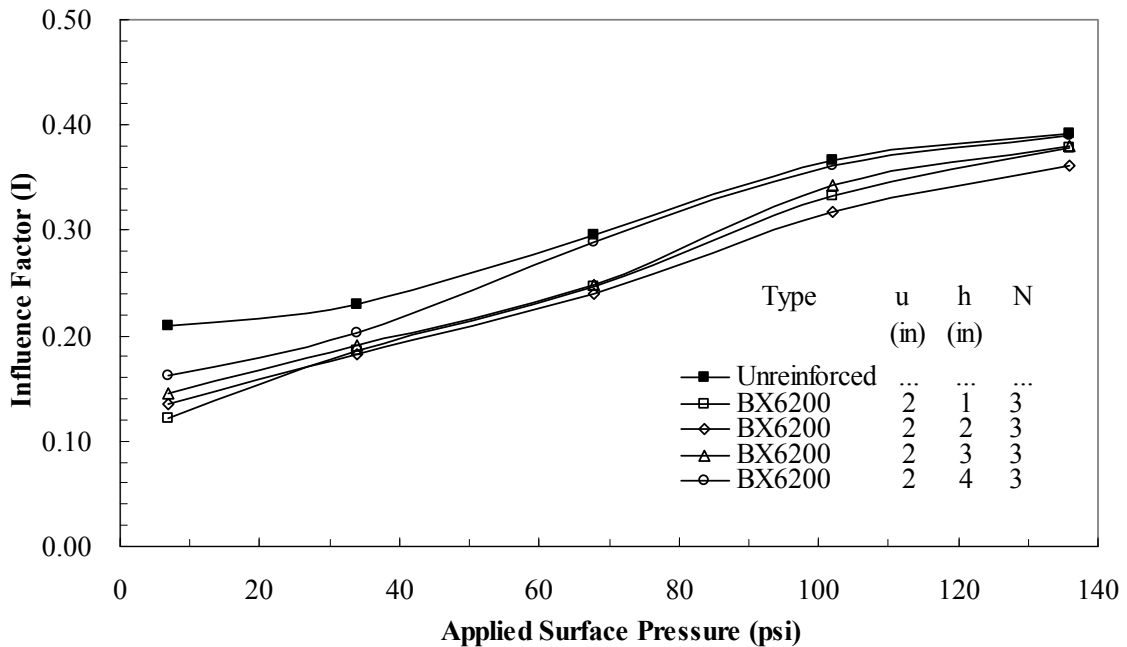
Figure 33
Stress influence factor (I) at a depth of 10 in. (1.67B) below the center of footing versus applied footing pressure for three layers of BX6200 geogrid at different vertical spacing
(B × L: 6 in. × 6 in.)
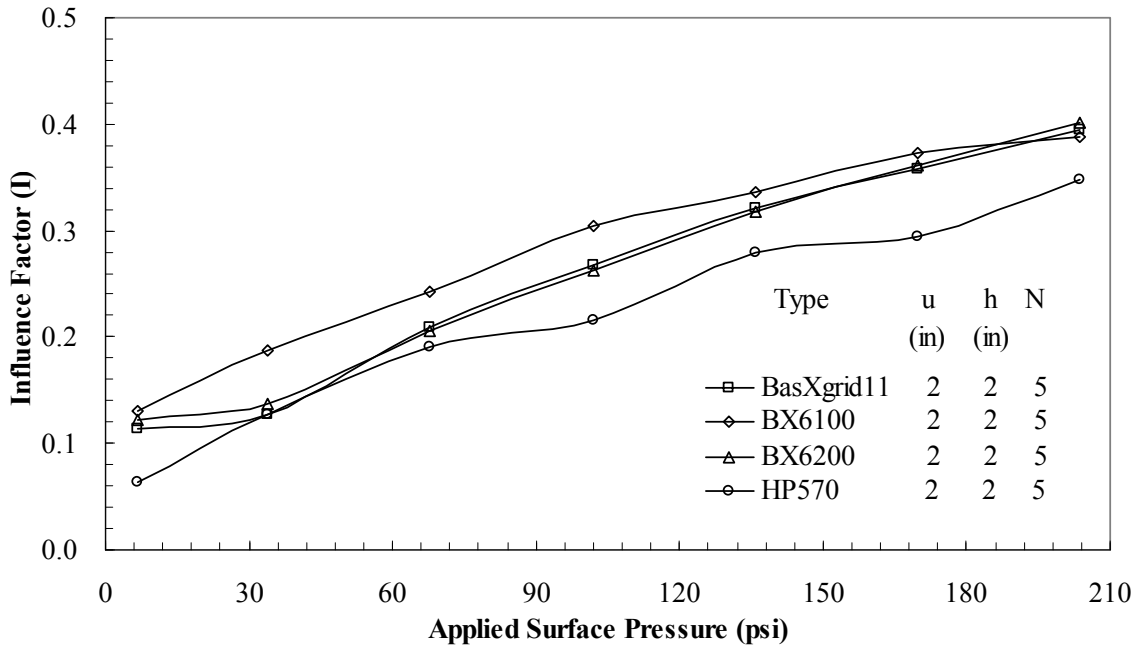
Figure 34
Stress influence factor (I) at a depth of 10 in. (1.67B) below the center of footing versus applied footing pressure for five layers of different types of reinforcement
(B × L: 6 in. × 6 in.)
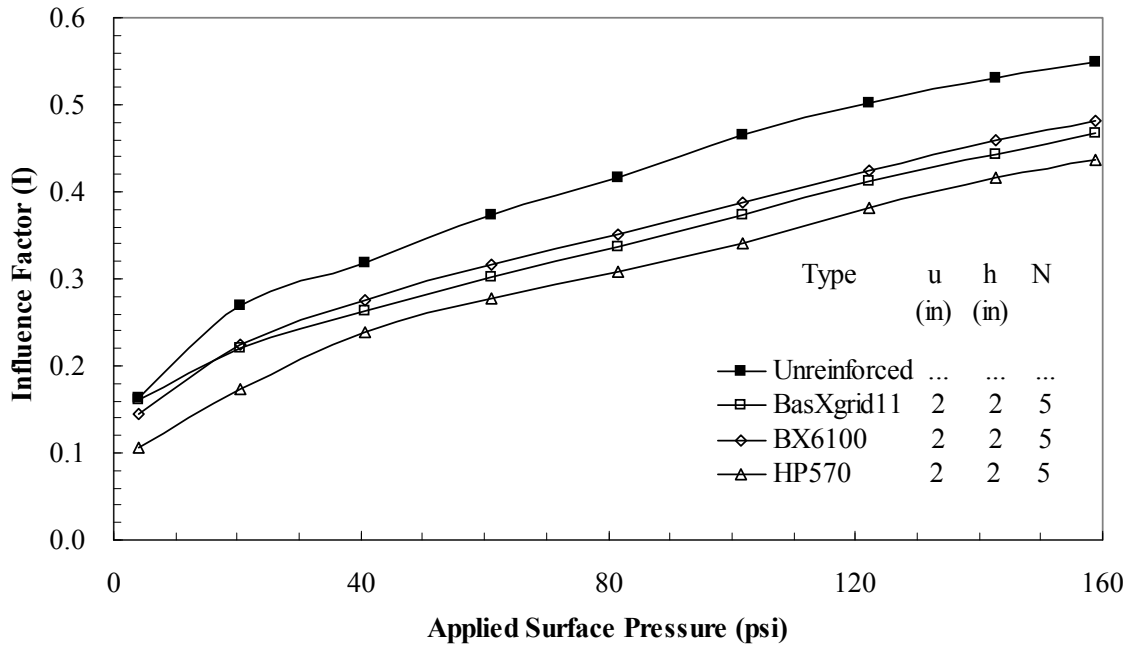
Figure 35
Stress influence factor (I) at a depth of 10 in. (1.67B) below the center of footing versus applied footing pressure for five layers of different types of reinforcement
(B × L: 6 in. × 10 in.)
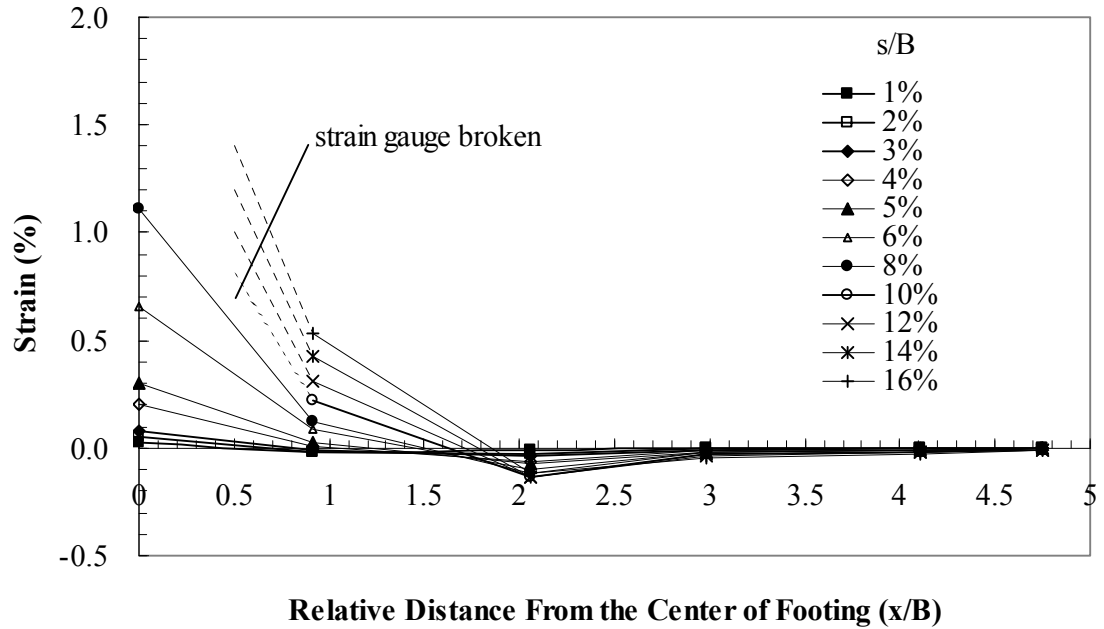
(a) at a depth of 2 in.
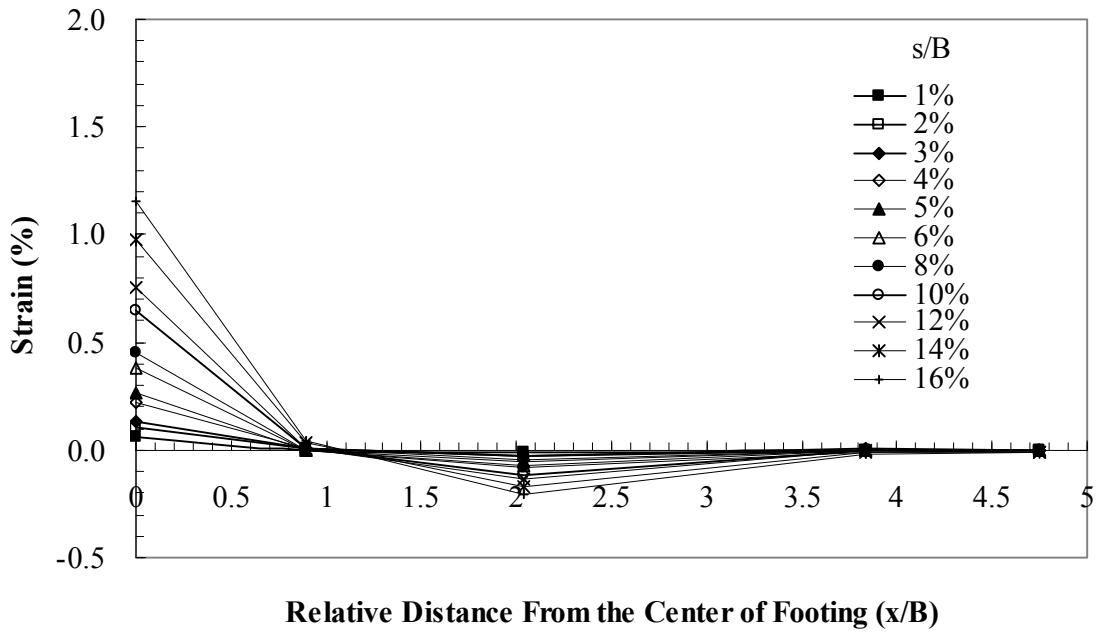
(b) at a depth of 8 in.

Figure 36
Strain distribution along the center line of BX6100 geogrid
(B × L: 6 in. × 6 in.)
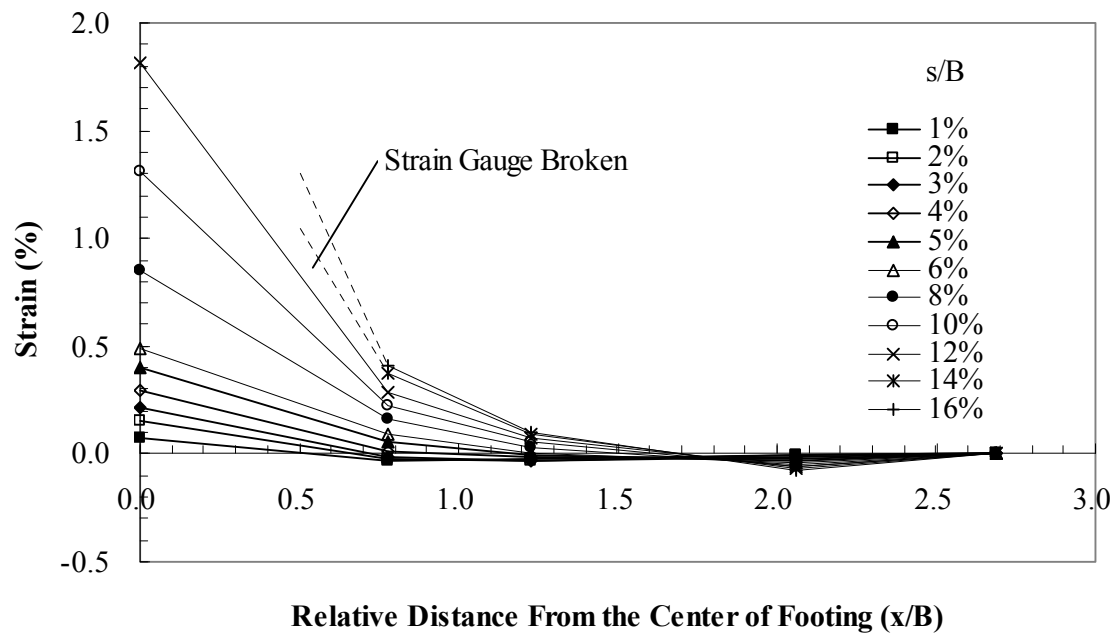
(a) at a depth of 2 in.
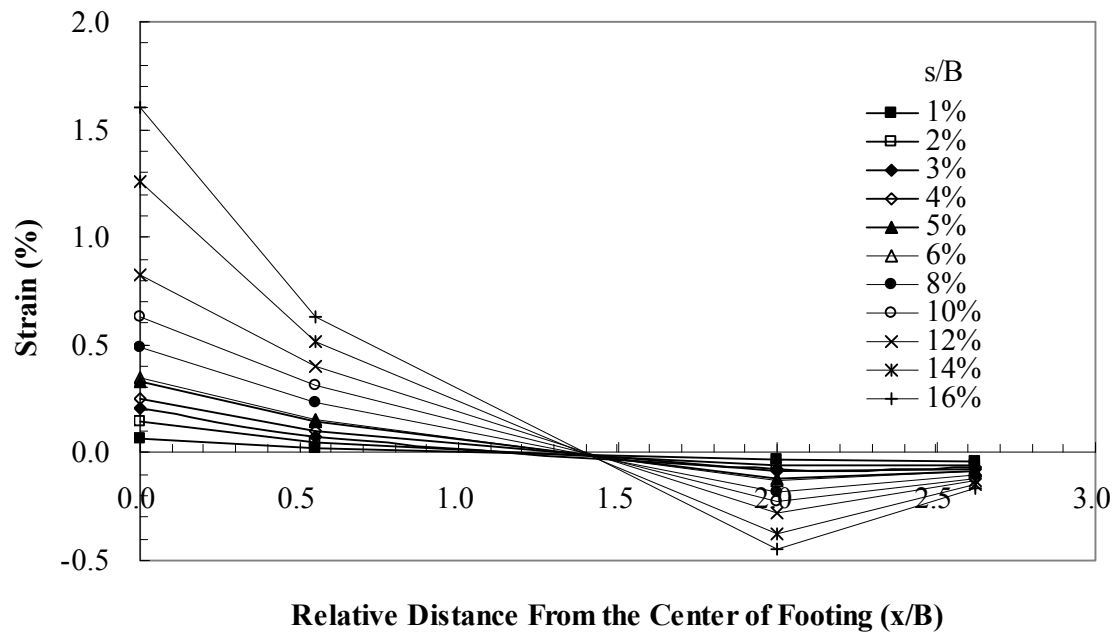
(b) at a depth of 8 in.

Figure 37
Strain distribution along the center line of BX6100 geogrid in the width direction of footing (B × L: 6 in. × 10 in.)

54
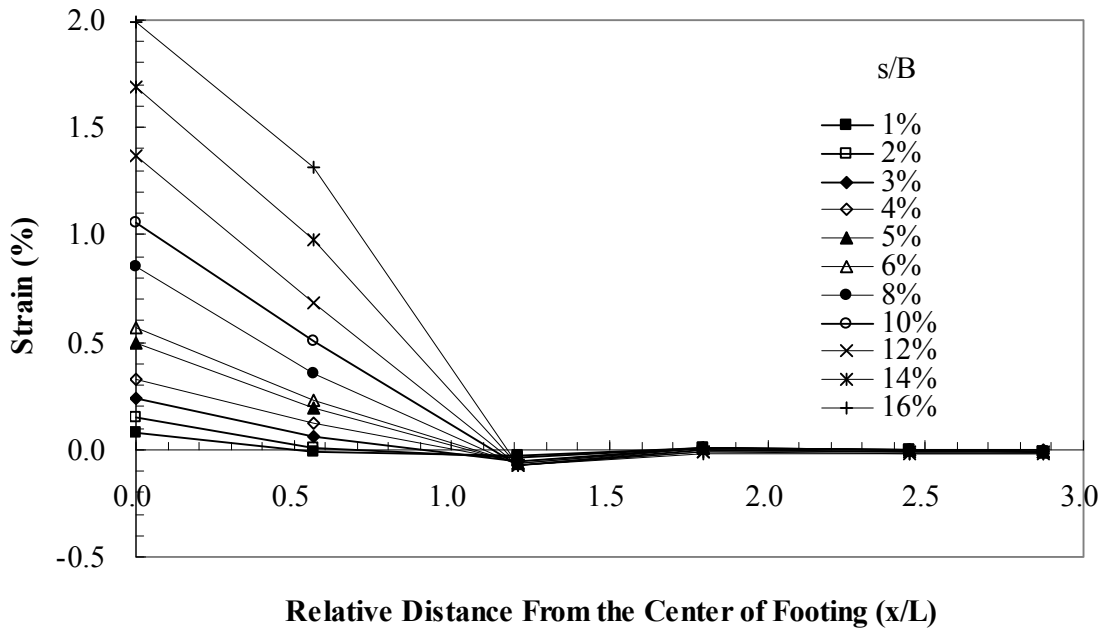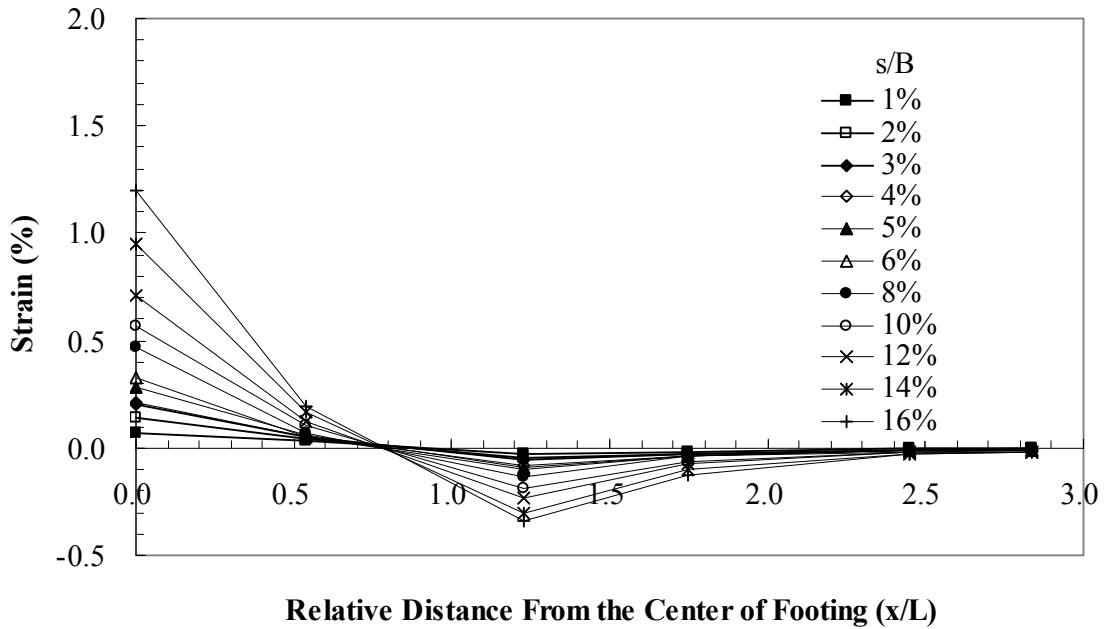
(a) at a depth of 2 in.

(b) at a depth of 8 in.

Figure 38
Strain distribution along the center line of BX6100 geogrid in the length
direction of footing (B × L: 6 in. × 10 in.)

Small-Scale Laboratory Tests on Reinforced Sand

The main objective of this study was to investigate the potential benefits of using the RSFs to improve the bearing capacity and reduce the settlement of shallow foundations on sand. For this purpose, extensive laboratory model tests were conducted on geosynthetic reinforced sandy soils. Due to the fact that, in engineering practices, footings are usually built at a certain embedment depth, most of tests in this research study were conducted on footings with embedment. The parameters investigated in the model tests included: the top layer spacing (u), the number of reinforcement layers (N), the vertical spacing between reinforcement layers (h), the tensile modulus and type of reinforcement, embedment depth (D_f), and shape of footing. The experimental study also includes investigating the stress distribution in sand and the strain distribution along the reinforcement.

Three types of geogrids were used as reinforcement in the tests, BasXgrid11, Miragrid 8XT and BX6100 and one type of geotextile, HP570. A composite, which is a combination of BX6100 geogrid and HP570 geotextile (i.e., HP570 geotextile is placed directly on the top of BX6100 geogrid to form a new reinforcement), was also used in the present study. The physical and mechanical properties of these geosynthetics, as provided by the manufacturers, were presented earlier in table 2.

The measured dry densities for sand test sections with and without reinforcement inclusion varied from 106 to 110 lb/ft^3 (1,690 to 1,763 kg/m^3), with the moisture contents ranging from 4.5 to 5%. The corresponding geogauge stiffness moduli were in the range of 7,252 to 8,702 psi (50 to 60 MPa).

The results of the laboratory model tests conducted, using a 6 in. × 6 in. model footing for no embedment depth are summarized in table 5. Table 6 and table 7 present the results of laboratory model tests conducted at an embedment depth ratio (D_f/B) of 1.0 for square and rectangular footings with dimensions of 6 in. × 6 in. and 6 in. × 10 in., respectively. These tables present the bearing capacity ratios (BCRs) obtained at the ultimate capacity, at a settlement ratio (s/B) = 3%, and at the residual. The results of the model footing tests are also graphically shown in figures 39 through 40 and figures C.1 through C.10 in Appendix C. Figures 39 and C.1 through C.6 present the pressure-settlement curves for 6 in. × 6 in. square footing at a footing embedment depth equal to 6 in. (D_f = 1.0B). Figures 40 and C.7 through C.9 present the pressure-settlement curves for 6 in. × 6 in. footing placed on surface (no embedment). Figure C.10 depicts the pressure-settlement curves obtained for model

footing tests with four layers of different reinforcement for 6 in. $\times$ 10 in. rectangular footing at a footing embedment depth equal to 6 in. (D_f = 1.0B).

It can be seen from these figures that the magnitude of settlement ratio (s/B) at ultimate bearing capacity is about 7-10% for embedded footing and 4-7% for surface footing on both unreinforced and reinforced sands. It is clear that, although the inclusion of geogrid/geotextile reinforcement can increase the ultimate bearing capacity of sand, the effect of reinforcement on footing settlement at ultimate load is minimal.

Effect of Reinforcement's Top Spacing

The optimum location (top layer spacing) of the first reinforcement layer for sand was investigated for both confined (embedded footing) and unconfined (surface footing) conditions.

Table 5
Summary of model tests for sand with 6 in. × 6 in. square footing on surface

Test No.	Reinforcement configuration	u in.	h in.	Ultimate		@ s/B = 3%		Residual @ s/B = 12%	
				q_u, psi	BCR	q_s, psi	BCR	q_r, psi	BCR
SNR[*]	Unreinforced	...	...	135.9	...	99.8	...	51.5	...
SGG11-1	N=1, BasXgrid11	1	...	200.4	1.47	129.2	1.30	137.6	2.67
SGG11-2		2	...	166.5	1.23	132.5	1.33	138.8	2.70
SGG11-3		3	...	163.0	1.20	115.3	1.16	54.4	1.06
SGG11-4		4	...	156.2	1.15	109.9	1.10	48.3	0.94
SGG11-5		6	...	137.6	1.01	103.4	1.04	44.1	0.86
SGG31-1	N=1 2xMiragrid 8XT each layer	1.2	...	183.4	1.35	135.7	1.36	129.2	2.51
SGG31-2		1.8	...	176.6	1.30	138.6	1.39	127.9	2.49
SGG31-3		2.4	...	157.9	1.16	131.5	1.32	...	...
SGG31-4		3	...	163.0	1.20	120.1	1.20	97.0	1.89
SGG12[*]	N=2, BasXgrid11	2	2	179.9	1.32	149.6	1.50	141.8	2.76
SGG13[*]	N=3, BasXgrid11	2	2	193.6	1.42	156.6	1.57	143.7	2.79
SGG14[*]	N=4, BasXgrid11	2	2	193.6	1.42	162.4	1.63	152.0	2.95
SGT12[*]	N=2, HP570	2	2	163.1	1.20	107.6	1.08	184.7	3.59
SGT13[*]	N=3, HP570	2	2	183.4	1.35	138.5	1.39	192.4	3.74
SGT14[*]	N=4, HP570	2	2	183.4	1.35	144.3	1.45	198.8	3.86

* Instrumented with pressure cell

Table 6
Summary of model tests for sand with 6 in. × 6 in. square footing at an embedment depth of 6 in.

Test No.	Reinforcement configuration	u in.	h in.	Ultimate		@ s/B = 3%		Residual @ s/B = 12%	
				q_u, psi	BCR	q_s, psi	BCR	q_r, psi	BCR
SDNR[*]	Unreinforced	…	…	527.7	…	377.6	…	362.8	…
SDGG11-0		0	…	562.3	1.07	361.6	0.96	540.6	1.49
SDGG11-1		1	…	617.8	1.17	394.1	1.04	568.4	1.57
SDGG11-2		2	…	666.4	1.26	411.9	1.09	502.9	1.39
SDGG11-3	N=1,BasXgrid11	3	…	666.4	1.26	395.1	1.05	411.4	1.13
SDGG11-4		4	…	638.7	1.21	399.6	1.06	348.9	0.96
SDGG11-5		6	…	638.7	1.21	396.6	1.05	382.5	1.05
SDGG11-6		8	…	583.2	1.11	370.2	0.98	384.5	1.06
SDGG31-0		0	…	562.3	1.07	382.8	1.01	542.7	1.50
SDGG31-1	N=1	1	…	583.2	1.11	396.3	1.05	539.1	1.49
SDGG31-2	2xMiragrid 8XT	2	…	652.6	1.24	407.7	1.08	626.4	1.73
SDGG31-3	each layer	3	…	624.8	1.18	396.7	1.05	587.5	1.62
SDGG31-4		4	…	597.1	1.13	384.0	1.02	300.7	0.83
SDGG12	N=2,BasXgrid11	2	2	749.8	1.42	477.9	1.27	584.5	1.61
SDGG13-1	N=3,BasXgrid11	2	1	805.3	1.53	473.4	1.25	779.8	2.15
SDGG13-2	N=3,BasXgrid11	2	2	777.5	1.47	488.2	1.29	613.4	1.69
SDGG13-3	N=3,BasXgrid11	2	3	744.3	1.41	449.5	1.19	595.8	1.64
SDGG14[*]	N=4,BasXgrid11	2	2	791.4	1.50	492.0	1.30	668.2	1.84
SDGG21	N=1,BX6100	2	…	708.2	1.34	434.6	1.15	618.3	1.70
SDGG22[*]	N=2,BX6100	2	2	749.8	1.42	483.3	1.28	553.0	1.52
SDGG23[*]	N=3,BX6100	2	2	777.5	1.47	483.6	1.28	584.4	1.61
SDGG24[*#]	N=4,BX6100	2	2	777.5	1.47	491.4	1.30	639.7	1.76
SDGT11	N=1,HP570	2	…	708.2	1.34	435.7	1.15	676.3	1.86
SDGT12[*]	N=2,HP570	2	2	749.8	1.42	405.1	1.07	735.9	2.03
SDGT13[*]	N=3,HP570	2	2	791.4	1.50	409.0	1.08	749.8	2.07
SDGT14[*]	N=4,HP570	2	2	805.3	1.53	413.1	1.09	777.5	2.14
SDGGT11	N=1,Composite	2	…	777.5	1.47	440.5	1.17	730.1	2.01
SDGGT12	N=2,Composite	2	2	833.0	1.58	503.4	1.33	859.7	2.37
SDGGT13	N=3,Composite	2	2	860.9	1.63	513.4	1.36	863.9	2.38
SDGGT14[*]	N=4,Composite	2	2	860.9	1.63	515.2	1.36	871.9	2.40

* Instrumented with pressure cell   # Instrumented with strain gauge

Table 7
Summary of model tests for sand with 6 in. × 10 in. rectangular footing at an embedment depth of 6 in.

Test No.	Reinforcement configuration	u in.	h in.	Ultimate		@ s/B = 3%		Residual @ s/B = 12%	
				q_u, psi	BCR	q_s, psi	BCR	q_r, psi	BCR
SDFNR[*]	Unreinforced	...	...	516.5	...	326.7	...	342.2	...
SDFGG14[*]	N=4,BasXgrid11	2	2	683.1	1.32	387.6	1.19	573.2	1.67
SDFGG24[*]	N=4, BX6100	2	2	666.4	1.29	398.8	1.22	457.0	1.34
SDFGT14[*]	N=4, HP570	2	2	683.1	1.32	345.7	1.06	663.7	1.94
SDFGGT14[*]	N=4, Composite	2	2	783.1	1.52	414.0	1.27	763.3	2.23

* Instrumented with pressure cell

For footing embedment depth equal to 6 in., figures 41a and 41b show that the BCR at a 3% settlement ratio and the ultimate loads generally increase with increasing the top layer spacing ratio (u/B) up to a maximum value at u/B = 0.33 for both BasXgrid 11 and Miragrid 8XT geogrid, after which it decreases. The optimum location of the top layer is then estimated to be about 2 in., which is equivalent to 0.33B, and appears to be unrelated to the modulus of geogrid.
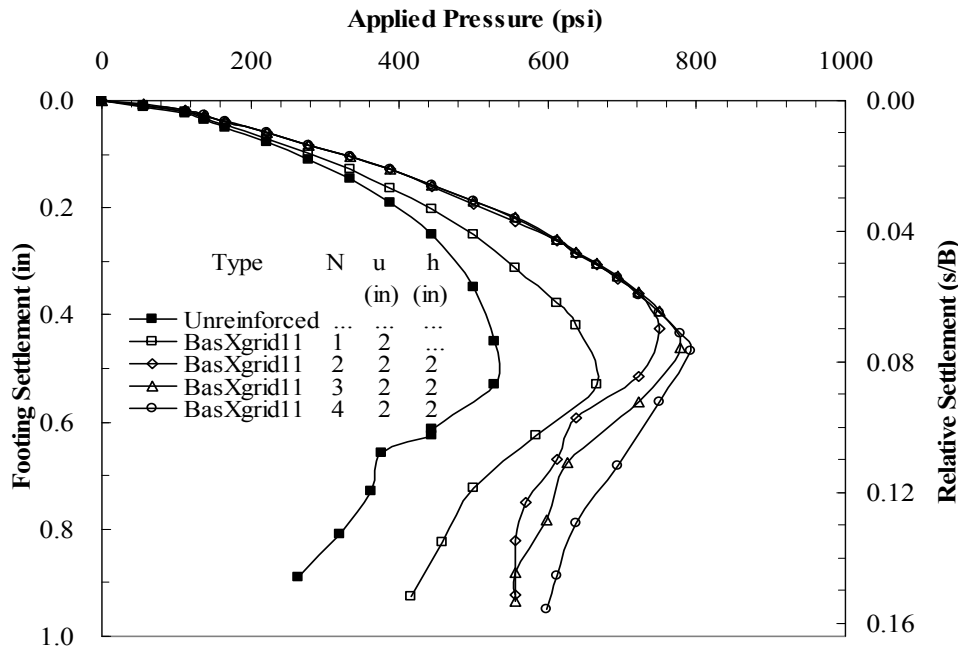
Figure 39
Pressure-settlement curves for model footing tests with different number of layers of BasXgrid11 geogrid (B × L: 6 in. × l6 in.; D_f / B: 1.0)
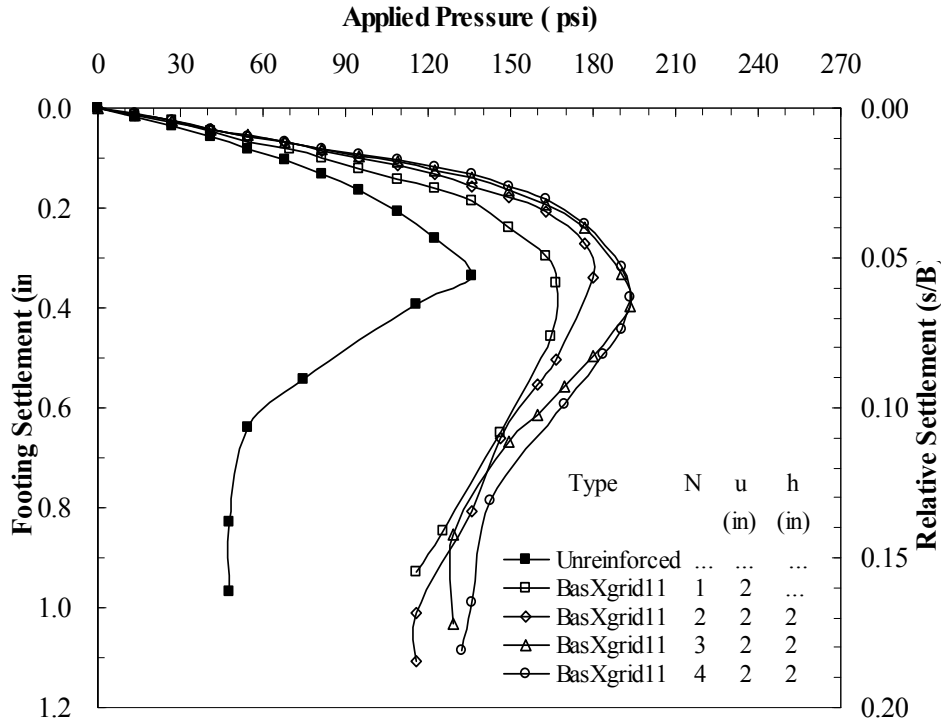
Figure 40
Pressure-settlement curves for model footing tests with different number of layers of BasXgrid11 geogrid (B × L: 6 in. × 6 in.; D_f / B: 0.0)

For the surface footing condition, the variations of BCRs obtained at 3% settlement ratio and the ultimate loads for different top layer spacing (u) are shown in figures 42a and 42b. Figure 42a shows that the BCR values for BasXgrid 11 geogrid reinforced sand generally decrease with increasing top layer spacing. This behavior is different from that for the footing with 6 in. embedment, in which the BCR first increases to an optimum value and then decreases. The same phenomenon was also obtained for model tests with Miragrid 8XT geogrid reinforcement as can be seen in figure 42b. No clear optimum top layer spacing was obtained for geogrid reinforced sand for surface footing condition. However, the use of u/B value of 0.33 seems to be reasonable, based on the figures.

The results of laboratory model tests on sand with one layer of reinforcement show that there are two different types of failure modes for reinforced soil, as described below:

(1) When the top layer spacing is greater than 0.5B, the failure surface in the sands extends to the surface and the load decreases rapidly after failure. The settlement pattern for this kind of failure resembles typical general shear failure. For this kind of failure mode, it is believed that lateral soil shear flow happens above the

reinforcement. The visual inspection of the reinforcement after tests also confirms this point. The deformation of the reinforcement beneath the footing is not clear. This failure mode was first reported by Binquet and Lee [2]. In this model, the top layer of reinforcement acted as a rigid boundary.

(2) When the top layer spacing is less than 0.5B, the failure surface in the sands never extends to the surface of the sands, indicating a punching type of failure. Here the load decreases slowly after failure. For this kind of failure mode, it is believed that lateral soil shear flow crosses the reinforcement. The visual inspection of the reinforcement after the test shows that the deformation of the reinforcement beneath the footing is significant.

Effect of Number of Reinforcement Layers

A series of laboratory model footing tests were conducted on the sand reinforced with multiple layers of four different types of geosynthetics placed at a spacing of 2 in. for both surface footing and embedded footing conditions. Figures 39, 40, C.3 through C.5 and C.9 present the pressure-settlement curves of these model tests. As shown for model tests on reinforced silty clay soil, the similar phenomenon was also observed in reinforced sand soil. The bearing capacity increased with an increasing number of reinforcement layers. However, the significance of an additional reinforcement layer decreases with the increase in number of layers. This effect becomes negligible below the influence depth. The variations of BCRs obtained at settlement ratio of s/B=3% and the ultimate loads for different numbers of reinforcement layers (N) and reinforcement depth ratios (d/B) are shown in figures 43a through 43d for embedded footing and figures 44a through 44b for surface footing. It can be seen from these figures that the BCRs increase with N and d/B and appear to become almost constant after N=3, which are located at a depth of 1.0B for both surface and embedded footing for all types of reinforcement. Accordingly, the influence depth can be estimated to be 1.25B. This result suggests that the type and modulus of reinforcement within the examined range have minimal effect on the influence depth. The influence depth also seems to be independent of footing embedment depth.

Effect of Vertical Spacing of Reinforcement Layers

The effect of vertical spacing of reinforcement layers in sand was investigated using three layers of BasXgrid11 with a top layer spacing of 2 in. (0.33B) and vertical spacing varied from 0.167B to 0.5B. Figure 45 depicts the variation in the BCR values of the loads corresponding to settlement ratios s/B=3% and the ultimate loads as a function of the vertical spacing ratio (h/B). It is obvious that the BCR values decrease with increasing vertical
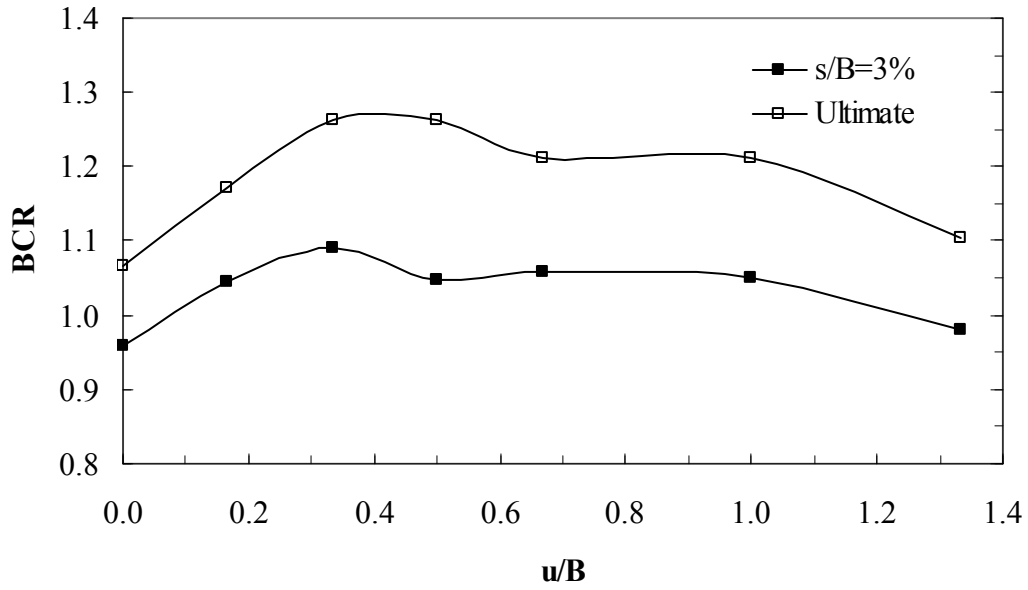
(a) BasXgrid11
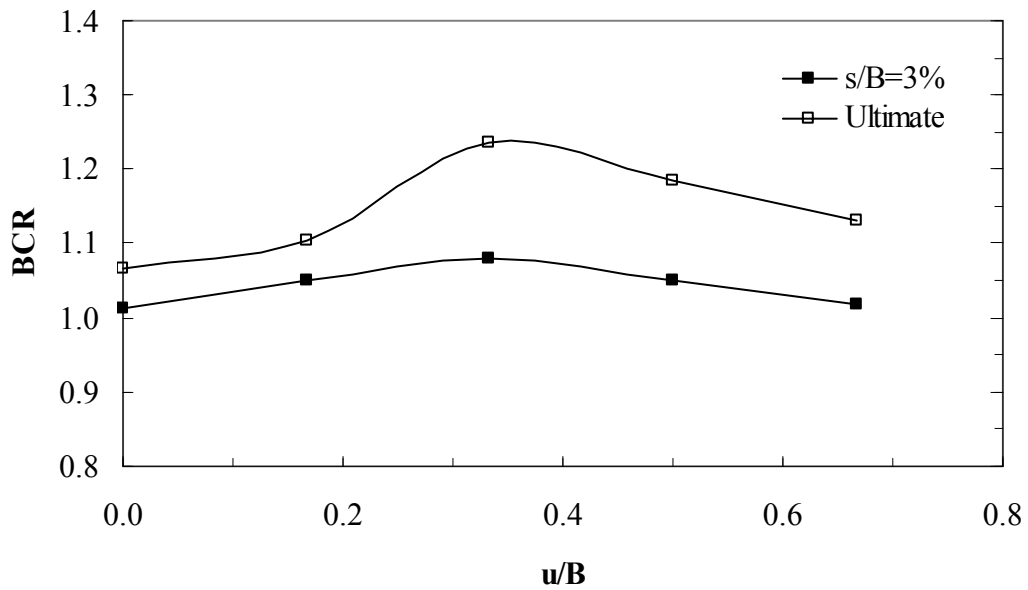
(b) Miragrid 8XT

Figure 41
BCR versus *u/B* for one layer of reinforcement
(B × L: 6 in. × 6 in.; *D_f /B* = 1.0)
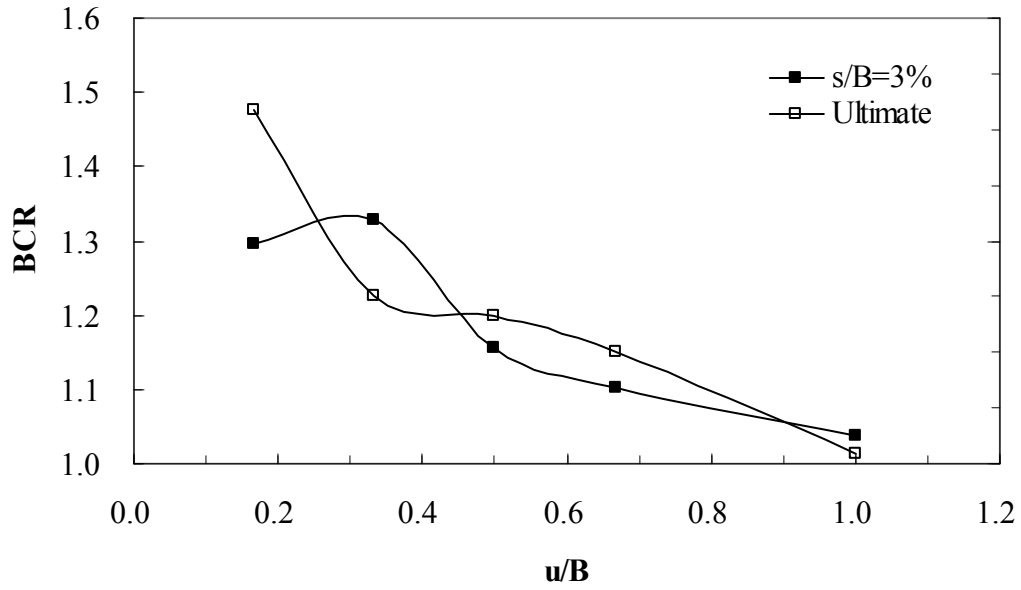
(a) BasXgrid11
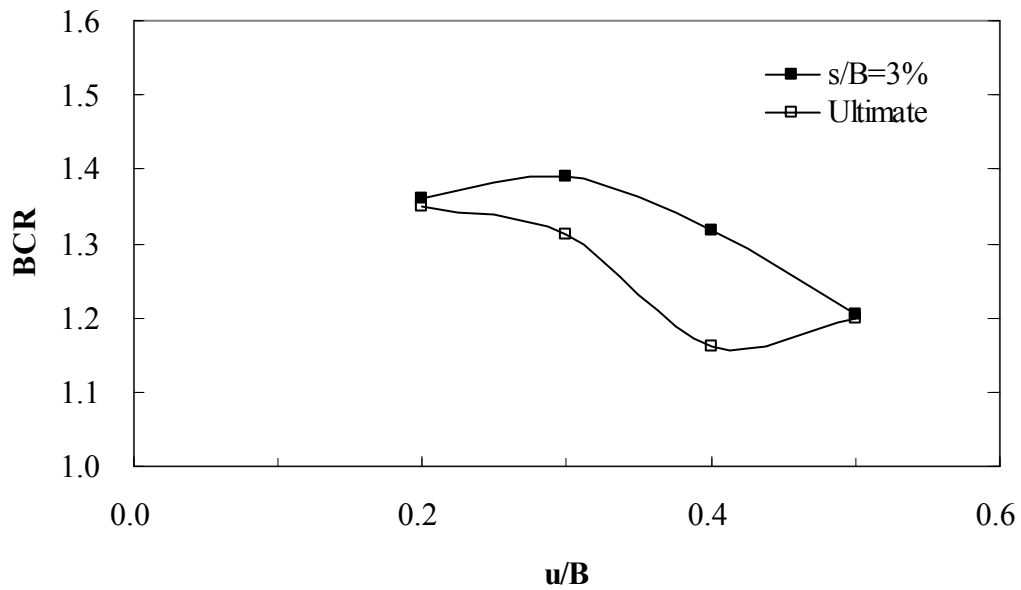
(b) Miragrid 8XT

Figure 42
BCR versus *u/B* for one layer of reinforcement
(B × L: 6 in. × 6 in.; *D_f/B*: 0.0)
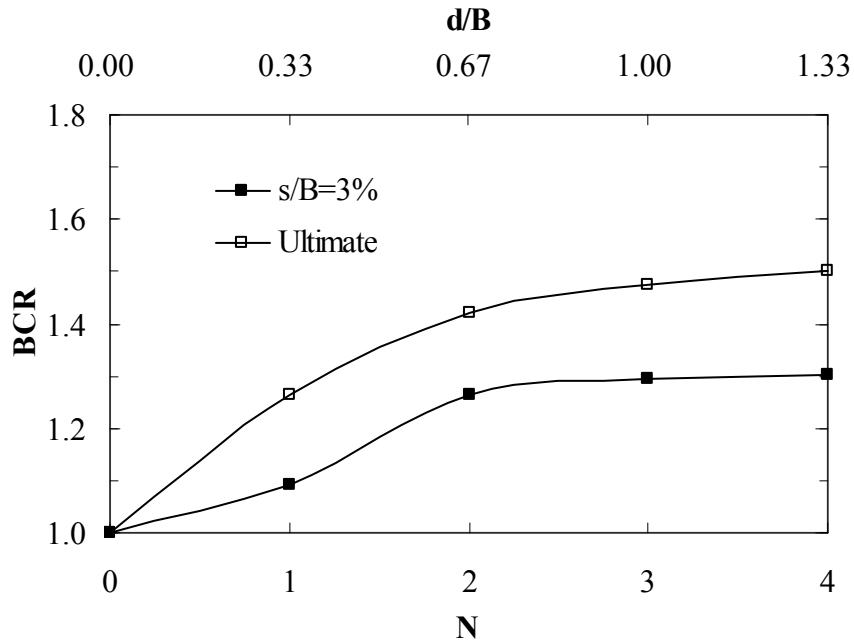
(a) BasXgrid11 geogrid
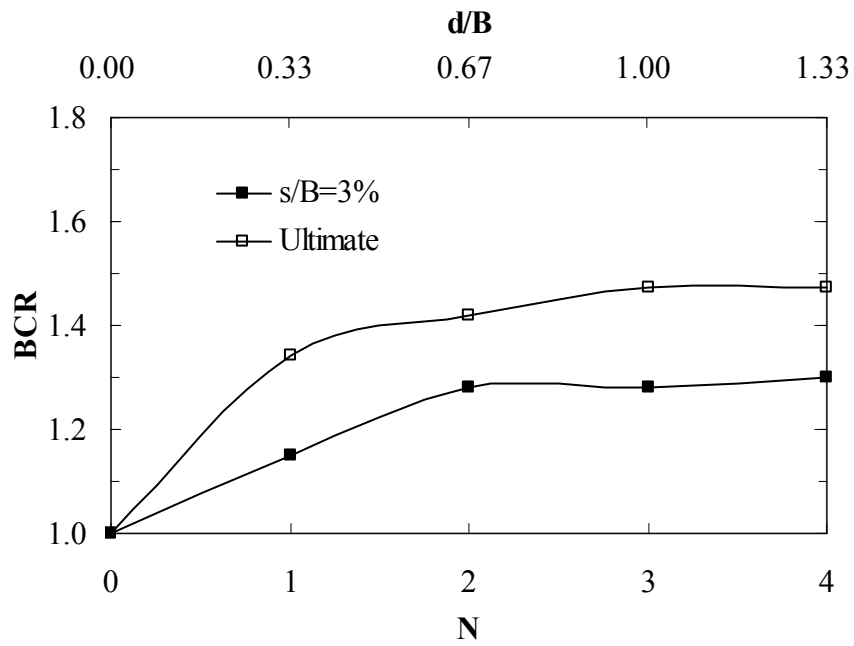
(b) BX6100 geogrid

Figure 43
BCR versus *N* and *d/B*
(B × L: 6 in. × 6 in.; *D_f/B* = 1.0)
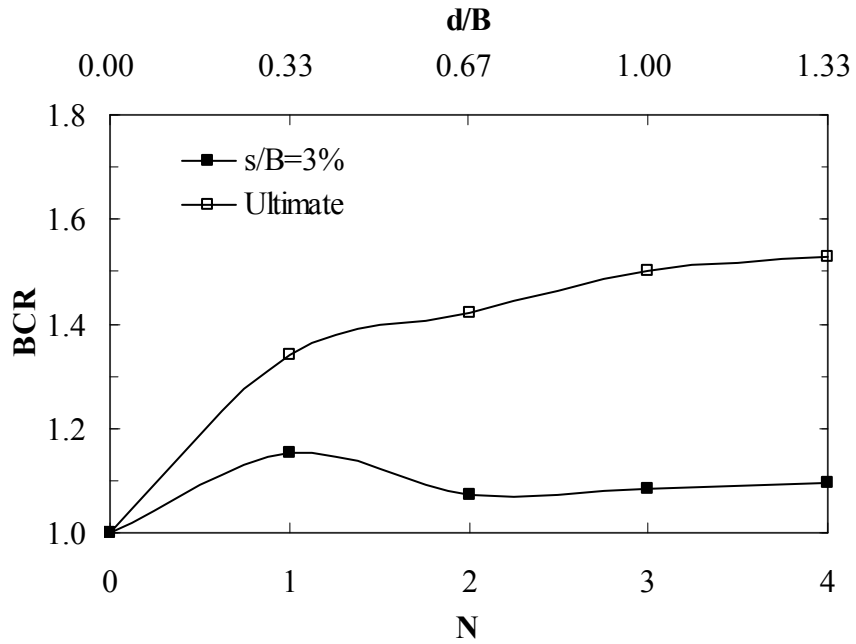
(c) HP570 geotextile
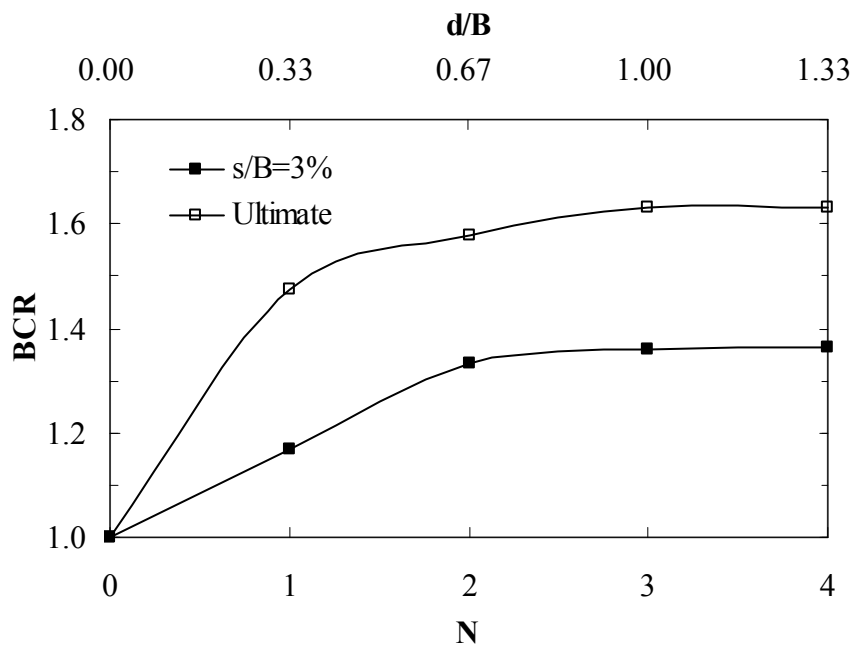
(d) HP570/BX6100 Composite

Figure 43
(continued)
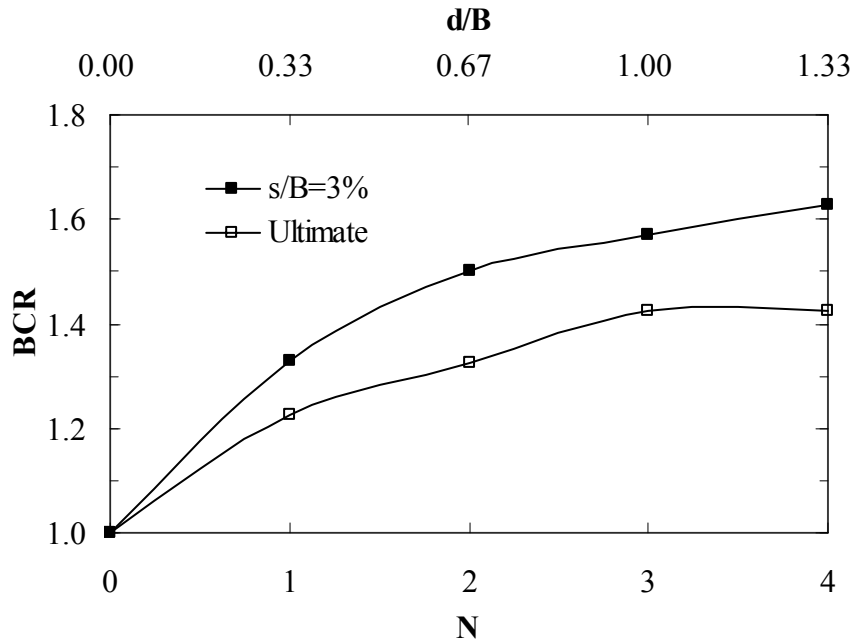
(a) BasXgrid11 geogrid
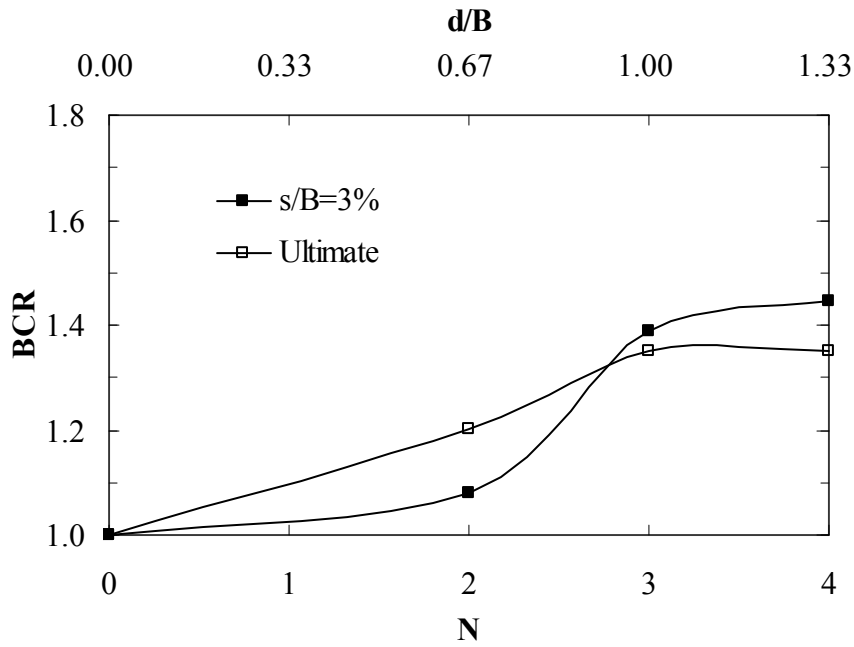
(b) HP570 geotextile

Figure 44
BCR versus *N* and *d/B*
(B × L: 6 in. × 6 in.; *D_f/B* = 0.0)

spacing of reinforcement layers with maximum BCR at $h = 0.167B$. No optimum vertical spacing was obtained for the BasXgrid11 geogrid reinforced sand tested. As indicated in the previous discussion of model tests on reinforced silty clay soil, in order to fully understand the effect of vertical spacing on bearing capacity separately, other influencing factors, such as the top layer spacing (u), number of layers (N), and geogrid modulus should be considered. Once again, for the sand and geogrid reinforcement tested in this study, one can realize that the smaller the spacing, the higher the BCR. For design purpose, engineers need balance between reducing spacing and increasing geogrid modulus. The author believes a value of $h/B = 0.33$ can be a reasonable value for use in the design of reinforced sand.
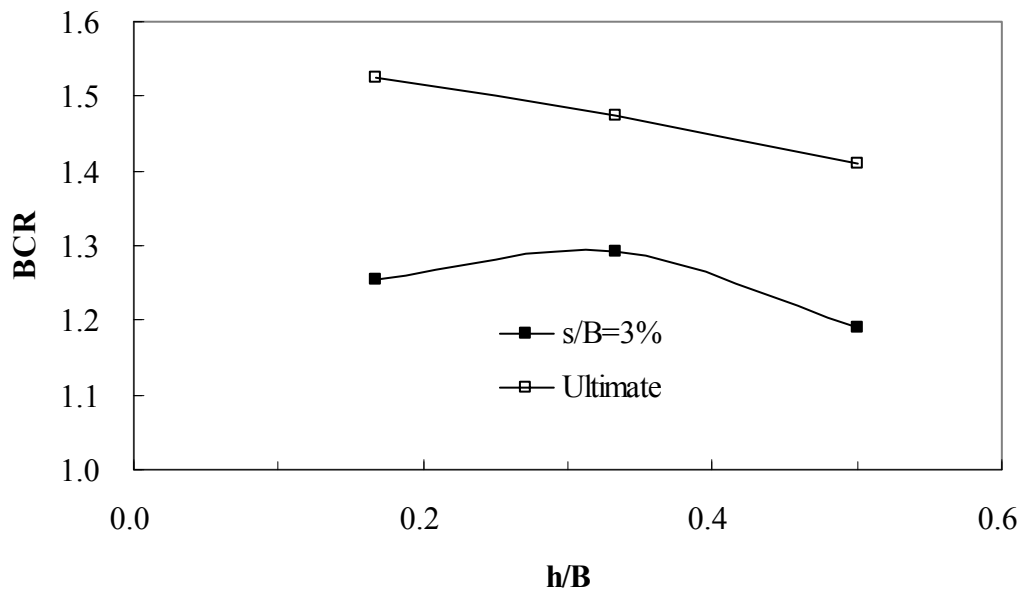
Figure 45
BCR versus h/B for three layers of BasXgrid11
(B × L: 6 in. × 6 in.; D_f/B: 1.0)

Effect of Footing Depth and Shape
The effect of embedment depth on the BCR of reinforced sand was investigated by conducting two sets of model tests, one without embedment depth (footing on surface), and one at an embedment depth equal to the footing width ($D_f=B=6$ in.). The tests conducted in the present study indicated that at the same settlement ratio (s/B), the BCRs for surface footing are generally greater than those for 6 in. embedded footing (figure 46). The BCRs also increase with an increase in the settlement ratio. It is also shown in the present study that the BCRs at ultimate bearing capacity for surface footings are generally smaller than those for footing with 6 in. embedment (figure 47). This finding can be expected in the light of the

fact that the settlement ratios (s/B) at the ultimate bearing capacity for 6 in. embedded footing are greater than those for surface footing.

The effect of footing shape on the BCR of reinforced sand was also investigated by conducting two sets of model tests, one with a 6 in. × 6 in. square footing, and one with a 6 in. × 10 in. rectangular footing. The test results show that the ultimate bearing capacity of unreinforced sand for 6 in.-wide square footing is greater than that for 6 in. × 10 in. rectangular footing (table 6 and 7), which is consistent with the theoretical analysis by using bearing capacity formula suggested by Vesic [27]. Figure C.11 indicates that, at the same settlement, the bearing capacity of unreinforced sand for 6 in.-wide square footing is also greater than that for 6 in. × 10 in. rectangular footing. Similarly, in reinforced sand, higher bearing capacity (both at ultimate and the same settlement) was also observed for 6 in.-wide square footing (figures C.12 through C.15). The comparison of BCRs obtained for these two different shape footings is shown in figure 48. Figure 48 clearly shows that the BCRs at ultimate bearing capacity for 6 in.-wide square footing are greater than those obtained for 6 in. × 10 in. rectangular footing. The similar trend was identified for the BCRs at settlement ratio less than 12% (figure 49).

Effect of Tensile Modulus and Type of Reinforcement
Four different types of reinforcement with different tensile modulus were used in the model footing tests on sand. These include BasXgrid11 geogrid, BX6100 geogrid, HP570 geotextile, and HP570/BX6100 composite. The properties of these reinforcements were presented earlier in table 2. Figures C.10 and C.16 through C.19 compare the pressure-settlement curves obtained for different types of reinforcements on model tests conducted with multiple reinforcement layers placed at top layer spacing and vertical spacing of 2 in. As seen in these figures, the performance of BasXgrid11 geogrid and BX6100 geogrid is very similar until ultimate bearing capacity reached, after which the sand reinforced by BasXgrid11 geogrid, which has a higher tensile modulus and smaller aperture size than BX6100 geogrid, performs appreciably better than that reinforced by BX6100 geogrid. This point is more clearly demonstrated in figure 50.

The variations of BCRs with settlement ratios (s/B) for model tests with multiple layers of different types of reinforcement are presented in figures 51a through 51d. It can be seen that the BCR generally increases with the increase of settlement ratio (*s/B*). Before the ultimate bearing capacity is reached, the BCRs of geotextile reinforced sand are smaller than those of
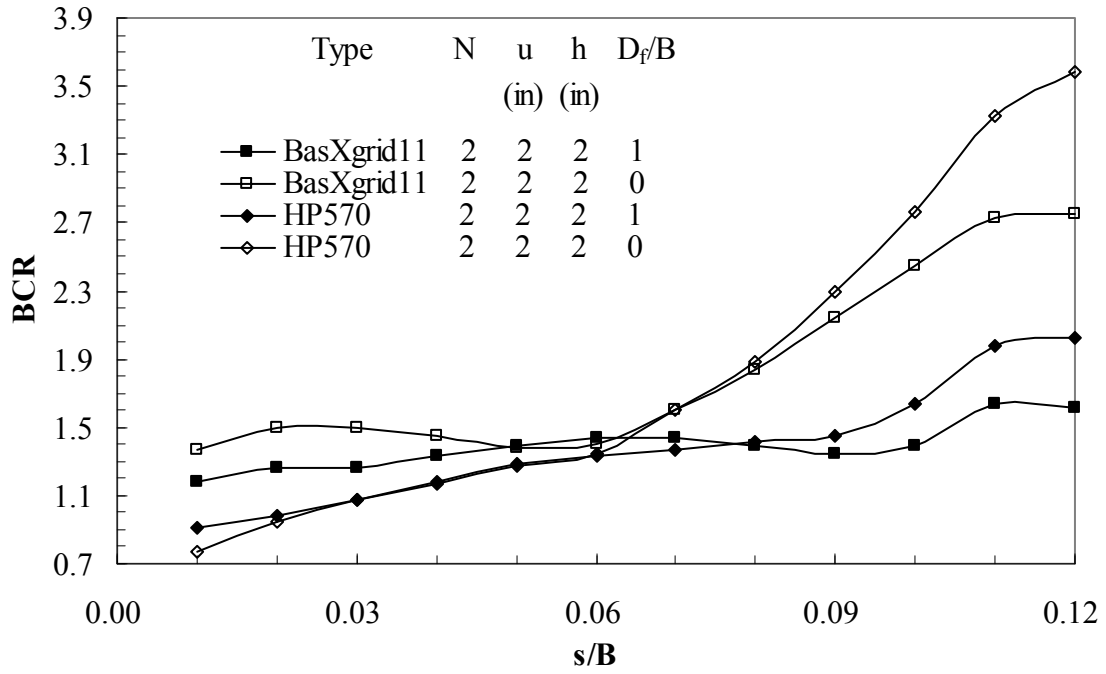
(a) Two layers of reinforcement
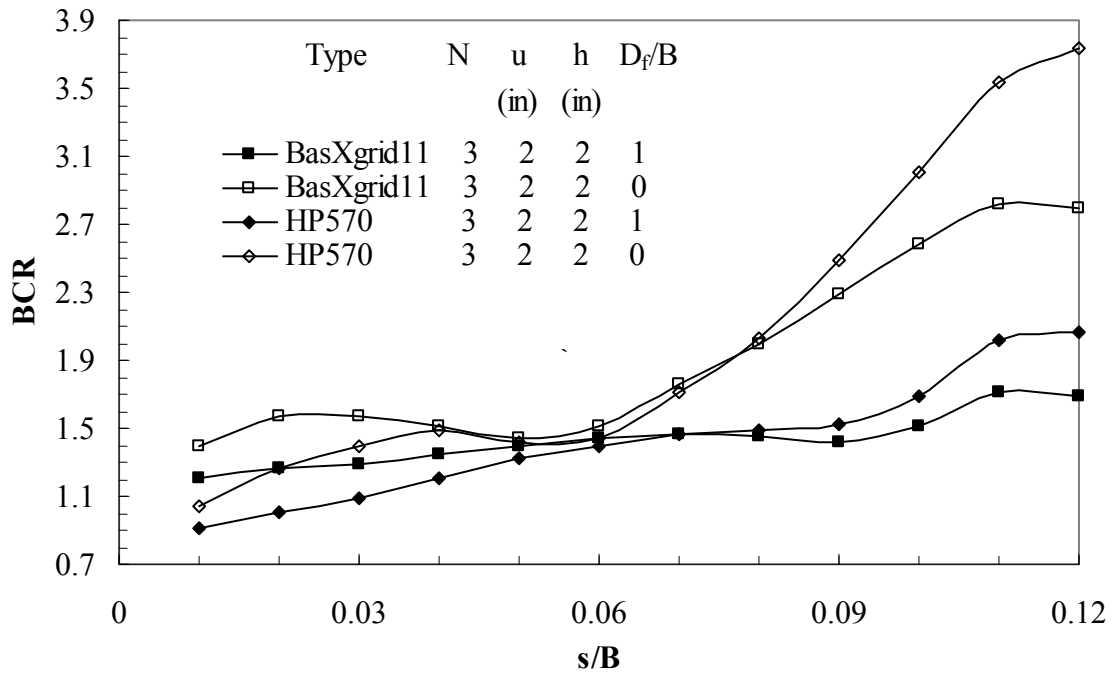
(b) Three layers of reinforcement

Figure 46
BCR versus settlement ratio (s/B)
(B × L: 6 in. × 6 in.)
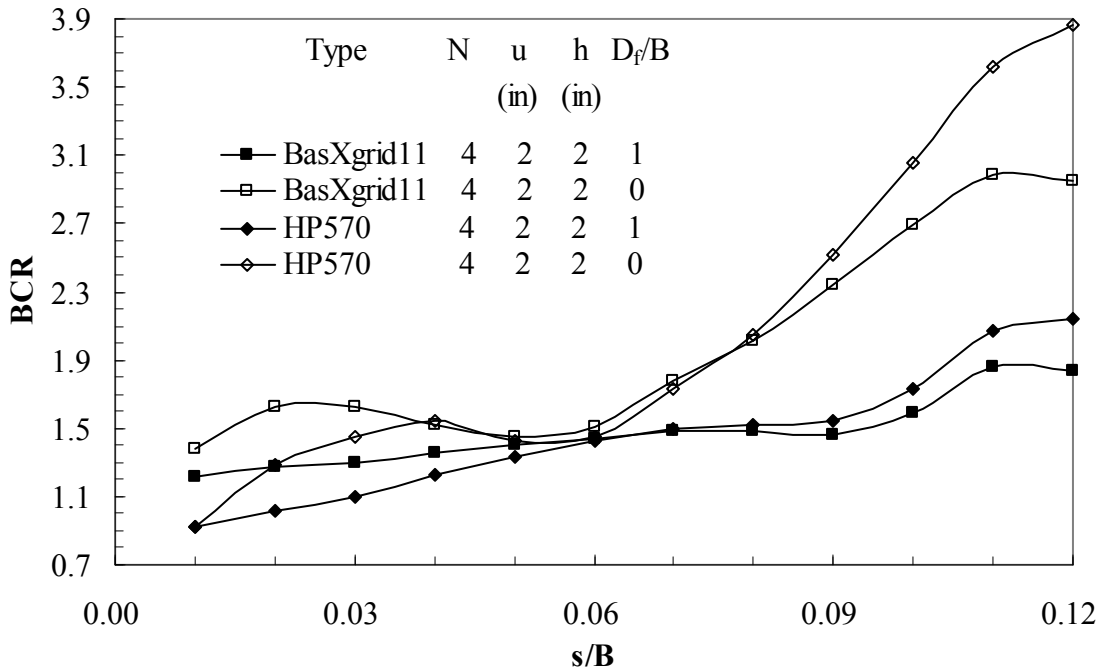
(c) Four layers of reinforcement

Figure 46
(continued)
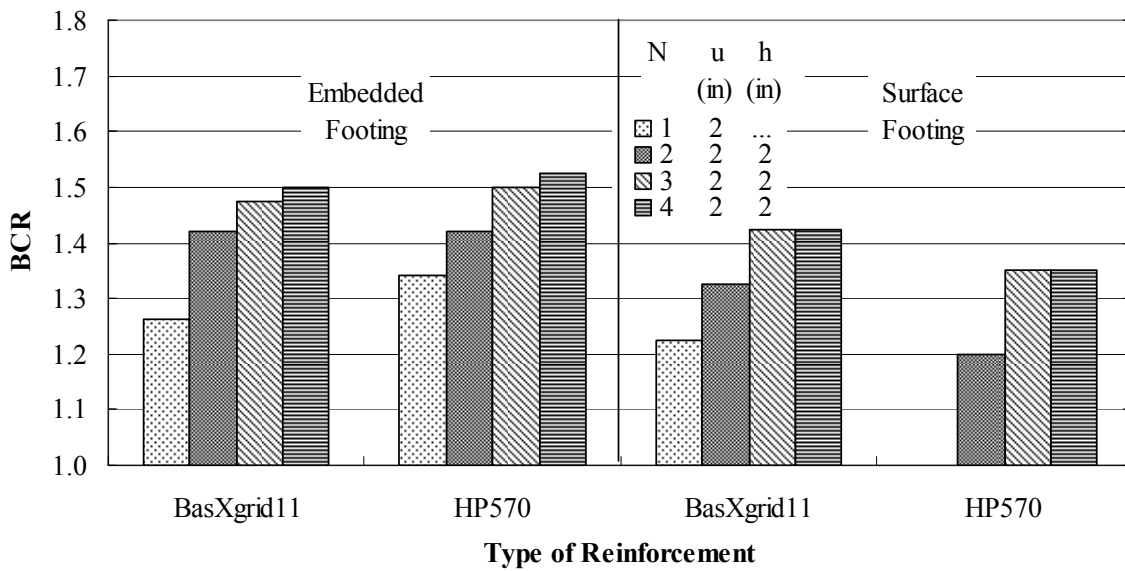
Figure 47
BCR versus type of reinforcement for both embedded footing and surface footing at the
ultimate bearing capacity (B × L: 6 in. × 6 in.)
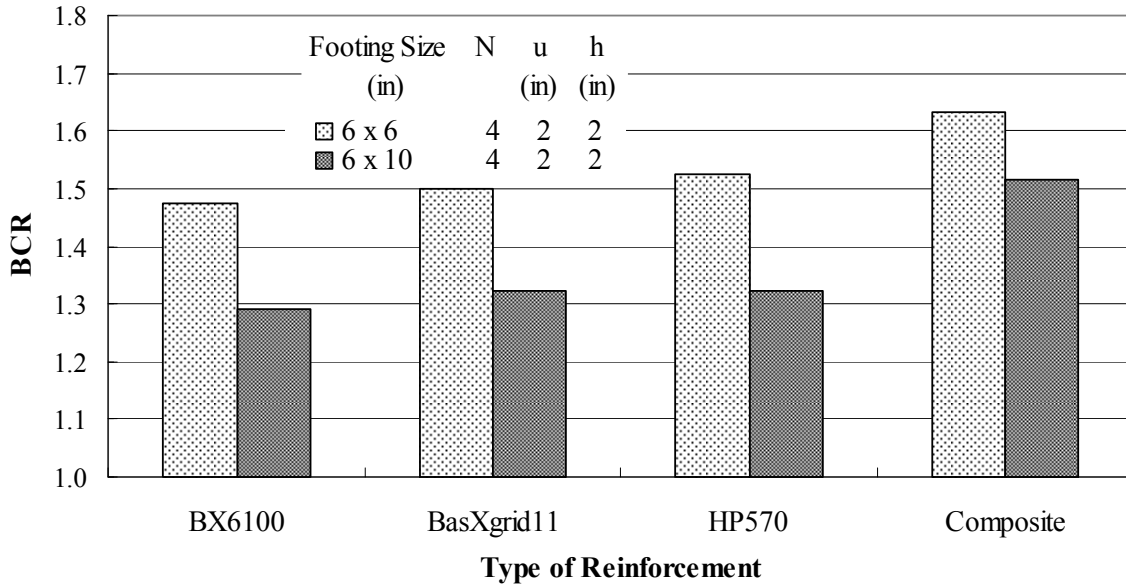
Figure 48
BCR versus type of reinforcement for two different size footings at the ultimate bearing capacity ($D_f/B = 1.0$)
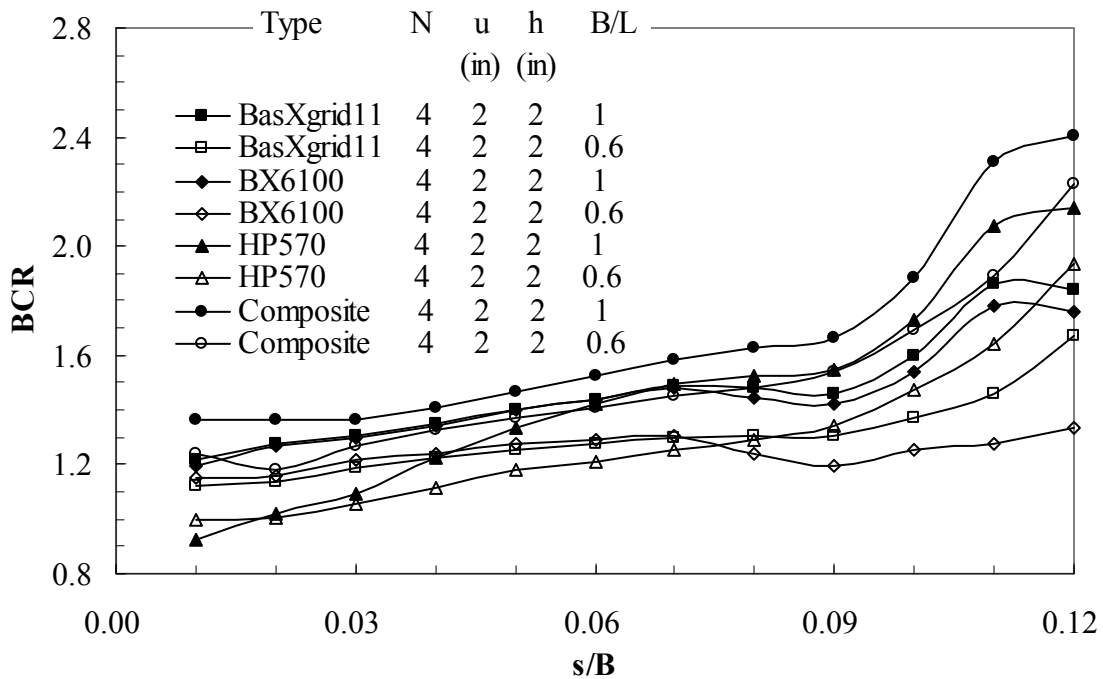
Figure 49
BCR versus settlement ratio (s/B) ($D_f/B = 1.0$)

geogrid reinforced sand, except for one layer. However, the rate of increase of BCRs with the increase of settlement for geotextile reinforced sand is higher compared to that for geogrid

reinforced sand. Consequently, at post failure stage, the BCRs of geotextile reinforced sand are much greater than those of geogrid reinforced sand. This point can also be clearly seen in figures 50 and 51. Furthermore, the bearing capacity of geotextile reinforced sand at low settlement level (s/B < 2% for embedded footing and s/B < 1.5% for surface footing) is even less than that of unreinforced sand. As discussed in model tests on silty clay, this behavior is due to the slack of woven geotexitle. It is also interesting to note that the ultimate bearing capacity of geotextile reinforced sand is somewhat higher than that of geogrid reinforced sand for embedded footing, while it is obviously lower for surface footing (table 5 and 6). Figures C.10 and C.16 through C.19 show that the sand reinforced by HP570/BX6100 composite performed better than that reinforced by geogrid or geotextile alone. This better performance of HP570/BX6100 composite becomes pronounced at post failure stage.

Again, because of a serviceability requirement, geogrid reinforcement is generally considered to perform better for sand foundation than geotextile.

The settlement reduction factors (SRF) at different footing pressure (q) for the model tests with multiple layers of different types of reinforcement are presented in figures 52a through 52d. It is obvious that the inclusion of the reinforcement would reduce the settlement except for geotextile at low to medium footing pressure (q < 290.1 psi (2000 kPa)). With two or more layers of geogrid, the settlement can be reduced by 20% at all pressure levels. This study showed that modulus of geogrid has minimal effect on reducing the settlement in this study of sand. The rate of decrease of SRF with the increase of applied footing pressure for geotextile reinforced sand is higher compared to that for geogrid reinforced sand. HP570/BX6100 composite provides the best effect on reducing the footing settlement.

Stress Distribution in Sand
Several laboratory model tests were conducted to evaluate the stress distribution in sand with and without reinforcement inclusion. The measured stress distributions along the center line of the footing at the depth of 10 in. (1.67B) below the footing for both embedded and surface footing with different number of layers of geogrid (BX6100 for embedded footing and BasXgrid11 for surface footing) are shown in figures 53 and 54, respectively. Figures 55 and 56 present the stress distributions at the depth of 10 in. (1.67B) below the footing for 6 in. × 6 in. and 6 in. × 10 in. footing at an embedment depth of 6 in. with four layers of different types of reinforcement, respectively. Here, only limited cases of stress distributions are presented; the vertical stress distributions at the other applied footing pressures can be found in Chen [26].
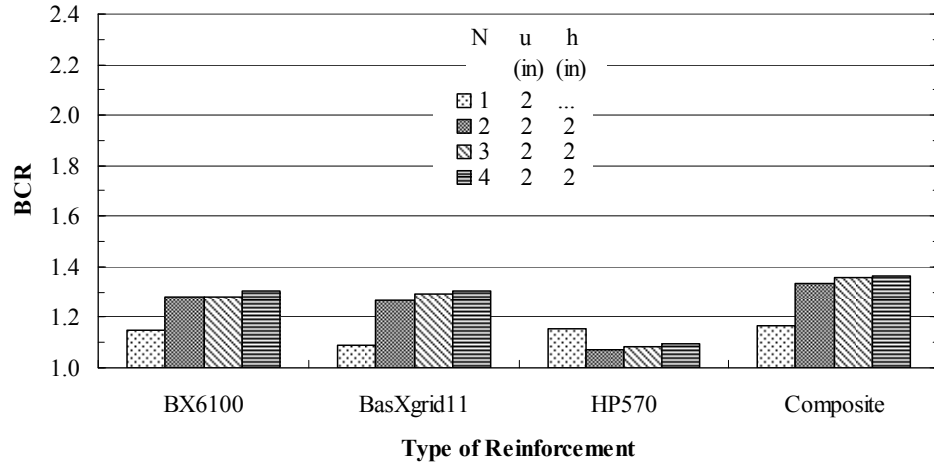
(a) s/B=3%
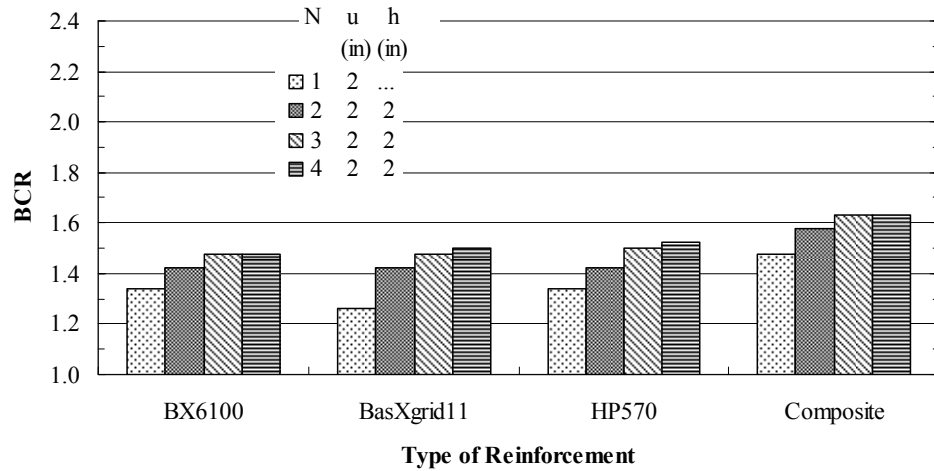
(b) at ultimate load
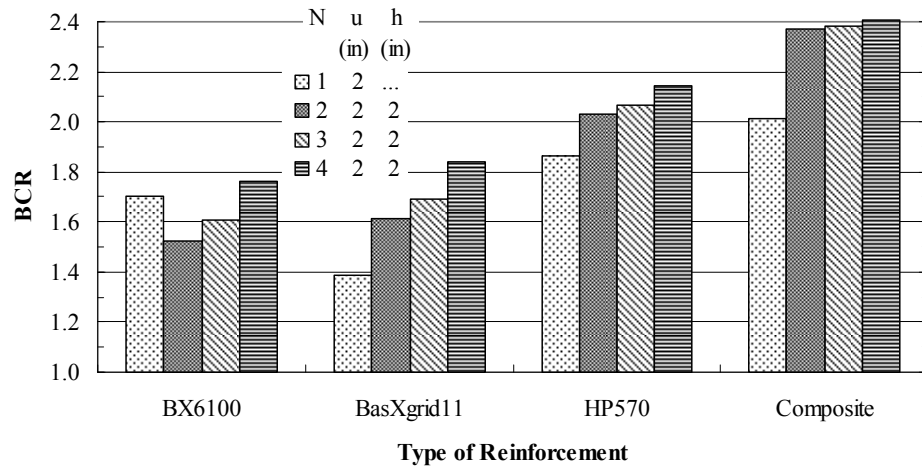
(c) s/B=12%

Figure 50

BCR versus type of reinforcement for clay (B × L: 6 in. × 6 in.; $D_f / B = 1.0$)
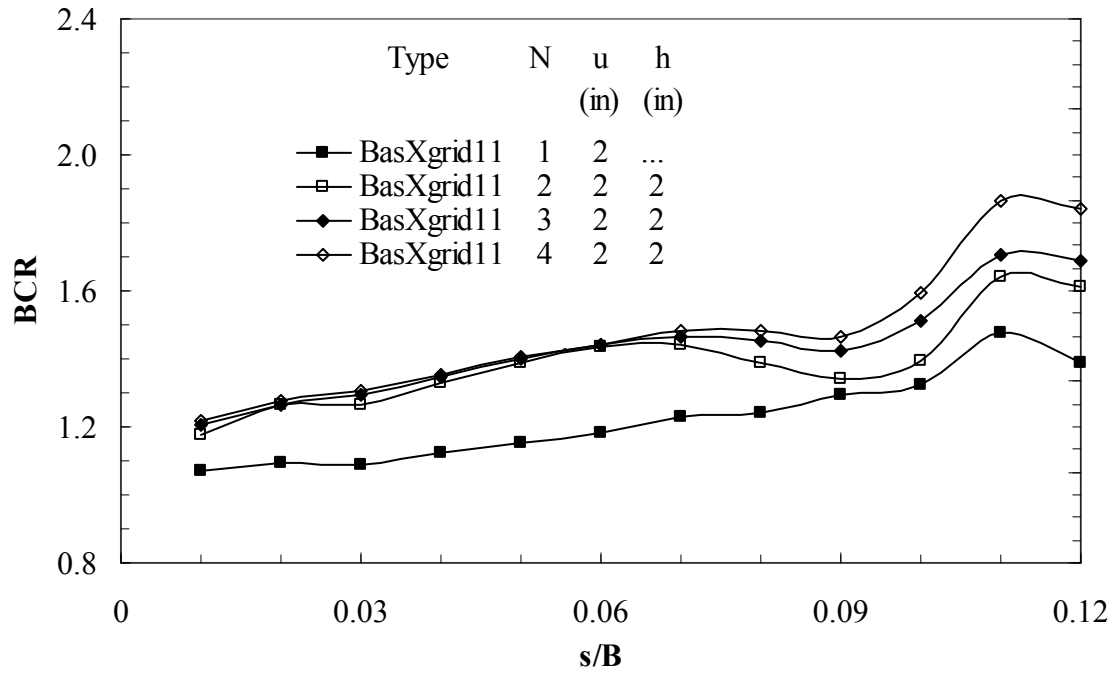
(a)
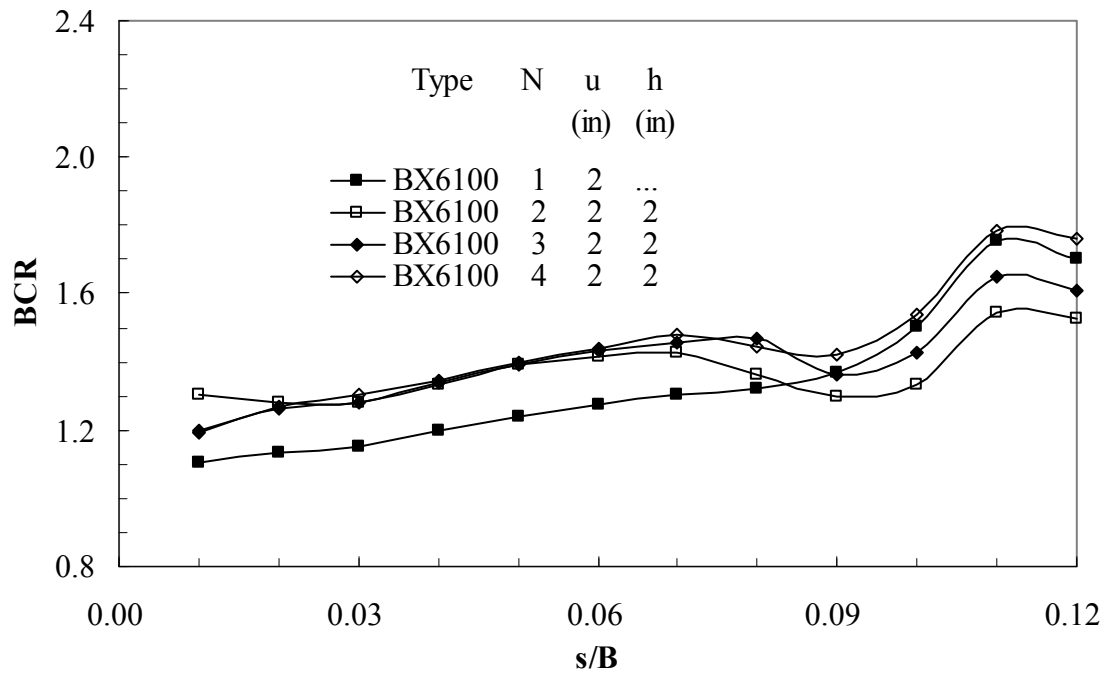
(b)

Figure 51
BCR versus settlement ratio (s/B) (B × L: 6 in. × 6 in.; $D_f / B = 1.0$)
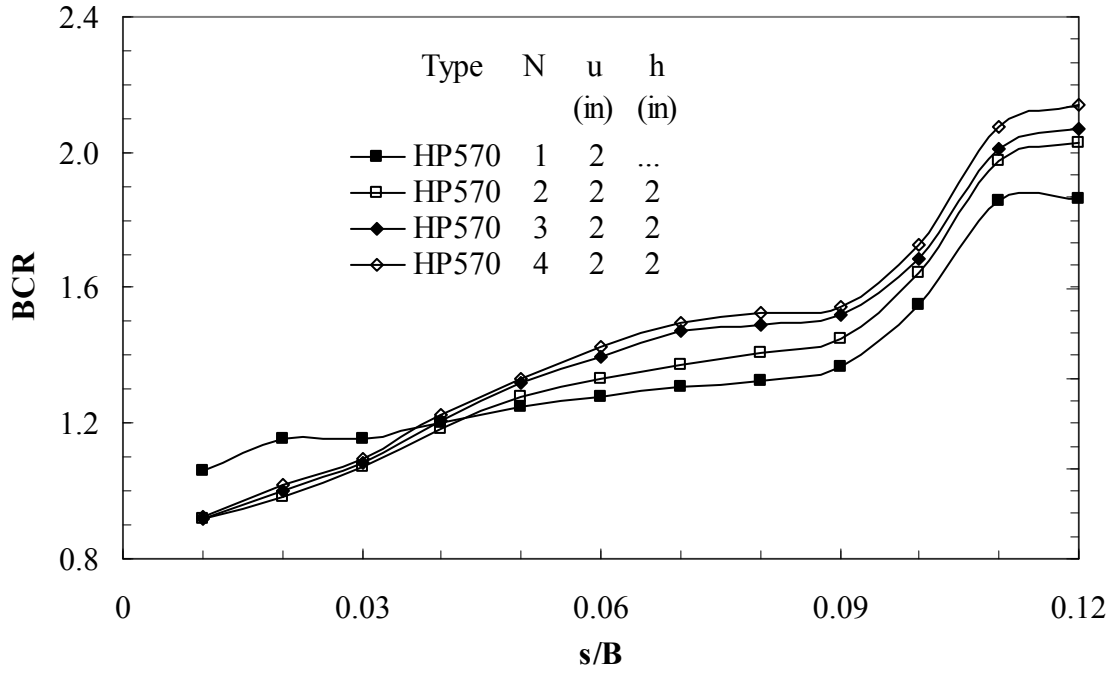
(c)
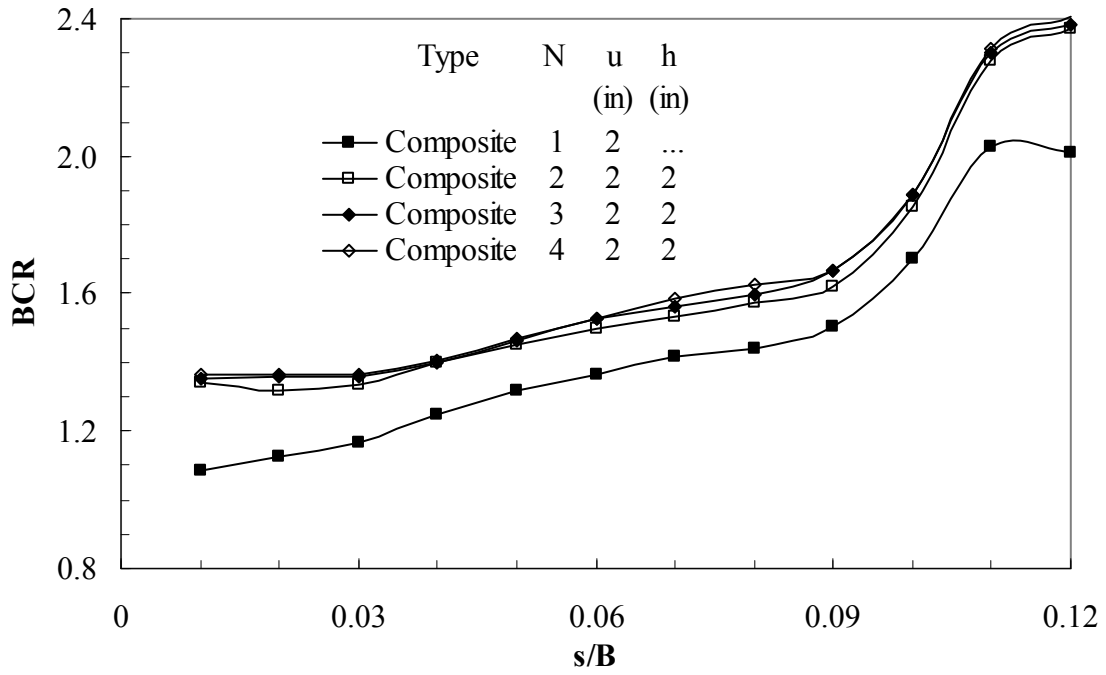
(d)

Figure 51
(continued)
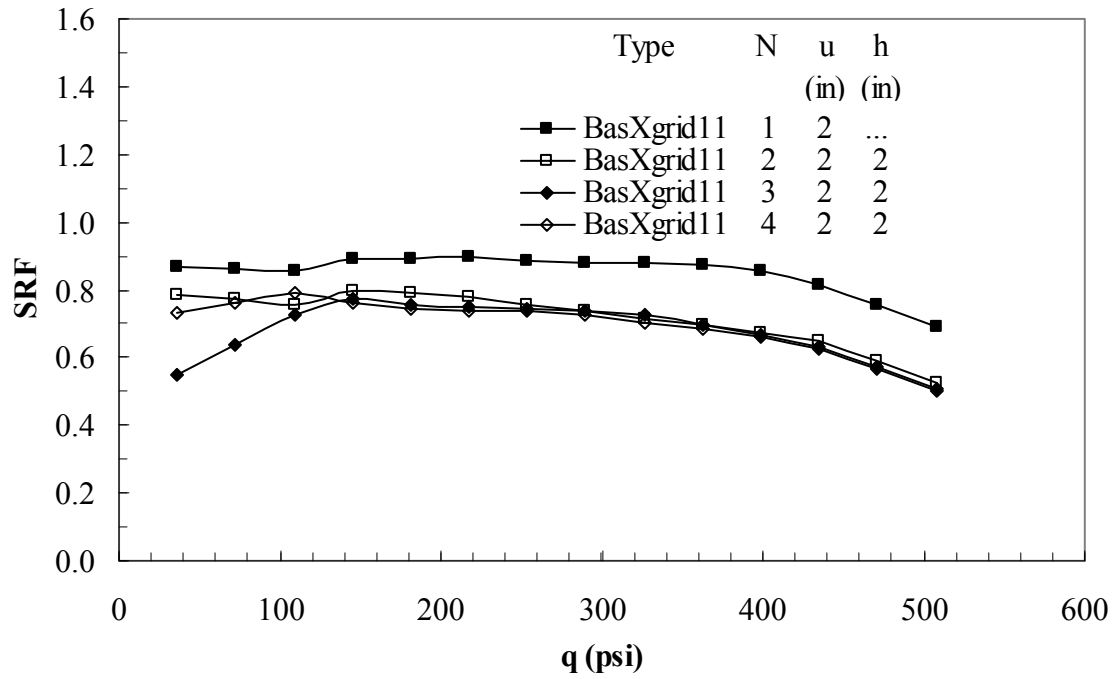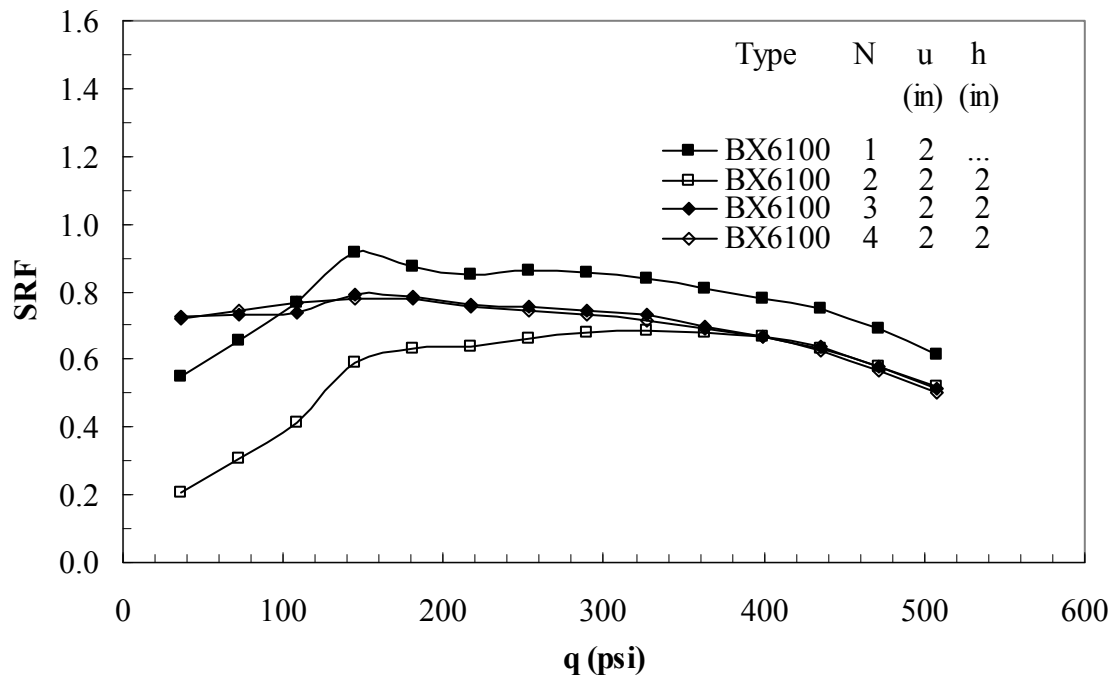
Figure 52
SRF versus applied footing pressure (q)
(B × L: 6 in. × 6 in.; D_f / B = 1.0)
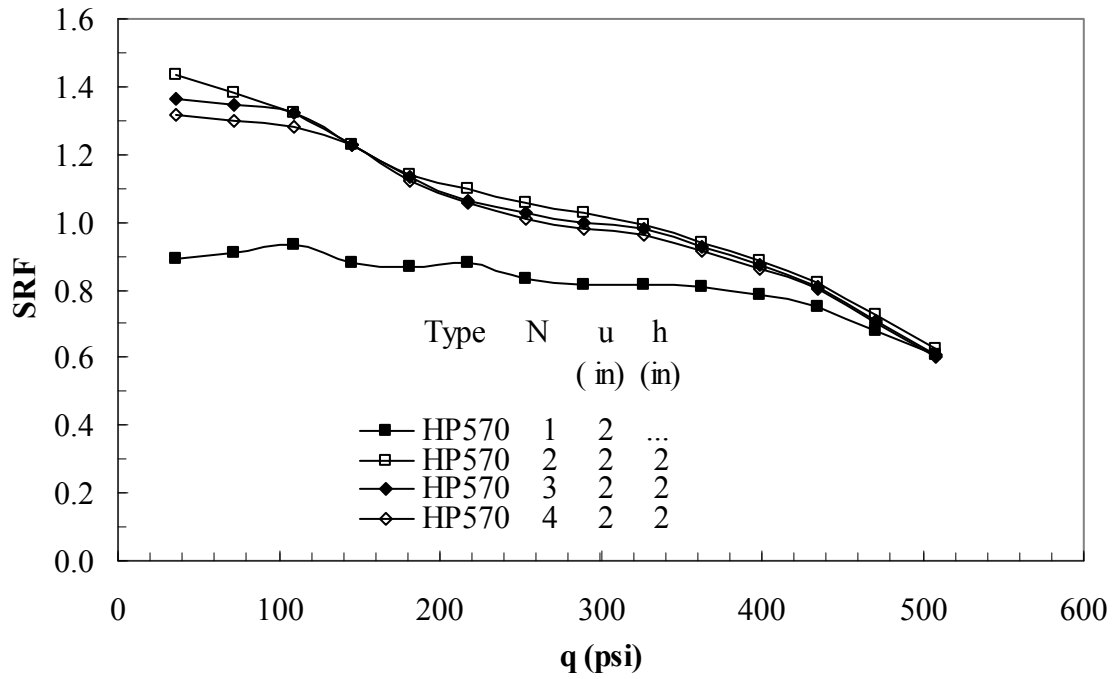
(c)
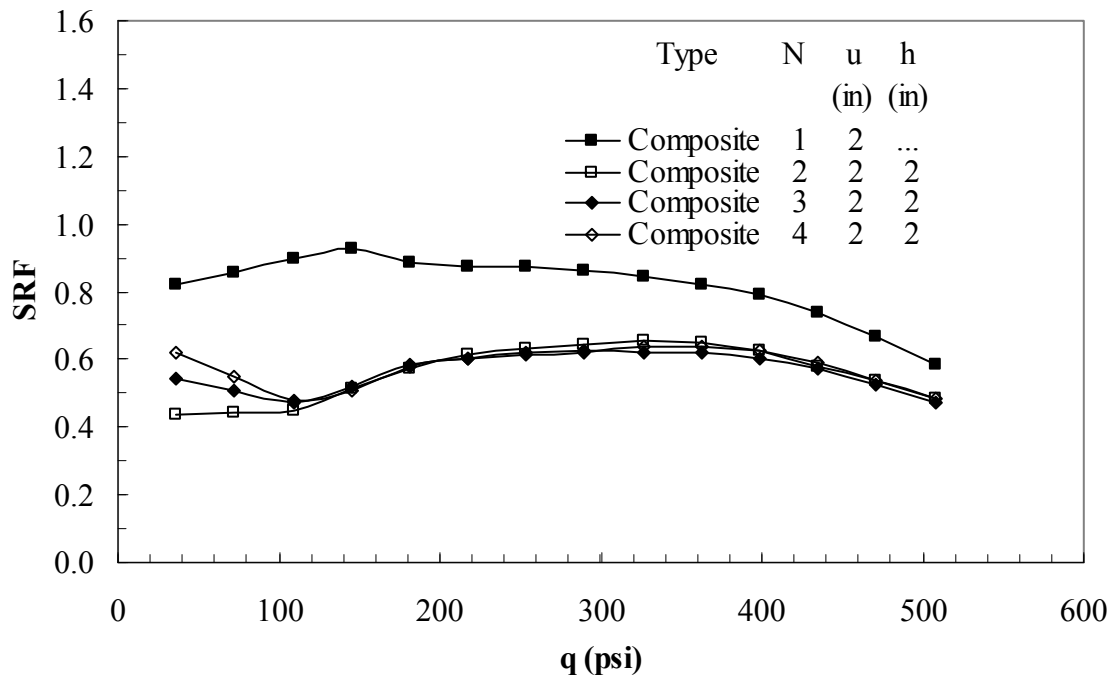
(d)

Figure 52
(continued)

As can be seen from these figures, the reinforcement results in redistribution of the applied load to a wider area, thus avoiding stress concentration and achieving improved stress distribution. The induced maximum stresses beneath the center of the footing in reinforced sand are appreciably reduced compared to those in unreinforced sand, especially for surface footing condition. For embedded 6 in. wide square footing with four layers of different types of reinforcement, the reduction in maximum stress ranges from 14% to 28% and from 12% to 19% at a footing pressure of 111.1 psi and 388.8 psi (766 kPa and 2681 kPa), respectively, while for surface footing with four layers of different types of reinforcement, the reduction in stress varies from 43% to 56% and from 31% to 34% at a footing pressure of 13.6 psi and 108.8 psi (94 kPa and 750 kPa), respectively. The redistribution of load to a wider area below the reinforced zone usually results in reducing the consolidation settlement of underlying weak clayey soil, which is directly related to the induced stress.

Generally, for the same applied footing pressure, the vertical stresses under the center decrease with increasing number of layers (figures 53 and 54). As shown in figures 57 and 58, under the same footing pressure, the stress influence factor (I) decreases with the increase of the number of reinforcement layers.

Among the geogrids used, the geogrid (BasXgrid11) with a higher modulus resulted in a better reduction of the center stresses than geogrid (BX6100) with a lower modulus. HP570 geotextile, which has a higher tensile modulus than the geogrids used in this study, showed better attenuation of the stresses under the center of footing than the geogrids. However, HP570/BX6100 composite provided the best attenuation of the center stresses among four types of reinforcement used in the present study for sand. It is interesting to mention here that that the improved performance of reinforced sand is also not always compatible with the improved stress distribution, similar to the observation on reinforced silty clay soil. As shown earlier, before the ultimate bearing capacity is reached, geogrid reinforced sand generally performs better than geotextile reinforced sand, but the induced stresses under the center of the footing in the geogrid reinforced sand are higher than those in the geotextile reinforced sand. As indicated in the previous discussion of model tests on silty clay, it seems that improvement of stress distribution in reinforced sand is closely related to the tensile modulus of reinforcement and that better tension membrane effect provides better improvement in stress distribution.

Negative stresses were measured in unreinforced sand for surface footing at approximately 2.5B from the center of footing. This result indicates that the sand is pushed upward at a

distance of around 2.5B from the center of footing. It confirms again that the inclusion of reinforcement could develop a "surcharge effect."

Figures 57 through 60 show that the stress influence factor (I) in sand is a load-dependent value instead of a constant value and it increases with the increase of the footing pressures. It is also indicated in figures 57 and 58 that the stress influence factors (I) for embedded footing were smaller than those for surface footing. This behavior can be expected in the light of the heterogeneity of sand and attributed to the variation of sand modulus with confining pressure, which increases with the depth.

Strain Distribution Along Reinforcement
One laboratory model test using a 6 inch-wide square footing at an embedment depth of 6 in. was conducted to evaluate the strain distribution along the reinforcement. Four layers of BX6100 geogrid placed at a spacing of 2 in. were used in the test. The geogrids with strain gauges instrumentation were placed at the top and bottom layers (at a depth of 2 in. (0.33B) and 8 in. (1.33B) below the footing, respectively). The variations of strains along the centerline of the geogrid at different settlement ratios (s/B) are presented in figure 61. The tensile strain is the largest at the point beneath the center of the footing and becomes almost negligible at about 3.0B from the center of footing. It also indicates that the geogrid beyond the effective length of $l_e = 6.0B$ results in insignificant mobilized tensile strength, and thus provides negligible effects on the improved performance of reinforced sand foundation. This observation is the same as that observed for reinforced silty clay foundation.

Compressive strains were measured in the geogrid located beyond 0.85B and 1.15B from the center of footing for geogrid placed at a depth of 2 in. and 8 in. below the footing, respectively. As stated before in reinforced silty clay, this means that the geogrid past this length cannot restrain lateral soil shear flow and works as an anchorage unit to prevent geogrid from failing by pull out. The compressive strain measured in the reinforcement beyond a certain length may be due to the reason that the direction of reinforcement past this length is coincidental with the direction of compressive strains in the soil [17]. This point was clearly described by Michalowski [31] through limit analysis.
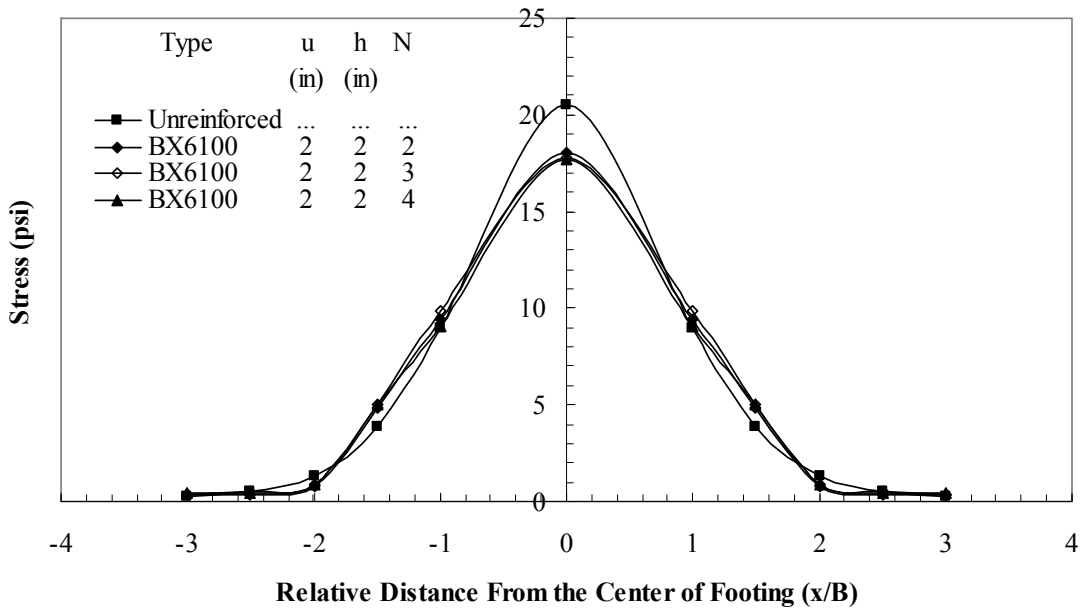
(a) Applied footing pressure q=111.1 psi
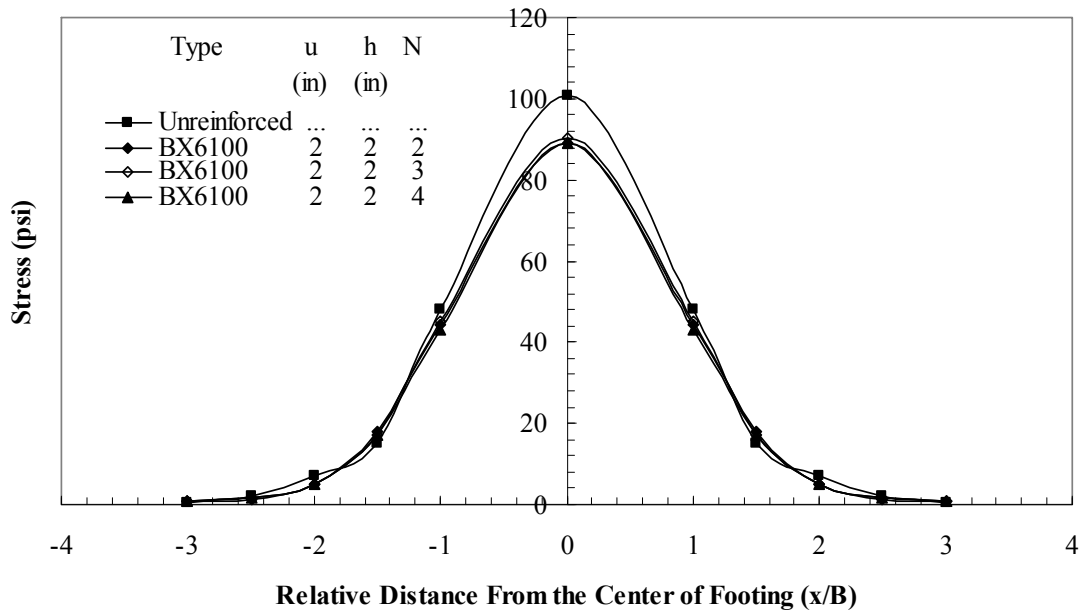
(b) Applied footing pressure q=388.8 psi

Figure 53
Vertical stress distribution along the center line of footing at a depth of 10 in. below the footing with multilayer of BX6100 geogrid
(B × L: 6 in. × 6 in., $D_f/B = 1.0$)
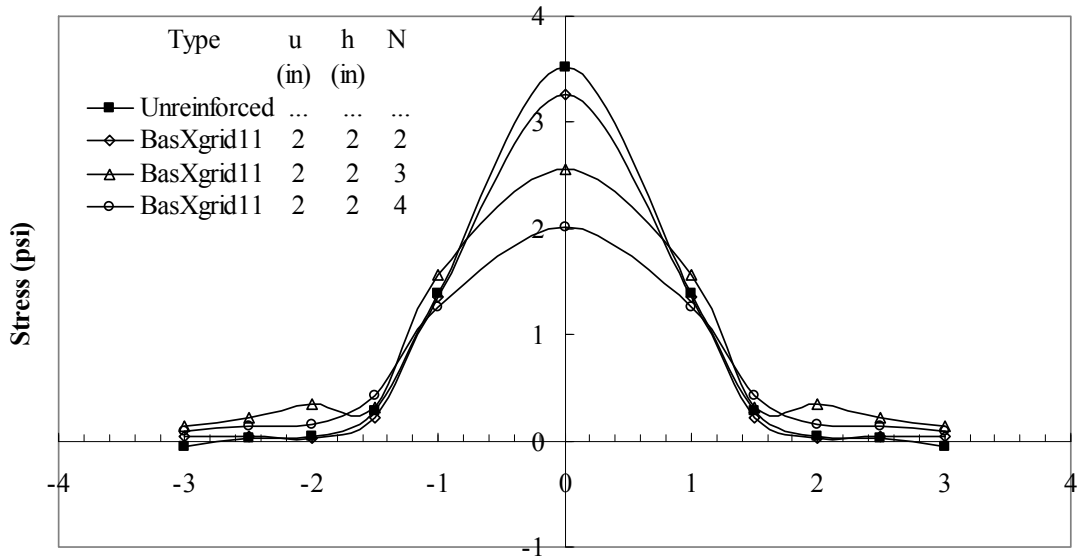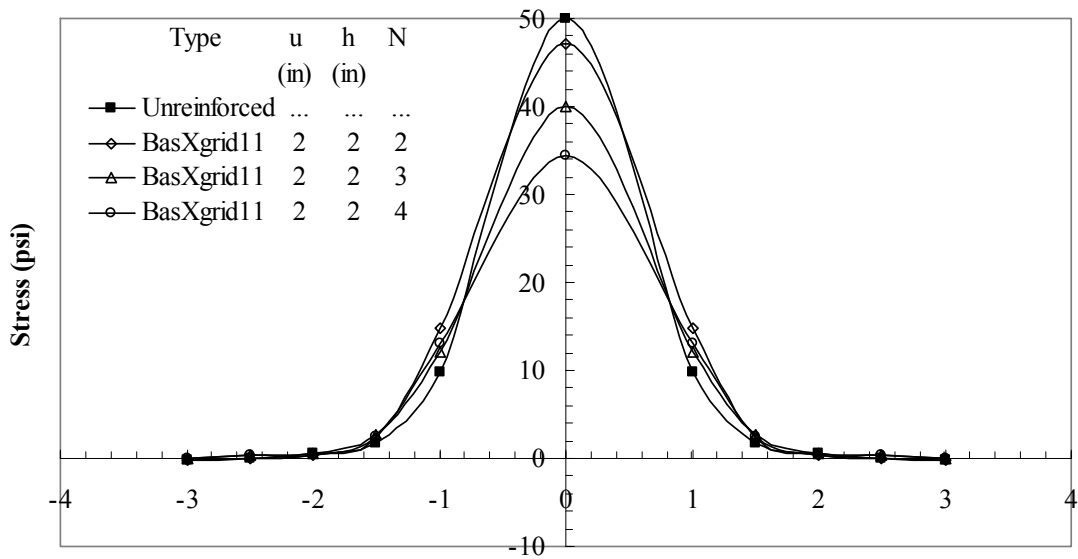
(a) Applied footing pressure q=13.6 psi

(b) Applied footing pressure q=108.8 psi

Figure 54
Vertical stress distribution along the center line of footing at a depth of 10 in. below the footing with multilayer of BasXgrid11 geogrid
(B × L: 6 in. × 6 in., D_f/B = 0.0)
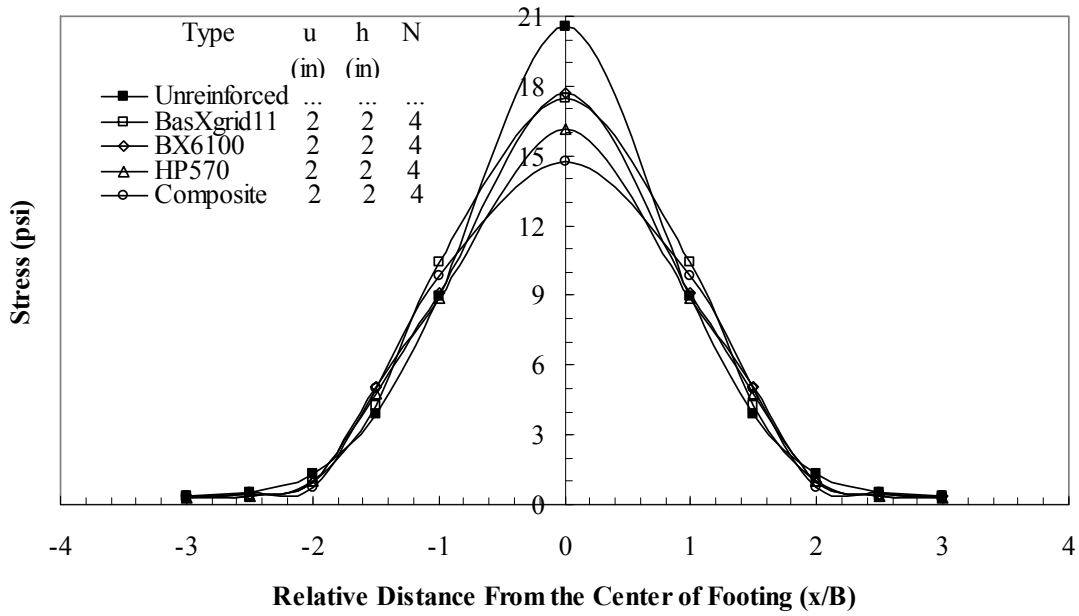
(a) Applied footing pressure q=111.1 psi
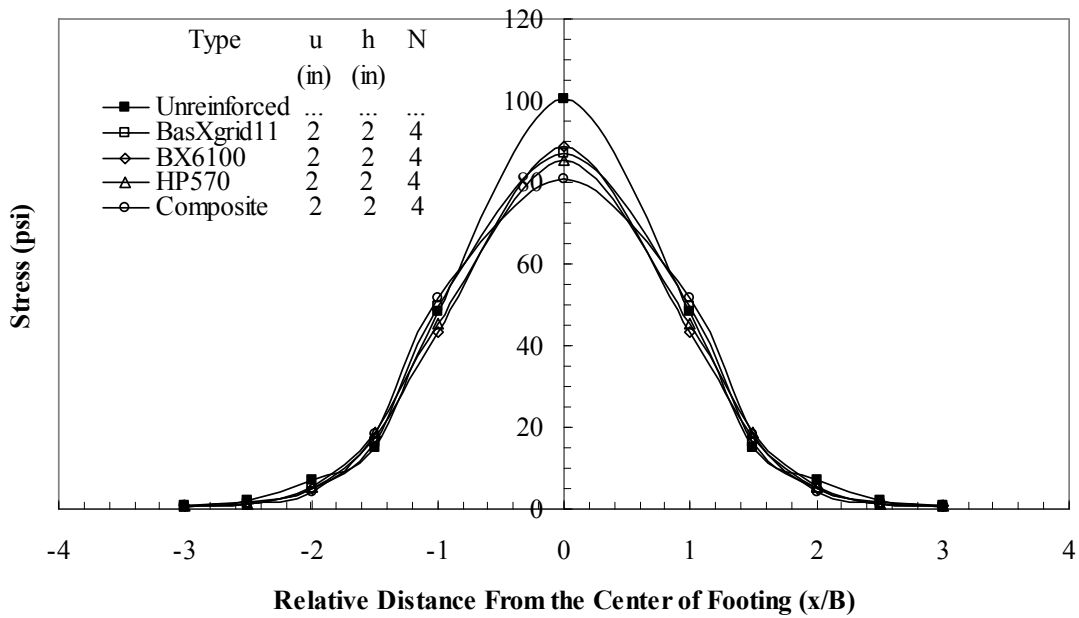
(b) Applied footing pressure q=388.8 psi

Figure 55

Vertical stress distribution along the center line of footing at a depth of 10 in. below the footing with four layers of different types of reinforcement
(B × L: 6 in. × 6 in., D_f/B = 1.0)
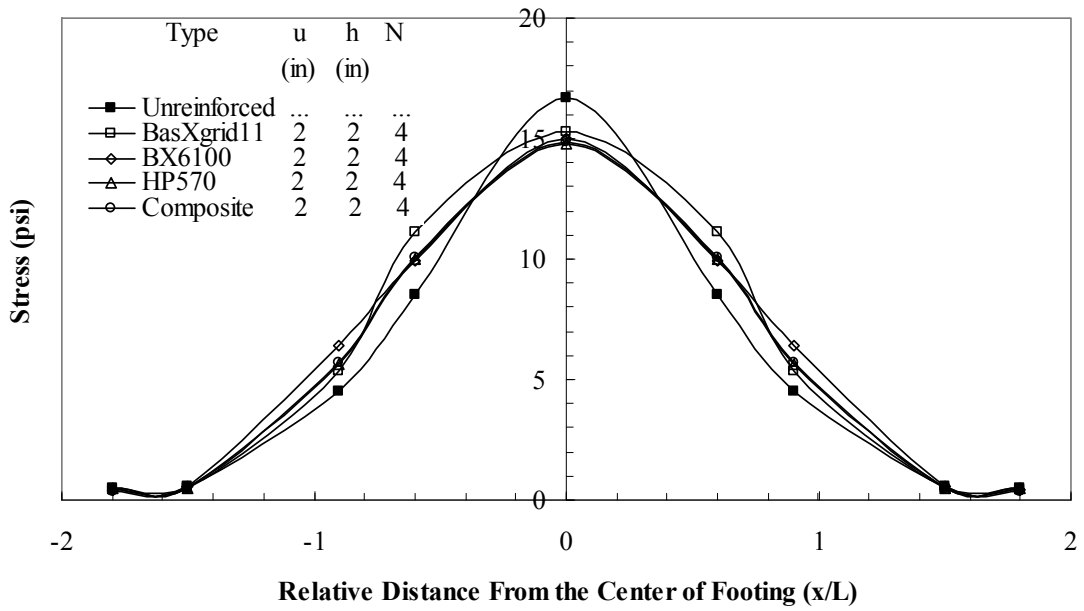
(a) Applied footing pressure q=66.7 psi
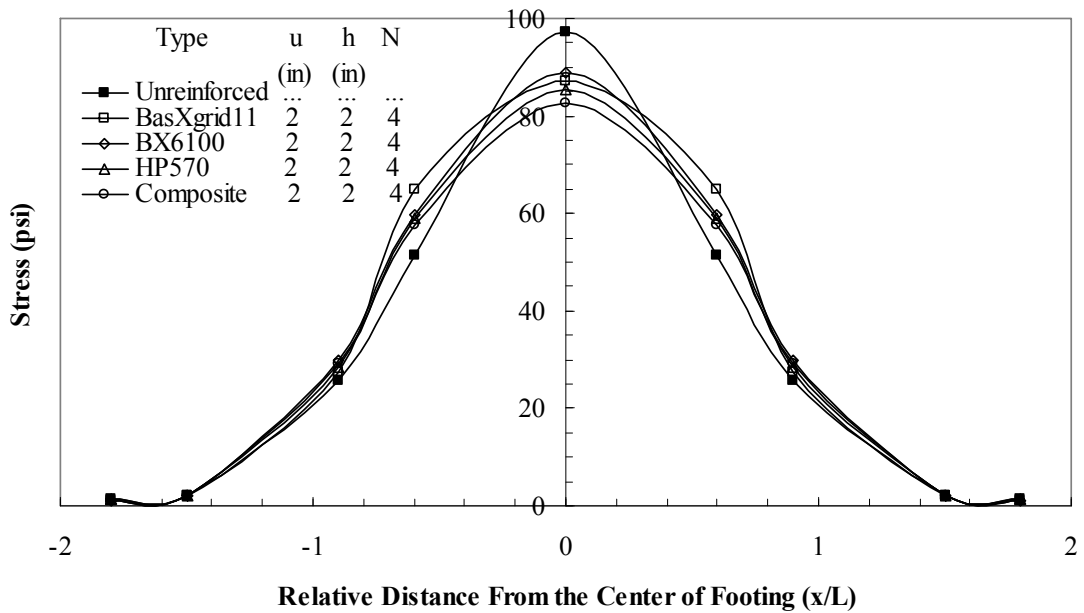
(b) Applied footing pressure q=266.6 psi

Figure 56
Vertical stress distribution along the center line of footing at a depth of 10 in. below the footing with four layers of different types of reinforcement
(B × L: 6 in. × 10 in., $D_f/B = 1.0$)
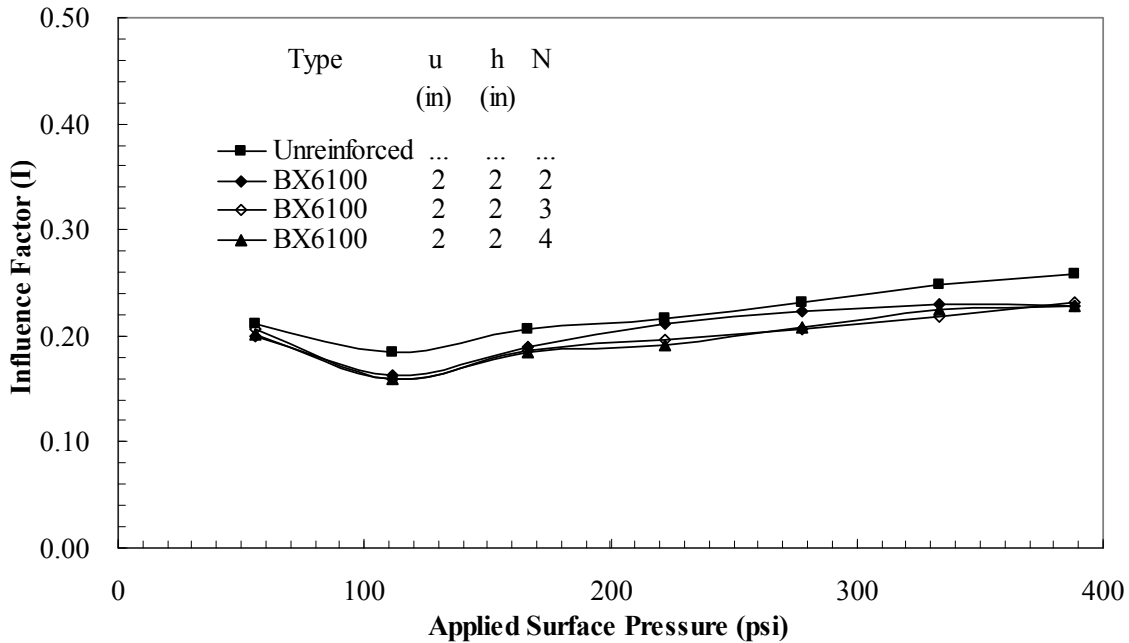
Figure 57
Stress influence factor (I) at a depth of 10 in. (1.67B) underneath the center of footing versus applied footing pressure for multilayer of BX6100 geogrid
(B × L: 6 in. × 6 in., D_f/B = 1.0)
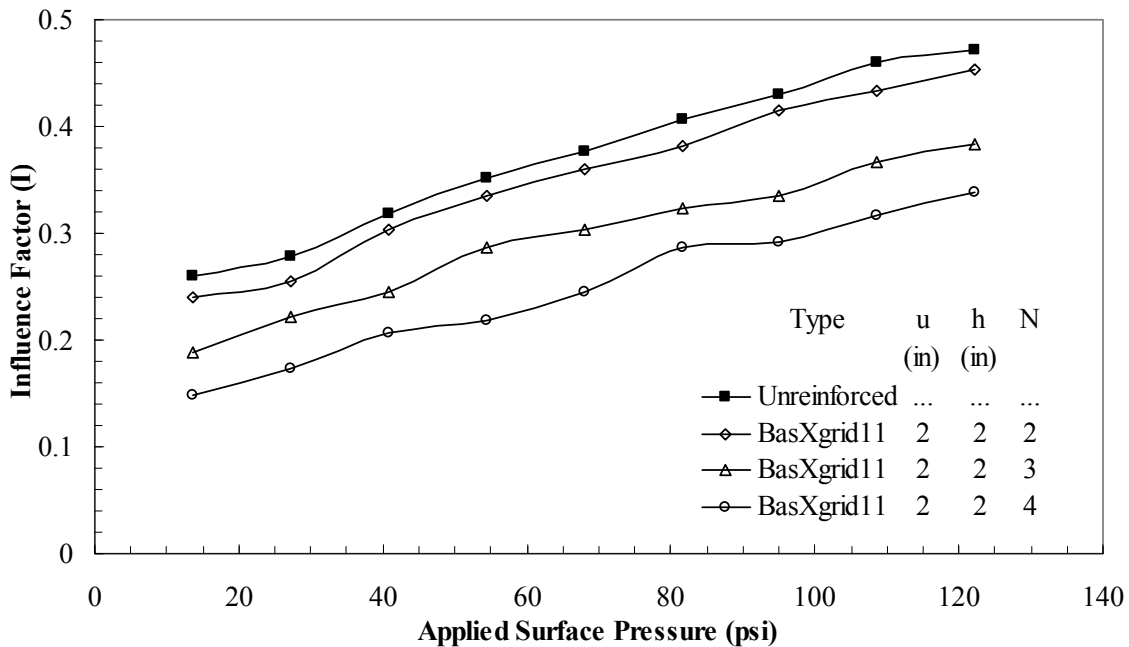
Figure 58
Stress influence factor (I) at a depth of 10 in. (1.67B) underneath the center of footing versus applied footing pressure for multilayer of BasXgrid 11 geogrid
(B × L: 6 in. × 6 in., D_f/B = 0.0)
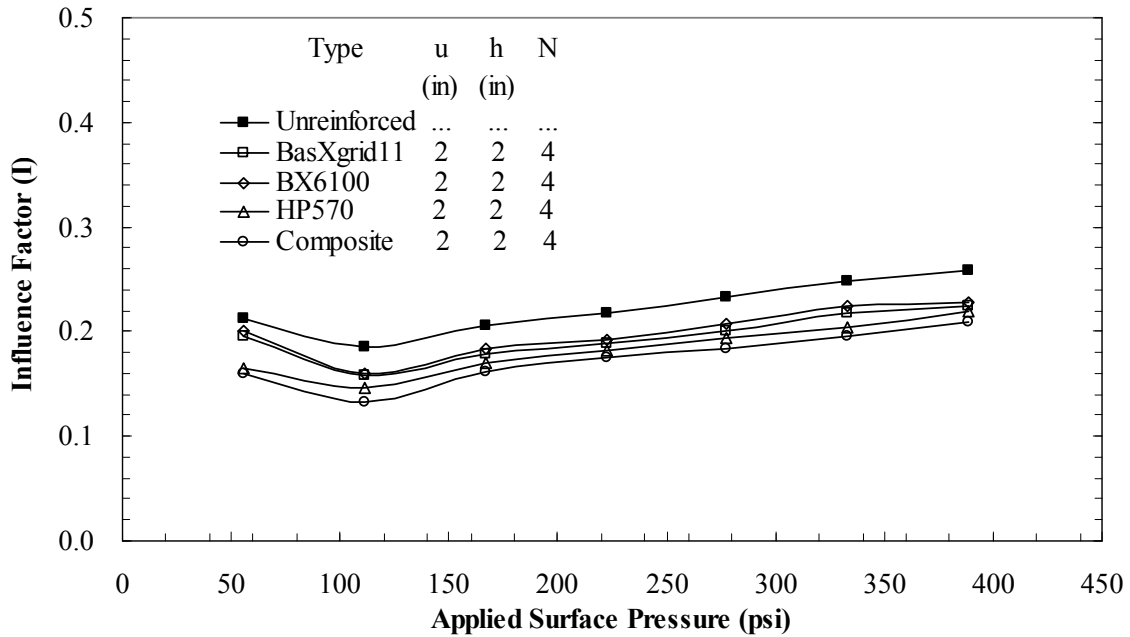
Figure 59
Stress influence factor (I) at a depth of 10 in. (1.67B) underneath the center of footing versus applied footing pressure for four layers of different types of reinforcement (B × L: 6 in. × 6 in., D_f / B = 1.0)
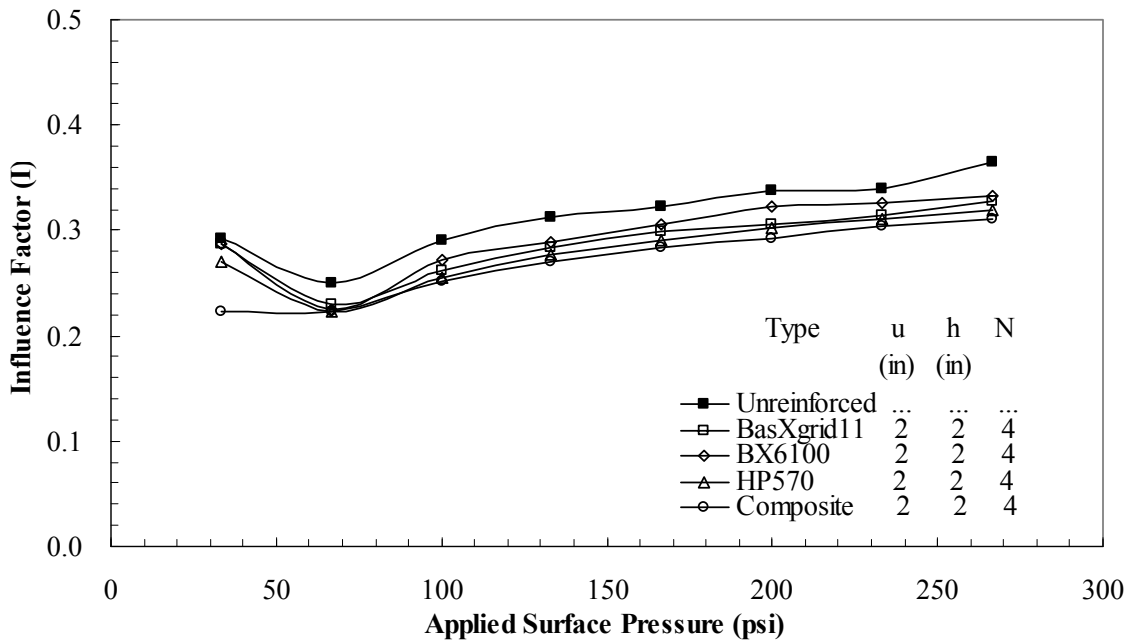
Figure 60
Stress influence factor (I) at a depth of 10 in. (1.67B) underneath the center of footing versus applied footing pressure for four layers of different types of reinforcement (B × L: 6 in. × 10 in., D_f / B = 1.0)
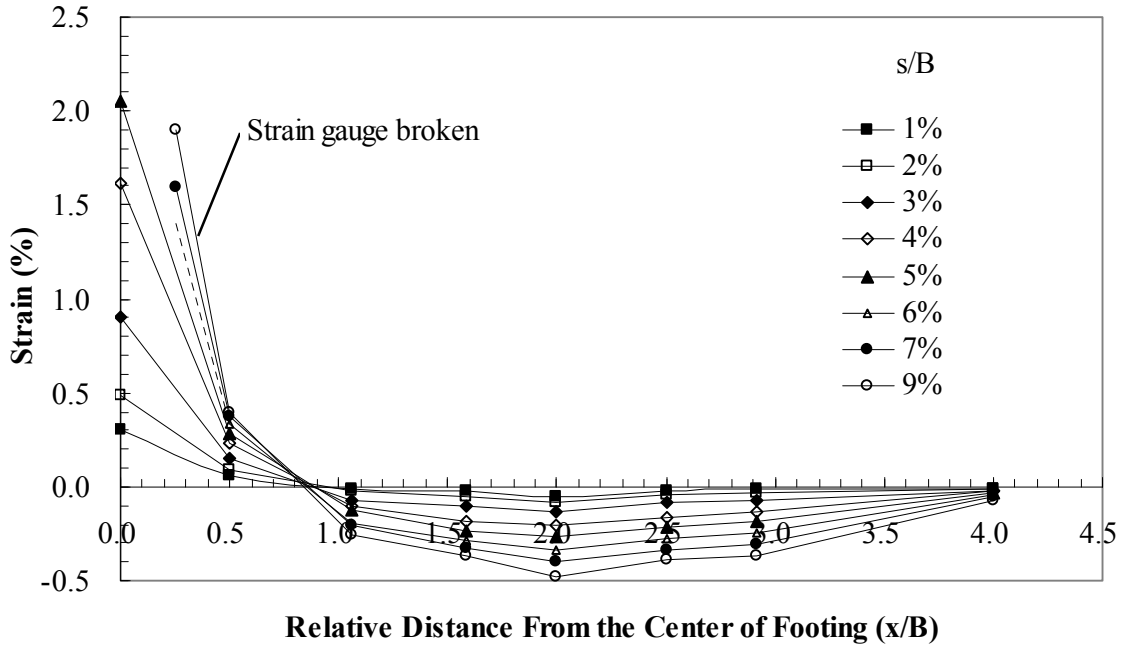
(a) at a depth of 2 in. (0.33B) below the footing
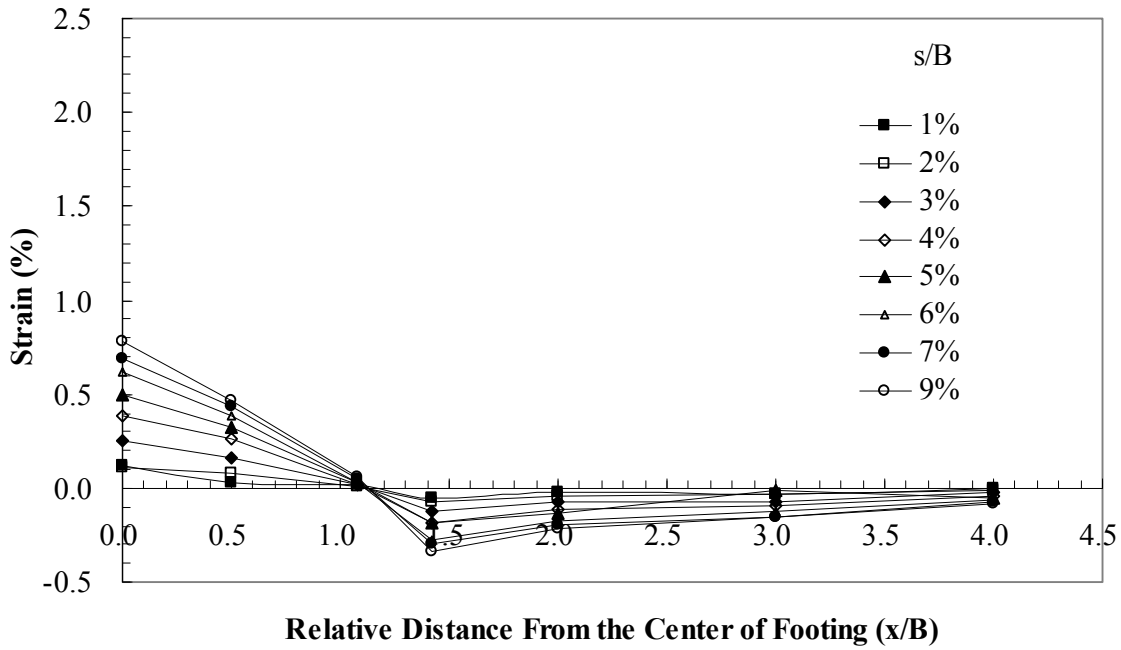
(b) at a depth of 8 in. (1.33B) below the footing

Figure 61
Strain distribution along the center line of geogrid
(B × L: 6 in. × 6 in.; D_f / B = 1.0)

Small-Scale Laboratory Tests on Reinforced Kentucky Crushed Limestone

The main objective of this study was to investigate the potential benefits of using the RSFs to improve the bearing capacity and reduce the settlement of shallow foundations on crushed limestone. For this purpose, extensive laboratory model tests were conducted on reinforced crushed limestone. The parameters investigated in the model tests include the number of reinforcement layers (N), and the tensile modulus of reinforcement.

Five types of geogrids including BX1100, BX1200, BX1500, BasXgrid 11 and MS330, one type of steel wire mesh, and one type of steel bar mesh, were used as reinforcements. The physical and mechanical properties of these reinforcements were presented earlier in table 2.

The measured dry densities for Kentucky crushed limestone test sections with and without reinforcement inclusion varied from 140 lb/ft^3 to 146 lb/ft^3 (2,243 to 2,333 kg/m^3), with moisture contents ranging from 5.5 to 6%. The corresponding geogauge stiffness moduli were in the range of 10,153 to 13,053 psi (70 to 90 MPa).

The results of the laboratory model tests for all crushed limestone test sections are summarized in table 8. In this table the BCRs obtained at settlement ratios, (s/B) = 3%, 5% and 10%, are presented. The results of the model footing tests are also graphically presented in figures 62 through 64. Figure 62 depicts the pressure-settlement curves measured for model footing tests on limestone reinforced with a single layer of different types of reinforcements. The measured pressure-settlement curves for model footing tests with two and three layers of different types of reinforcements are presented in figure 63 and figure 64, respectively. Because of the loading capacity limitation of the hydraulic jack used in this study, some tests were not possible to be loaded to failure. The bearing capacity is then obtained at different settlement ratios and used to calculate the BCRs.

Effect of Number of Reinforcement Layers

Several laboratory model footing tests were conducted on the crushed limestone reinforced with multiple layers of reinforcement. Seven different types of reinforcement were used: geogrid, including BX1100, BX1200, BX1500, BasXgrid11, and MS330; and steel, including steel wire mesh, SWM, and steel bar mesh, SBM. The reinforcement layers were placed at a spacing of 2 in. (h/B=0.33). Figures 62 through 64 show that the performance of crushed limestone foundation was improved noticeably for all types of reinforcement with even one layer of reinforcement. The effect of number of reinforcement layers on the BCRs is presented in figure 65 at settlement ratios of *s/B*=3% and 10%. As shown in the figures, the BCRs increase with increasing number of reinforcement layers. Figure 65 illustrates that the

effect of number of layers is more appreciable at s/B = 10% than at s/B = 3%. It is obvious that the reinforced benefit is directly related to the footing settlement, which can be explained by achieving better mobilizing of the reinforcements. The effect of number of reinforcement layers on the settlement reduction factor (SRF) is shown in figure 66 at footing pressures of 290.1 psi and 797.7 psi (2000 kPa and 5500 kPa). The inclusion of the reinforcement obviously reduces the immediate footing settlement. The figure also shows that the SRFs decrease with increasing number of reinforcement layers. With three layers of reinforcement, the immediate footing settlement can even be reduced by about 60% at a footing pressure of 797.7 psi (5500 kPa) for all types of reinforcement.

Table 8
Summary of model tests for crushed limestone

Test No.	Reinforcement configuration	u in.	h in.	s/B = 3%		s/B = 5%		s/B = 10%.	
				q, psi	BCR	q, psi	BCR	q, psi	BCR
LNR	Unreinforced	...	...	430.5	...	584.6	...	750.7	...
LGG41	N=1, BX1100	2	...	442.0	1.03	605.2	1.04	828.1	1.10
LGG42	N=2, BX1100	2	2	447.3	1.04	618.7	1.06	942.8	1.26
LGG43	N=3, BX1100	2	2	464.1	1.08	685.4	1.17	1143.9	1.52
LGG51	N=1, BX1200	2	...	474.7	1.10	681.6	1.17	962.2	1.28
LGG52	N=2, BX1200	2	2	502.4	1.17	742.8	1.27	1107.8	1.48
LGG53	N=3, BX1200	2	2	512.4	1.19	764.2	1.31	1260.8	1.68
LGG61	N=1, BX1500	2	...	476.5	1.11	694.7	1.19	1004.7	1.34
LGG62	N=2, BX1500	2	2	503.6	1.17	750.7	1.28	1247.3	1.66
LGG63	N=3, BX1500	2	2	530.6	1.23	799.5	1.37	1346.9	1.79
LGG11	N=1, BasXgrid11	2	...	455.0	1.06	654.4	1.12	891.0	1.19
LGG12	N=2, BasXgrid11	2	2	459.1	1.07	668.0	1.14	972.4	1.30
LGG13	N=3, BasXgrid11	2	2	485.2	1.13	734.1	1.26	1268.3	1.69
LGG71	N=1, MS330	2	...	443.6	1.03	641.0	1.10	965.6	1.29
LGG72	N=2, MS330	2	2	446.6	1.04	649.6	1.11	1066.2	1.42
LGG73	N=3, MS330	2	2	466.2	1.08	709.2	1.21	1240.5	1.65
LSWM1	N=1, SWM	2	...	505.5	1.17	720.9	1.23	1049.1	1.40
LSWM2	N=2, SWM	2	2	519.1	1.21	804.5	1.38	1498.4	2.00
LSWM3	N=3, SWM	2	2	599.0	1.39	951.9	1.63	1788.0	2.38
LSBM1	N=1, SBM	2	...	538.0	1.25	784.0	1.34	1199.3	1.60
LSBM2	N=2, SBM	2	2	664.1	1.54	1079.5	1.85	2017.5	2.69
LSBM3	N=3, SBM	2	2	669.5	1.56	1081.0	1.85	2137.9	2.85
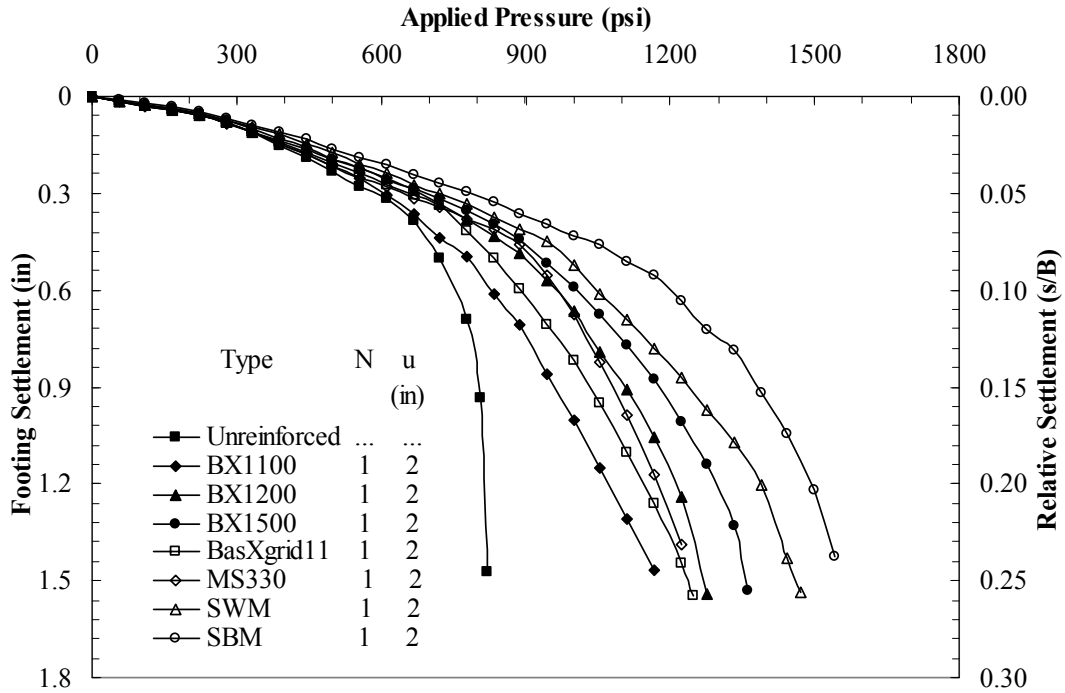
Figure 62
Pressure-settlement curves for model footing tests with single layer of different types of reinforcements
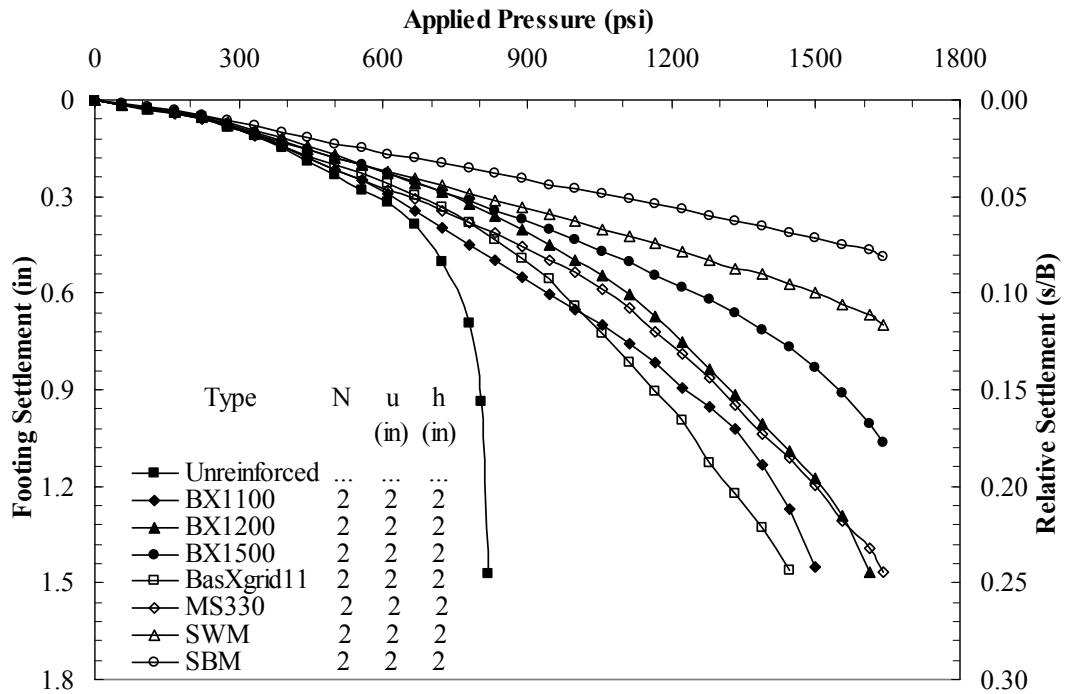
Figure 63
Pressure-settlement curves for model footing tests with two layers of different types of reinforcements
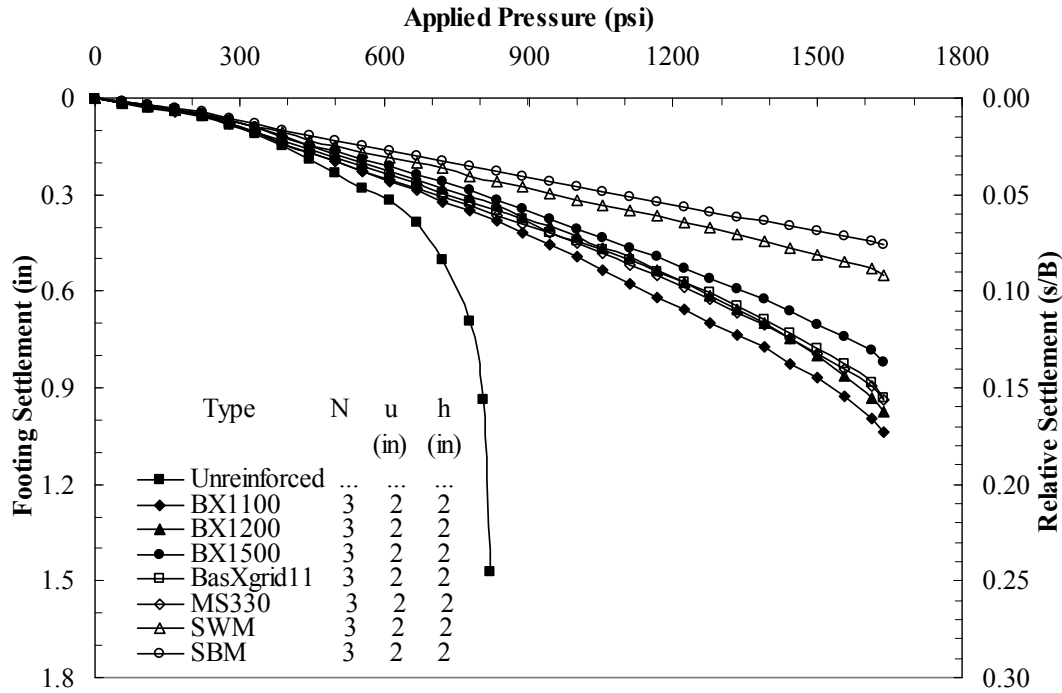
Figure 64
Pressure-settlement curves for model footing tests with three layers of different types of reinforcements

Effect of Tensile Modulus and Type of Reinforcement

Seven different types of reinforcements were used to reinforce crushed limestone in the model footing tests. The properties of these reinforcements were presented earlier in table 2. The BX1100, BX1200, and BX1500 geogrids are made of the same material and have similar structure (single layer/extruded). BX1200 geogrid has higher tensile modulus than BX1100 geogrid. As seen in figures 62 through 64, the crushed limestone reinforced by BX1200 geogrid performs better than that reinforced by BX1100 geogrid. BX1500 geogrid, which has the highest tensile modulus among these three geogrids, has the best performance. As compared to BX1200 geogrid, BasXgrid11 geogrid (woven) and MS330 geogrid (multilayer/extruded) have different structure and smaller aperture sizes but with almost similar tensile modulus. In the meanwhile, the similar performance of crushed limestone reinforced with BX1200 geogrid, BasXgrid11 geogrid, and MS330 geogrid was observed in the present study. This result suggests that the structure and aperture size of geogrid within the examined range have minimal influence on the performance of the reinforced crushed limestone, which indicates similar degree of geogrid-crushed limestone interlocking. To further study the effect of tensile modulus, two stiff metal grid reinforcements were used in
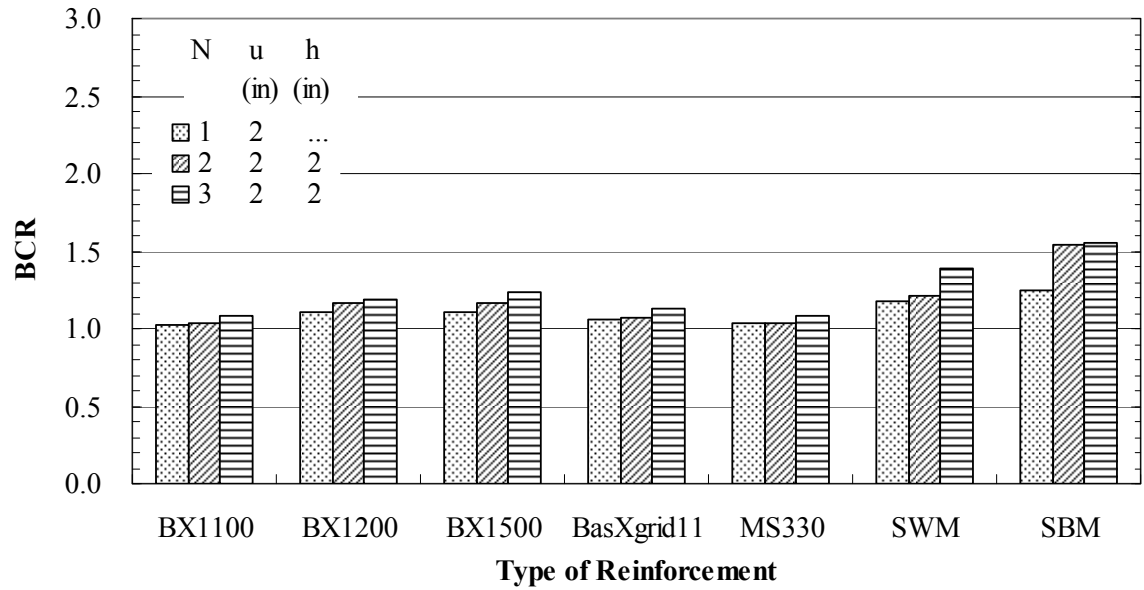
(a) s/B = 3%
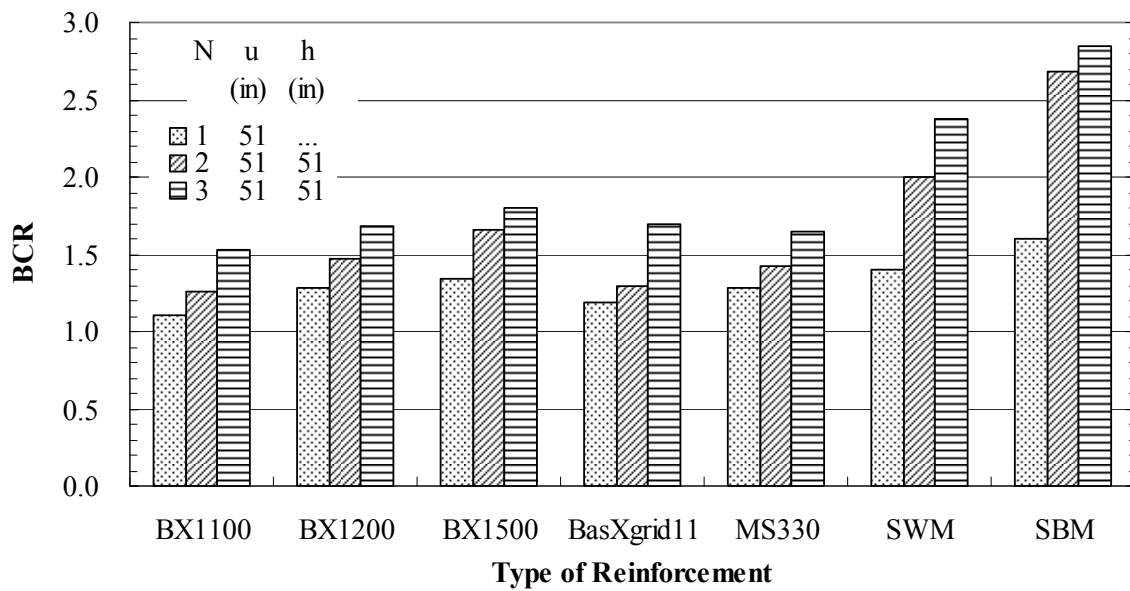
(b) s/B = 10%

Figure 65
BCR versus type of reinforcement
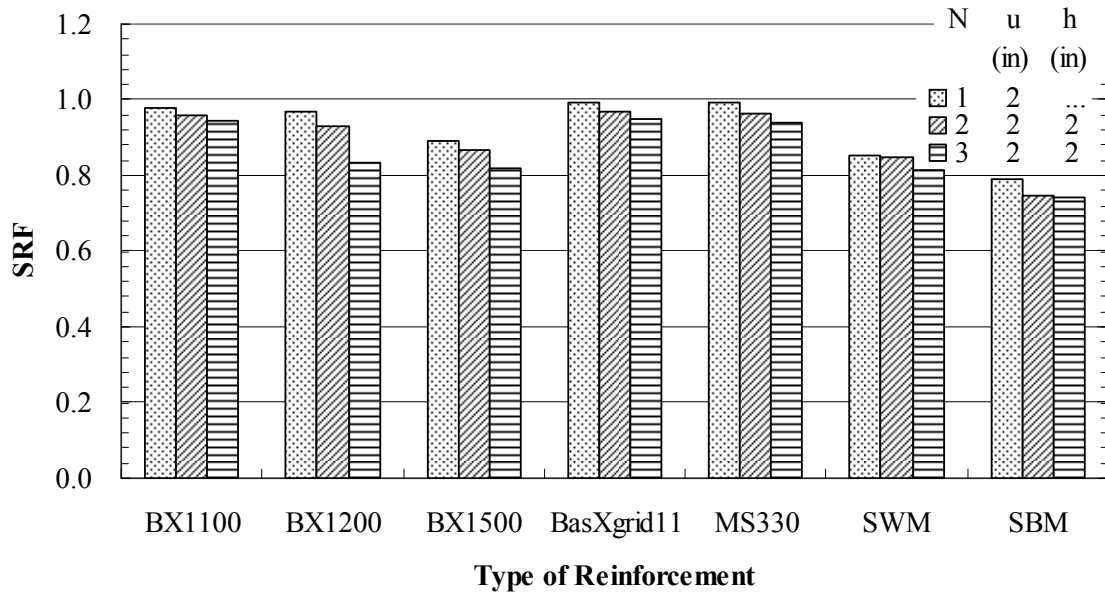
(a) q = 290.1 psi
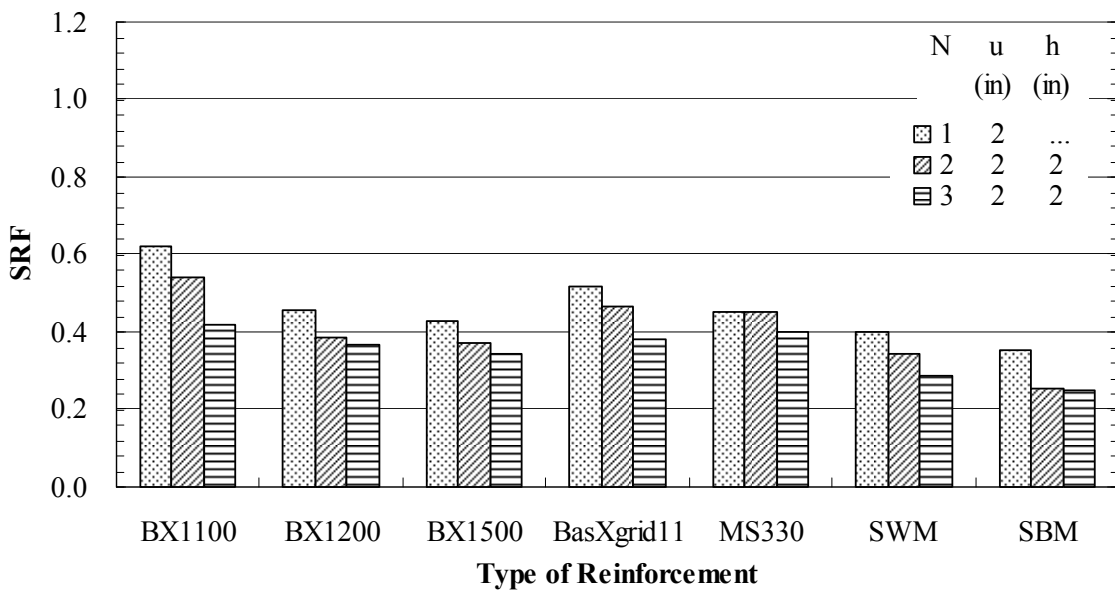
(b) q = 797.7 kPa

Figure 66
SRF versus type of reinforcement

the present study: steel wire mesh (SWM) and steel bar mesh (SBM). SWM has a tensile modulus of about 30 times higher than the geogrids used in the present study, and the tensile modulus of SBM is approximately three times higher than that of SWM. Figures 62 through 64 indicate that the crushed limestone reinforced with SWM and SBM performs much better than those reinforced with geogrids. For three layers of reinforcement at settlement ratio of s/B=10%, BCRs of SWM and SBM reinforced crushed limestone are nearly 1.4 and 1.6 times larger than that for geogrid reinforced crushed limestone, respectively. As shown in figures 65, this study clearly demonstrates that the performance of reinforced crushed limestone improves with increasing the tensile modulus of reinforcement. However, the effect of reinforcement tensile modulus at low settlement ratio (e.g., s/B=2%) is not significant when compared to that at a settlement ratio of s/B=10%. For example, at s/B=2%, the BCR of reinforced crushed limestone for three layers of SBM (with the highest tensile modulus) is 29% higher than that for three layers of BX1100 geogrid (with the lowest tensile modulus); while this difference increases to 88% as the settlement ratio increases to s/B=10%. So the effect of reinforcement modulus seems to be a function of footing settlement. Again, this can be explained by achieving better mobilization of the reinforcement with increasing footing settlement.

The BCRs at different settlement ratios (*s/B*) for the model tests on crushed limestone section reinforced with multiple layers of different types of reinforcement are presented in figure 67. It can be seen that the BCRs increase with the increase of settlement ratio (*s/B*). At relatively low settlement ratio (*s/B*), the increase of the bearing capacity of SWM and SBM reinforced sections has marginal difference from geogrid reinforced sections. However, with the increase of settlement ratio (*s/B*), the BCRs of footings on SWM and SBM reinforced sections increase at a faster rate compared to those on geogrid reinforced sections

Figure 68 depicts the settlement reduction factors (SRF) as a function of applied footing pressure (*q*) for the model tests on crushed limestone section reinforced with multiple layers of different types of reinforcement. As shown in figure 68, higher modulus geogrids provide better reduction in settlement than lower modulus geogrids, while the settlements of SWM and SBM reinforced sections are much smaller than those of geogrid reinforced sections. In all cases, the SRFs decrease with increasing the footing pressure, and the rate of decrease of SRFs increases suddenly at footing pressure of about 652.7 psi (4500 kPa). This trend may be expected in the light of the fact that the ultimate bearing capacity of unreinforced crushed limestone is close to 652.7 psi (4500 kPa).
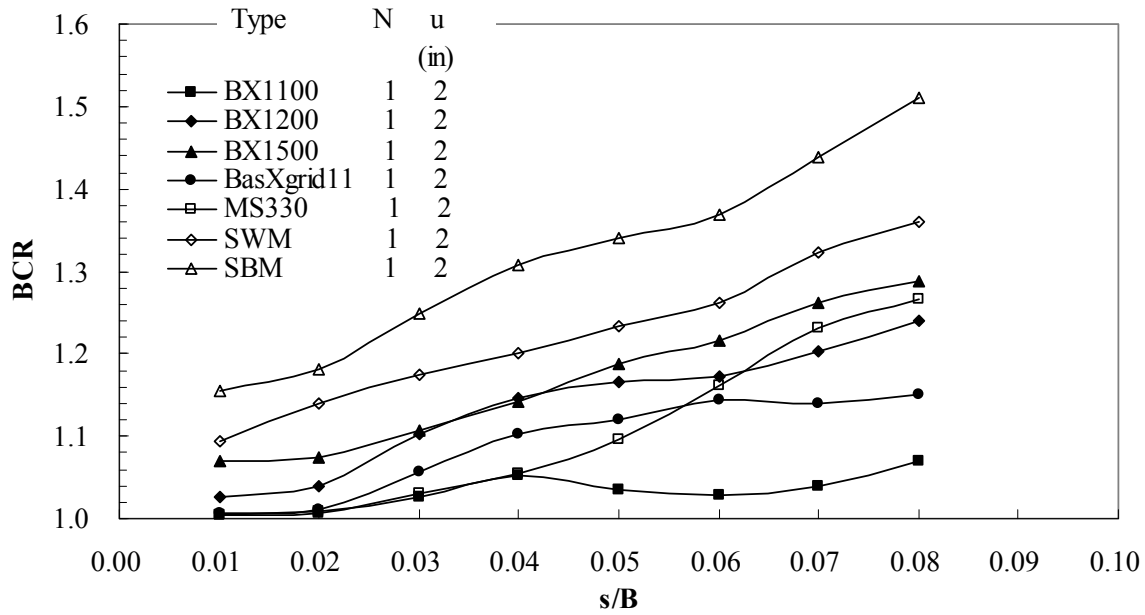
(a) One layer of reinforcement
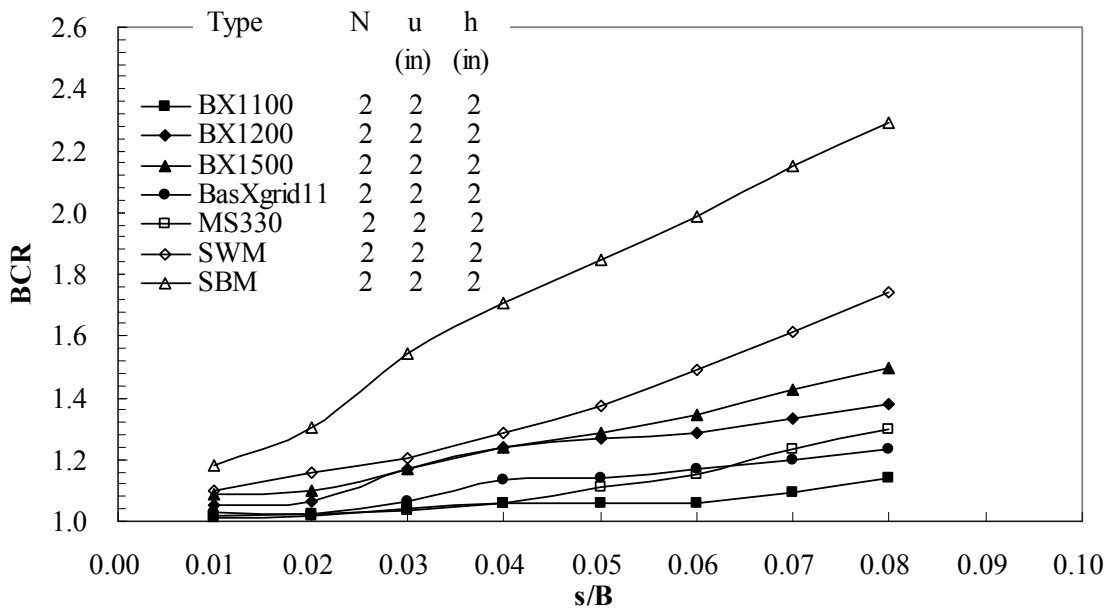
(b) Two layers of reinforcement

Figure 67
BCR versus settlement ratio (s/B)
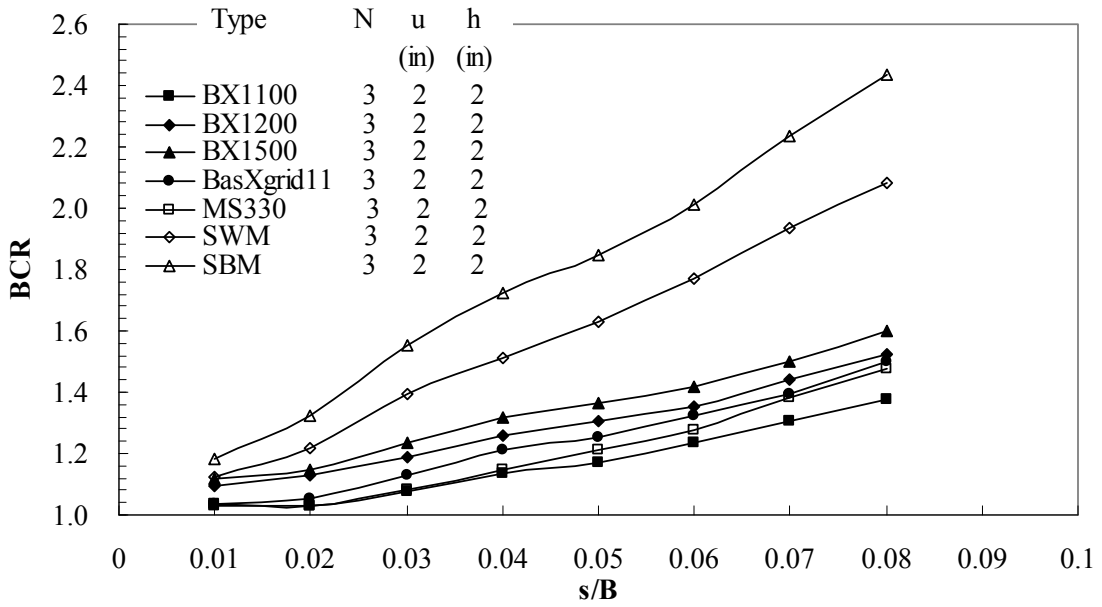
(c) Three layers of reinforcement

Figure 67
(continued)
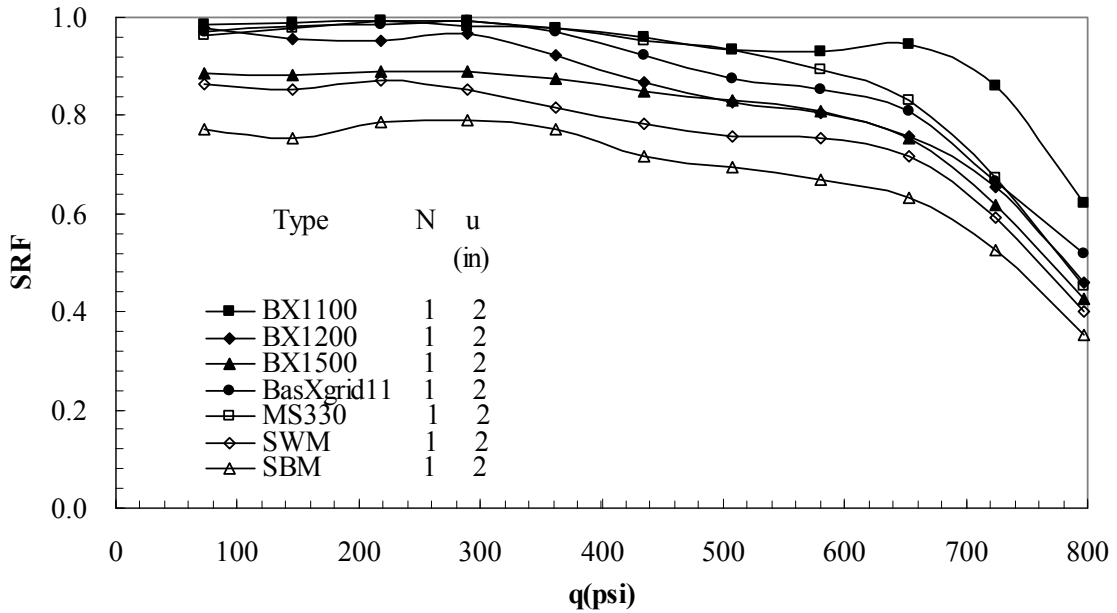
(a) One layer of reinforcement

Figure 68
SRF versus applied footing pressure (q)
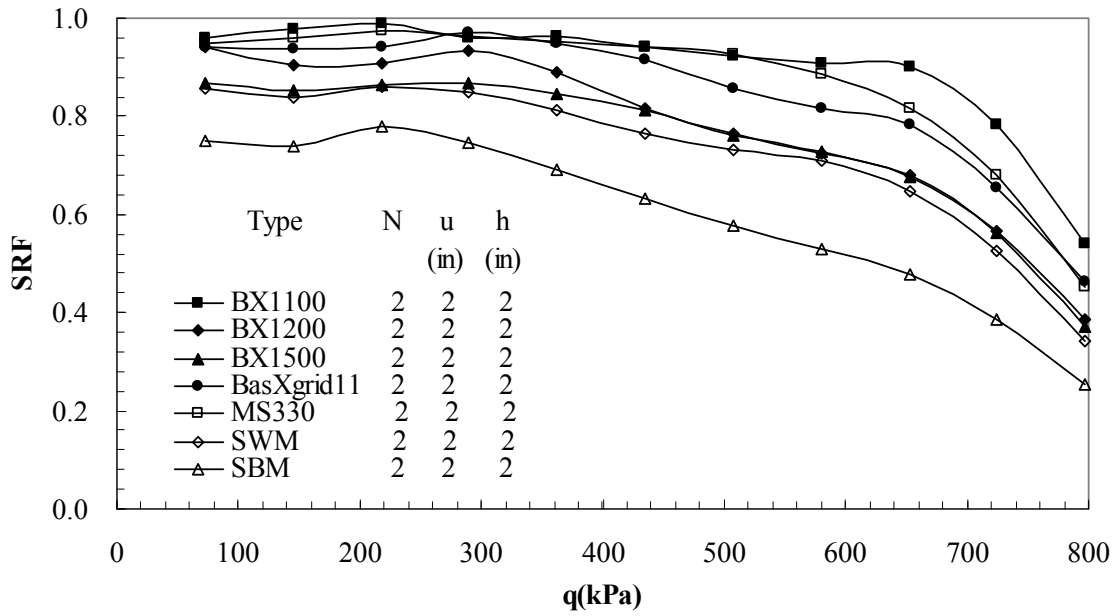
(b) Two layers of reinforcement
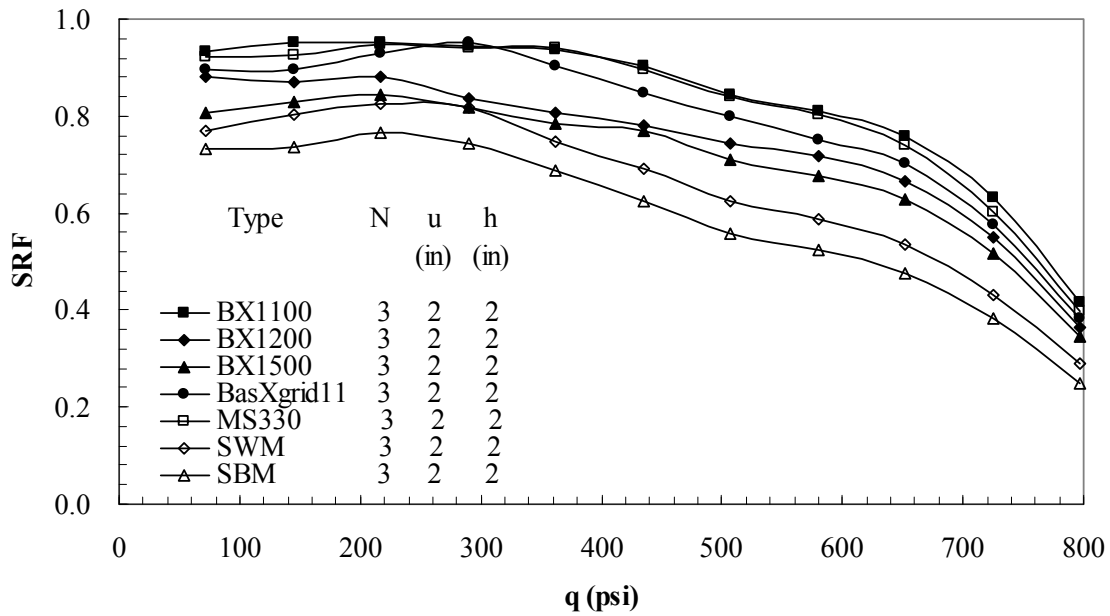
(c) Three layers of reinforcement

**Figure 68
(continued)**

Large-Scale Field Tests on Reinforced Silty Clay Embankment Soil

A review of existing literature revealed that most of experimental studies on geosynthetic reinforced soils were conducted using small-scale laboratory tests. Due to scale effect, it is not easy to accurately model the full-scale behavior of reinforced soil with small-scale laboratory tests. Six large scale field tests, therefore, were conducted on geosynthetic reinforced silty clay embankment soils to investigate the potential benefits of using the RSFs to improve the bearing capacity and to reduce the settlement of shallow foundations. The parameters investigated in the field tests include the number of reinforcement layers (N), the vertical spacing between reinforcement layers (h), and the tensile modulus of reinforcement. The experimental study also includes investigating the vertical stress distribution in the silty clay embankment soils and the strain distribution along the reinforcement.

Three types of geogrids, BX6100, BX6200, and BX1500, were used as reinforcement in the field tests. The physical and mechanical properties of these reinforcements were presented in table 2. The measured dry densities for Kentucky crushed limestone test sections with and without reinforcement inclusion varied from 109.9 pcf to 112.9 pcf (1,760 to 1,808 kg/m³), with moisture contents ranging from 15.81 to 16.84%.

Based on the laboratory model test results, the top layer spacing of geogrid for all field tests were kept constant with the value of u=0.33B. For all tests, all geogrids were placed within the depth of d=1.67B with the bottom layer kept at a depth of 1.67B. The vertical spacing between reinforcement layers can then be determined for each test as:

$$h = \frac{d - u}{N - 1} \tag{4}$$

The results of the field tests for unreinforced and reinforced silty clay test sections are summarized in table 9. In this table, the BCRs obtained at settlement ratios of $s/B = 3\%$, 5% and 10% are presented. The results of the model footing tests are also graphically drawn in figure 69. Investigating the pressure-settlement curves, we can see that the pressure keeps increasing with an increase in the settlement for both unreinforced and reinforced silty clay test sections. This settlement pattern resembles a typical punching-shear failure. Since the failure point is not well defined, the bearing capacity obtained at different settlement ratios is used to calculate the BCRs.

Table 9
Summary of field tests for silty clay embankment soil

Reinforcement configuration	u in.	h in.	s/B = 3%		s/B = 5%		s/B = 10%	
			q, psi	BCR	q, psi	BCR	q, psi	BCR
Unreinforced[*]	...	...	72.5	...	92.5	...	129.9	...
N=4, BX6100[*#]	6	8	85.7	1.18	111.8	1.21	160.7	1.24
N=3, BX6200[*]	6	12	80.9	1.12	105.1	1.14	153.0	1.18
N=4, BX6200[*#]	6	8	92.9	1.28	119.6	1.29	172.0	1.32
N=5, BX6200[*]	6	6	102.8	1.42	136.7	1.48	191.6	1.48
N=4, BX1500[*#]	6	8	98.5	1.36	132.4	1.43	188.8	1.45

* Instrumented with pressure cell
# Instrumented with strain gauge
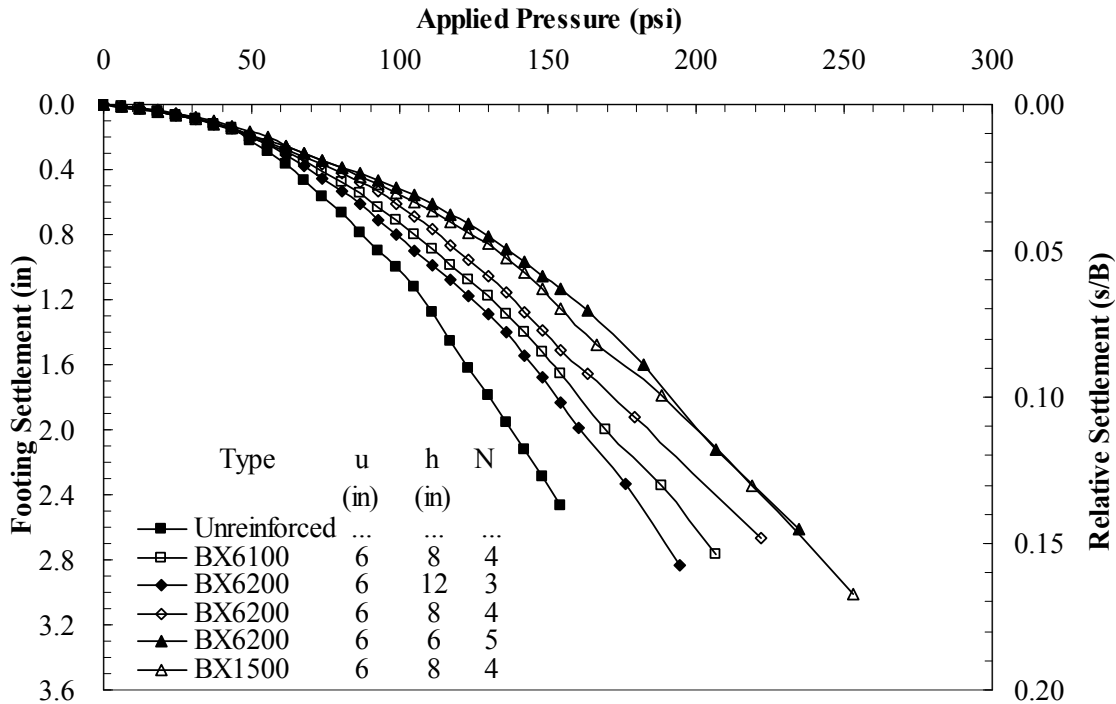
Figure 69
Pressure-settlement curves for large-scale model footing tests

Effect of Number and Vertical Spacing of Reinforcement Layers

The effect of number and vertical spacing of reinforcement layers was investigated using multilayers of BX6200 with a top layer spacing of 6 in. (0.33B). The following reinforcement layers/spacing combinations were chosen to study this effect in the present study: three layers placed at 12 in. spacing; four layers placed at 8 in. spacing; and five layers

placed at 6 in. spacing. Figure 69 presents the pressure-settlement curves of these model tests as compared with unreinforced section. Figure 70 depicts the variations of BCRs obtained at settlement ratios of s/B=3%, 5%, and 10% for different numbers of reinforcement layers (N) and reinforcement spacing ratios (*h/B*). It is obvious that the BCR values increase with increasing number of reinforcement layers and decreasing vertical spacing of reinforcement layers with maximum BCR at N = 5 and h = 0.33B. Therefore, for all geogrids placed within influence depth, smaller reinforcement spacing (i.e., more reinforcement layers) should always be examined as an alternative of using higher geogrid tensile modulus, provided that its cost is justified. This subject is discussed later in the report.

Investigating the load-settlement curves, we can see that the shapes and slopes of curves of reinforced soil foundations are very similar to those of unreinforced soil foundations when the settlement ratio (s/B) is less than 0.01; and that the reinforcement effect starts being mobilized when the s/B ratio is greater than 0.01.
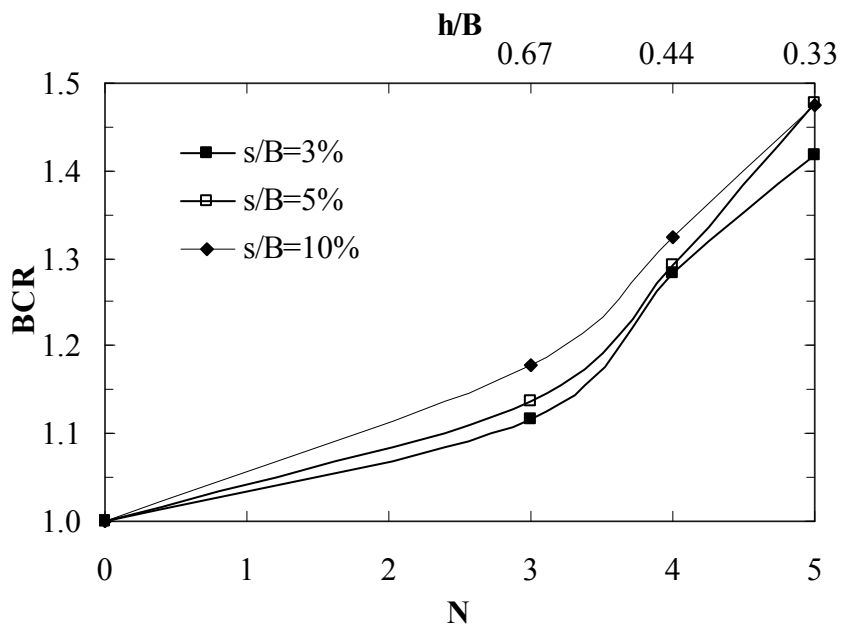
Figure 70
BCR versus *N* and *h/B* at different settlement ratios (s/B)

Effect of Tensile Modulus of Reinforcement

Three different types of geogrid with different tensile modulus were used in the large scale field tests. These include BX6100 geogrid, BX6200 geogrid, and BX1500 geogrid, the properties of which were presented in table 2. Figure 69 compares the pressure-settlement curves obtained for the different types of reinforcements on model tests conducted with four

reinforcement layers placed at top layer spacing of 6 in. and vertical spacing of 8 in. The BX6100 and BX6200 geogrids are made of the same material and have similar aperture size, but BX6200 has a higher tensile modulus than BX6100. Figure 69 shows that the silty clay reinforced by BX6200 geogrid performs better than that reinforced by BX6100 geogrid. The figures also show that BX1500 geogrid, which has the highest tensile modulus and smallest aperture size, has the best performance of the three types of geogrid used. This effect can be more clearly seen in figure 71.

The BCRs at different settlement ratios (s/B) for model tests with multiple layers of different types of reinforcement are presented in figure 72. It can be seen that the BCR generally increases with the increase of settlement ratio (s/B). It is also noted that the *BCR* increases significantly only after the s/B ratio becomes greater than 1% at which it is believed that the reinforcing effect of geogrid starts to be mobilized. However, BCR only keeps substantially increasing up to a settlement ratio of s/B≈3%, and it remains more or less constant thereafter.

Figure 73 depicts the variation of the settlement reduction factors (*SRF*) as a function of footing pressure (*q*) for the model tests with multiple layers of different types of reinforcement. It is obvious that the inclusion of the reinforcement would reduce the immediate settlement significantly. With five layers of reinforcement, the settlement can be reduced by 40% at a relatively medium footing pressure (72.5 psi (500kPa)). The geogrid with higher modulus provides better reduction in immediate settlement than geogrid with lower modulus. In all cases, the SRF decreases with increasing footing pressure. It is also noted that the SRF decreases suddenly at a footing pressure of about 43.5 psi (300 kPa), and it becomes stabilized at a footing pressure of 101.5 psi (700 kPa) and higher. This behavior may be expected in light of the fact that the settlement ratio (s/B) is close to 1% at a footing pressure of 43.5 psi (300 kPa). As indicated earlier, the reinforcing effect of geogrid starts to be mobilized at $s/B = 1\%$.
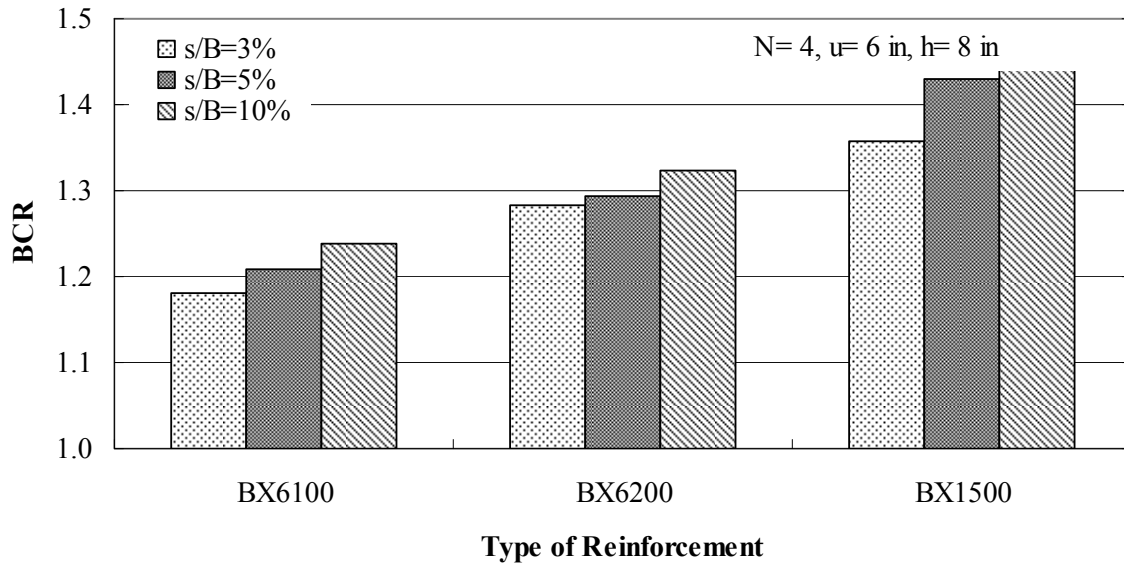
Figure 71
BCR versus type of reinforcement for silty clay
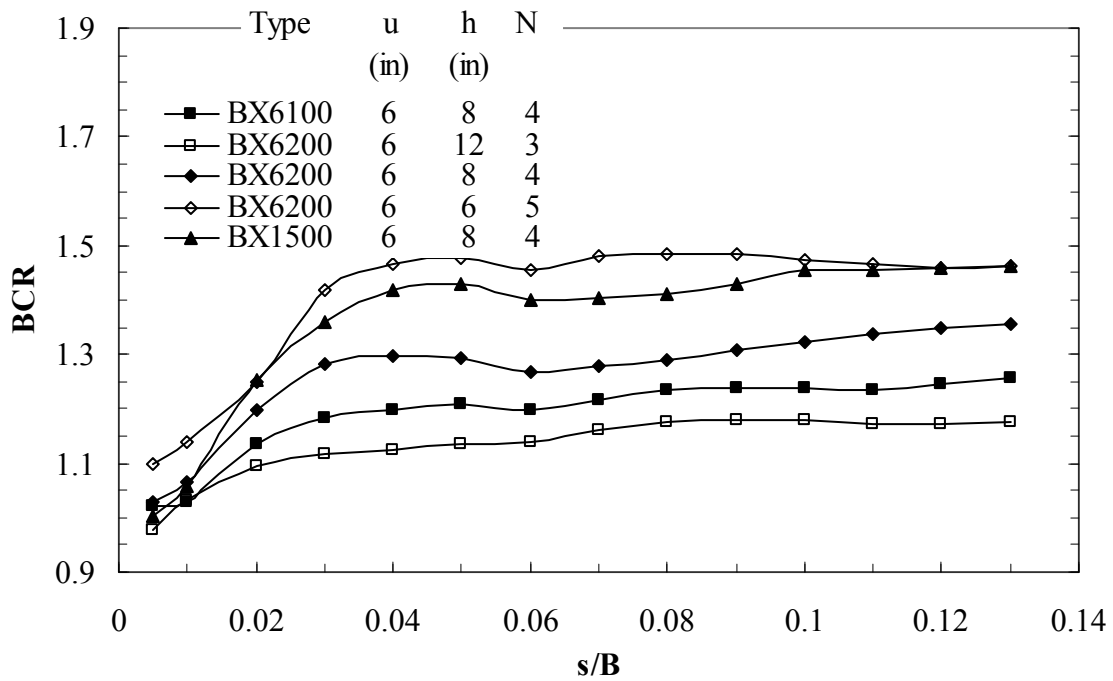
Figure 72
BCR versus settlement ratio (s/B)
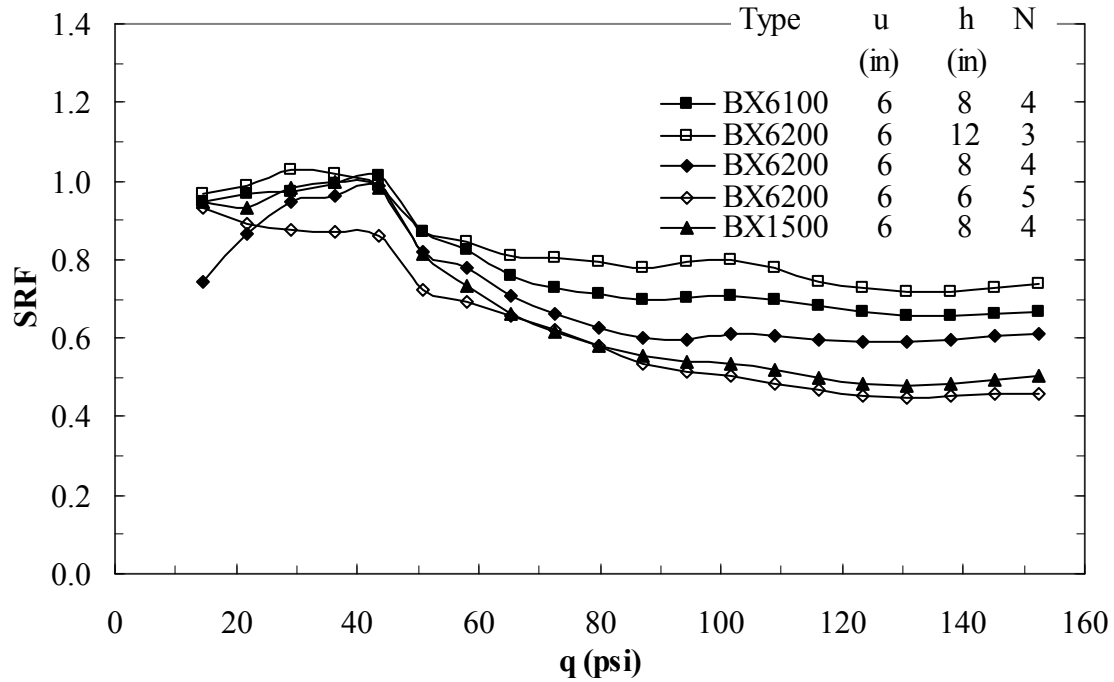
Figure 73
SRF versus applied footing pressure (q)

For all geogrids placed within influence depth, it is necessary to determine whether the design priority should be given for the number of reinforcement layers or for the reinforcement tensile modulus. The average modulus of reinforcement (E_{avg}) is introduced to help quantify the decision process. The average modulus of reinforcement is defined as the sum of tensile modulus of reinforcement for each layer, divided by the total depth of reinforcement. Because the tensile modulus of geogrid in machine direction and cross-machine direction is different, the mean value of tensile modulus in two directions is then used to calculate the average modulus of reinforcement.

$$E_{avg} = \frac{\sum\limits_{i=1}^{N}(J_{MDi} + J_{CDi})/2}{d} = \frac{N(J_{MD} + J_{CD})/2}{u + (N-1)h} \qquad (5)$$

where, J_{MDi} and J_{CDi} are tensile modulus in machine direction and cross machine direction for the ith layer of reinforcement, (lb./in.).

The average modulus of reinforcement for the five large-scale field tests on reinforced silty clay is calculated and presented in table 10. It can be seen from table 10 that the average modulus of the four layers of BX6100 placed at 8 in. spacing is smaller than that of the three layers of BX6200 placed at 12 in.; However, the four layers of BX6100 placed at 8 in.

spacing has better performance as compared to the three layers of BX6200 placed at 12 in. The same observation was also obtained for the five layers of BX6200 placed at 6 in. and the four layers of BX1500 placed at 8 in. Therefore, the design priority should be given for the number of reinforcement layers over the reinforcement tensile modulus when all geogrids are placed within influence depth and its cost is justified.

Table 10
Average modulus

Reinforcement configuration	u (in.)	h (in.)	E_{avg} (psi)
N=4, BX6100	6	8	166.7
N=3, BX6200	6	12	184.4
N=4, BX6200	6	8	245.8
N=5, BX6200	6	6	307.3
N=4, BX1500	6	8	352.8

Stress Distribution in Silty Clay Embankment Soil

All field tests were instrumented with pressure cells to evaluate the vertical stress distribution in silty clay embankment soil with and without reinforcement inclusion. Pressure cells were placed at specified locations/depth for this purpose. Figure 74 shows the measured vertical stress distributions along the center line of the footing at a depth of 30 in. (1.67B). The measured vertical stress distributions along the center line of the footing at a depth of 24 in. (1.33B) are presented in figure 75. For the unreinforced section of this depth, the vertical stress was only measured at the point under the center of footing due to the fact that not enough pressure cells were available at that time. Figure 76 depicts the measured vertical stress distributions along the center line of the footing at a depth of 18 in. (1.0B). Again, for the unreinforced section, the vertical stress was only measured at the point under the center of footing. The measured vertical stress distributions with depth below the center of footing are shown in figure 77. The variation of the stress influence factors (I) were computed at different depths under the center of the footing with applied footing pressures and presented in figures 78 through 80.

As can be seen from these figures, the reinforcement results in redistribution of the applied load to a wider area, thus avoiding stress concentration and achieving improved stress distribution. The induced maximum stresses beneath the center of the footing in reinforced silty clay are appreciably reduced compared to those in unreinforced silty clay. At a surface pressure of 6.2 psi and 67.9 psi (43 kPa and 468 kPa), the stress can be reduced up to 20%

and 26% at a depth of 18 in. (1.0B), 27% and 27% at a depth of 24 in. (1.33B), and 40% and 35% at a depth of 30 in. (1.67B) for five layers of BX6200 geogrid. The redistribution of load to a wider area below the reinforced zone usually results in reducing the consolidation settlement of underlying weak clayey soil, which is directly related to the induced stress.

Generally, for the same applied footing pressure, the vertical stresses under the center of footing decrease with increasing number of layers and decreasing vertical spacing of reinforcement layers (figures 74 through 76). As shown in figures 78 through 80, under the same footing pressure, the stress influence factor (*I*) decreases with the increase of the number of reinforcement layers and decrease of vertical spacing.

Among geogrids with the same material and aperture size, the geogrid with higher tensile modulus (BX6200) results in a better reduction of center stresses than the geogrid with lower tensile modulus (BX6100). The BX1500 geogrid, which has the highest tensile modulus and smallest aperture size among three types of geogrid, provides the best attenuation of the stresses below the center of footing.

The four layers of BX6100 placed at 8 in. spacing results in a better reduction of center stresses as compared to the three layers of BX6200 placed at 12 in. The same observation was also obtained for the five layers of BX6200 placed at 6 in. and the four layers of BX1500 placed at 8 inch. Again, the measured stress distribution shows that the benefit of increasing the number of geogrid layers on improved performance of reinforced soil foundation is larger than that of increasing the tensile modulus of geogrid when all geogrids are placed within influence depth.

Negative stresses were measured in unreinforced silty clay at approximately 3.0B from the center of footing. This result indicates that the soil is pushed upward at a distance of around 3.0B from the center of footing. The similar behavior is observed only in reinforced silty clay with three layers of BX6200 geogrid placed at a spacing of 12 in., but the values of measured negative stresses are smaller than those in unreinforced silty clay. This again confirms that the inclusion of reinforcement can develop a "surcharge effect" to prevent soil from moving upward, and thus improve the bearing capacity of silty clay.

Because of a serviceability requirement, the design of foundations is generally controlled by settlement criterion. To evaluate the settlement of foundation, the stress distribution in soil due to applied load should be evaluated. Currently, methods based on elastic solutions such as the Boussinesq solution and Westergaard solution are generally used to evaluate the stress

distribution in foundation application. The comparison between the measured values and those calculated from using these elastic methods can help understanding the application of these methods for reinforced soil.

Based on the Boussinesq solutions, the vertical stress in soil at a depth z under the corner of a uniformly loaded rectangular area can be computed from the following equation:

$$\Delta\sigma_z = qI_B$$
(6)

where, $\Delta\sigma z$ is the increase in vertical stress due to the applied load, q is the applied footing pressure, I_B is the stress influence factor for Boussinesq solution.

For soil reinforced by stiff horizontal layers which prevent horizontal deformation, the elastic solution was given by Westergaard [28]. Similar to the Boussinesq solution, the vertical stress in Westergaard material is at a depth of z. Under the corner of a rectangular uniformly loaded area can be evaluated as:

$$\Delta\sigma_z = qI_W$$
(7)

where, I_W is the stress influence factor for the Westergaard solution.

The comparisons between the measured and calculated vertical stress distributions are presented in figures 74 through 77 for footing pressures of 6.2 psi (43 kPa) and 67.9 psi (468 kPa). The comparison at other applied footing pressures can be found in Chen [26]. Figures 78 through 80 show the comparison between the corresponding measured and calculated stress influence factors.

For vertical stress distribution along the centerline of the footing (figures 74 through 76), Boussinesq solution matches the measured values for some cases of reinforced soil at a footing pressure of 67.9 psi (468 kPa) and lower, except for overestimation of vertical stress distribution at a depth of 24 in. for a footing pressure of 6.2 psi (43 kPa). On the other hand, Westergaard solution matches the measured values for some cases of reinforced soil at a depth of 30 in. and 24 in. for a footing pressure of less than 37 psi (255 kPa), while it underestimates the measured vertical stress distribution in reinforced soil immediately below the footing at a depth of 18 in. for all footing pressure levels. Both solutions underestimate the measured vertical stresses in reinforced soil at higher footing pressures immediately below the footing, especially at the point where the maximum vertical stress occurred. As compared to unreinforced case, it can be seen from figure 74 that Boussinesq solution

underestimates the maximum vertical stress beneath the center of footing at a depth of 30 in., but with wider stress distribution.

For vertical stress distribution along the depth at the center of footing (figures 77 through 80), the match between the Boussinesq and measured vertical stress distribution for unreinforced soil at a relatively low footing pressure of 6.2 psi (43 kPa) is fairly good while Westergaard solution underestimates the measured vertical stress distribution for reinforced soil. At relatively medium footing pressures of 37 psi (255 kPa) and 67.9 psi (468 kPa), Boussinesq solution matches the measured vertical stress distribution for some cases of reinforced soil. At a footing pressure of 104.9 psi (723 kPa) and higher, both Boussinesq and Westergaard solutions underestimate the measured vertical stress distributions for all cases. This behavior may be expected in the light of the fact that Boussinesq and Westergaard solutions assume elasticity and constant modulus of elasticity of soil. These assumptions may be justified at low footing pressures, but at high footing pressures, it cannot stand. Figures 78 through 80 also show that the stress influence factors (I) are load dependent values, which increase with the increase of footing pressures, instead of a constant value as indicated by the elastic solutions such as Boussinesq and Westergaard solutions.

The above comparison showed that elastic solutions have some limitations in predicting the vertical stress distribution in unreinforced and reinforced silty clay soil. However, under a relatively medium applied pressure, these elastic solutions can give an acceptable estimation of the stress distribution in silty clay soil, while at a relatively high applied pressure, a correction coefficient needs to be applied for underestimated values.

Strain Distribution Along Reinforcement
Three field tests on silty clay reinforced with four layers of geogrids (BX6100, BX6200, BX1500) were instrumented with strain gauges to evaluate the strain distribution along the reinforcement. The geogrids with instrumentations were placed at the top and bottom layers (at a depth of 6 in. (0.33B) and 30 in. (1.67B), respectively). During the installment of the geogrid in the test, considerable care was taken to place the geogrid as flat as possible, but local bending was still likely to happen, especially during the subsequent compaction and loading process. In order to cancel/minimize the influence of bending of the geogrid on the interpretation of tensile force, therefore, a pair of strain gauges system was installed on the geogrids (one attached to the top face of geogrid and the other one attached to the bottom face of geogrid). The average reading from the pair of strain gauges was then used to calculate the strain and eventually the tensile force developed in the geogrid. The variations
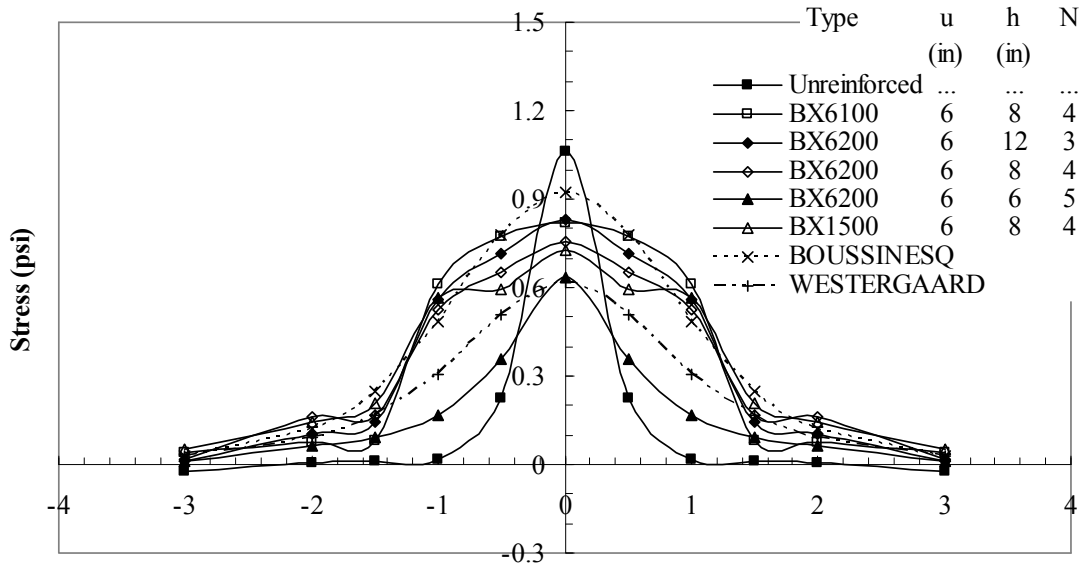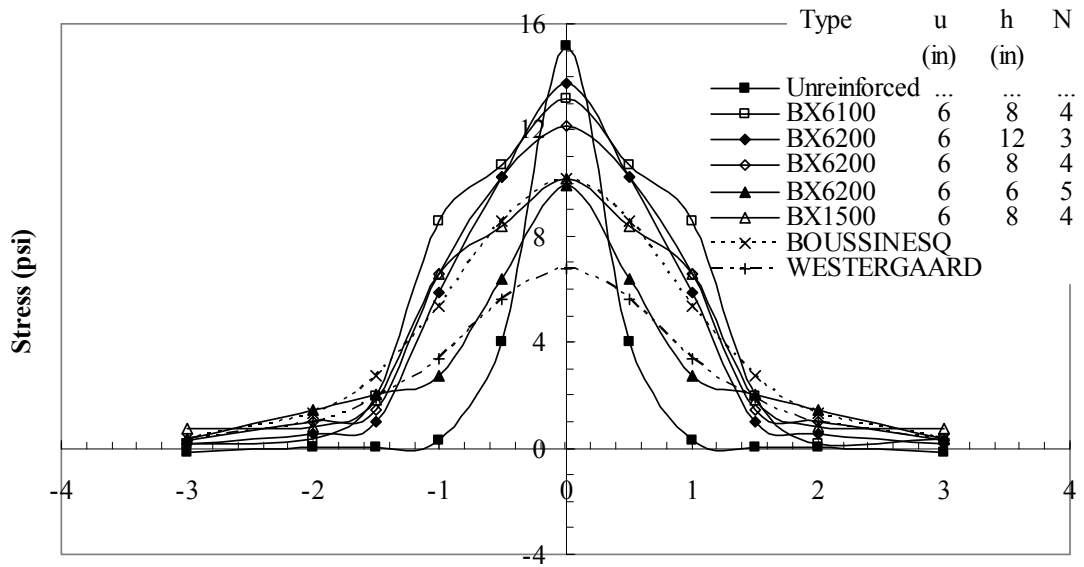
(a) Applied footing pressure q = 6.2 psi

(b) Applied footing pressure q = 67.9 psi

Figure 74
Measured and calculated stress distribution along the center line of footing at a depth of 30 in.
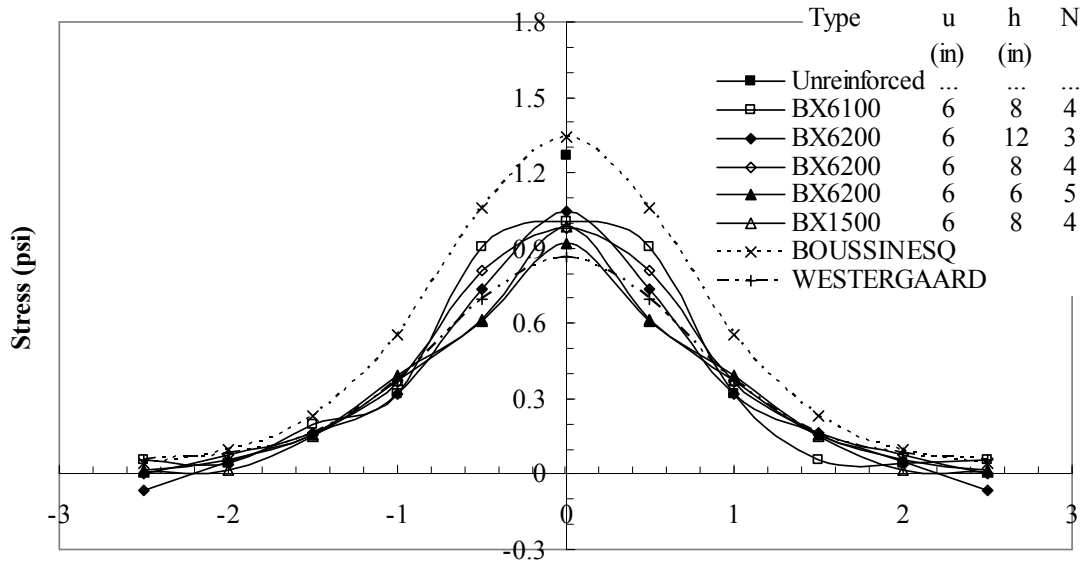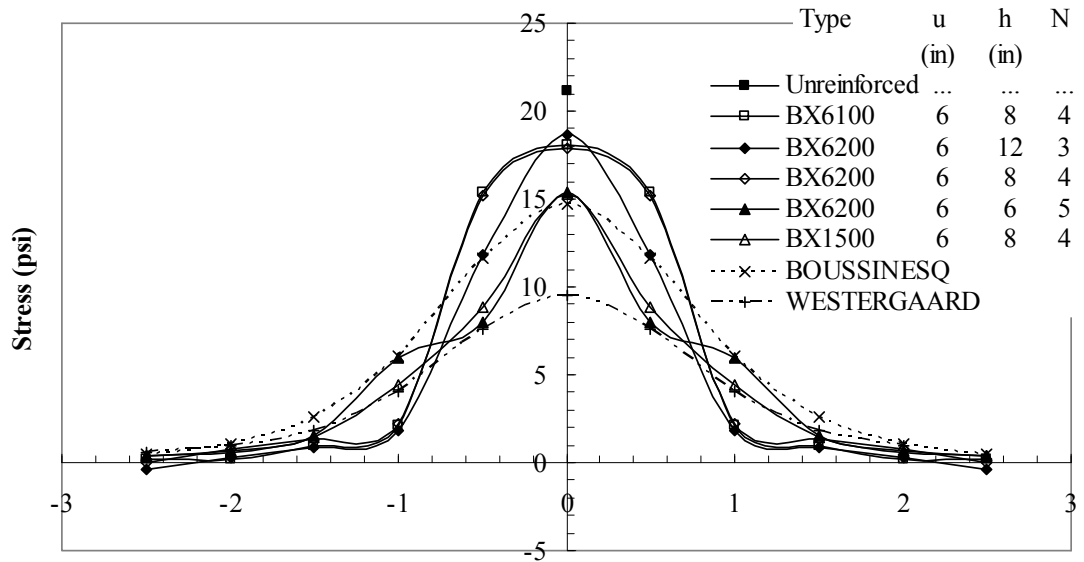
(a) Applied footing pressure q = 6.2 psi

(b) Applied footing pressure q = 67.9 psi

Figure 75
Measured and calculated stress distribution along the center line of footing at a depth of 24 in.
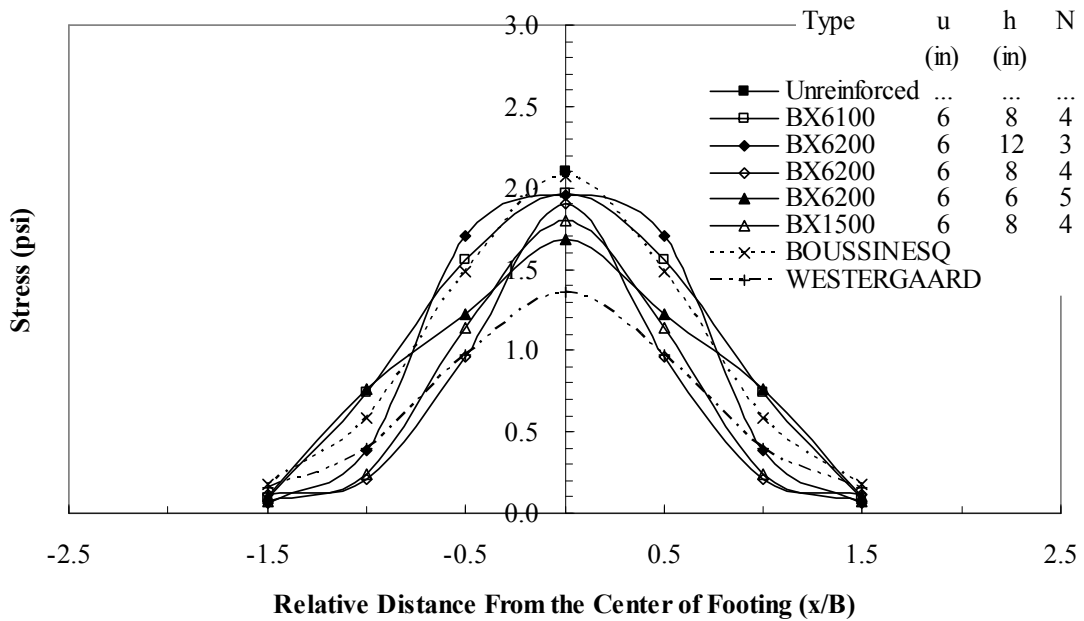
(a) Applied footing pressure q = 6.2 psi
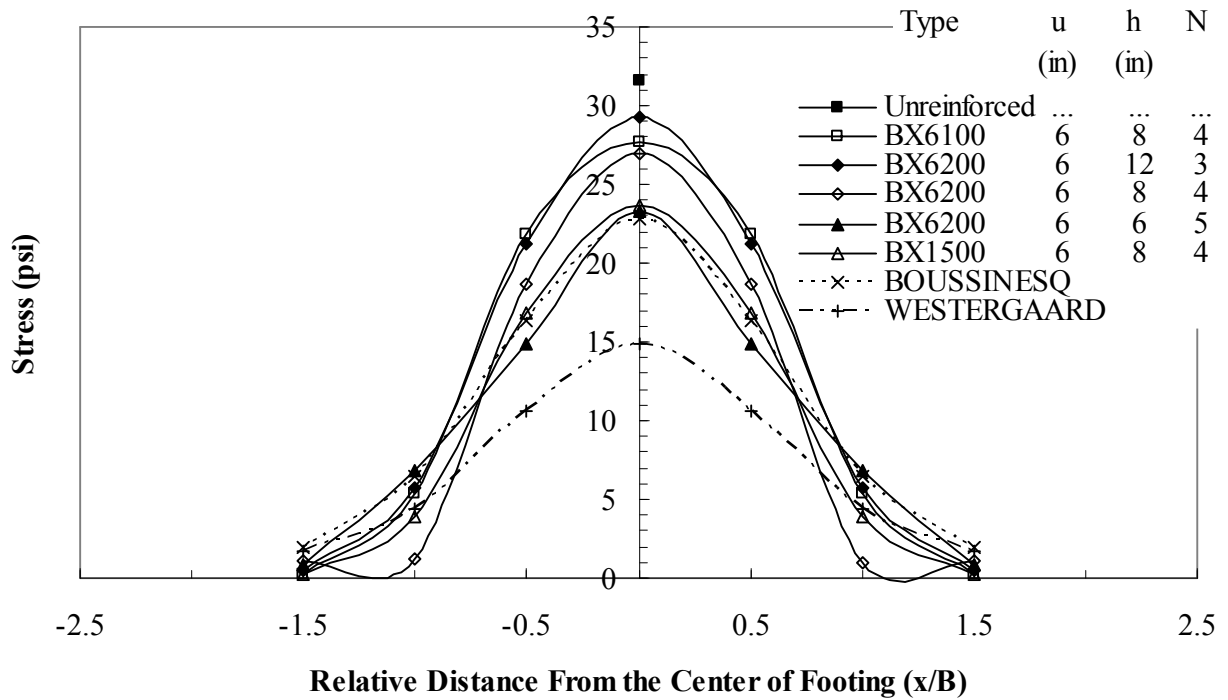
(b) Applied footing pressure q = 67.9 psi

Figure 76
Measured and calculated stress distribution along the center line of footing at a depth of 18 in.
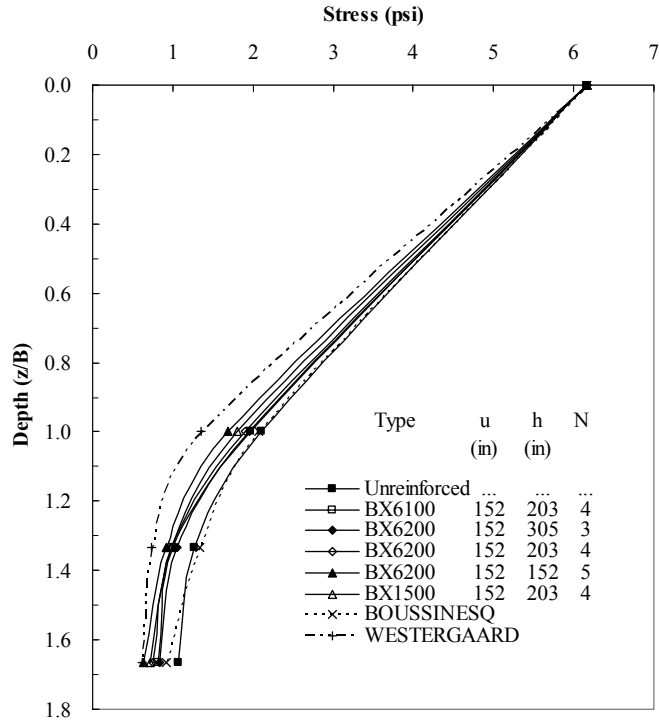
(a) Applied footing pressure q = 6.2 psi
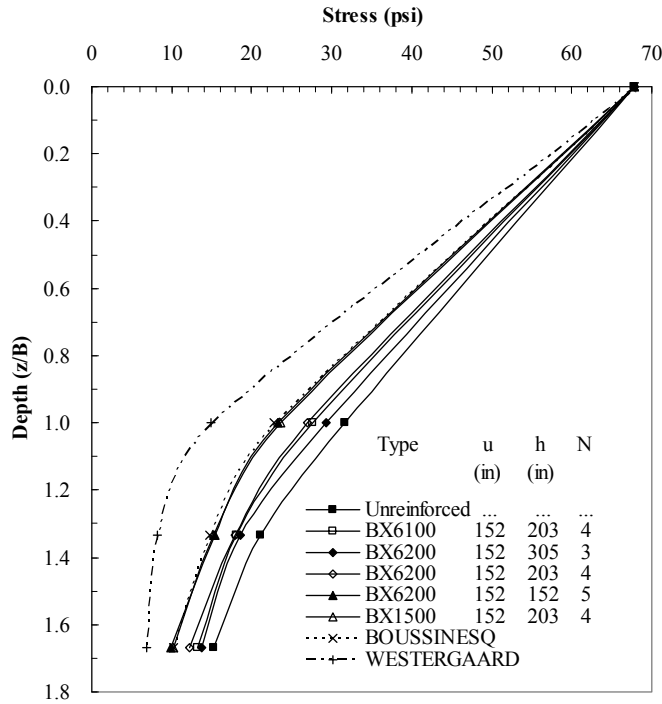
(b) Applied footing pressure q = 67.9 psi

Figure 77
Measured and calculated stress distribution with the depth
at the center of footing
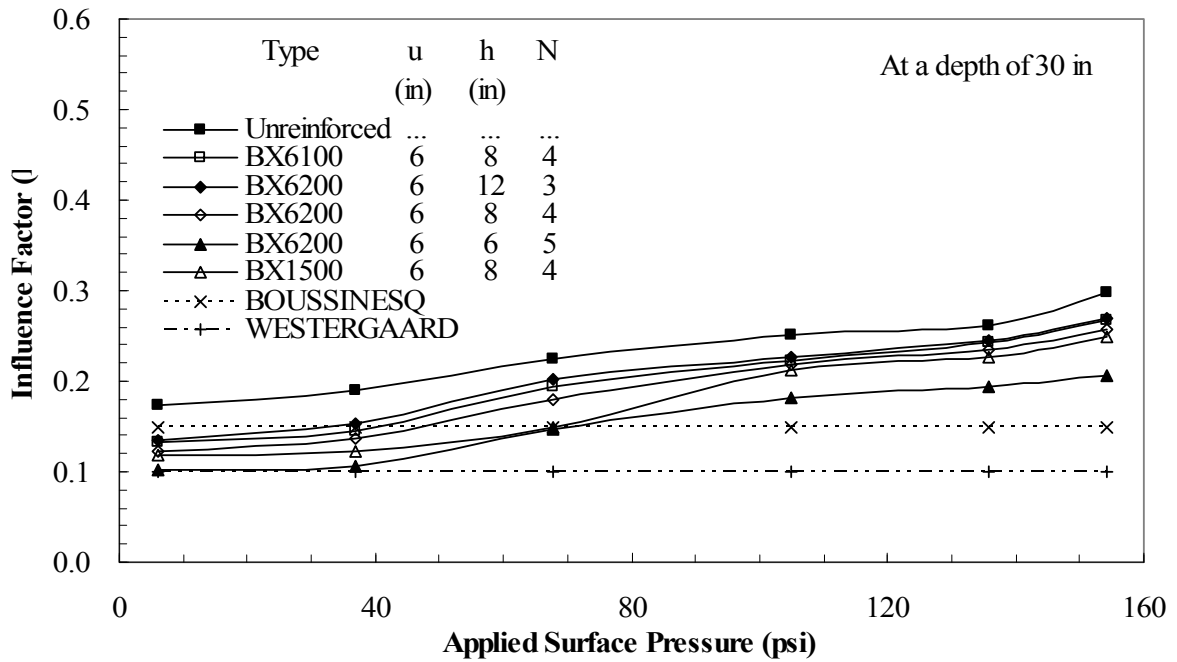
Figure 78
Stress influence factor (I) at a depth of 30 in. (1.67B) underneath the center of footing versus applied footing pressure
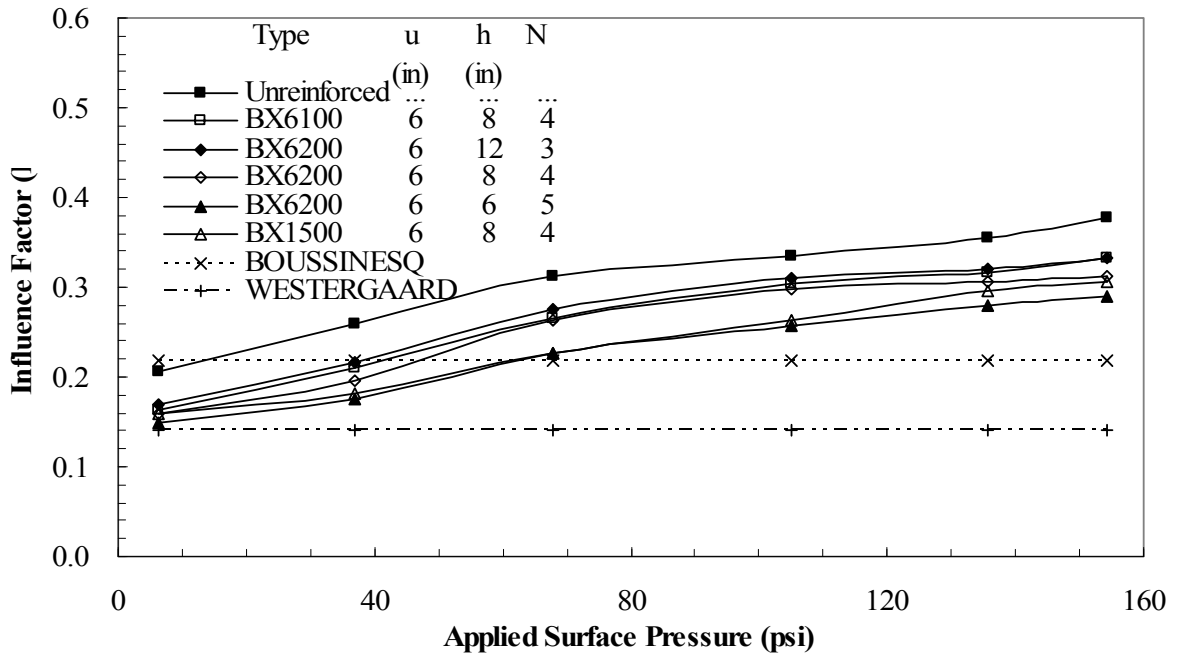
Figure 79
Stress influence factor (I) at a depth of 24 in. (1.33B) underneath the center of footing versus applied footing pressure
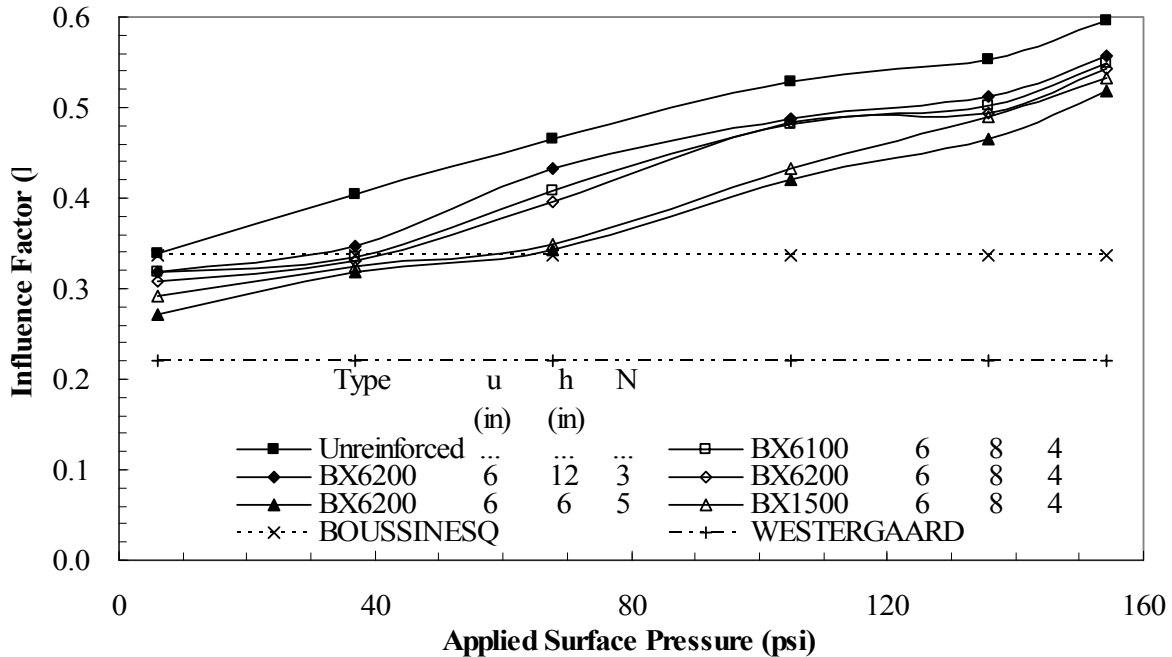
Figure 80

Stress influence factor (I) at a depth of 18 in. (1.0B) underneath the center of footing versus applied footing pressure

of strains measured along the centerline of the geogrid for different settlement ratios(s/B) are presented in figures 81 through 84. The measured tensile strain is the highest at the point beneath the center of the footing and becomes almost negligible at about 2.0B from the center of footing. It indicates that the geogrid beyond the effective length (4.0B) results in insignificant mobilized tensile strength, and thus provides negligible effects on the improved performance of reinforced silty clay soil.

It can be seen from the figures that the strain distribution along machine direction of geogrid is almost the same as that along cross machine direction, in spite of the relatively lower tensile modulus in machine direction for geogrids. The BX6100 geogrid, BX6200 geogrid, and BX1500 geogrid, all of which are made of the same material, have obviously different tensile modulus; however, the developed strains along these geogrids are very similar at the same settlement. This finding suggests that the strain developed along the geogrid seems to be directly related to the settlement, which is independent of geogrid tensile modulus. At the same settlement, the higher tension, therefore, would be developed in higher tensile modulus geogrid, and the improved performance of reinforced soil foundation is believed to be directly related to the tension developed in the geogrid. Again, it shows that the performance of reinforced silty clay would be improved with increasing the geogrid tensile modulus.

Compressive strain was measured in geogrid located beyond 0.75~1.0B from the center of footing. This means that the geogrid past this length cannot restrain lateral soil shear flow and works as an anchorage unit to prevent geogrid from failing by pull out.
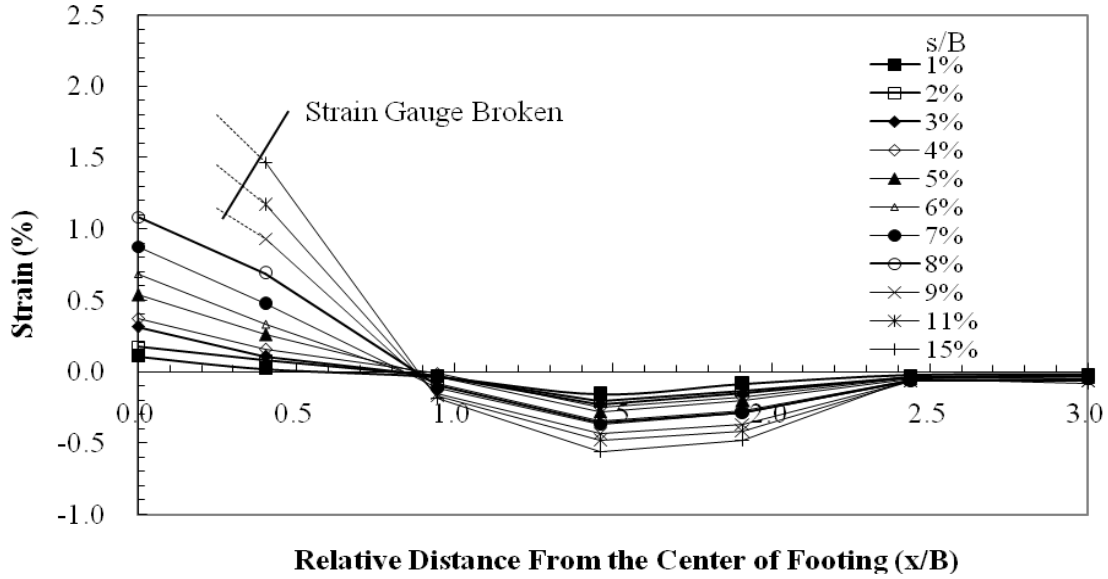
(a) Machine direction
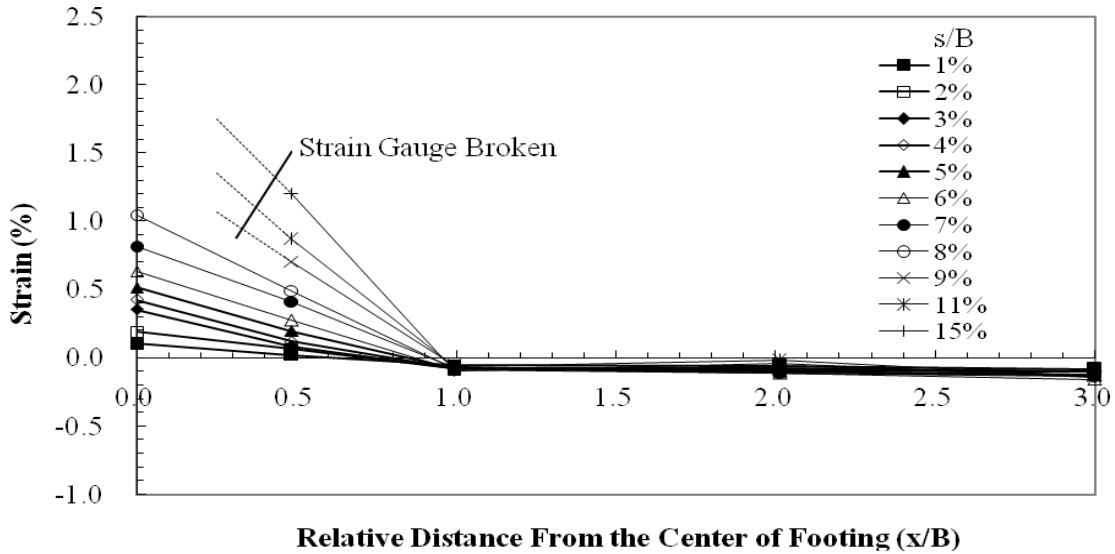
(b) Cross machine direction

Figure 81
Strain distribution along the center line of BX6100 geogrid at a depth of 6 in.
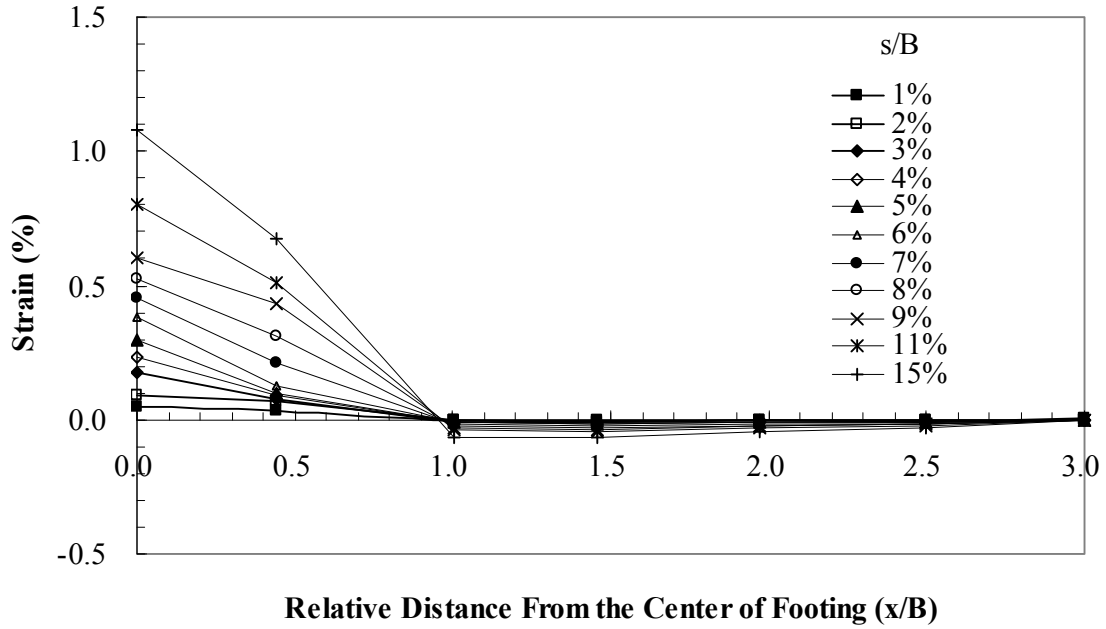
(a) Machine direction
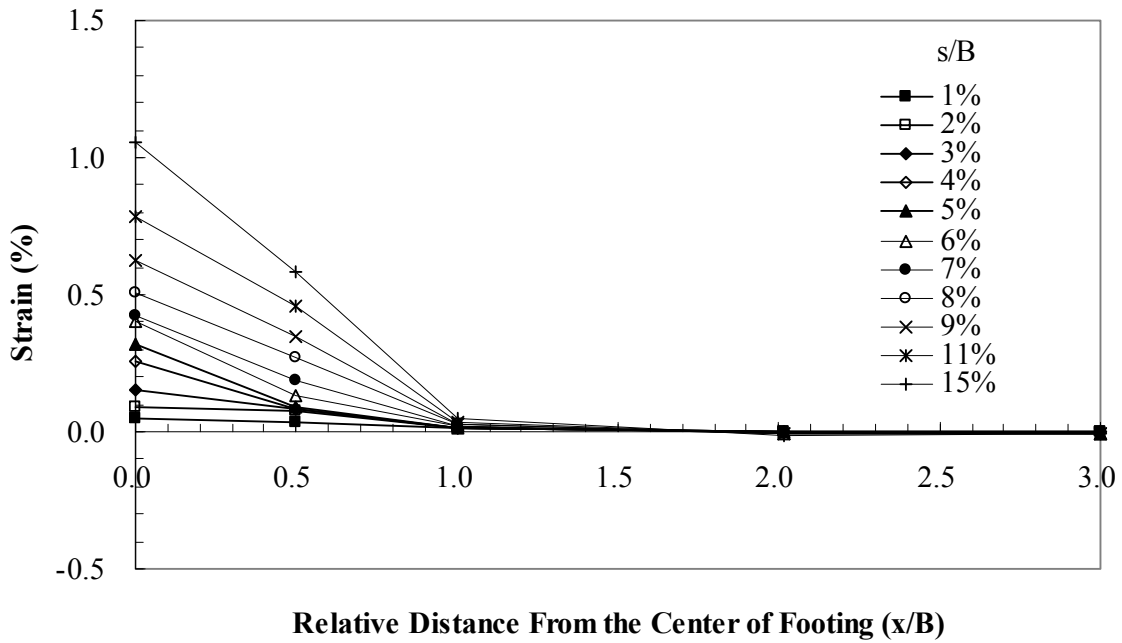
(b) Cross machine direction

Figure 82
Strain distribution along the center line of BX6100 geogrid at a depth of 30 in.
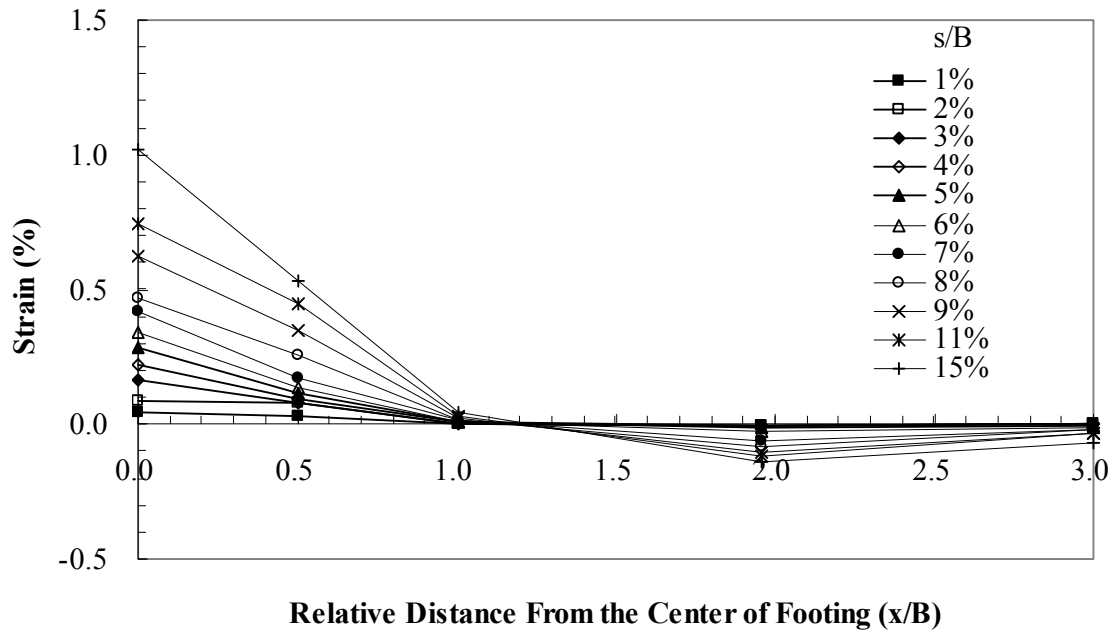
Figure 83
Strain distribution along the center line of BX6200 geogrid in cross machine direction at a depth of 30 in.
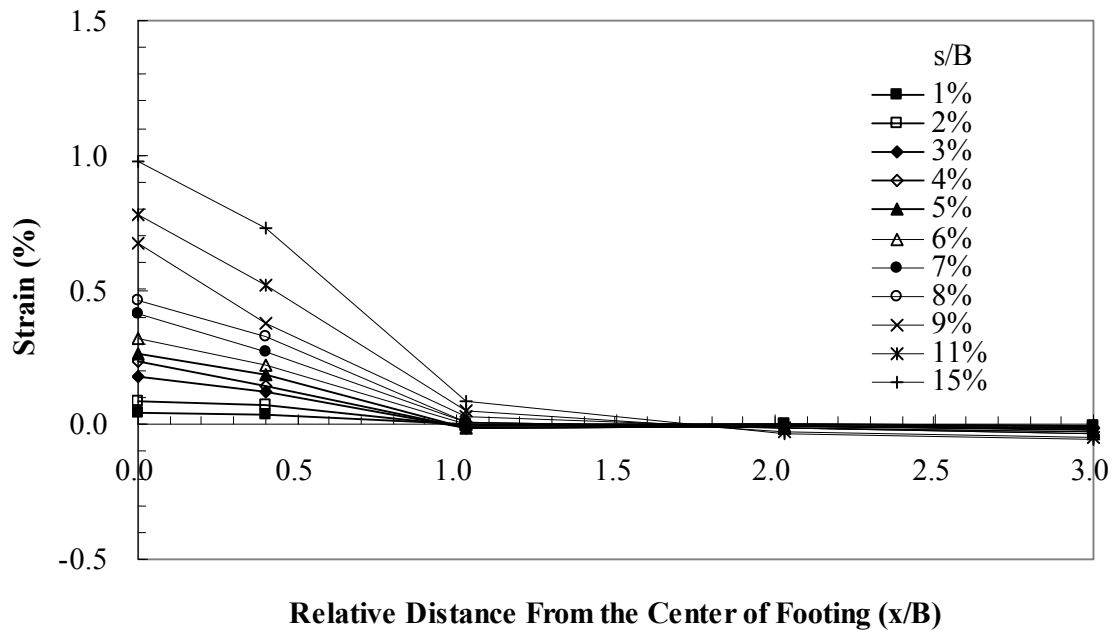
Figure 84
Strain distribution along the center line of BX1500 geogrid in cross machine direction at a depth of 30 in.

Numerical Parametric Study of Strip Footing on Reinforced Soil Foundation

Results on Reinforced Embankment Soil

Comprehensive finite element parametric study was conducted to evaluate the influence of various factors on the performance of a strip footing on reinforced studied soil. The footing performance was assessed in terms of increased bearing capacity and/or reduced settlement of the footing. The factors included in this study for geogrid-reinforced embankment soil are the effective depth of reinforced zone, spacing between geogrid layers, stiffness of geogrid, geogrid-soil interaction coefficient, optimum top spacing for the single-layer and multilayer reinforced soil, footing width, and the embedment depth of footing.

For each case, the load-deformation curve obtained from the finite element simulation was used to determine the bearing capacity and settlement of the footing. The ultimate bearing capacity of the footing was defined as the bearing capacity that corresponds to a settlement ratio (s/B) of 10%. The influence of these factors will be discussed in the following sections.

Stress distributions and developed plastic zones within the foundation soil with and without geogrid reinforcement layers are first presented, which will shed light on the reinforcement mechanisms. The vertical stress distributions within unreinforced soil and soil reinforced with three-layer and six-layer Type VI geogrid, are shown in figures 85a and 85b, respectively. All of these stresses are corresponding to the moment when the footing sitting on unreinforced soil reaches its ultimate bearing capacity. The vertical stress distribution shown in figure 85a is along a horizontal line at a distance of 2B underneath the footing bottom. The inclusion of a reinforcement layer resulted in reducing the magnitude of vertical stress compared to the unreinforced soil, and more reduction is achieved with more reinforcement layers. A similar trend, as illustrated in figure 85b, is observed in the distributions of vertical stress along the central axis of the footing. The inclusion of reinforcement layers helps spread the load applied on the footing onto a wider range of the foundation soil and thus helps reduce the ultimate consolidation settlement of the footing that will develop. Also, the more reinforcement layers included in the foundation soil, the more remarkable the reinforcement effect in the sense of reducing stresses in the foundation soil.

When the footing reinforced with Type VI geogrid reaches its ultimate bearing capacity, axial strain developed in geogrid layers within the half of the reinforced soil is shown in figure 86. Figure 86a shows the geogrid strain distribution in a three-layer reinforced soil, and figure 86b shows the geogrid strain distribution in a five-layer reinforced soil. In both

(a)Vertical stress distribution along a horizontal line 2B beneath the footing

(b) Vertical stress distribution along the central axis
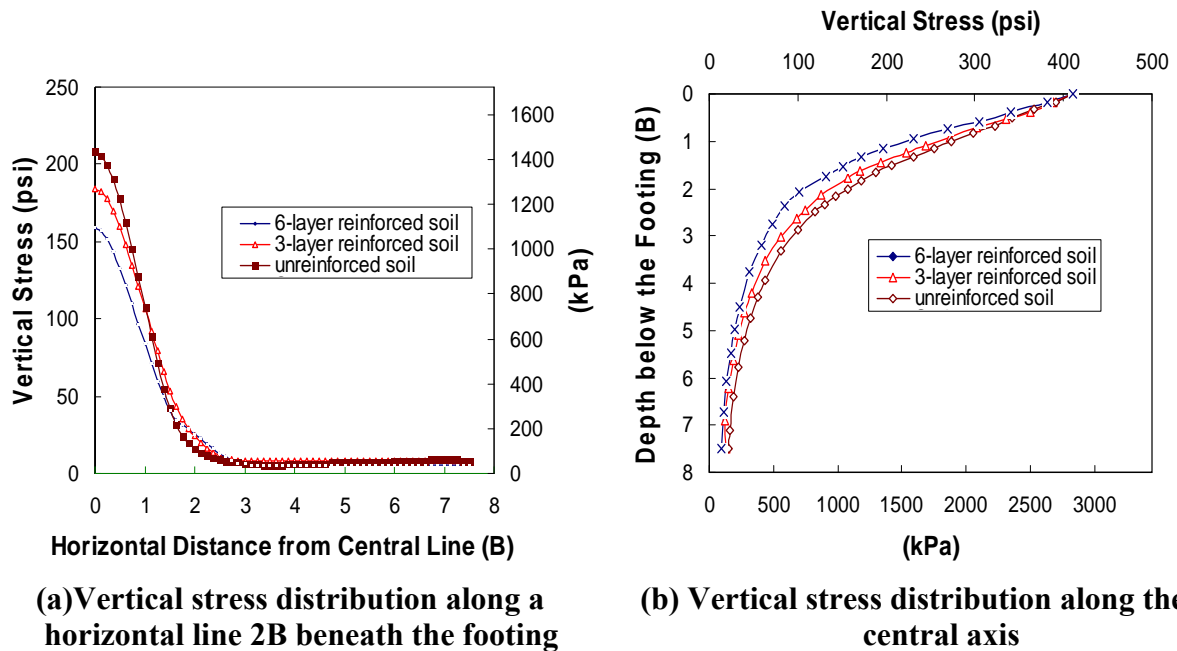
Figure 85
Stress distribution for cases reinforced with Type VI geogrid at s/B=10%

cases, the bottom geogrid layer (i.e., the third or the fifth layer in figure 86) is embedded 1.5B beneath the footing bottom. Figure 86 indicates that the greatest strain occurs at the geogrid location underneath the axis of the footing and dramatically drops off at geogrid locations further away from the footing center. As would be expected, the first geogrid layer always experiences the greatest strain, and the second geogrid layer experiences the second greatest strain, and so on in both cases. In addition, the strains in the three-layer case are larger than their counterparts in the five-layer case. Figure 86 indicates that a tensile strain (positive in the figure) is developed within a 2B range in the geogrid. The development of a tensile strain in geogrids implies the mobilization of geogrids, and thus the reinforcing benefits of geogrids in foundation can be realized. It follows that the reinforcement effect of a geogrid in a foundation soil can fully be mobilized, provided that its length is larger than 4B.

Effect of Depth of First Reinforcement Layer

The depth of the first reinforcement layer (u) was found to have considerable effect on the bearing capacity in single- and multiple-layered reinforced soils. To evaluate its effect on bearing capacity of reinforced soil, the bearing capacity ratio (BCR) was used. The top layer spacing ratio (u/B) is adopted to discuss the influence of the depth of the first reinforcement layer.

The influence of the top layer spacing ratio on the BCR for geogrid-reinforced embankment soil is discussed in this section, based on the FEM analyses for the footing placed on single-layer, two-layer and three-layer geogrid-reinforced studied soil at varying top layer spacing ratios. The typical variations of the BCR with top layer spacing ratios (u/B) for single-layer, two-layer and three-layer Type VI reinforced soil are shown in figure 87.

(a) Three-layer system   (b) Five-layer system
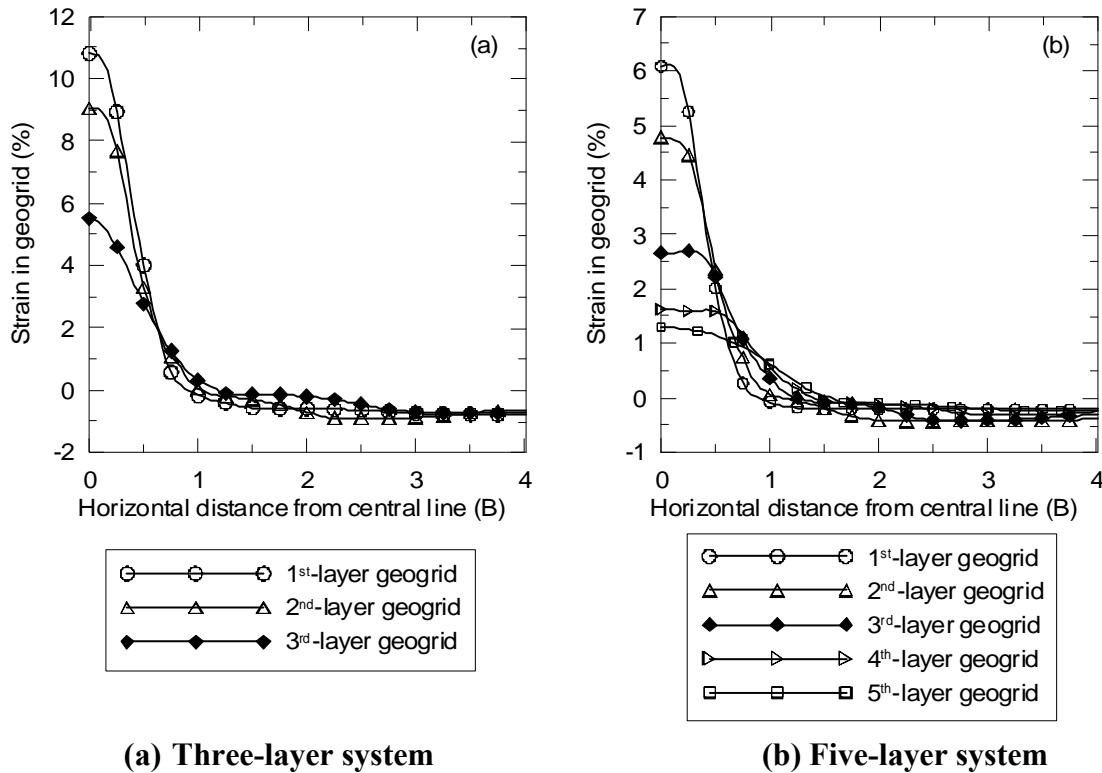
Figure 86
Strain developed in geogrid of Type VI

In the single-layer reinforcement case, the BCR increases first with the increase of the top layer spacing ratios (u/B) and then decrease after a threshold value of u/B. This threshold top layer spacing ratio (u/B) is around 0.5 where the BCR is the highest. The variation of the BCR with top layer spacing ratios (u/B) is similar in the two-layer and three-layer reinforcement cases. However, the threshold top layer spacing ratio slightly decreases with the number of reinforcement layers–around 0.4 in the two-layer reinforcement case and around 0.3 in the three-layer reinforcement case. The threshold top layer spacing ratio is used in the following sections in which the influence of other reinforcement factors on the reinforced footing is investigated.
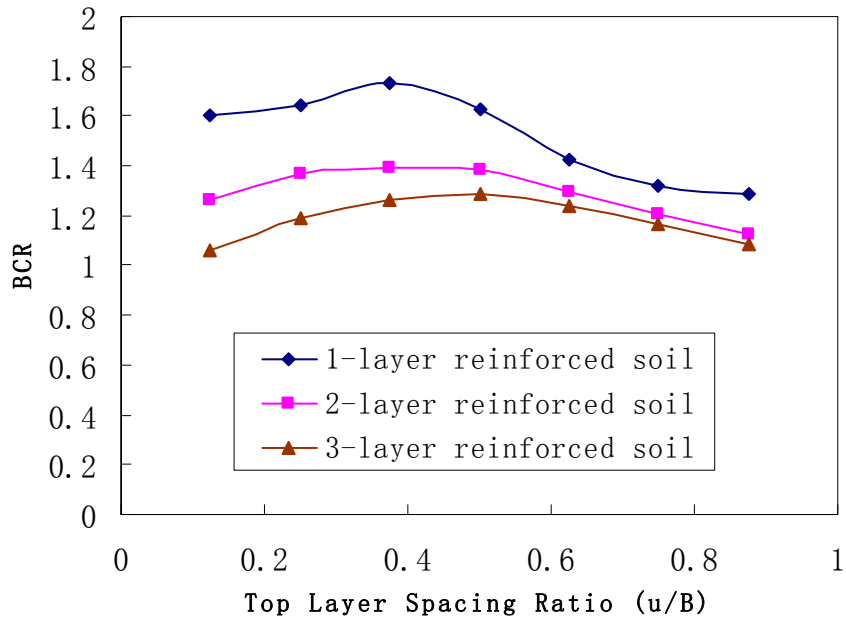
Figure 87
Variation of BCR with top layer spacing ratio in one-layer, two-layer, and three-layer reinforced soil (s/B=10%)

Effective Depth of Reinforced Zone

The design of reinforced soil foundations requires the determination of the effective (or influence) depth of reinforced zone, below which reinforcement inclusion will not have appreciable benefit on footing performance.

To identify the effective depth, finite element analyses were conducted on 4 ft. wide footing using three types of geogrid reinforcements (III, VI, and VIII) placed either at 12 in. or 24 in. uniform spacing (for both u and h). Type III geogrid has a relatively low stiffness and Type VI has a medium stiffness, while type VIII is a stiff geogrid. For each reinforcement spacing, a series of finite element analyses were conducted with the number of reinforced layers increasing until the reinforced depth reached 2.5B. The load-deformation curve for each case was determined and used to calculate the bearing capacity ratio (BCR) at s/B equal to 10%. Figure 88a presents the BCRs at s/B = 10%, for the 12 in. reinforcement spacing, as the number of reinforcement layers increases from one to ten. The variations in the BCRs at s/B = 10% versus the number of reinforcement layers for the 24 in. reinforcement spacing are shown in figure 88b.

As expected, the BCR of the reinforced footing increased as the number of reinforcement layers increased, but did so at a decreasing rate. For the 12 in. spacing cases, there is no significant improvement in the BCR when the number of reinforcement layers exceeds 6,

which corresponds to a depth of 6 ft. (1.5B). Similarly, no further significant improvement in BCR was achieved for the 24 in. spacing as the number of layers exceeds 3, which also corresponded to 6 ft. (1.5B). Accordingly, the effective reinforcement depth expressed as the strip footing's width was equal to 1.5B for the soil in question. The figures also indicated that the effective reinforcement depth was independent of the geogrid type.

(a) 12 inch spacing   (b) 24 inch spacing
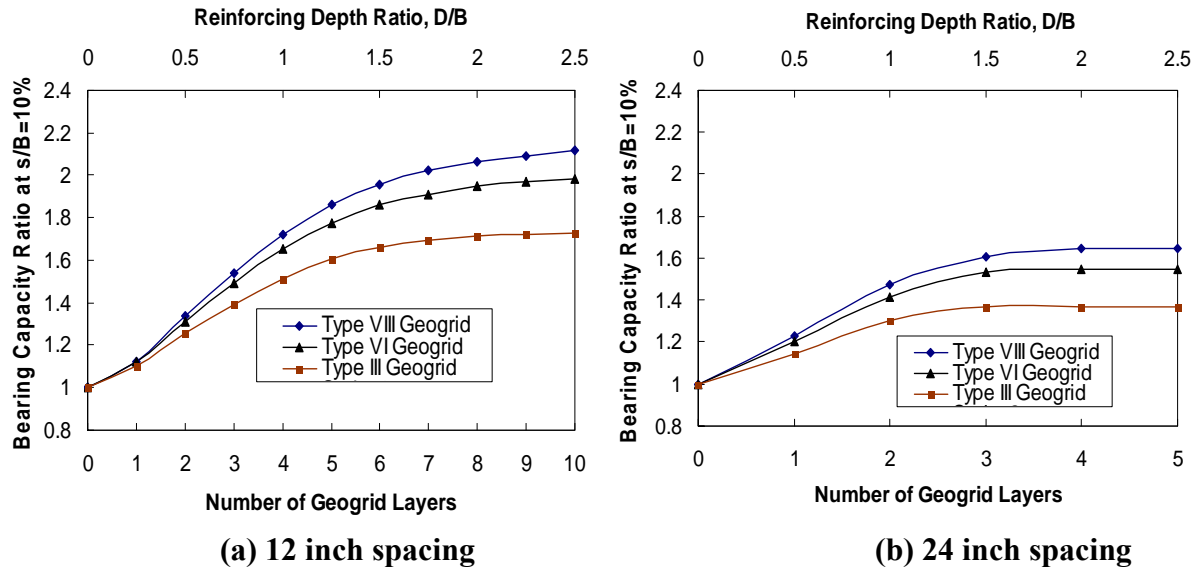
Figure 88
Variation of BCR with reinforcement layers for multilayer reinforced soil

Effect of Reinforcement Spacing

The effect of reinforcement spacing on the footing's bearing capacity and settlement was investigated by changing the number/spacing of reinforcement layers within the effective reinforcement depth of 1.5B. A series of finite element analyses were conducted on the footing-reinforced soil model using three geogrid types (III, VI, and VIII) at five different spacing. The following reinforcement layers/spacing configurations were examined: three layers placed at 24 in. spacing, four layers placed at 18 in. spacing, six layers placed at 12 in. spacing, nine layer placed reinforcement at 9 in. spacing, and twelve layers placed at 6 in. spacing. For each case, the BCR at s/B =10% and the settlement ratio (s/B) at the ultimate load capacity of a three-layer Type VI reinforced soil were calculated. Figures 89a and 89b depict the relationship between the reinforcement spacing and the BCR and s/B, respectively. For three geogrids used, the figures show that at a given settlement the load capacity of the footing decreases with increasing reinforcement spacing, with larger decrease rates at small spacing. In addition, the footing settlement at the ultimate load capacity of a three-layer Type VI reinforced soil is smaller for closer reinforcement spacing. The reduction effect of footing

settlement is more remarkable when the vertical spacing ratio (h/B) is reduced from 0.5 to 0.2. Therefore, smaller reinforcement spacing should always be desirable, provided that its cost is justified.

(a) Variation of BCR with reinforcement spacing

(b) Variation of settlement ratio with reinforcement spacing
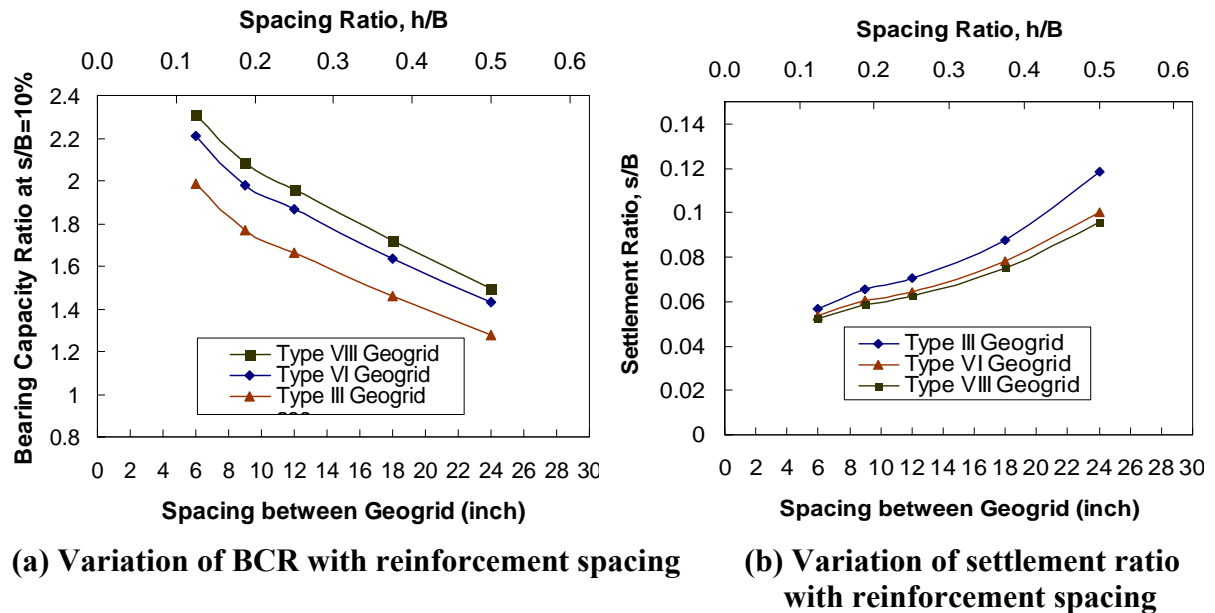
Figure 89
Effect of reinforcement spacing

Effect of Reinforcement Stiffness

Stiffness is one of the most important properties of geogrids, which has significant influence on the geogrid-soil interaction and, thus, the performance of footing on reinforced soils. In the study of geogrid-reinforced embankment soil, eight uniaxial geogrids with varying stiffness were analyzed to examine the influence of their stiffness from the perspective of the ultimate bearing capacity and settlement of the footing. The geogrid's elastic modulus was taken as its tensile strength (at 5% strain) per unit width divided by its thickness. All the geogrids here are assumed to have the same nominal thickness of 0.04in. (1 mm). Since both the soil's elastic modulus and geogrid's elastic modulus have significant effects on the behavior of the reinforced soil-footing system, a normalized geogrid's stiffness is used here. The normalized geogrid stiffness is defined as the ratio of the geogrid's elastic modulus to the soil's elastic modulus. A series of finite element analysis were conducted for each geogrid stiffness using 3, 4, 6, 8, and 12 reinforcement layers placed within the effective depth at a uniform spacing. The calculated BCR values at s/B=10% versus the normalized geogrid stiffness are presented in figure 90a. The relationship between the footing's s/B ratio and the normalized geogrid's stiffness is presented in figure 90b. Regardless of the number

of reinforcement layers, the footing with stiffer geogrids has a larger bearing capacity than that with weaker geogrids. However, this stiffness-related increase in the BCR is more remarkable at low normalized geogrid stiffness and gradually decreases as the normalized geogrid stiffness exceeds 1.5. On the other hand, the settlement ratio decreases with the increase in reinforcement stiffness, at a gradually reducing rate. In general, the figures indicate that a better reinforcement effect can be achieved in terms of higher ultimate bearing capacity and smaller settlement when the geogrid is stiffer. For the soil studied herein, a geogrid with a normalized stiffness ranging from 2 to 3.5 will maximize the benefits of the reinforced embankment soil footing.
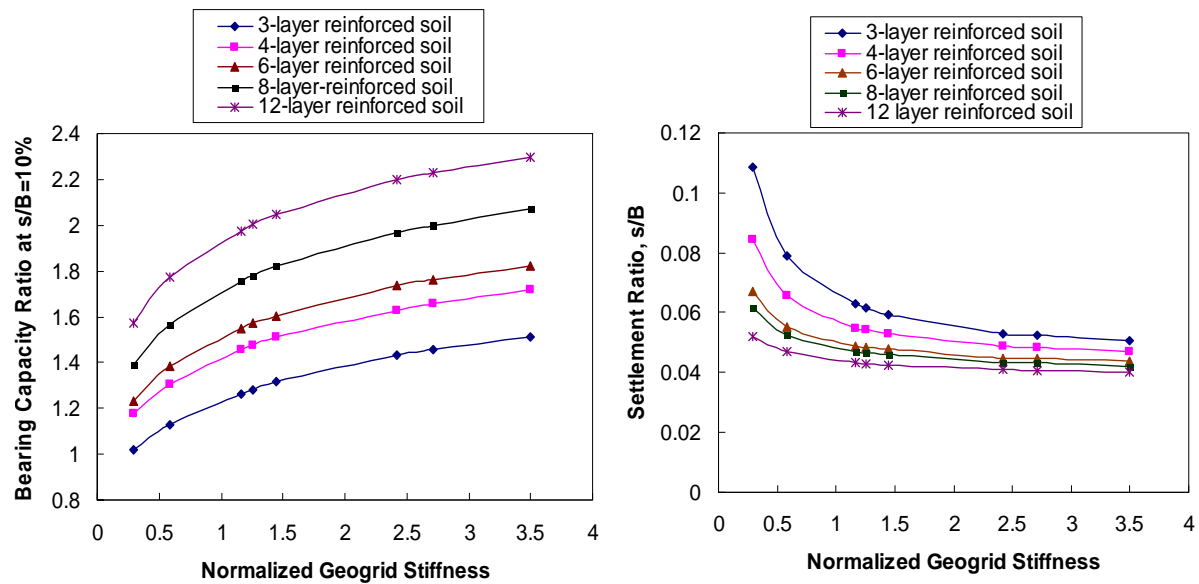
(a) BCR versus normalized geogrid stiffness (b) s/B versus normalized geogrid stiffness

Figure 90
Effect of reinforcement stiffness for the footing overlying multilayer reinforcement soil

Effect of Geogrid-Soil Interaction

The geogrid-soil interaction coefficient measures the interface friction between the geogrid and soil. Its effect on the reinforced footing was examined here by modeling a footing placed on a six-layer, reinforced soil at 12 in. reinforcement spacing. The investigated geogrids included type III, VI, and VIII, with their interaction coefficients ranging from 0.4 to 0.8. The influence of the interaction coefficient on the BCR and settlement ratio is illustrated in figures 91a and 91b, respectively. As the interaction coefficient increases, the BCR increases and the settlement ratio decreases for all studied geogrids. Figures 91a and 91b indicate that the increase rate in the BCR or the decrease rate in the settlement ratio is relatively independent of the type of geogrids. It can also be noticed that the variations of the

BCR and settlement ratio are relatively small as the interaction coefficient varies from 0.6 to 0.8, which represents typical interaction coefficient values in most geogrid-reinforced soils used in engineering applications.

(a)BCR vs. geogrid-soil interaction coefficient

(b) Settlement ratio vs. geogrid-soil interaction coefficient
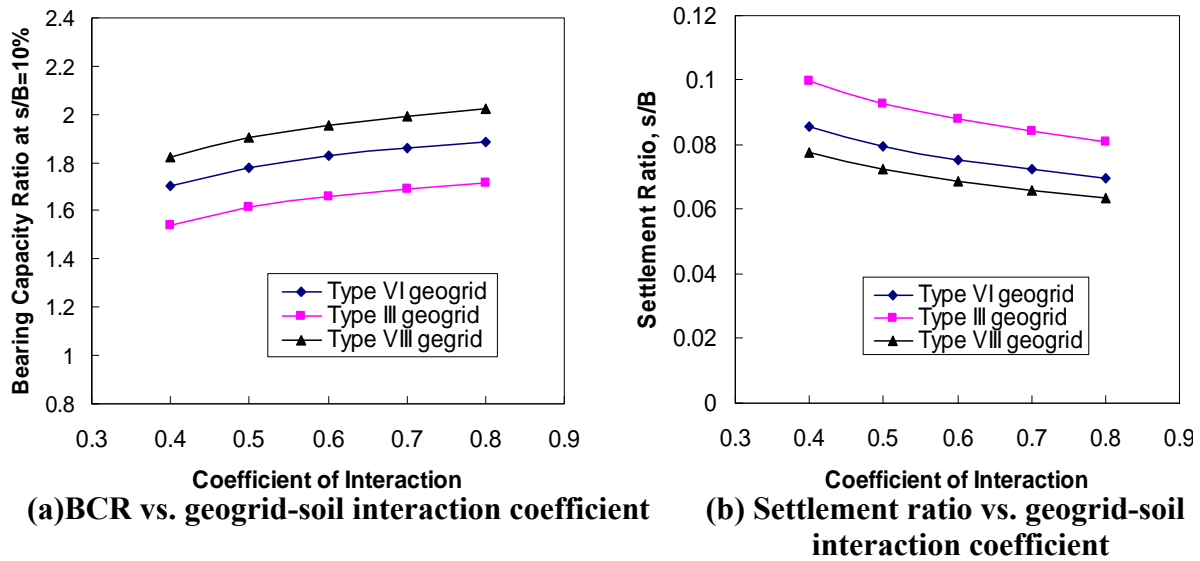
Figure 91
Effect of geogrid-soil interaction for a footing on 6-layer reinforced soil

Effect of Footing Embedment Depth

Embedment depth of an unreinforced footing has significant effect on its performance, which has been studied extensively and is well understood. However, its influence on the reinforced footing is less understood and is discussed in this section. A footing with different embedment depths (including 0B, 0.25B, 0.5B, 0.75B, and 1B) placed on a multilayer reinforced embankment soil was analyzed, using the FEM model presented in a previous section. The variation of the BCR and the variation of settlement ratio with footing embedment depth are shown in figures 92a and 92b, respectively. With the increase in embedment depth of the footing, both the bearing capacity and the settlement ratio reduce at an approximately linear manner. The reduction trend of the BCR with the increase in the embedment depth, as illustrated in figure 92a, can be explained by the fact that the increase in the embedment depth increases the bearing capacity of the unreinforced footing more than that of the reinforced footing.

Effect of Footing Width

In this study, the effect of footing width on the BCR and settlement ratio of reinforced embankment soil footings was studied by changing the width of strip footing from 3 ft. to 6 ft., and the results are shown in figures 93a and 93b, respectively. With the increase in

footing width, both the bearing capacity and the settlement ratio reduce in a linear manner. Again, this is due to a larger increase in the bearing capacity of the unreinforced footing compared to the reinforced footing brought up by the increase in the footing's width, which consequently causes a decrease trend in the BCR, as illustrated in figure 93a.
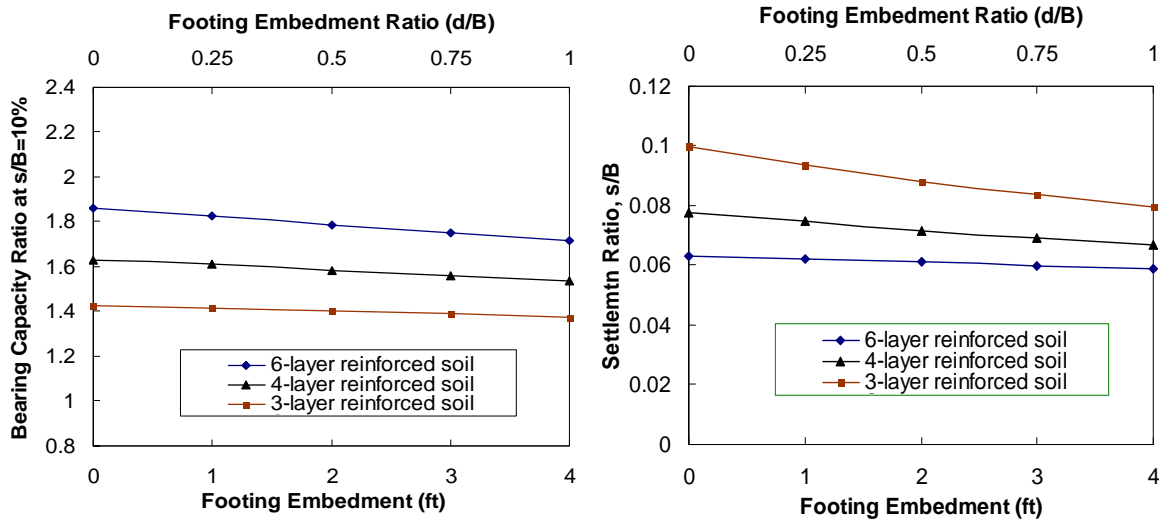
(a)Variation of BCR with footing embedment with footing

(b)Variation of settlement ratio embedment

Figure 92
Effect of footing embedment depth for footing reinforced with Type VI geogrid at s/B=10%
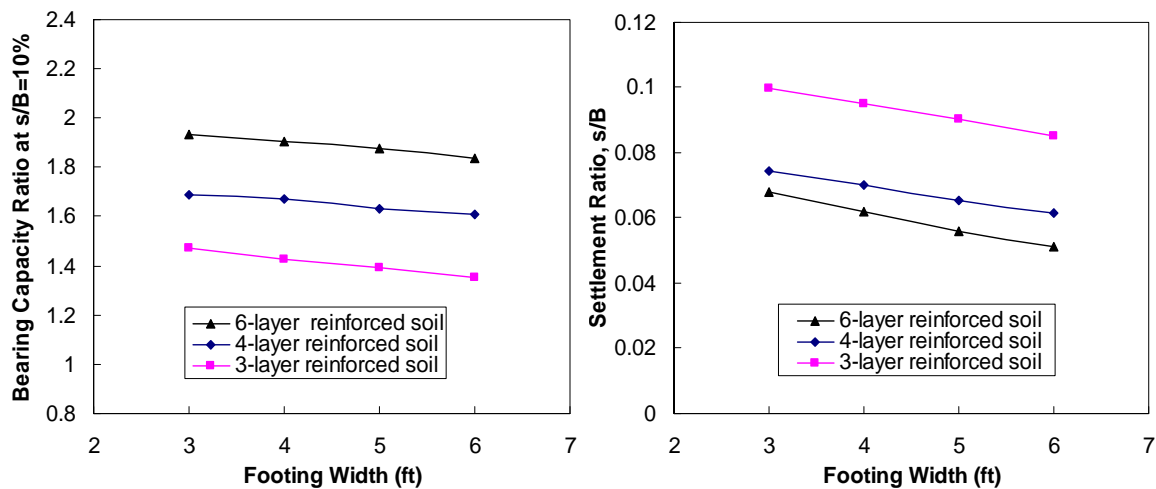
(a)Variation of BCR with footing width

(b)Variation of settlement ratio with footing width

Figure 93
Effect of footing width for footing reinforced with Type VI geogrid at s/B=10%

Finite Element Analyses Result for Reinforced Crushed Lime Stone

Based on findings from a previous analysis, we will replace the embankment soil under the proposed strip footing to a certain depth (1.5 B under the footing) with crushed lime stone, then reinforce it. A comprehensive finite element parametric study was conducted to evaluate the influence of various factors on the performance of strip footing on reinforced studied soil. The factors included in the study for reinforced crushed limestone are the spacing between reinforcement layers, stiffness of reinforcement, optimum top layer spacing for single-layer and multilayer reinforced soil, footing width, and the embedment depth of the footing.

Effect of Reinforcement Spacing

A series of finite element analyses were conducted on the footing-reinforced soil model at five different spacings. Within the 1.5 B depth under the strip footing (B=4ft), the following reinforcement layers/spacing configurations were examined: three layers placed at 24 in. spacing, four layers placed at 18 in. spacing, six layers placed at 12 in. spacing, and twelve layers placed at 6 in. spacing. The corresponding pressure-settlement curves are shown in figure 94. In this figure, all the reinforcements were steel wire mesh.
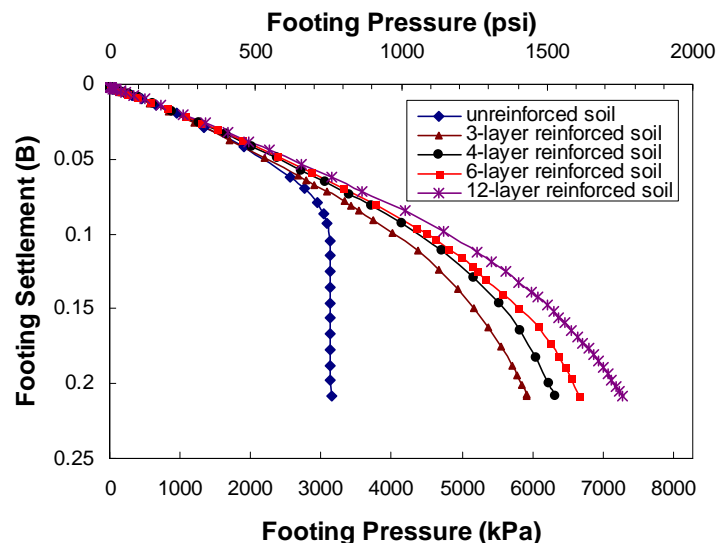
Figure 94
Typical curves of footing pressure versus footing settlement

For each case, the BCR at s/B =10% and the SRF at a footing pressure of 700 psi (4823 kPa) were calculated. Figures 95a and 95b depict the relationship between the reinforcement spacing and the BCR and SRF, respectively. For the reinforcements used, the figures show the same trend as reinforced embankment soil that at a given settlement the load carrying capacity of the footing decreases with the increase in reinforcement spacing, with larger decrease rates at small spacing. Besides, the footing settlement at the same load is smaller for

a closer reinforcement spacing. Therefore, smaller reinforcement spacing should always be desirable, provided that its cost is justified.

(a) BCR versus reinforcement spacing   (b) SRF versus reinforcement spacing
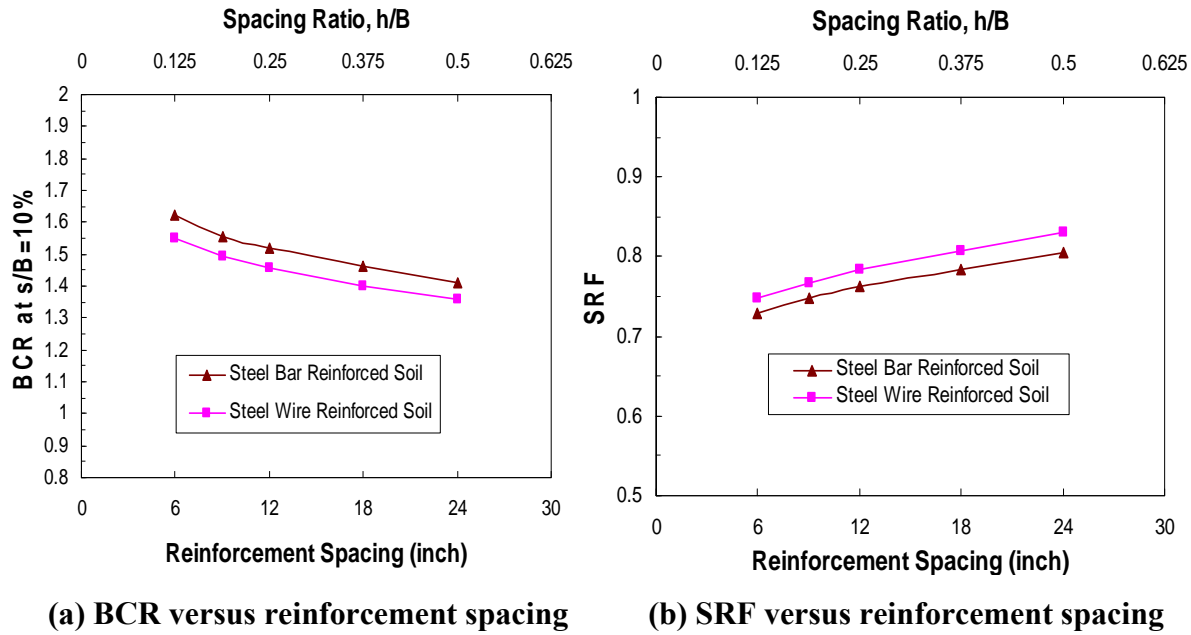
Figure 95
Effect of reinforcement spacing

Effect of Top Layer Spacing

Based on the FEM analyses for the footing placed on single-layer, two-layer and three-layer steel wire reinforced studied soil at varying top layer spacing ratios, the typical variations of the BCR with top layer spacing ratios (u/B) for single-layer, two-layer, and three-layer steel wire reinforced soil was shown in figure 96.

In the single-layer reinforcement case, the BCR increases first with the increase of the top layer spacing ratio (u/B) and then decreases after a threshold value of u/B. This threshold top layer spacing ratio (u/B) is approximately 0.35 where the BCR is the highest. The variation of the BCR with top layer spacing ratios (u/B) is similar in the two-layer and three-layer reinforcement cases. The threshold top layer spacing ratio slightly decreases with the number of reinforcement layers. It is approximately 0.25-0.3.

Effect of Reinforcement Stiffness

In this study for the reinforced crushed limestone, different reinforcements with varying stiffness were analyzed to examine the influence of their stiffness from the perspective of the ultimate bearing capacity and settlement of the footing. Since different reinforcements may
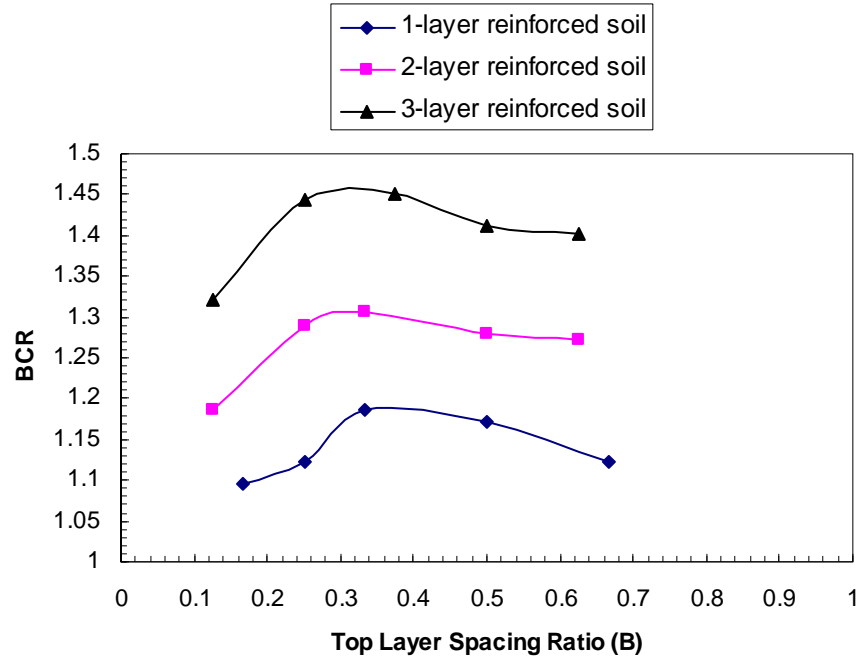
Figure 96
Variation of BCR with top layer spacing ratio in one-layer, two-layer, and three-layer reinforced soil (s/B=10%)

have different thickness and both the soil's elastic modulus and reinforcement's elastic modulus have significant effects on the behavior of the reinforced soil-footing system, a normalized reinforcement's stiffness is used here.

$$E_{normal}=T_{reinforcement}*t*1/(E_{soil}*D) \tag{8}$$

where, $E_{normal:}$ the normalized stiffness of reinforcement; $T_{reinforcement}$: the tensile strength of reinforcement at 5%; t : the thickness of reinforcement; E_{soil} : the elastic modulus of soil; D: the reinforcing depth of the reinforced soil; 1: unit width in the longitudinal direction of the strip footing.

A series of finite element analyses were conducted for different assumed normalized reinforcement stiffness for 3-layer, 6-layer, and 12-layer reinforced crushed lime stone with uniform spacing between reinforcement layers. The calculated BCR values at s/B=10% versus the normalized reinforcement's stiffnesses are presented in figure 97a. The relationship between the footing's SRF (at p=700psi) and the normalized reinforcement's stiffness is presented in figure 97b.

Similar to the trend shown by the reinforced embankment soil section, regardless of the number of reinforcement layers, the footing with stiffer reinforcements has a larger bearing
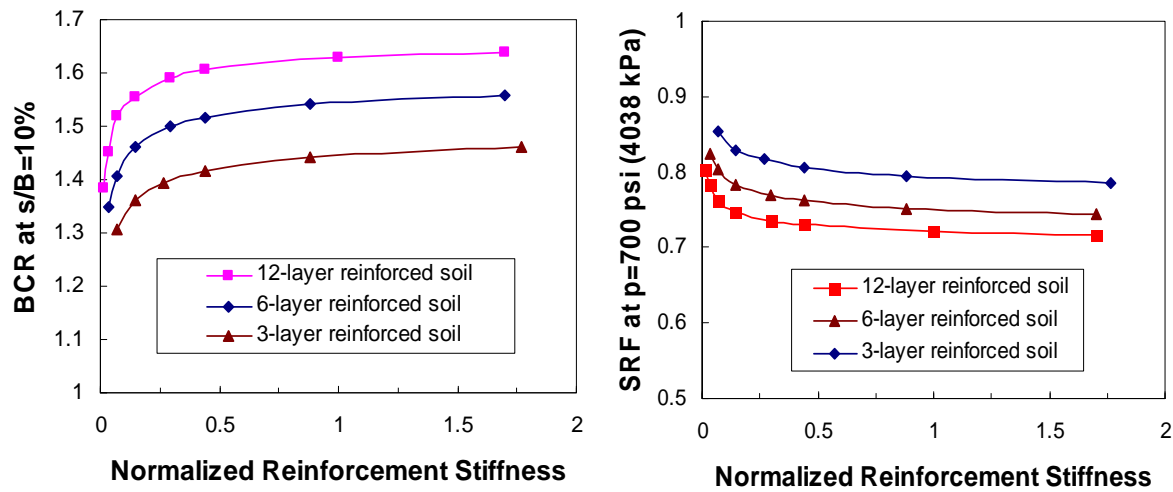
(a) BCR versus reinforcement' stiffness (b) SRF versus reinforcement's stiffness

Figure 97
Effect of reinforcement stiffness for the footing overlying multilayer reinforcement soil

capacity than that with weaker reinforcements. However, this stiffness-related increase in the BCR is more remarkable at low normalized reinforcement's stiffness and gradually decreases as the normalized reinforcement's stiffness exceeds 0.5. On the other hand, the settlement decreases with the increase in reinforcement stiffness, at a gradually reducing rate. In general, the figures indicate that a better reinforcement effect can be achieved in terms of higher ultimate bearing capacity and smaller settlement when the reinforcement is stiffer. For the crushed limestone studied herein, reinforcement with a normalized stiffness ranging from 0.5 to 1 will maximize the benefits of the reinforced soil footing.

Effect of Footing Embedment Depth
A footing with different embedment depths (including 0B, 0.25B, 0.5B, 0.75B, and 1B) placed on a multilayer reinforced crushed limestone was analyzed using the FEM model presented in a previous section. The variation of the BCR and the variation of settlement ratio with footing embedment depth are shown in figures 98a and 98b, respectively. With the increase in the embedment depth of the footing, the bearing capacity reduces in an approximately linear manner and the settlement reduction factor increases. The reduction trend of the BCR with the increase in the embedment depth, as illustrated in figure 98a, also can be explained by the fact that the increase in the embedment depth increases the bearing capacity of the unreinforced footing more than that of the reinforced footing.

(a) BCR versus embedment ratio   **(b) SRF versus embedment ratio**
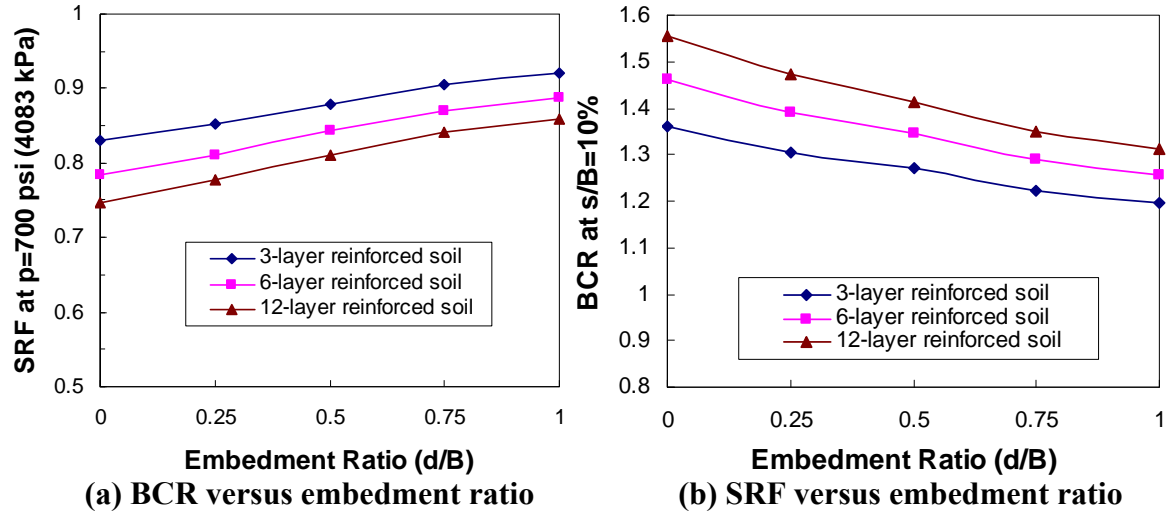
Figure 98
Effect of footing embedment depth for footing reinforced with steel wire at s/B=10%

Effect of Footing Width

The effect of footing width on the BCR and SRF of footing on reinforced crushed limestone was studied by changing the width of strip footing from 3 ft. to 6 ft.; and the results are shown in figures 99a and 99b, respectively. With the increase in footing width, the settlement reduction factor increases and the bearing capacity reduces in a linear manner. Again, this is due to larger increases in the bearing capacity of the unreinforced footing, compared to the reinforced footing brought up by the increase in the footing's width, consequently causing a decreasing trend in the BCR, as illustrated in figure 99a.


(a) BCR versus footing width   **(b) SRF versus footing width**
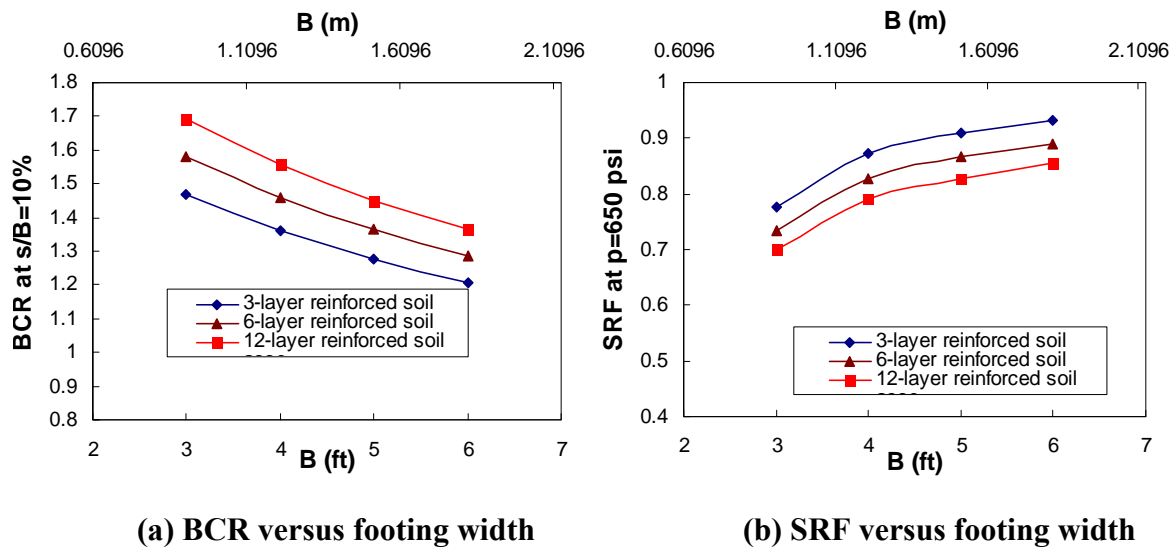
Figure 99
Effect of footing width for footing reinforced with steel wire at s/B=10%

Statistical Regression Analysis

Development of the BCR Regression Model for Reinforced Embankment Soil

As confirmed by the finite element analyses, the behavior of a strip footing sitting on geogrid-reinforced soil depends on multiple factors, including the geogrid spacing, geogrid stiffness, soil-geogrid interaction, footing width, and footing embedment depth. The effect of these factors should be appropriately determined to ensure a rational design of a geogrid-reinforced footing. Therefore, based on most of the finite element results (45 cases), a multi-regression statistical analysis was conducted to develop a BCR model that can facilitate the design of a reinforced soil footing. The rest of finite element results (20 cases) were used for model verification. In developing the BCR regression model, all the geogrid layers were assumed to lie within the effective reinforced depth and have enough length to fully mobilize their tensile contribution. The Statistical Analysis Software (SAS) package was used in this study. The full model described in equation (9) was first analyzed, which includes the effects of all variables and their interactions.

$$BCR = \beta_0+\beta_1*X1+\beta_2*X2+\beta_3*X3+\beta_4*X4+\beta_5*X5+\beta_6*X1X2+\beta_7X1X3+\beta_8X1*X4+\beta_9*X1X5+\beta_{10}*X2X3+\beta_{11}*X2X4+\beta_{12}*X2X5+\beta_{13}*X3X4+\beta_{14}*X3X5+\beta_{15}*X4X5 \tag{9}$$

where, BCR: the ultimate bearing capacity ratio of the reinforced soil; X1: the vertical spacing ratio between geogrid layers (h/B); X2: the stiffness ratio of reinforcement included in the reinforced soil; (i.e., $E_{reinforcement}/E_{soil}$); X3: the interaction coefficient between reinforcement layers and soil; X4: the footing embedment ratio (D_f/B); X5: the footing width ratio (B/4ft).

A stepwise variable selection procedure was then performed on the general model shown in equation (9) to remove insignificant variables. The statistical variable selection procedure showed that no interaction between these variables is significant and that geogrid spacing, geogrid stiffness, soil-geogrid interaction coefficient, footing embedment, and footing width are the statistically significant variables for the BCR at the 95% confidence level. The multiple regression analysis was then conducted on the reduced model, and the results yielded the model below:

$$BCR=1.7761-2.0237*X1+0.12367*X2+0.56264*X3-0.01889*X4-0.08193*X5$$
$$R^2=0.98 \tag{10}$$

130

Verification of the BCR Regression Model for Reinforced Embankment Soil

The regression BCR model in equation (10) was further verified by comparing the results of regression model with the results from the rest of the 20 finite element analysis cases. The detailed variables and their comparison are presented in table D.1. The absolute error in predicting the BCR value was calculated for each case and presented in the table. The absolute errors range from 0.16 % to 4.79 %, which suggests that the BCR values predicted by the regression model in equation (10) have acceptable accuracy. Limitation on this regression model is as follows:

A footing width from 3ft. to 6 ft. with embedment from 0 to 1 ft, sitting on 3 to 12 layers reinforced embankment soil (E=37700 psi, $\varphi = 48°$, c=11.5 psi).

Development of the BCR Regression Model for Reinforced Crushed Limestone

Again, as confirmed by the finite element analyses, the behavior of a strip footing sitting on reinforced crushed limestone depends on multiple factors, including the reinforcement spacing, reinforcement stiffness, and footing embedment depth. The effect of these factors should be appropriately determined to ensure a rational design of a reinforced footing. Therefore, based on 39 of the finite element results of reinforced crushed limestone, a multi-regression statistical analysis was conducted to develop a BCR model that can facilitate the design of a reinforced soil footing. Another 24 finite element analyses were run for model verification. In developing the BCR model, all the reinforcement layers were assumed to lie within the effective reinforced depth and have enough length to fully mobilize its tensile contribution. The full model, including the effects of all variables and their interactions, is described in equation (11).

$$BCR = \beta_0 + \beta_1*X1 + \beta_2*X2 + \beta_3*X3 + \beta_4*X4 + \beta_5*X1X2 + \beta_6 X1X3 + \beta_7 X1*X4$$
$$\beta_8*X2X3 + \beta_9*X2X4 + \beta_{10}*X3X4 \tag{11}$$

where, BCR: is the ultimate bearing capacity ratio of the reinforced soil (at s/B=10); X1: is the vertical spacing ratio between reinforcement layers (h/B); X2: is the normalized stiffness of reinforcement included in the reinforced soil; X3: is the footing embedment ratio (D_f/B); X4: is the footing width ratio (B/4ft).

A stepwise variable selection procedure was then performed on the general model shown in equation (11) to remove insignificant variables from the general model. The statistical variable selection procedure showed that no interaction between these variables is significant and that reinforcement spacing, reinforcement stiffness, footing embedment, and footing width are the statistically significant variables for the BCR at the 95% confidence level. The multiple regression analysis was then conducted on the reduced model, and the results yielded the model shown in equation (12):

$$BCR=1.89666-0.39396*X1+0.09554*X2-0.20263*X3-0.34838*X4 \qquad (12)$$

Verification of the BCR Regression Model for Reinforced Crushed Limestone

The regression BCR model in equation (12) was also further verified by comparing the results of regression model with the results from the rest of the 24 finite element analysis cases. The detailed variables and their comparisons are presented in table D.2. The absolute error in predicting the BCR value was calculated for each case and presented in the table. The absolute errors range from 0.083% to 3.856%, which suggests that the BCR values predicted by the regression model in equation (12) have acceptable accuracy. Limitation on this regression model is as follows:

A footing width from 3ft. to 6 ft. with embedment from 0 to 1 ft; sitting on 3- to 12- layer reinforced crushed limestone (E=17420 psi, $\varphi = 48°$).

Expansion of the BCR Regression Model for Reinforced Embankment Soil

In order to expand the use of the BCR regression model, more finite element analyses were run to include the effect of soil's parameters. For embankment soil, the soil friction angle was varied by 25, 30, and 35 degrees, and the soil cohesion was varied by 9 psi, 11.5 psi, and 14 psi.

Now the full model, including all the variables and their interactions, is described below.

$$BCR = \beta_0+\beta_1*X1+\beta_2*X2+\beta_3*X3+\beta_4*X4+\beta_5*X5+\beta_6*X6+\beta_7*X7+\beta_8 X1X2+\beta_9 X1*X3+\beta_{10}*X1X4+\beta_{11}*X1X5+\beta_{12}*X1X6+\beta_{13}*X1X7+\beta_{14}*X2X3+\beta_{15}*X2X4+\beta_{16}*X2X5+\beta_{17}*X2X6+\beta_{18}*X2X7+\beta_{19}*X3X4+\beta_{20}*X3X5+\beta_{21}*X3X6+\beta_{22}*X3X7+\beta_{23}*X4X5+\beta_{24}*X4X6+\beta_{25}*X4X7+\beta_{26}*X5X6+\beta_{27}*X5X7+\beta_{28}*X6X7 \qquad (13)$$

where, BCR: is the ultimate bearing capacity ratio of the reinforced soil; X1: is the vertical spacing ratio between geogrid layers (h/B); X2: is the stiffness ratio of reinforcement included in the reinforced soil (i.e. $E_{reinforcement}/E_{soil}$); X3: is the interaction coefficient between reinforcement layers and soil; X4: is the footing embedment ratio (D_f/B), X5: is the footing width ratio (B/4ft); X6: is the normalized soil friction angle ($\varphi/30$); X7: is the normalized soil cohesion (c/11.5 psi).

The statistical variable selection procedure showed that no interaction between variables is significant and that geogrid spacing, geogrid stiffness, soil-geogrid interaction coefficient, footing embedment, footing width, soil friction angle, soil cohesion are statistically significant variables for the BCR at the 95% confidence level. The multiple regression

analysis was then conducted on the reduced model, and the results yielded the model shown below:

$$BCR=3.84848-1.99668*X1+0.12434*X2+0.57453*X3-0.01057*X4-0.06924*X5-1.28114*X6-0.81625*X7 \tag{14}$$

Verification of the Expanded BCR Regression Model for Reinforced Embankment Soil

The expanded regression BCR model in equation (14) was further verified by comparing the results of regression model with the results obtained from finite element analysis. The detailed variables and comparison are presented in table D.3. The absolute error in predicting the BCR value was calculated for each case and presented in the table. The absolute errors range from 0.16% to 4.79%, which suggests that the BCR values predicted by the regression model in equation (14) have acceptable accuracy.

Expansion of the BCR Regression Model for Reinforced Crushed Limestone

In order to expand the use of the BCR regression model for crushed limestone, more finite element analyses were run to include the effect of soil's parameters. In this study, the soil friction angle was varied by 48, 50 and 52 degrees; and the soil's elastic modulus was varied by 14510 psi (100 MPa), 17420 psi (120 MPa), and 20320 psi (140 MPa).

The full model including all the variables and their interactions is described as below.

$$BCR=\beta_0+\beta_1*X1+\beta_2*X2+\beta_3*X3+\beta_4*X4+\beta_5*X5+\beta_6X6+\beta_7X1*X2+\beta_8*X1X3+\beta_9*X1X4+\beta_{10}*X1X5+\beta_{11}*X1X6+\beta_{12}*X2X3+\beta_{13}*X2X4+\beta_{14}*X2X5+\beta_{15}*X2X6+\beta_{16}*X3X4+\beta_{17}*X3X5+\beta_{18}*X3X6+\beta_{19}*X4X5+\beta_{20}*X4X6+\beta_{21}*X5X6 \tag{15}$$

where, BCR: is the ultimate bearing capacity ratio of the reinforced soil (at s/B=10); X1: is the vertical spacing ratio between reinforcement layers (h/B); X2: is the normalized stiffness of reinforcement included in the reinforced soil; X3: is the footing embedment ratio (D_f/B); X4: is the footing width ratio (B/4ft); X5: is the normalized friction angle of soil ($\varphi/48$); X6: is the normalized elastic modulus of soil (E/17420 psi or E/120 MPa).

The statistical variable selection procedure showed that no interaction between these variables is significant and that reinforcement spacing, reinforcement stiffness, footing embedment, and footing width, soil friction angle, and soil elastic modulus are statistically significant variables for the BCR at the 95% confidence level. The multiple regression analysis was then conducted on the reduced model, and the results yielded the model shown in equation (16):

$$BCR=3.17874-0.41281*X1+0.07947*X2-0.21817*X3-0.37297*X4-$$
$$1.65633*X5+0.41759*X6 \tag{16}$$

Verification of the Expanded BCR Regression Model for Reinforced Crushed Limestone

The expanded regression BCR model for crushed limestone in equation (16) was further verified by comparing the results of regression model with the results obtained from finite element analysis. The detailed variables and comparison are presented in table D.4. The absolute error in predicting the BCR value was calculated for each case and presented in the table D.4. The absolute errors range from 0.072% to 4.869%, which suggests that the BCR values predicted by the regression model in equation (16) have acceptable accuracy.

DESIGN OF REINFORCED SOIL FOUNDATION

The benefits of using reinforcements to increase the bearing capacity and reduce the settlement of soil foundation have been widely recognized. The experimental results of this study clearly substantiated this point. It is therefore necessary to develop a new stability analysis technique for reinforced soil foundations to account for this positive effect from reinforcement. During the past thirty years, many hypotheses have been postulated to describe the reinforcing mechanism and determine the possible failure modes of RSF, but as compared to RSF's engineering application, the development of its design method and theory is relatively slow. The stability analysis of reinforced soil foundation in this chapter, including the effect of reinforcement, is an attempt to examine existing methods and/or develop reasonable design methods for different soil types.

Stability Analysis of Reinforced Soil Foundation

Based on the literature review, experimental study, and numerical study, five different failure modes can be identified as shown in figure 100: failure above reinforcement [2], failure between reinforcement [19], failure like footing on a two-layer soil system (strong soil layer over weak soil layer) [19], failure in reinforced zone, and partial punching-shear failure in reinforced zone. The first two failure modes can be avoided by keeping the top layer spacing (u) and the vertical spacing between reinforcement layers (h) small enough. Based on the experimental results of the present study, the top layer spacing (u) and the vertical spacing (h) are recommended to be less than $0.5B$ to prevent these two failure modes from occurring. This requirement should not be difficult to fulfill in engineering practice; therefore, the discussion here is focused on the latter three failure modes only. As mentioned in the literature review, the reinforcement can restrain lateral deformation or potential tensile strain of the soil (confinement effect), and the deformed reinforcement can also develop an upward force (tension membrane effect). All these effects lead to an increase in bearing capacity. So, the contribution of reinforcements to bearing capacity needs to be included in the bearing capacity calculation.

Failure like Footings on Two-Layer Soil System (Strong Soil Layer Over Weak Soil Layer)

If the strength of the reinforced zone is much larger than that of the underlying unreinforced zone, and the reinforcement depth ratio (d/B) is relatively small, a punching shear failure will occur in the reinforced zone followed by a general shear failure in the unreinforced zone as shown in figure 100c. This failure mode was first suggested by Meyerhof and Hanna [29] for

stronger soil underlying by weaker soil. With some modification, Meyerhof and Hanna's solution can be used to calculate the bearing capacity of a reinforced soil foundation [29].
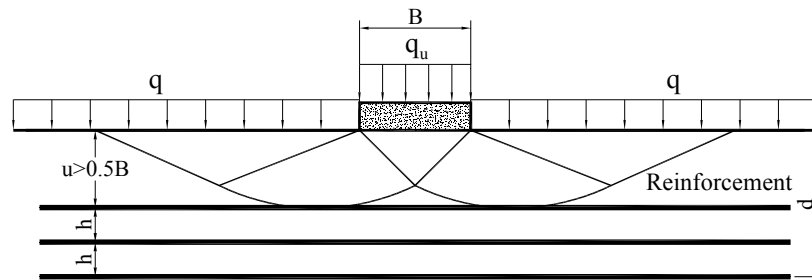
(a) Failure above top layer reinforcement (after Binquet and Lee, 1975)
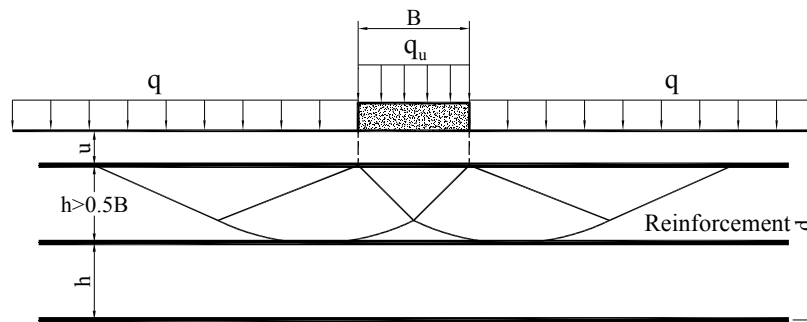
(b) Failure between reinforcement layers (after Wayne et al., 1998)
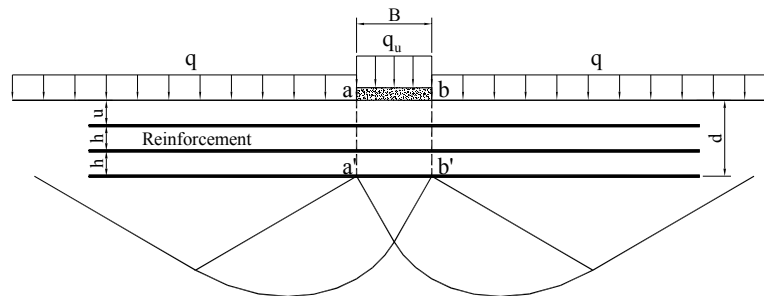
(c) Failure like footings on a two-layer soil system (after Wayne et al., 1998)
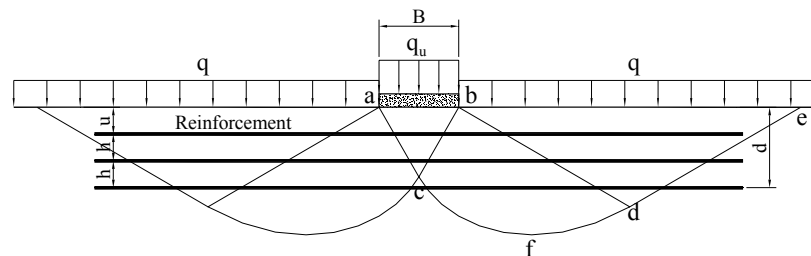
(d) Failure in reinforced zone

Figure 100
Failure modes of reinforced soil foundation
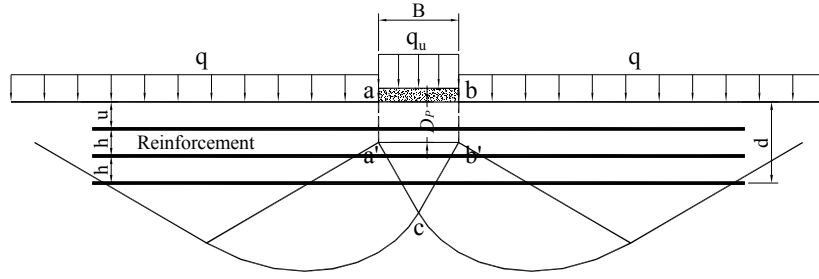
(e) Partial punching shear failure

Figure 100
(continued)

The determination of the exact shape of reinforcement at the ultimate load is not easy. Two different reinforcing mechanisms are discussed here, therefore: horizontal confinement effect of reinforcement and vertical reinforcement tension along the punching failure surfaces aa' and bb' (tension membrane effect). The actual reinforcing effect should be the combination of these two reinforcing mechanisms.

Horizontal Confinement Effect of Reinforcement

Considering the strip footing case as shown in figure 100c, the forces on the vertical punching failure surfaces *aa'* and *bb'* in the upper soil layer include the total passive earth pressure P_p, inclined at an average angle δ, and adhesive force $C_a = c_a d$ acting upwards. c_a is the unit adhesion of soil along two sides. With the inclusion of reinforcement, there is an upward shear force induced by the tension of the reinforcement on the vertical failure surface.

The ultimate bearing capacity can be given as follows for strip footing on a reinforced soil foundation with horizontal reinforcement:

$$q_{u(R)} = q_b + \frac{2c_a d}{B} + \gamma_t d^2 \left(1 + \frac{2D_f}{d}\right) \frac{K_s \tan \phi_t}{B} + \frac{2\sum_{i=1}^{N} T_i \tan \delta}{B} - \gamma_t d \qquad (17)$$

where $q_{u(R)}$ is the ultimate bearing capacity of reinforced soil foundation; q_b is the ultimate bearing capacity of the underlying unreinforced soil; γ_t is the unit weight of soil in the reinforced zone; D_f is the embedment depth of the footing; K_s is the punching shear coefficient, which depends on the friction angle of soil in the reinforced zone and the ultimate bearing capacity of soil in both the reinforced zone and the underlying unreinforced zone; ϕ_t is the friction angle of soil in the reinforced zone. T_i is the tensile force in the ith layer of reinforcement; δ is the mobilized friction angle along two sides; N is the number of

reinforcement layers. An estimate of the punching shear coefficient, K_s, and unit adhesion of soil, c_a, can be obtained from Meyerhof and Hanna [29].

Similar to equation (17), the ultimate bearing capacity formula for square footings on a reinforced soil foundation with horizontal reinforcement can be given as:

$$q_{u(R)} = q_b + \frac{4c_a d}{B} + 2\gamma_t d^2 \left(1 + \frac{2D_f}{d}\right)\frac{K_s \tan\phi_t}{B} + \frac{4\sum_{i=1}^{N} T_i \tan\delta}{B} - \gamma_t d \qquad (18)$$

This failure mechanism most likely controls the performance of reinforced clayey soil.

Vertical Reinforcement Tension along the Punching Failure Surfaces aa' and bb'

For the reinforcement turning vertically along the punching failure surfaces at the ultimate load, the solution proposed by Wayne, et al [19] can be used to calculate the ultimate bearing capacity of reinforced soil foundation.

For strip footing on a reinforced soil foundation with vertical reinforcement (Wayne, et al):

$$q_{u(R)} = q_b + \frac{2c_a d}{B} + \gamma_t d^2 \left(1 + \frac{2D_f}{d}\right)\frac{K_s \tan\phi_t}{B} + \frac{2\sum_{i=1}^{N} T_i}{B} - \gamma_t d \qquad (19)$$

For square footing on a reinforced soil foundation with vertical reinforcement (Wayne, et al):

$$q_{u(R)} = q_b + \frac{4c_a d}{B} + 2\gamma_t d^2 \left(1 + \frac{2D_f}{d}\right)\frac{K_s \tan\phi_t}{B} + \frac{4\sum_{i=1}^{N} T_i}{B} - \gamma_t d \qquad (20)$$

This kind of failure mechanism most likely occurs in the reinforced clayey soil with large deformation.

Failure in Reinforced Zone

If the strength of the reinforced zone is slightly larger than that of the underlying unreinforced zone or if the reinforcement depth ratio (d/B) is relatively large, the failure will occur in the reinforced zone as shown in figure 100d. Again, two different reinforcing mechanisms are discussed here: horizontal confinement effect of reinforcement and reinforcement tension along the faces *ac* and *bc* of soil wedge *abc* (tension membrane effect).

Horizontal Confinement Effect of Reinforcement

The classic bearing capacity formula, also known as the "triple N formula", includes three items which account for the contributions of surcharge q, cohesion c, and the weight of soil γ.

Superposition is applied to add these three items together. The general form of the bearing capacity formula for a strip footing is given by:

$$q_u = cN_c + qN_q + 0.5\gamma BN_\gamma \tag{21}$$

where, q_u is the ultimate bearing capacity of unreinforced soil foundation; c is the cohesion of soil; q is the surcharge load; γ is the unit weight of soil; B is the width of footing; and N_c, N_q, and N_γ are bearing capacity factors, which are dependent on the friction angle of soil ϕ.

To include the contribution of reinforcement, the method of superposition can be used, and an additional item Δq_T is then added in terms of tensile force T. The bearing capacity formula now takes the following form:

$$q_{u(R)} = cN_c + qN_q + 0.5\gamma BN_\gamma + \Delta q_T \tag{22}$$

where $q_{u(R)}$ is the ultimate bearing capacity of reinforced soil foundation; Δq_T is the increased bearing capacity due to the tensile force of the reinforcement.

First, consider the strip footing case and the single layer of reinforcement. The failure surface in the soil for the strip footing at the ultimate load is shown in figure 100d. The reinforcement is located at a depth of u.

Considering the soil wedge abc, the passive force P_p acting on the faces ac and bc includes four components as shown in figure 101 and can be written as:

$$P_p = P_{pc} + P_{pq} + P_{p\gamma} + P_{pT} \tag{23}$$

where $P_{pc}, P_{pq}, P_{p\gamma},$ and P_{pT} are the passive forces due to surcharge q, cohesion c, weight of soil γ, and the tensile force of reinforcement T.
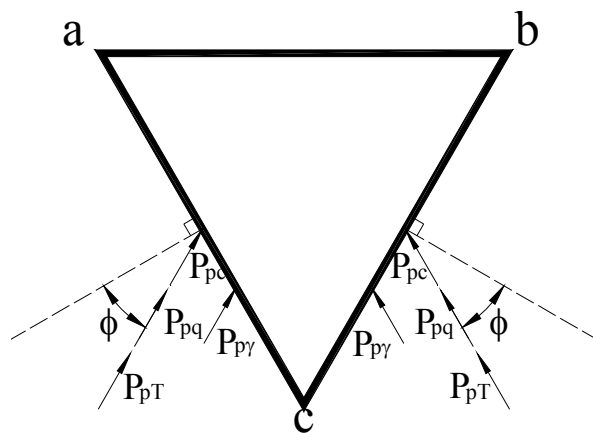
Figure 101
Passive forces on the triangular wedge *abc*

Derivation of P_{pc}, P_{pq}, and $P_{p\gamma}$ can be found in many foundation engineering books (e.g., 30). Therefore, the discussion will only focus on the derivation of P_{pT} here.

Considering the free body diagram of the soil wedge *bcdg* shown in figure 102, the forces per unit length of the wedge *bcdg*, due to the tensile force of reinforcement T, include P_{pT}, tensile force of reinforcement, T_L and T_R, and the resisting force along the log spiral *cd, F* as shown in figure 102.
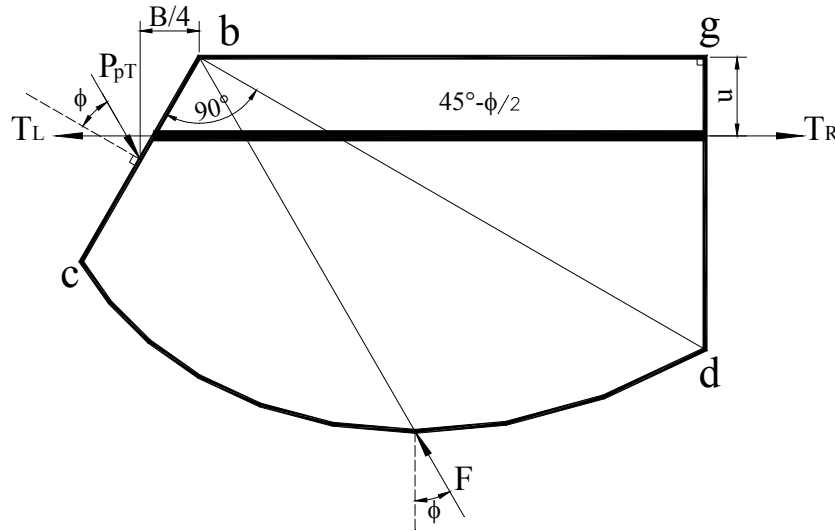
Figure 102
Free body diagram of the soil wedge *bcdg*

The log spiral is described by the equation $r = r_0 e^{\theta \tan \phi}$. This means that the radial line at any point makes an angle ϕ with the normal direction of the log spiral. The resisting force F also makes an angle ϕ with the normal direction of the log spiral. Taking the moment about center of the log spiral, *b*

$$P_{pT} = \frac{4(T_L - T_R)u \cos(\pi/4 + \phi/2) \times 1}{B \cos \phi}$$

(24)

Considering the equilibrium of the soil wedge *abc* shown in figure 103.

$$\Delta q_T = \frac{4(T_L - T_R)u}{B^2}$$

(25)

The distance that the tensile force T_R is applied from the center of footing x_{T_R} is the function of the friction angle of soil ϕ. The variation of x_{T_R}/B with the soil friction angle ϕ is given in figure 104. From this figure, it can be seen that the distance that the tensile force T_R is applied from the center of footing is greater than *2B* when soil friction angle ϕ is greater than

25°. Based on the measured strain distribution along the reinforcement in this study, the tensile force in the reinforcement at this distance is negligible; therefore, the tensile force T_R can be taken as zero, and the equation (25) can then be simplified as:

$$\Delta q_T = \frac{4T_L u}{B^2} = \frac{4Tu}{B^2} \tag{26}$$
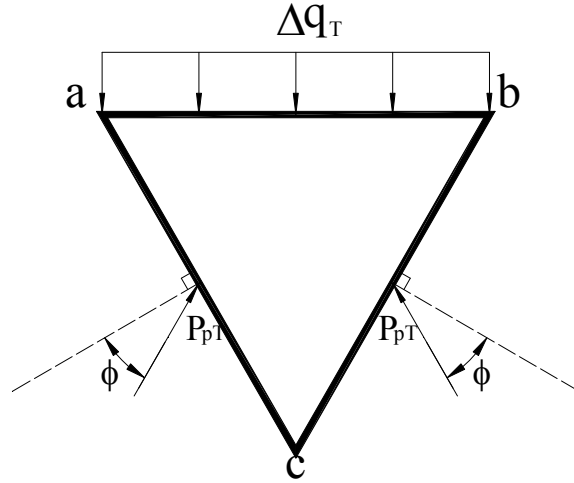
Figure 103
Free body diagram of the soil wedge *abc*

For two or more layers of reinforcement, the increased bearing capacity Δq_T can be easily shown to be:

$$\Delta q_T = \sum_{i=1}^{N} \frac{4T_i [u + (i-1)h]}{B^2} \tag{27}$$

where T_i is the tensile force in the ith reinforcement layer; N is the number of reinforcement layers; u is the top layer spacing of reinforcement; h is the vertical spacing between reinforcement layers. It should be noted that all reinforcement layers must be placed above the failure zone, i.e. above the point f as shown in figure 100d, to contribute to improving the performance of the soil foundation. The ultimate bearing capacity of the strip footing on a soil with horizontal reinforcement can now be given as:

$$q_{u(R)} = cN_c + qN_q + 0.5\gamma BN_\gamma + \sum_{i=1}^{N} \frac{4T_i [u + (i-1)h]}{B^2} \tag{28}$$

For square footings, the increased bearing capacity Δq_T can be simply calculated as:

$$\Delta q_T = \sum_{i=1}^{N} \frac{12T_i [u + (i-1)h] r_T}{B^2} \tag{29}$$

where:

$$r_T = \begin{vmatrix} \left[1 - 2\dfrac{u+(i-1)h}{B}\tan\left(\dfrac{\pi}{4}-\dfrac{\phi}{2}\right)\right] & u+(i-1)h < \dfrac{B}{2}\tan\left(\dfrac{\pi}{4}+\dfrac{\phi}{2}\right) \\[3mm] \dfrac{1}{2}-\dfrac{u+(i-1)h}{2H_f} & u+(i-1)h \geq \dfrac{B}{2}\tan\left(\dfrac{\pi}{4}+\dfrac{\phi}{2}\right) \end{vmatrix} \tag{30}$$

where, H_f is the depth of failure surface and can be evaluated as:

$$H_f = \frac{B}{2\cos(\pi/4+\phi/2)}e^{(\pi/4+\phi/2)\tan\phi}\cos\phi \tag{31}$$
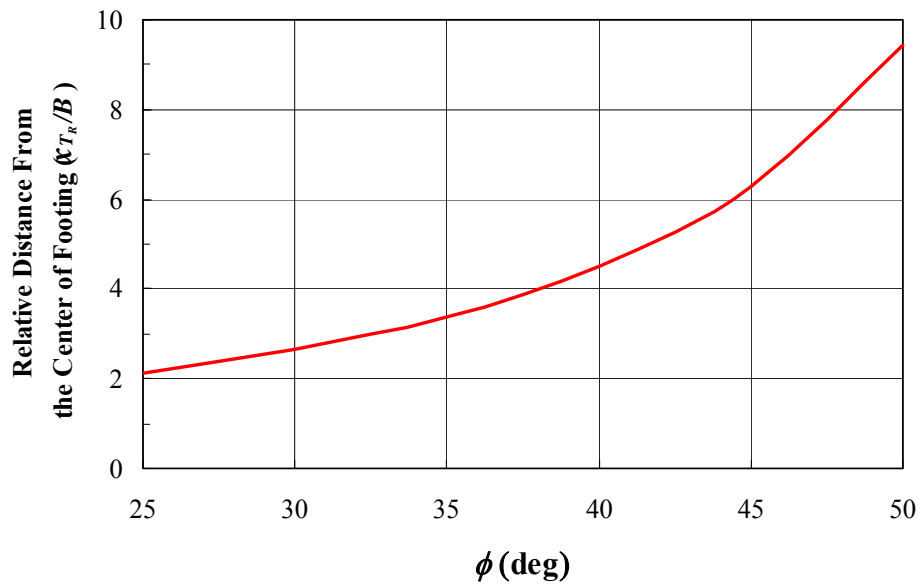
Figure 104
Variation of x_{T_R} with soil friction angle ϕ

The ultimate bearing capacity of the square footing on a reinforced soil foundation with horizontal reinforcement can now be given as:

$$q_{u(R)} = 1.3cN_c + qN_q + 0.4\gamma BN_\gamma + \sum_{i=1}^{N}\frac{12T_i[u+(i-1)h]r_T}{B^2} \tag{32}$$

This type of failure mechanism most likely controls the performance of the reinforced sandy soil.

Reinforcement Tension along the Faces *ab* and *bc* of Soil Wedge *abc*
The strip footing with a single layer of reinforcement is first discussed here. The increased bearing capacity due to the tensile force of the single layer of reinforcement Δq_T can be evaluated by considering the equilibrium of the soil wedge *abc* as shown in figure 105.

142

$$\Delta q_T = \frac{2T \sin(\pi/4 + \phi/2)}{B} \tag{33}$$
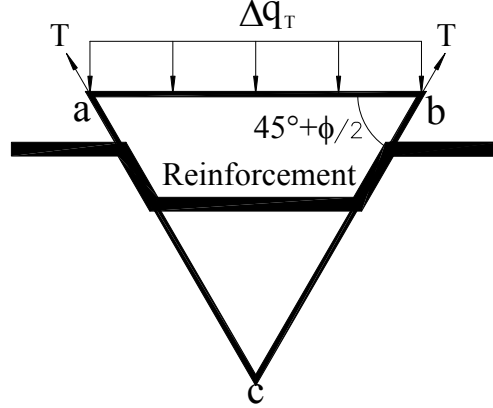
Figure 105
Free body diagram of the soil wedge *abc*

For two or more layers of reinforcement, the increased bearing capacity *Δq_T* can be easily shown to be:

$$\Delta q_T = \sum_{i=1}^{N} \frac{2T_i \sin\left(\frac{\pi}{4} + \frac{\phi}{2}\right)}{B} \tag{34}$$

It should be noted that all reinforcement layers must be placed above the triangle wedge *abc*, i.e. above the point *c* as shown in figure 100d, to contribute to improving the performance of the soil foundation for this case. The ultimate bearing capacity of strip footing on a reinforced soil foundation with the inclusion of reinforcement can now be given as:

$$q_{u(R)} = cN_c + qN_q + 0.5\gamma BN_\gamma + \sum_{i=1}^{N} \frac{2T_i \sin\left(\frac{\pi}{4} + \frac{\phi}{2}\right)}{B} \tag{35}$$

For square footings, the ultimate bearing capacity of reinforced soil foundation can be given as:

$$q_{u(R)} = 1.3cN_c + qN_q + 0.4\gamma BN_\gamma + \sum_{i=1}^{N} \frac{4T_i \sin\left(\frac{\pi}{4} + \frac{\phi}{2}\right)\left\{B - 2[u + (i-1)h]\tan\left(\frac{\pi}{4} - \frac{\phi}{2}\right)\right\}}{B^2} \tag{36}$$

This kind of failure mechanism most likely occurs in the reinforced soil with large particle size.

Partial Punching-Shear Failure

If the strength of the reinforced zone is moderately larger than that of the underlying unreinforced zone (i.e., between aforementioned two cases), a punching shear failure may occur partially in the reinforced zone followed by a general shear failure as shown in figure 100e. Again, two different reinforcing mechanisms are discussed here: horizontal confinement effect of reinforcement and reinforcement tension along the faces *aa'c* and *bb'c* of soil wedge *abb'ca'* (tension membrane effect).

Horizontal Confinement Effect of Reinforcement

For a strip footing with the horizontal confinement effect of reinforcement, the ultimate bearing capacity of reinforced soil foundation can be calculated by combining equations (17) and (28) with some modification as follows:

$$q_{u(R)} = q_g + \frac{2c_a D_P}{B} + \gamma_t D_P^2 \left(1 + \frac{2D_f}{D_P}\right)\frac{K_s \tan \phi_t}{B} - \gamma_t D_P + \Delta q_T \tag{37}$$

where:

$$\Delta q_T = 2\sum_{i=1}^{N_P} \frac{T_i}{B} \tan \delta + \sum_{i=N_P+1}^{N} \frac{4T_i [u + (i-1)h - D_P]}{B^2} \tag{38}$$

where, q_g is the ultimate bearing capacity of unreinforced soil located in the general shear failure zone; N_p is the number of reinforcement layers located in the punching shear failure zone; D_P is the depth of the punching shear failure in the reinforced zone.

Similarly, the ultimate bearing capacity of the square footing on a reinforced soil foundation with horizontal reinforcement can be evaluated as:

$$q_{u(R)} = q_g + \frac{4c_a D_P}{B} + 2\gamma_t D_P^2 \left(1 + \frac{2D_f}{D_P}\right)\frac{K_s \tan \phi_t}{B} - \gamma_t D_P + \Delta q_T \tag{39}$$

where:

$$\Delta q_T = 4\sum_{i=1}^{N_P} \frac{T_i}{B} \tan \delta + \sum_{i=N_P+1}^{N} \frac{12T_i [u + (i-1)h - D_P]r_T}{B^2} \tag{40}$$

This first failure mechanism most likely occurs in the reinforced clayey soil with low reinforced ratio (R_r). The reinforced ratio (R_r) is defined as:

$$R_r = \frac{E_R A_R}{E_S A_S} \tag{41}$$

where, E_R is the elastic modulus of the reinforcement $= J/t_R$; J is the tensile modulus of reinforcement; A_R is the area of reinforcement per unit width $= Nt_R \times 1$; t_R is the thickness of

the reinforcement; N is the number of reinforcement layers; E_s is the modulus of elasticity of soil; A_s is the area of reinforced soil per unit width $= d \times 1$; d is the total depth of reinforcement $= u + (N-1)h$.

Reinforcement Tension along the Faces aa'c and bb'c of Soil Wedge abb'ca'

For strip footing with reinforcement along the shear failure surface *aa'c* and *bb'c*, the ultimate bearing capacity of reinforced soil foundation can be written by combining equations (19) and (35) with some modification as follows:

$$q_{u(R)} = q_g + \frac{2c_a D_P}{B} + \gamma_t D_P^{\,2}\left(1 + \frac{2D_f}{D_P}\right)\frac{K_s \tan\phi_t}{B} - \gamma_t D_P + \Delta q_T \tag{42}$$

where:

$$\Delta q_T = 2\sum_{i=1}^{N_P}\frac{T_i}{B} + \sum_{i=N_P+1}^{N}\frac{2T_i \sin\left(\dfrac{\pi}{4} + \dfrac{\phi}{2}\right)}{B} \tag{43}$$

Similarly, the ultimate bearing capacity of the square footing on a reinforced soil foundation can be given as:

$$q_{u(R)} = q_g + \frac{4c_a D_P}{B} + 2\gamma_t D_P^{\,2}\left(1 + \frac{2D_f}{D_P}\right)\frac{K_s \tan\phi_t}{B} - \gamma_t D_P + \Delta q_T \tag{44}$$

where:

$$\Delta q_T = 4\sum_{i=1}^{N_P}\frac{T_i}{B} + \sum_{i=N_P+1}^{N}\frac{4T_i \sin\left(\dfrac{\pi}{4} + \dfrac{\phi}{2}\right)\left\{B - 2[u + (i-1)h - D_P]\tan\left(\dfrac{\pi}{4} - \dfrac{\phi}{2}\right)\right\}}{B^2} \tag{45}$$

This failure mechanism most likely controls the performance of the reinforced soil with large particle size such as crushed limestone.

Tensile Force in Reinforcement

In the experimental work of this study, the strain distribution along the reinforcement was measured by strain gauges. The tensile force developed along the reinforcement can be evaluated based on this measured strain. In real world design, the mobilized tensile force in reinforcement is unknown and has to be estimated. The following analysis is made to obtain a reasonable estimation on the tensile force along the reinforcement for a foundation on reinforced sand.

Experimental test results of this study showed that the strain developed along the reinforcement is directly related to the settlement. At the same footing settlement, the vertical

settlement distribution in the reinforced soil is assumed to be the same as that in unreinforced soil. At a certain settlement level, the shape of deformed reinforcement should be compatible with vertical settlement distribution.

In the absence of a rigorous solution for the vertical settlement distribution at a certain depth, it may be assumed that the shape of reinforcement at that certain depth is of the form as shown in figure 106 for sand. The reinforcement beneath the footing is assumed to move downward uniformly (lines *bc*). The reinforcement located outside of a certain boundary (lines *a-a'* and *d-d'*) is considered to have negligible strain. Based on the measured strain distribution along the reinforcement in the present study, the slope of the boundary lines *a-a'* and *d-d'* can be taken as about 2:1 (vertical : horizontal), which is the same as the simplified 2:1 stress distribution lines.

Since the distribution of vertical settlement is now known, the next step is to determine the amount of settlement at a certain depth beneath the footing (S_e). The following formula suggested by Schmertmann [31] and Schmertmann, et al. [32] can be used to calculate the elastic settlement S_e in sand:

$$S_e = C_1 C_2 C_3 \left(q - \gamma D_f \right) \sum \frac{I_\varepsilon \Delta z}{E_s} \tag{46}$$

where C_1 is a correction factor for the depth of embedment; C_2 is a correction factor for secondary creep; C_3 is a correction factor for the footing shape; q is the surcharge load; γ is the unit weight of soil; D_f is the embedment depth of the footing; I_ε is the strain influence factor; Δz is the thickness of subdivided sand layer; E_s is the elastic modulus of sand.
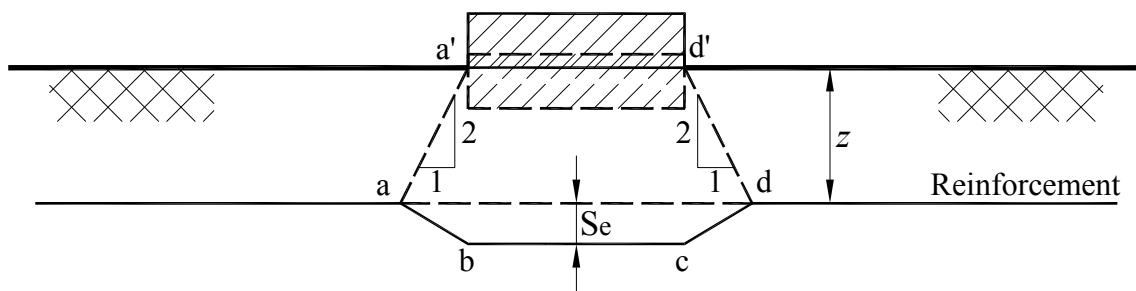
Figure 106

Simplified distribution of vertical settlement in sand

$$\varepsilon_{avg} = \frac{L_{ab} + L_{bc} + L_{cd} - L_{ad}}{L_{ad}} \tag{47}$$

$$L_{ab} = L_{cd} = \sqrt{S_e^2 + (z/2)^2} \tag{48}$$

$$L_{bc} = B \tag{49}$$

$$L_{ad} = B + z \tag{50}$$

where, S_e is the settlement at a depth of z beneath the center of the footing; z is the depth of reinforcement $= u+(i-1)h$. The average tensile force, T_{avg}, developed in reinforcement, can then be evaluated by the following equation:

$$T_{avg} = J\varepsilon_{avg} \tag{51}$$

where, J is the tensile modulus of reinforcement.

The measured strain showed that the strain distribution along the reinforcement is not uniform. The tensile strain is the largest at the point beneath the center of the footing and decreases with the distance away from the center of footing. A triangle distribution as shown in figure 107 is assumed here to approximately describe the real strain distribution along the reinforcement. The maximum strain in this triangle distribution can be calculated as:

$$\varepsilon_{max} = 2\varepsilon_{avg} \tag{52}$$
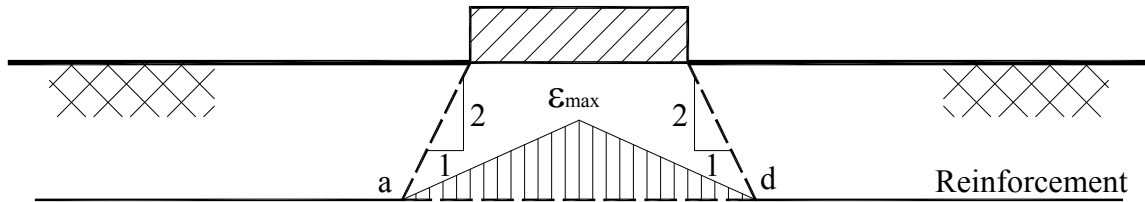
Figure 107
Simplified strain distribution along the reinforcement

For crushed limestone, due to its relatively larger particle size, the reinforcement is believed to move together with the soil wedge *abc* or *abb'ca'* as shown in figure 100d and 100e. It may then be assumed that the shape of reinforcement at the certain depth is of the form as shown in figure 108. The reinforcement in the soil wedge beneath the footing is assumed to move down uniformly (lines *cd* or *c'd'*). The reinforcement outside of the wedge is taken as horizontal. The strain of the reinforcement beyond a certain boundary (lines *a-a'-a''* and *f-f'-f''*) is considered to be insignificant. Without measuring strain data, the boundary lines *a-a'-a''* and *f-f'-f''* are assumed to have a slope of 2 which is the same as that for sand. The

amount of settlement at a certain depth beneath the footing (S_e) can be approximately evaluated by Schmertmann's method.
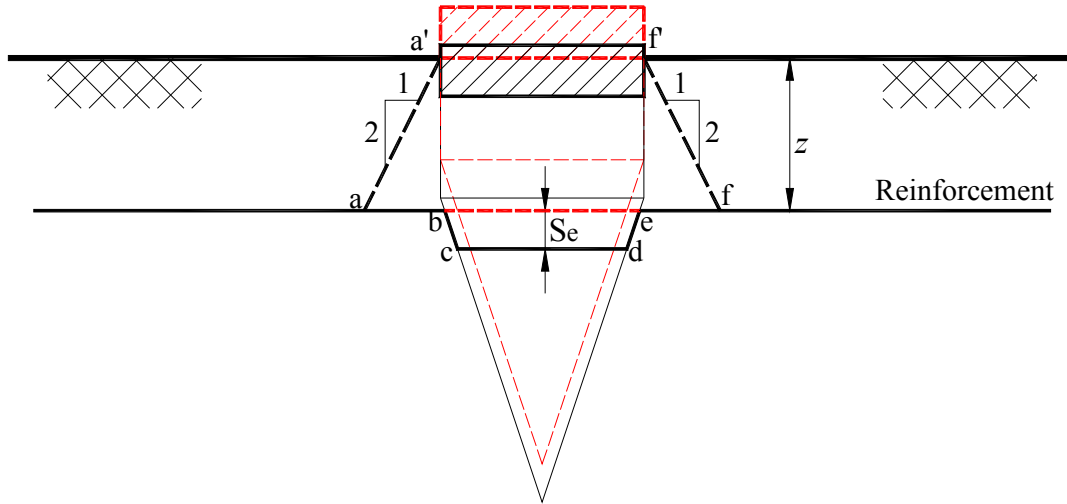
Figure 108
Simplified shape of reinforcement in crushed limestone

The average strain in reinforcement at a certain footing settlement can now be calculated as:

$$\varepsilon_{avg} = \frac{L_{ab} + L_{bc} + L_{cd} + L_{de} + L_{ef} - L_{af}}{L_{af}} = \frac{\Delta L}{L_{af}} \tag{53}$$

$$\Delta L = 2S_e - 2A + 2A \left/ \sin\left(\frac{\pi}{4} + \frac{\phi}{2}\right) - 2A \cdot tg\left(\frac{\pi}{4} - \frac{\phi}{2}\right) \right. \tag{54}$$

where:

$$A = \begin{vmatrix} 0 & \text{for } z \le D_P \\ S_e & \text{for } z > D_P \text{ and } S_e \le z - D_P \\ z - D_P & \text{for } z > D_P \text{ and } S_e > z - D_P \end{vmatrix} \tag{55}$$

The average tensile force T_{av} developed in reinforcement can then be evaluated by equation (51). A triangle distribution, as shown in figure 107, is again assumed here to approximately describe the real strain distribution along the reinforcement. The maximum strain in this triangle distribution can be calculated by equation (52).

For silty clay foundations with all geosynthetics reinforcement placed in the influence depth, it is recommended for design purposes that the tensile strain takes the value of 1.5~2% and 0.5~0.8% at the point beneath the center of footing for the top and bottom layer geosynthetics, respectively. The corresponding strain for geosynthetics located between the

148

top and bottom layers can be approximately linearly interpolated. A triangular distribution as shown in figure 107 is again assumed here to approximately describe the real strain distribution along the reinforcement.

Verification of Analytical Model

In verifying the analytical model, the test results obtained by Adams and Collin [37] are compared with the calculated bearing capacities. A comparison is also made between the field test data of this study and the analytical results. Because of the flowability of sand, the failure of reinforced sand most likely occurs in the reinforced zone with the reinforcement close to the horizontal direction. Due to the cohesive native of silty clay, the "deep footing" effect is likely to develop in the reinforced silty clay with the proper reinforcement configuration. The first failure mechanism (failure-like footings on a two-layer soil system) would then control the performance of reinforced silty clay. It should be noted that the concept of "deep footing" is different from the traditional concept of "deep foundation." Traditionally, "deep foundation" refers to piles and drilled shafts. Here, the "deep footing" effect suggests that the performance of reinforced soil is very similar to that of unreinforced soil, with a rigid footing having an additional embedment depth equal to the depth of the reinforced zone.

Comparison with Adams and Collin's Test Results

A series of large scale model tests on reinforced sand has been reported by Adams and Collin [33]. The ultimate bearing capacities were obtained at a settlement ratio s/B=10%. As the friction angle of soil was provided in the work of Adams and Collin [33], it was back-calculated from the model test results for the unreinforced case by using the bearing capacity formula suggested by Vesic [27]. The elastic modulus of sand was also back-calculated from the model test results on unreinforced case by substituting settlement $s = 0.1B$ in equation (46). The failure of reinforced sand is believed to occur in the reinforced zone with the reinforcement close to the horizontal direction.

Table 11 presents a comparison of the measured and estimated bearing capacities for the large scale model tests conducted by Adams and Collin [33]. The predicted values by using the analytical solution of this study are in agreement with the test results of TL286, TL2861, and TL386.

The soil properties of sand in the test TL3861 were the same as those in the test TL386. The same type and size of geogrid were also used in both tests. The only difference was the number of reinforcement layers. Test TL3861 used two layers of reinforcement, while test

TL 386 used only one layer of reinforcement. The ultimate bearing capacity of the test TL 3861 should be higher than that of the test TL386, but the measured data was the opposite. This may be why the predicted value for TL3861 is much higher than the measured data.

The predicted values for the tests TL166 and TL169 are relatively lower as compared to measured data. This is also due to the test variation. The density of the tests TL166 and TL169 was higher than the density in the tests TL286 and TL2861, but the ultimate bearing capacity of unreinforced sand corresponding to the tests TL166 and TL169 was lower than that of unreinforced sand corresponding to the tests TL286 and TL2861. This is not usual because a footing is expected to have a higher ultimate bearing capacity on denser sand if the other conditions are kept the same.

Table 11
Measured and estimated bearing capacities for the experiments conducted by Adams and Collin [33]

Test ID	q_u (psi)	B (in.)	γ (pcf)	u/B	h/B	N	$q_{u(R)}$ (psi) (measured)	$q_{u(R)}$ (psi) (calculated)	Error
TL286	39.2	24	92.3	0.25	…	1	53.7	48.6	9.5%
TL2861	39.2	24	92.3	0.25	0.25	2	53.7	54.7	1.9%
TL386	20	24	90.4	0.25	…	1	29.4	29.4	0.0%
TL3861	20	24	90.4	0.25	0.25	2	26.8	35.2	31.4%
TL166	34.8	24	93.6	0.25	…	1	52.2	44.2	15.3%
TL169	34.8	24	93.6	0.375	…	1	57.7	43.7	24.4%

Comparison with Large-Scale Field Test Results of this Study

A comparison between the measured and calculated bearing capacities for all five field tests is presented in table 12.

It can be seen from table 12 that the predicted values by using the analytical solution with the first failure mechanism (failure like footings on a two-layer soil system) are in agreement with the test results of four layers of BX1500 geogrid placed at 8 in. spacing or five layers of BX6200 geogrid placed at 6 in. spacing. This suggests that the reinforced zone with four layers of BX1500 geogrid placed at 8 in. spacing or five layers of BX6200 geogrid placed at 6 in. spacing is strong enough to develop "deep footing" effect. For four layers of BX6100 and BX6200 geogrid placed at 8 in. spacing, the predicted values are relatively higher as compared to measured data. The reinforced zone in these two sections may not be strong

enough to form perfect "deep footing" effect. The back calculation by applying partial punching shear failure mechanism indicates that the depth of the punching shear failure (D_P) is equal to *3d/5*. For three layers of BX6200 geogrid placed at 12 in. spacing, the vertical spacing ratio (*h/B*) is equal to 2/3. The failure of reinforced silty clay most likely occurred between the top two layers of geogrid. This failure mode should be avoided in engineering practice. As mentioned before, this failure mode can be prevented from occurring by keeping vertical spacing (*h*) less than 0.5*B*.

Table 12
Measured and estimated bearing capacities for the field tests

Geogrid Type	B (in.)	u/B	h/B	N	$q_{u(R)}$ (psi) (measured)	$q_{u(R)}$ (psi) (calculated)	Error
BX6100	18	1/3	4/9	4	160.7	199.4	24.1%
BX6200	18	1/3	2/3	3	153	199.6	30.4%
BX6200	18	1/3	4/9	4	172	200.9	16.8%
BX6200	18	1/3	1/3	5	191.6	202	5.5%
BX1500	18	1/3	4/9	4	188.8	202.2	7.1%

Comparison of Analytical Solutions with Laboratory Model Test Results
A large number of model tests in the present study provide experimental data to compare the analytical solution described herein. For obtaining the predicted ultimate bearing capacity ratio of reinforced soil, the ultimate bearing capacity ratios were calculated based on the aforementioned failure modes. Based on the observation during the model tests, the failure of reinforced sand most likely occurred in the reinforced zone with reinforcement close to the horizontal direction (failure mode 1); the reinforced silty clay in lab tests behaved like a footing on a two layer soil system (failure mode 2); and the partial punching failure in the reinforced zone is most likely to happen in geosynthetic-reinforced, crushed limestone in this study. The design methods from Kumar and Saran [16], Huang and Tatsuoka [17], Huang and Menq [18], and Wayne, et al. [19] are also compared with proposed analytical solution.

Laboratory Model Test Series for Silty Clay (Figures E.1 through E.4 on Appendix E))
Only the design methods of Huang and Menq [18] and Wayne, et al. [19] can be applied for cohesive soil. Compared with laboratory test results, Huang and Menq's method underestimates the bearing capacity of reinforced silty clay. This may be expected in the light of the fact that the regression model for the estimate of the load-spreading angle (the wide-slab effect) developed in their study was based on model test results for sand. On the other

hand, the method of Wayne, et al., overpredicts the bearing capacity of reinforced clay. In their method, Wayne, et al., [19] assumed that the reinforcement sheet turns vertically at the punching failure surface due to the punching failure. This assumption requires a large deformation to be developed. The visual inspection of the reinforcement after the tests confirmed that this amount of deformation wasn't reached in this study. The proposed design method of this study assumed that the reinforcement remains horizontal at the ultimate bearing capacity. It can be seen from figures E.1 through E.4 on Appendix E that the assumption of the horizontal reinforcement gives a better prediction of bearing capacity as compared to the assumption of vertical reinforcement along the punching failure surface. This suggests that taking the reinforcement as horizontal is more appropriate for this study. The actual shape of the reinforcement at the ultimate bearing capacity should be between these two cases. The relatively poor match between measured and predicted BCR for geotextile reinforced silty clay, as show in E.4, may be due to the slack of woven geotexitle.

Laboratory Model Test Series for Sand (Figures E.5 through E.9 on Appendix E)
All other methods overestimated the performance of reinforced sand. The proposed design approach provides a better prediction. The "deep footing" effect is explicitly or implicitly implied in the design methods of Huang and Tatsuoka [17], Huang and Menq [18], and Wayne, et al. [19]. This effect results in an almost linear increase of the bearing capacity ratio with increasing the number of reinforcement layers or total depth of the reinforcement because of relatively high friction angle of sand. It appears that using geosynthetics to reinforce uniform sand cannot form this effect due to the flowability of sand. The design method of Kumar and Saran [16] assumes that all reinforcement layers either fail by tension rupture or by pull-out of reinforcement. This assumption leads to the result that the tensile force developed in reinforcement increases with increasing the depth of reinforcement (because normal load increases) which is obviously opposite to the measured data of this study.

Laboratory Model Test Series for Kentucky Crushed Limestone (Figures E.10 through E.16 on Appendix E)
The partial punching shear failure in the reinforced zone most likely occurs in the geosynthetics reinforced crushed limestone. The depth of the punching shear failure (D_P) is taken as one fourth of the total depth of reinforcement (*d*), i.e., $D_P = d/4$. Again, as indicated in the sand, all other methods overestimate the performance of crushed limestone reinforced by geosynthetics. The proposed design method provides a better prediction. However, the design method of Huang and Menq [18] gives a good prediction of BCR for crushed limestone reinforced by steel wire mesh and steel bar mesh. It appears that if the

reinforcement has a much higher stiffness, as compared to the crushed limestone, the reinforced mass would act as a rigid block and the "deep footing" effect can then be formed. In this case, Huang and Menq's method is recommended for use.

CONCLUSIONS

The benefits of using geosynthetics to reinforce soils have been widely recognized. Past research works available in the literature demonstrate that the use of reinforcements can significantly increase the bearing capacity of the soil foundations and reduce footing settlement.

This research is undertaken to investigate the potential benefits of using reinforcement to improve the bearing capacity and reduce the settlement of shallow foundations on soils. For this purpose, four series of tests were conducted, small-scale laboratory tests on silty clay soil, small-scale laboratory tests on sandy soil, small-scale laboratory tests on Kentucky crushed limestone, and large-scale field tests on silty clay embankment soil. The influences of different variables and parameters contributing to the improved performance of reinforced soil foundation (RSF) were examined in these tests. The investigated parameters include top layer spacing (u), number of reinforcement layers (N), vertical spacing between reinforcement layers (h), tensile modulus and type of reinforcement, embedment of the footing (D_f), shape of the footing, and type of soil. Also, an instrumentation program with pressure cells and strain gauges was designed to investigate the stress distribution in soil mass with and without reinforcement and the strain distribution along the reinforcement. In addition, the numerical study was conducted and statistical models for different soil conditions were proposed. The reinforcement can restrain lateral deformation or potential tensile strain of the soil (confinement effect) and the deformed reinforcement can also develop an upward force (tension membrane effect). All these effects lead to an increase in bearing capacity. So, the new bearing capacity formulas including the contribution of reinforcements to bearing capacity were developed for RSF with different soil types.

Based on the results of the present study, the following conclusions can be drawn:

(1) The inclusion of reinforcement generally increased the ultimate bearing capacity of granular soil and reducing footing settlement at ultimate load.

(2) The optimum depth to place the first reinforcement layer was estimated to be at 0.33B below the footing for all soil tested in this study.

(3) The bearing capacity of reinforced soil increases with increasing number of reinforcement layers. However, the significance of an additional reinforcement layer decreases with the increase in number of layers. The reinforcing effect becomes negligible below the influence depth. The influence depth of reinforced sand was

obtained at approximately 1.25B in this study regardless of the type of reinforcement and footing embedment depth, while the influence depth of geogrid and geotextile reinforced silty clay was obtained at approximately 1.5B and 1.25B, respectively.

(4) The BCR values decrease with increasing vertical spacing of reinforcement layers. No optimum vertical spacing was observed for the geogrid reinforced silty clay and sand. For the tested soil (silty clay and sand) and geogrid reinforcement, one can realize that the smaller the spacing, the higher the BCR. In practice, cost would govern the spacing and require 6 in. $\leq$ h $\leq$ 18 in. For design purposes, engineers need to balance between reducing spacing and increasing geogrid tensile modulus. The author believes that a value of $h/B = 0.33$ can be a reasonable value to use in the design of reinforced soil.

(5) Geogrid beyond the effective length (4.0-6.0B) results in insignificant mobilized tensile strength and thus provides negligible reinforcement effect.

(6) In general, the performance of reinforced soil improves with increasing the reinforcement tensile modulus. For a project controlled by settlement criteria, geogrid reinforcement is generally considered to perform better for soil foundation than geotextile.

(7) The inclusion of reinforcement will redistribute the applied load to a wider area, thus minimizing stress concentration and achieving a more uniform stress distribution. The redistribution of stresses below the reinforced zone will result in reducing the consolidation settlement of the underlying weak clayey soil, which is directly related to the induced stress. With the appropriate reinforcement configuration, the inclusion of reinforcement can develop a "surcharge effect" to prevent soil from moving upward, and thus improve the bearing capacity of the soil.

(8) The strain developed along the reinforcement is directly related to the settlement, and therefore higher tension would be developed for geogrid with higher modulus under the same footing settlement.

(9) The failure mechanisms of reinforced soil foundations were proposed for different soil types based on the literature review and the model test results of the present study. Stability analyses were then conducted on the proposed failure mechanisms of RSFs of tested soil types to evaluate the contribution of the reinforcement. New bearing capacity formulas that include the benefit of reinforcement to the increase in

bearing capacity were developed for the RSFs of three soil types. In the light of the fact that the mobilized tensile force in the reinforcement needs to be known to quantify the benefit of reinforcement, a reasonable estimation on the tensile force along the reinforcement was proposed. The predicted bearing capacities of reinforced soil foundation by using the methods of this study are generally in agreement with the field test results of previous research for reinforced sand and this study for reinforced silty clay. The proposed methods also provide good predictions of laboratory model test results of this study.

RECOMMENDATIONS

Based on extensive laboratory tests, field tests, and numerical study, the following step-by-step procedure is recommended for the design of reinforced soil foundation.

(1) Assume the footing width, *B*.

(2) Calculate the ultimate bearing capacity of unreinforced soil foundation, q_u.

(3) Determine the bearing pressure along the bottom of a shallow foundation, *q*.

(4) Select the geogrid with specific tensile modulus (*J*) and the proper reinforcement layout. Based on the experimental test results of this study, typical design parameters for reinforcement layout are recommended in table 13.

(5) Determine the possible failure mode of reinforced soil foundation

(6) Determine the tensile force, *T*, developed in the reinforcement using the method suggested in this study (refer to section "tensile force in reinforcement").

(7) Calculate the ultimate bearing capacity of reinforced soil foundation, $q_{u(R)}$ by using the equation (17) or (18) for clay, (28) or (32) for sand, and (42) or (44) for limestone.

(8) Calculate the allowable bearing capacity of reinforced soil foundation, $q_{a(R)}$ as

$$q_{a(R)} = \frac{q_{u(R)}}{F_S} \tag{56}$$

where, F_s is the factor of safety

(9) If the allowable bearing capacity of reinforced soil foundation, $q_{a(R)}$, is lower than the bearing pressure, *q*, repeat Steps (1) through (9).

Table 13
Recommended design parameters for reinforcement layout

Parameter	Typical value	Recommended
u/B	0.2 ~ 0.5	1/3
h/B	0.2 ~ 0.5	1/3
d/B	1.3 ~ 1.7	1.5
l/B	4 ~ 6	5

REFERENCES

1. Binquet, J., and Lee, K.L. "Bearing Capacity Tests on Reinforced Earth Slabs." *Journal of Geotechnical Engineering Division*, ASCE, Vol. 101, No.GT12, 1975a, pp. 1241-1255.

2. Binquet, J., and Lee, K.L. "Bearing Capacity Analysis of Reinforced Earth Slabs." *Journal of Geotechnical Engineering Division*, ASCE, Vol. 101, No.GT12, 1975b, pp. 1257-1276.

3. Akinmusuru, J.O., and Akinbolade, J.A. "Stability of Loaded Footing on Reinforced Soil." *Journal of Geotechnical Engineering*, ASCE, Vol. 107, No.6, 1981, pp. 819-827.

4. Fragaszy, J.R., and Lawton, E. "Bearing Capacity of Reinforced Sand Subgrades." *Journal of Geotechnical Engineering*, ASCE, Vol. 110, No.10, 1984, pp. 1500-1507.

5. Guido, V.A.; Chang, D.K.; and Sweeny, M.A. "Comparison of Geogrid and Geotextile Reinforced Slabs." *Canadian Geotechnical Journal*, Vol. 20, 1986, pp. 435-440.

6. Das, B.M. "Shallow Foundation on Sand Underlain by Soft Clay with Geotextile Interface." *ASCE special publication on Geosynthetics for Soil Improvement*, Holtz, R.D, ed., Geotechnical Special Publication No. 18, May, 1988, pp.112-126.

7. Yeo, C.Y.; Puri, V.K., Das, B.M., and Wright, M.A. "Laboratory Investigation Into the Settlement of Foundations on Geogrid-reinforced Sand Due to Cyclic Load." *Geotechnical ad Geological Engineering*, 11, 1993, pp. 1-14.

8. Omar, M.T.; Das, B.M.; Yen, S.C.; Puri, V.K.; and Cook, E.E. "Ultimate Bearing Capacity of Rectangular Foundations on Geogrid-reinforced Sand." *Geotechnical Testing Journal*, ASTM, Vol. 16, No. 2, 1993a, pp. 246-252.

9. Omar, M.T.; Das, B.M.; Puri, V.K.; and Yen, S.C. "Ultimate Bearing Capacity of Shallow Foundations on Sand with Geogrid Reinforcement." *Canadian Geotechnical Journal*, Vol. 20, No. 3, 1993b, pp. 435-440.

10. Khing, K.H.; Das, B.M.; Puri, V.K.; Cook, E.E.; and Yen, S.C. "The Bearing Capacity of a Strip Foundation on Geogrid-reinforced Sand." *Geotextiles and Geomembranes*, Vol. 12, 1993, pp. 351-361

11. Das, B.M., and Omar, M.T. "The Effects of Foundation Width on Model Tests for the Bearing Capacity of Sand with Geogrid-reinforcement." *Geotechnical and Geological Engineering*, Vol. 12, 1994, pp. 133-141.

12. Shin, E.C., Das, B.M., Puri, V.K., Yen, S.C., and Cook, E.E. "Bearing Capacity of Strip Foundation on Geogrid-reinforced Clay." *Geotechnical Testing Journal*, ASTM, Vol. 16, No. 4, 1993, pp. 534-541.

13. Shin, E.C., Das, B.M., Lee, E.S., and Atalar, C. "Bearing Capacity of Strip Foundation on Geogrid-reinforced Sand." *Geotechnical and Geological Engineering*, 20, 2002, pp. 169-180.

14. Mandal, J.N., and Sah, H.S. "Bearing Capacity Tests on Geogrid-reinforced Clay." *Geotextiles and Geomembranes*, Vol. 11, No. 3, 1992, pp. 327-333.

15. Ghosh, A., Ghosh, A., and Bera, A.K. "Bearing Capacity of Square Footing on Pond Ash Reinforced with Jute-geotextile." *Geotextiles and Geomembranes*, Vol. 23, No.2, 2005, pp. 144-173.

16. Kumar, A., and Saran, S. "Bearing Capacity of Rectangular Footing on Reinforced Soil." *Geotechnical and Geological Engineering*, Vol. 21, 2003, pp. 201-224

17. Huang, C.C., and Tatsuoka, F. "Bearing Capacity Reinforced Horizontal Sandy Ground." *Geotextiles and Geomembranes*, Vol. 9, 1990, pp. 51-82.

18. Huang, C.C., and Menq, F.Y "Deep-footing and Wide-slab Effects in Reinforced Sandy Ground." *Journal of Geotechnical and Geoenviromental Engineering*, ASCE, Vol. 123, No.1, 1997, pp. 30-36.

19. Wayne, M.H., Han, J., and Akins, K. "The Design of Geosynthetic Reinforced Foundations." *Proceedings of ASCE's 1998 Annual Convention & Exposition*, ASCE Geotechnical Special Publication, 76, 1998, pp. 1-18.

20. American Society for Testing and Materials, ASTM D 1196-93, *Standard Test Method for In Situ Compressive Stress within Solid Unit Masonry Estimated Using Flatjack Measurements*, Philadelphia, PA.

21. Hibbitt, Karlson, and Sorensen, *ABAQUS Standard User's Manuals*, Version 6.3-1, Pawtucket, RI, USA, 2002.

22. Perkins, S. W., and Edens, M. Q. "Finite Element Modeling of a Geosynthetic Pullout Test." *Geotechnical and Geological engineering*, Vol. 21, 2003, pp. 357-375.

23. Zhu, M., and Radoslaw, L. M. "Shape Factors for Limit Loads on Square and Rectangular Footings." *Journal of geotechnical and Geoenvironmental Engineering*, Vol. 131, No.2, 2005, pp. 223-231

24. Chungsik Y. "Laboratory Investigation of Bearing Capacity Behavior of Strip Footing on Reinforcement-reinforced Sand Slope," *Geotextiles and Geomembranes*, Vol. 19, 2001, pp. 279-298.

25. Guido, V.A., Biesiadecki, G.L., and Sullivan, M.J. "Bearing Capacity of a Geotextile Reinforced Foundation." *Proceedings of the 11th International Conference on Soil Mechanics and Foundation Engineering*, San Francisco, Vol. 3, 1985, pp.1777-1780.

26. Chen, Q.M. "An Experimental Study on Characteristics and Behavior of Reinforced Soil Foundation." PhD dissertation, Louisiana State University, Baton Rouge, LA, 2007.

27. Vesic, A.S. "Analysis of Ultimate Loads of Shallow Foundatins." *Journal of the Soil Mechanics and Foundations Division*, ASCE, Vol. 99, No.SM1, 1973, pp. 45-73.

28. Westergaard, H.M. "A Problem of Elasticity Suggested by a Problem in Soil Mechanics: Soft Material Reinforced by Numerous Strong Horizontal Sheets." Contributions to the *Mechanics of Solids*, Dedicated to Stephen Timoshenko, Macmillan, New York, 1938, pp 268 – 277.

29. Meyerhof, G.G., and Hanna, A.M. "Ultimate Bearing Capacity of Foundations on Layered Soils Under Inclined load." *Canadian Geotechnical Journal*, Vol. 15, No.4, 1978, pp. 565-572.

30. Das, B.M. *Shallow Foundations : Bearing Capacity and Settlement*, CRC Press, Boca Raton, 1999.

31. Schmertmann, J.H. "Static Cone to Compute Static Settlement Over Sand." *Journal of the Soil Mechanics and Foundations Division*, ASCE, Vol. 96, No.SM3, 1970, pp. 1011-1043.

32. Schmertmann, J.H., Hartman, J.P., and Brown, P.R. "Improved Strain Influence Factor Diagrams." *Journal of the Geotechnical Engineering Division*, ASCE, Vol. 104, No.GT8, 1978, pp. 1131-1135.

33. Adams, M.T., and Collin, J.G. "Large Model Spread Footing Load Tests on Geosynthetic Reinforced Soil Foundations." *Journal of Geotechnical and Geoenvironmental Engineering*, ASCE, Vol. 123, No.1, 1997, pp. 66-72.

34. Sakti, J., and Das, B.M. "Model Tests for Strip Foundation on Clay Reinforced with Geotextile Layers." *Transportation Research Record* No. 1153, National Academy of Sciences, Washington, D.C., 1987, pp. 40-45.

35. Ramaswamy, S.D., and Puroshothama, P. "Model Footings of Geogrid Reinforced Clay." *Proceedings of the Indian Geotechnical Conference on Geotechnique Today*, Vol. 1, 1992, pp. 183-186

36. Leng, J. *Characteristics and behavior of geogrid-reinforced aggregate under cyclic load*. PhD thesis, North Carolina State University, Raleigh, North Carolina, USA, 2002.

37.   Michalowski, R.L. "Limit Loads on Reinforced Foundation Soils", *Journal of Geotechnical and Geoenviromental Engineering*, ASCE, Vol. 130, No.4, 2004, pp. 381-390.

38.   Yetimoglu, T., Wu, J.T.H., and Saglamer, A. "Bearing Capacity of Rectangular Footings on Geogrid-reinforced Sand." *Journal of Geotechnical Engineering*, ASCE, Vol. 120, No.12, 1994, pp. 2083-2099.

39.   Patra, C.R., Das, B.M., and Atalar, C. "Bearing Capacity of Embedded Strip Foundation on Geogrid-reinforced Sand." *Geotextiles and Geomembranes*, Vol. 23, 2005, pp. 454-462.

40.   Lee, K.M., and Manjunath, V.R. "Experimental and Numerical Studies of Geosynthetics-reinforced Sand Slopes Loaded with a Footing." *Canadian Geotechnical Journal*, Vol. 37, 2000, pp. 828-842.

41.   Gabr, M.A., Dodson, R., and Collin, J.G. "A Study of Stress Distribution in Geogrid-reinforced Sand." *Proceedings of geosynthetics in foundation reinforcement and erosion control systems*, ASCE Geotechnical Special Publication, 76, 1998, pp. 62-76.

42.   James, R., and Raymond, G. "Strain/load on Geogrid-reinforcement of Aggregates Below Shallow Footings." *Proceedings of the 55th Canadian geotechnical and 3rd joint IAH-CNC and CGS groundwater specially conferences*, Niagara Falls, Ontario, 2002, pp. 783-790

43.   Uchimura, T., Tatsuoka, F., Hirakawa, D., and Shibata, Y. "Effects of Reinforcement Stiffness on Deformation of Reinforced Soil Structures Under Sustained and Cyclic Loading." *Proceedings of Asian Regional Conference on Geosynthetics*, Seoul, 2004, pp. 233-239.

44.   Das, B.M., Shin, E.C., and Omar, M.T. "The Bearing Capacity of Surface Strip Foundations on Geogrid-reinforced Sand and Clay – a comparative study." *Geotechnical and Geological Engineering*, Vol. 12, No. 1, 1994, pp. 1-14.

45.   Maharaj D. K. "Nonlinear Finite Element Analysis of Strip Footing on Reinforced Clay." *The Electronic Journal of Geotechnical Engineering*, Vol. 8, Bundle C, 2003.

46.   Singh, H. *Bearing capacity of reinforced soil beds*. Ph.D. dissertation, Indian Institute of Science, Bangalore, India, 1988.

47.   Elvidge, C., and Raymond, G. "Maximized Bearing Capacity From a Single Geosynthetic Reinforcement Layer." *Proceedings of the 54th Canadian Geotechnical Conference*, Calgary, Alberta, 2001, pp. 475-480.

APPENDIX A TEST FACTORIAL

Table A.1
Test factorial for silty clay soil

Test No.	Footing Dimensions	Embedment in.	Reinforcement configuration	u in.	h in.
CNR*	6 in.× 6 in.	0	Unreinforced	...	...
CGG11-1	6 in.× 6 in.	0		1	...
CGG11-2	6 in.× 6 in.	0		2	...
CGG11-3	6 in.× 6 in.	0		3	...
CGG11-4	6 in.× 6 in.	0	N=1, BasXgrid11	4	...
CGG11-5	6 in.× 6 in.	0		5	...
CGG11-6	6 in.× 6 in.	0		6	...
CGG11-7	6 in.× 6 in.	0		8	...
CGG12	6 in.× 6 in.	0	N=2, BasXgrid11	2	2
CGG13	6 in.× 6 in.	0	N=3, BasXgrid11	2	2
CGG14	6 in.× 6 in.	0	N=4, BasXgrid11	2	2
CGG15*	6 in.× 6 in.	0	N=5, BasXgrid11	2	2
CGG21	6 in.× 6 in.	0	N=1, BX6100	2	...
CGG22	6 in.× 6 in.	0	N=2, BX6100	2	2
CGG23	6 in.× 6 in.	0	N=3, BX6100	2	2
CGG24#	6 in.× 6 in.	0	N=4, BX6100	2	2
CGG25*	6 in.× 6 in.	0	N=5, BX6100	2	2
CGG31	6 in.× 6 in.	0	N=1, BX6200	2	...
CGG32	6 in.× 6 in.	0	N=2, BX6200	2	2
CGG33-1*	6 in.× 6 in.	0	N=3, BX6200	2	1
CGG33-2*	6 in.× 6 in.	0	N=3, BX6200	2	2
CGG33-3*	6 in.× 6 in.	0	N=3, BX6200	2	3
CGG33-4*	6 in.× 6 in.	0	N=3, BX6200	2	4
CGG34*	6 in.× 6 in.	0	N=4, BX6200	2	2
CGG35*	6 in.× 6 in.	0	N=5, BX6200	2	2
CGT11	6 in.× 6 in.	0	N=1, HP570	2	...
CGT12	6 in.× 6 in.	0	N=2, HP570	2	2
CGT13	6 in.× 6 in.	0	N=3, HP570	2	2
CGT14	6 in.× 6 in.	0	N=4, HP570	2	2
CGT15*	6 in.× 6 in.	0	N=5, HP570	2	2
CFNR	6 in.× 10 in.	0	Unreinforced	...	...

Table A.1
(continued)

CFGG15[*]	6 in.× 10 in.	0	N=5, BasXgrid11	2	2
CFGG21	6 in.× 10 in.	0	N=1, BX6100	2	...
CFGG22	6 in.× 10 in.	0	N=2, BX6100	2	2
CFGG23[*]	6 in.× 10 in.	0	N=3, BX6100	2	2
CFGG24[*#]	6 in.× 10 in.	0	N=4, BX6100	2	2
CFGG25[*]	6 in.× 10 in.	0	N=5, BX6100	2	2
CFGT15[*]	6 in.× 10 in.	0	N=5, HP570	2	2

* Instrumented with pressure cell, # Instrumented with strain gage

Table A.2
Test factorial for sand soil

Test No.	Footing Dimensions	Embedment in.	Reinforcement Configuration	u in.	h in.
SNR[*]	6 in.× 6 in.	0	Unreinforced	...	...
SGG11-1	6 in.× 6 in.	0		1	...
SGG11-2	6 in.× 6 in.	0		2	...
SGG11-3	6 in.× 6 in.	0	N=1, BasXgrid11	3	...
SGG11-4	6 in.× 6 in.	0		4	...
SGG11-5	6 in.× 6 in.	0		6	...
SGG81-1	6 in.× 6 in.	0		1.2	...
SGG81-2	6 in.× 6 in.	0	N=1 2xMiragrid 8XT each layer	1.8	...
SGG81-3	6 in.× 6 in.	0		2.4	...
SGG81-4	6 in.× 6 in.	0		3	...
SGG12[*]	6 in.× 6 in.	0	N=2, BasXgrid11	2	2
SGG13[*]	6 in.× 6 in.	0	N=3, BasXgrid11	2	2
SGG14[*]	6 in.× 6 in.	0	N=4, BasXgrid11	2	2
SGT12[*]	6 in.× 6 in.	0	N=2, HP570	2	2
SGT13[*]	6 in.× 6 in.	0	N=3, HP570	2	2
SGT14[*]	6 in.× 6 in.	0	N=4, HP570	2	2
SDNR[*]	6 in.× 6 in.	6	Unreinforced	...	...
SDGG11-0	6 in.× 6 in.	6		0	...
SDGG11-1	6 in.× 6 in.	6	N=1,BasXgrid11	1	...
SDGG11-2	6 in.× 6 in.	6		2	...
SDGG11-3	6 in.× 6 in.	6		3	...

SDGG11-4	6 in.× 6 in.	6		4	...
SDGG11-5	6 in.× 6 in.	6	N=1,BasXgrid11	6	...
SDGG11-6	6 in.× 6 in.	6		8	…
SDGG81-0	6 in.× 6 in.	6		0	...
SDGG81-1	6 in.× 6 in.	6	N=1	1	...
SDGG81-2	6 in.× 6 in.	6	2xMiragrid 8XT	2	...
SDGG81-3	6 in.× 6 in.	6	each layer	3	...
SDGG81-4	6 in.× 6 in.	6		4	...
SDGG12	6 in.× 6 in.	6	N=2,BasXgrid11	2	2
SDGG13-1	6 in.× 6 in.	6	N=3,BasXgrid11	2	1
SDGG13-2	6 in.× 6 in.	6	N=3,BasXgrid11	2	2
SDGG13-3	6 in.× 6 in.	6	N=3,BasXgrid11	2	3
SDGG14*	6 in.× 6 in.	6	N=4,BasXgrid11	2	2
SDGG21	6 in.× 6 in.	6	N=1,BX6100	2	...
SDGG22*	6 in.× 6 in.	6	N=2,BX6100	2	2
SDGG23*	6 in.× 6 in.	6	N=3,BX6100	2	2
SDGG24*#	6 in.× 6 in.	6	N=4,BX6100	2	2
SDGT11	6 in.× 6 in.	6	N=1,HP570	2	...
SDGT12*	6 in.× 6 in.	6	N=2,HP570	2	2
SDGT13*	6 in.× 6 in.	6	N=3,HP570	2	2
SDGT14*	6 in.× 6 in.	6	N=4,HP570	2	2
SDGGT11	6 in.× 6 in.	6	N=1,Composite	2	...
SDGGT12	6 in.× 6 in.	6	N=2,Composite	2	2
SDGGT13	6 in.× 6 in.	6	N=3,Composite	2	2
SDGGT14*	6 in.× 6 in.	6	N=4,Composite	2	2
SDFNR*	6 in.× 10 in.	6	Unreinforced	...	…
SDFGG14*	6 in.× 10 in.	6	N=4,BasXgrid11	2	2
SDFGG24*	6 in.× 10 in.	6	N=4, BX6100	2	2
SDFGT14*	6 in.× 10 in.	6	N=4, HP570	2	2
SDFGGT14*	6 in.× 10 in.	6	N=4, Composite	2	2

* Instrumented with pressure cell, # Instrumented with strain gage

Table A.3
Test factorial for Kentucky crushed limestone

Test No.	Footing Dimensions	Embedment in.	Reinforcement configuration	u in.	h in.
LNR-1	6 in.× 6 in.	0	Unreinforced	…	...
LGG41	6 in.× 6 in.	0	N=1, BX1100	2	...
LGG42	6 in.× 6 in.	0	N=2, BX1100	2	2
LGG43	6 in.× 6 in.	0	N=3, BX1100	2	2
LGG51	6 in.× 6 in.	0	N=1, BX1200	2	...
LGG52	6 in.× 6 in.	0	N=2, BX1200	2	2
LGG53	6 in.× 6 in.	0	N=3, BX1200	2	2
LGG61	6 in.× 6 in.	0	N=1, BX1500	2	...
LGG62	6 in.× 6 in.	0	N=2, BX1500	2	2
LGG63	6 in.× 6 in.	0	N=3, BX1500	2	2
LGG11	6 in.× 6 in.	0	N=1, BasXgrid11	2	...
LGG12	6 in.× 6 in.	0	N=2, BasXgrid11	2	2
LGG13	6 in.× 6 in.	0	N=3, BasXgrid11	2	2
LGG71	6 in.× 6 in.	0	N=1, MS330	2	...
LGG72	6 in.× 6 in.	0	N=2, MS330	2	2
LGG73	6 in.× 6 in.	0	N=3, MS330	2	2
LSWM1	6 in.× 6 in.	0	N=1, SWM	2	...
LSWM2	6 in.× 6 in.	0	N=2, SWM	2	2
LSWM3	6 in.× 6 in.	0	N=3, SWM	2	2
LSBM1	6 in.× 6 in.	0	N=1, SBM	2	...
LSBM2	6 in.× 6 in.	0	N=2, SBM	2	2
LSBM3	6 in.× 6 in.	0	N=3, SBM	2	2

Table A.4
Test factorial for large-scale test

Test No.	Soil	Footing Dimensions	Embedment in.	Reinforcement configuration	u in.	h in.
CLNR[*]	Silty clay	18 in.× 18 in.	0	Unreinforced	…	...
CLGG54[*#]	Silty clay	18 in.× 18 in.	0	N=4, BX6100	6	8
CLGG63[*]	Silty clay	18 in.× 18 in.	0	N=3, BX6200	6	12
CLGG64[*#]	Silty clay	18 in.× 18 in.	0	N=4, BX6200	6	8
CLGG65[*]	Silty clay	18 in.× 18 in.	0	N=5, BX6200	6	6
CLGG74[*#]	Silty clay	18 in.× 18 in.	0	N=4, BX1500	6	8

* Instrumented with pressure cell
# Instrumented with strain gage

APPENDIX B PRESSURE-SETTLEMENT CURVES FOR SMALL-SCALE LABORATORY MODEL TESTS ON SILTY CLAY
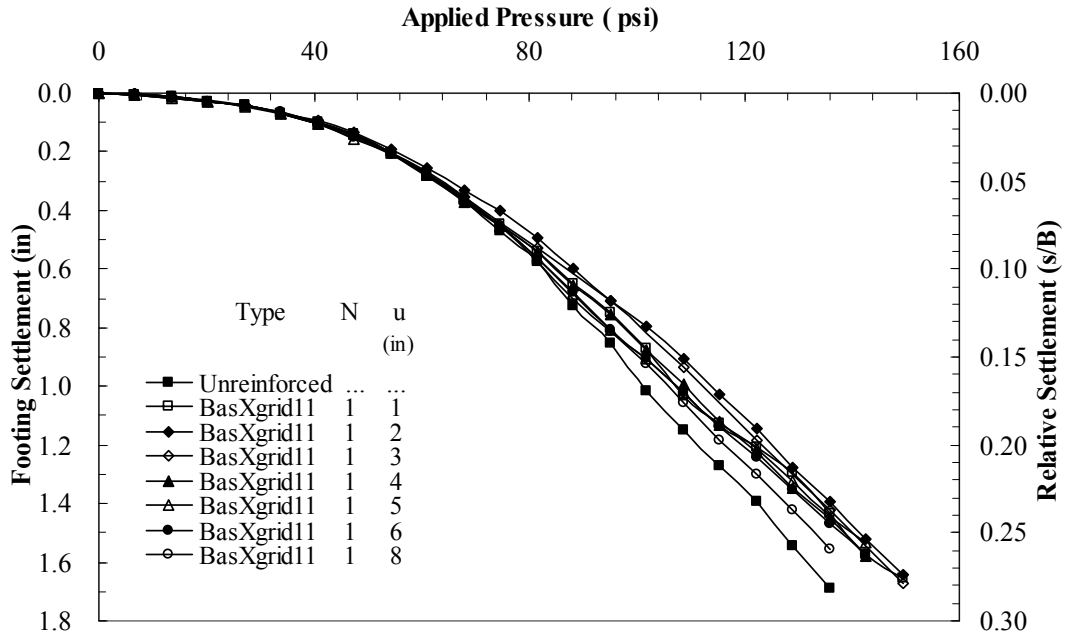
Figure B. 1
Pressure-settlement curves for model footing tests with single layer of BasXgrid11 placed at different top layer spacing in silty clay (B×L: 6 in. × 6 in.)
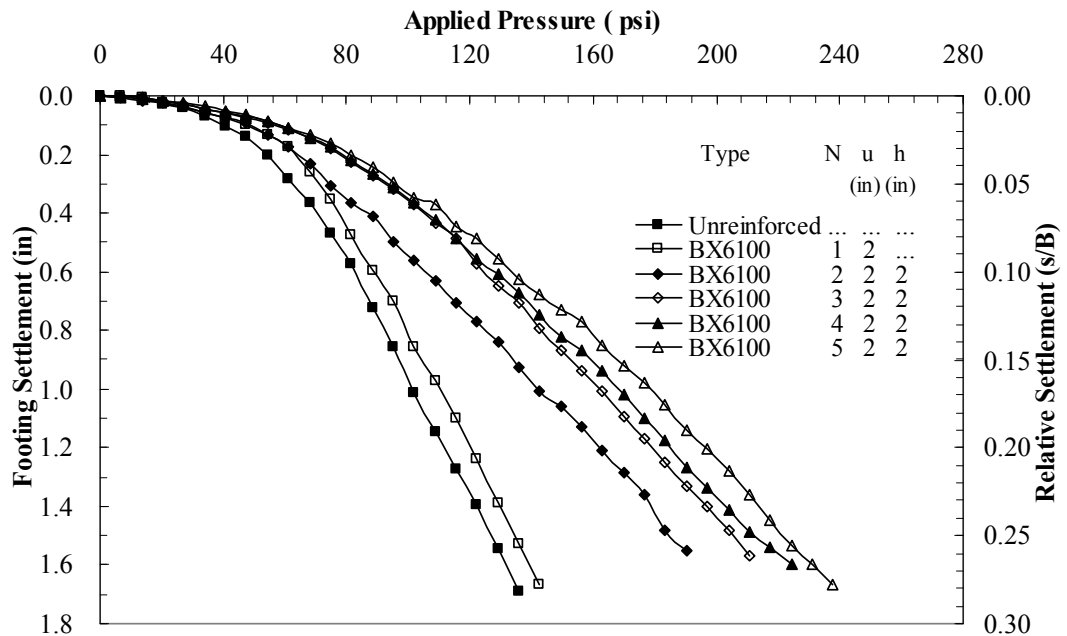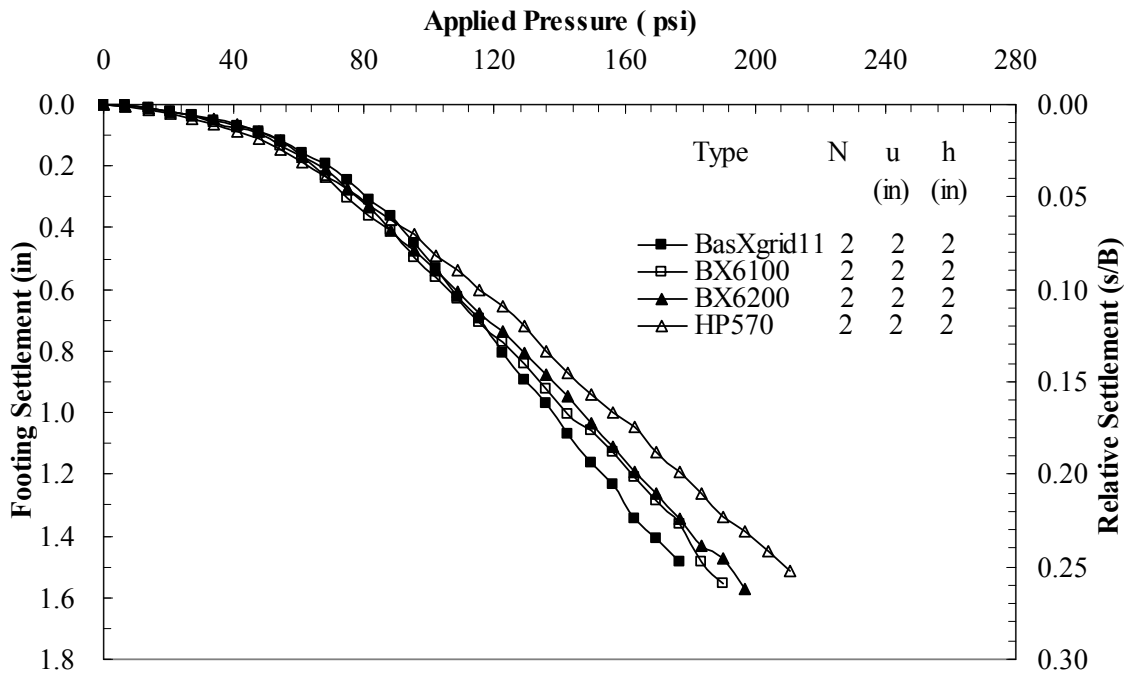

Figure B. 2
Pressure-settlement curves for model footing tests with different number of layers of BX6100 geogrid in silty clay (B×L: 6 in. × 6 in.)
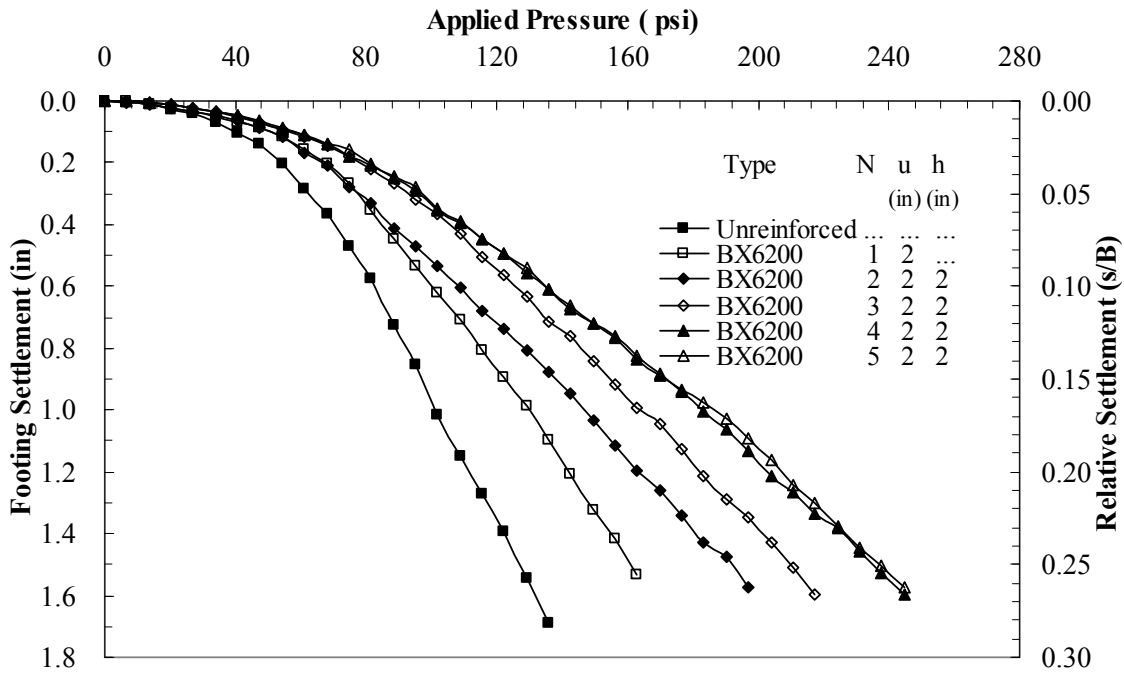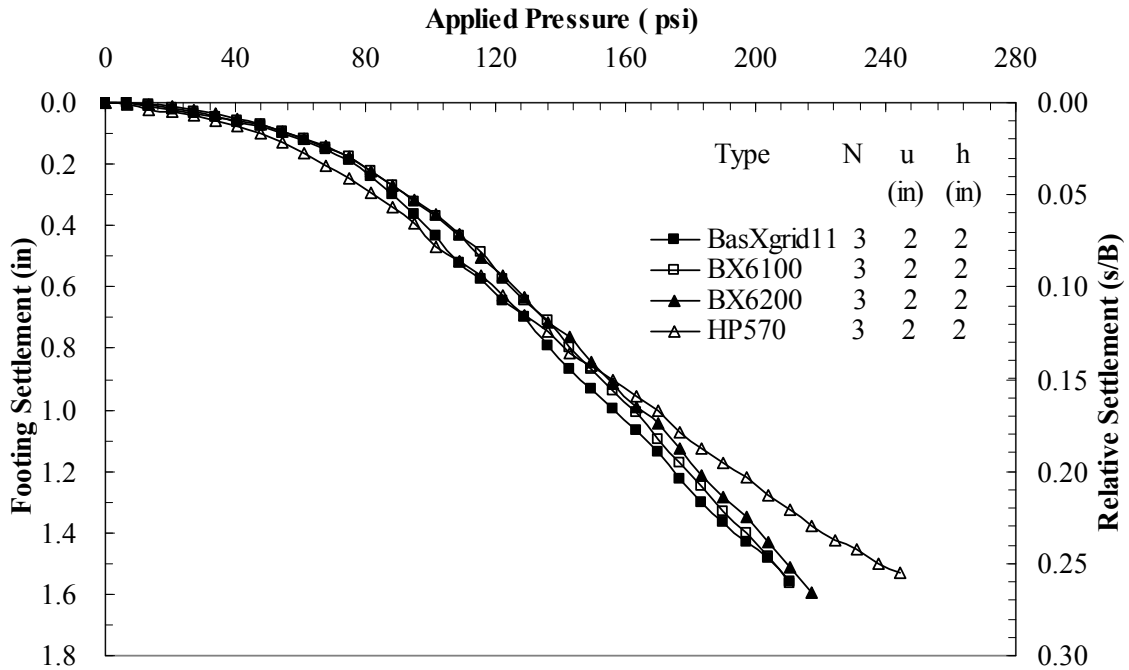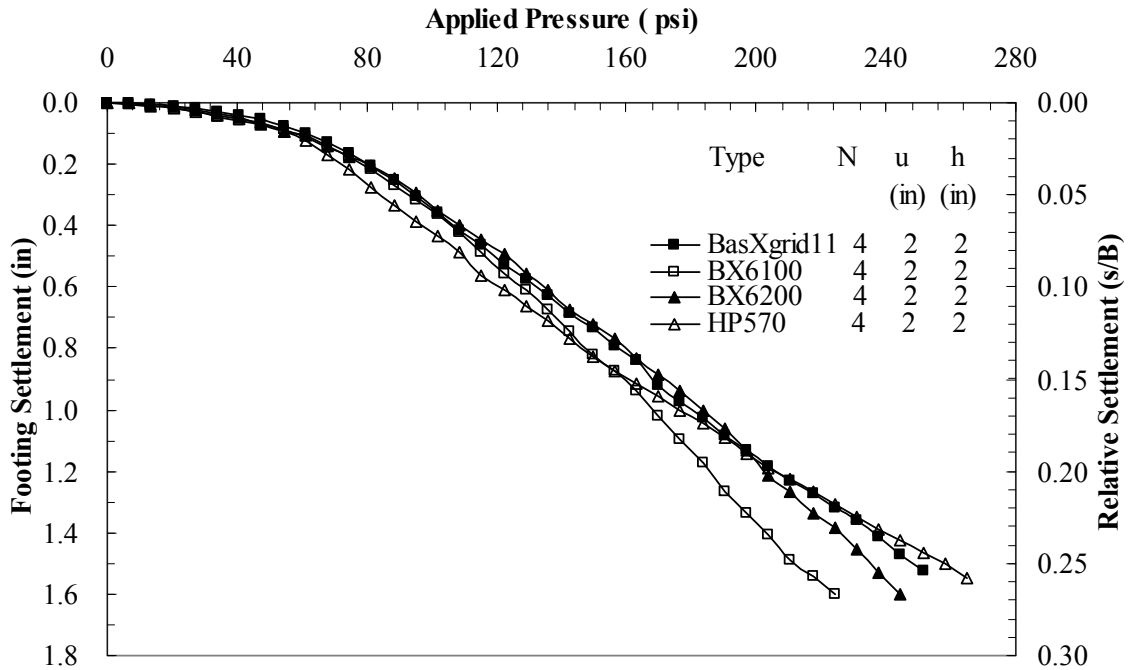
Figure B. 3
Pressure-settlement curves for model footing tests with different number of layers of BX6200 geogrid in silty clay (B×L: 6 in. × 6 in.)
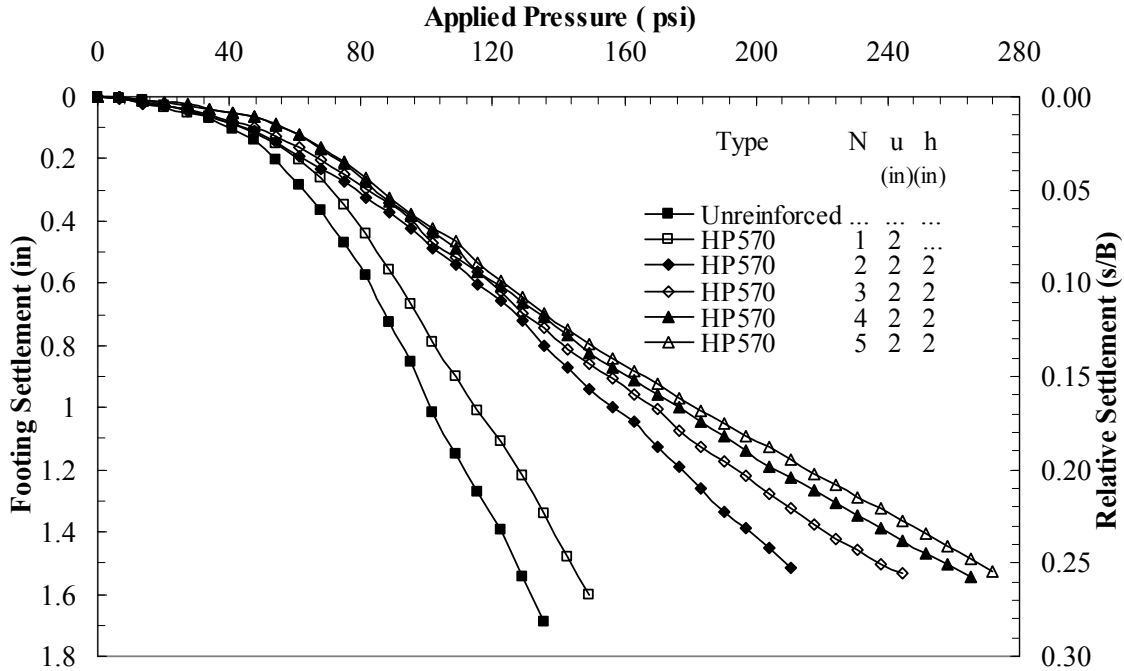
Figure B. 4
Pressure-settlement curves for model footing tests with different number of layers of HP570 geotextile in silty clay (B×L: 6 in. × 6 in.)
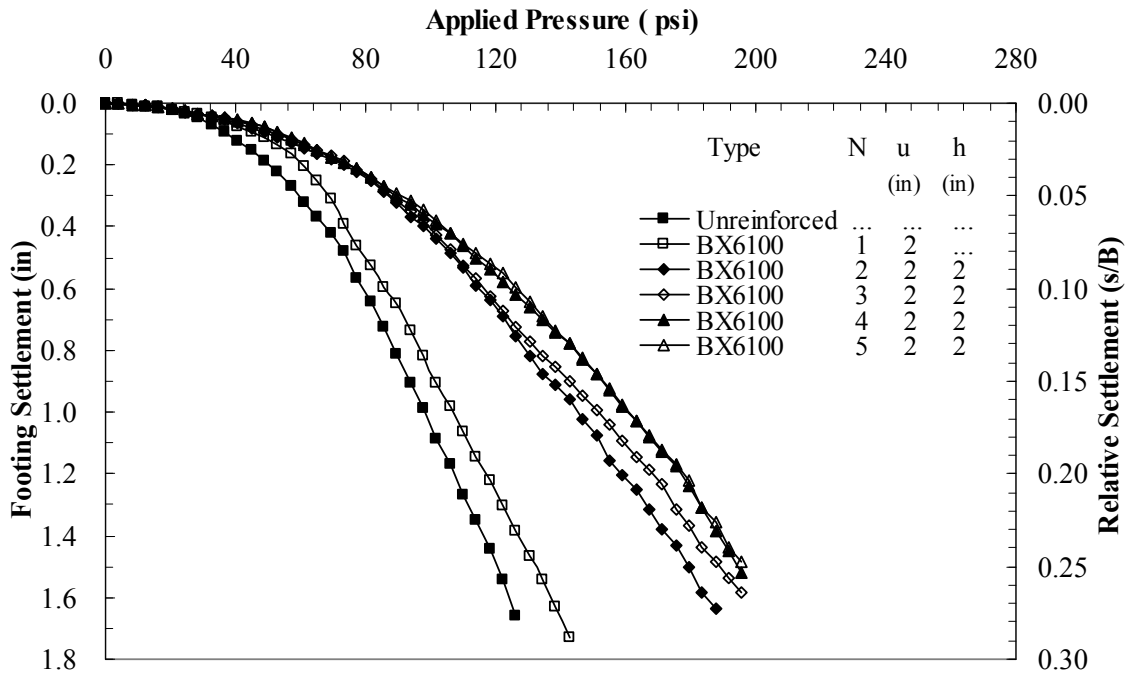
Figure B. 5

Pressure-settlement curves for model footing tests with different number of layers of BX6100 geogrid in silty clay (B×L: 6 in. × 10 in.)
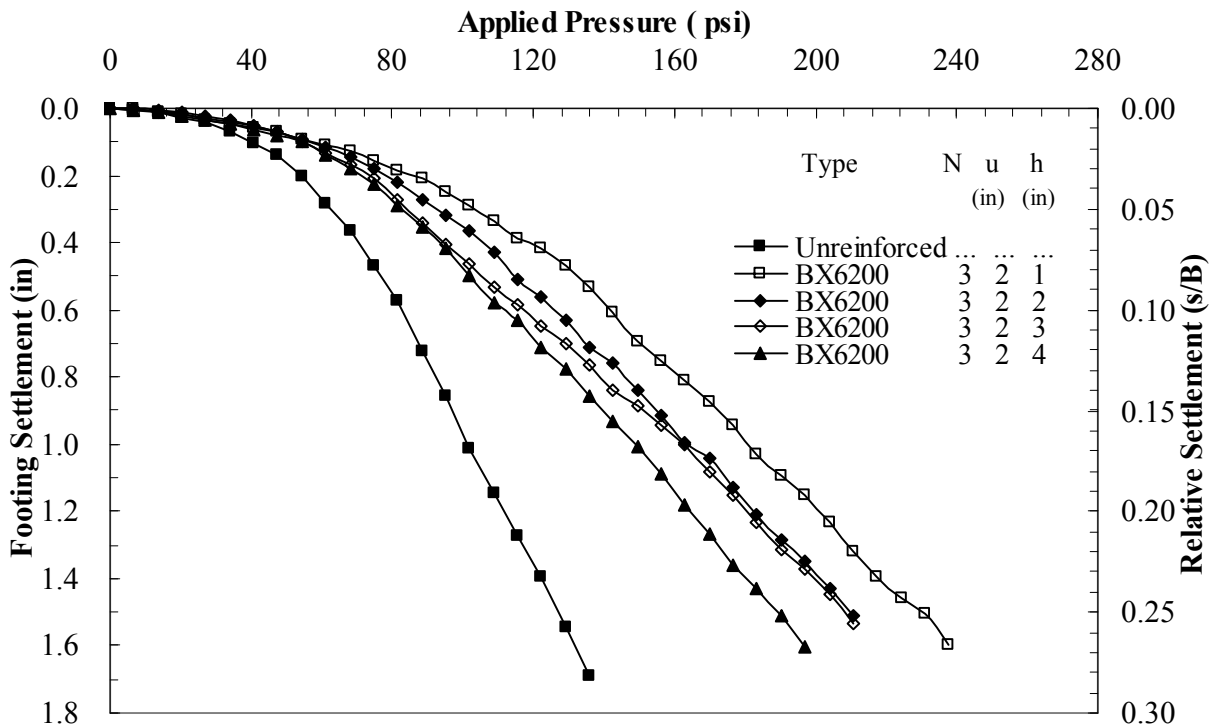
Figure B. 6

Pressure-settlement curves for model footing test with three layers of BX6200 placed at different vertical spacing in silty clay (B×L: 6 in. × 6 in.)
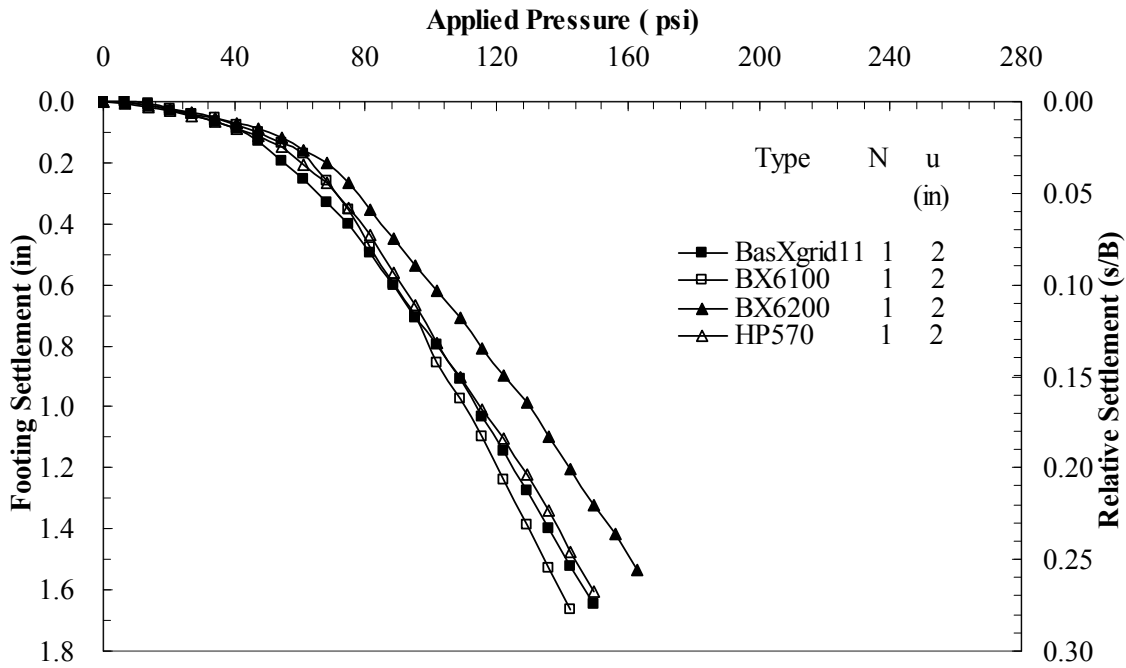
Figure B. 7
Pressure-settlement curves for model footing test with one layer of different types of reinforcements (B×L: 6 in. × 6 in.)
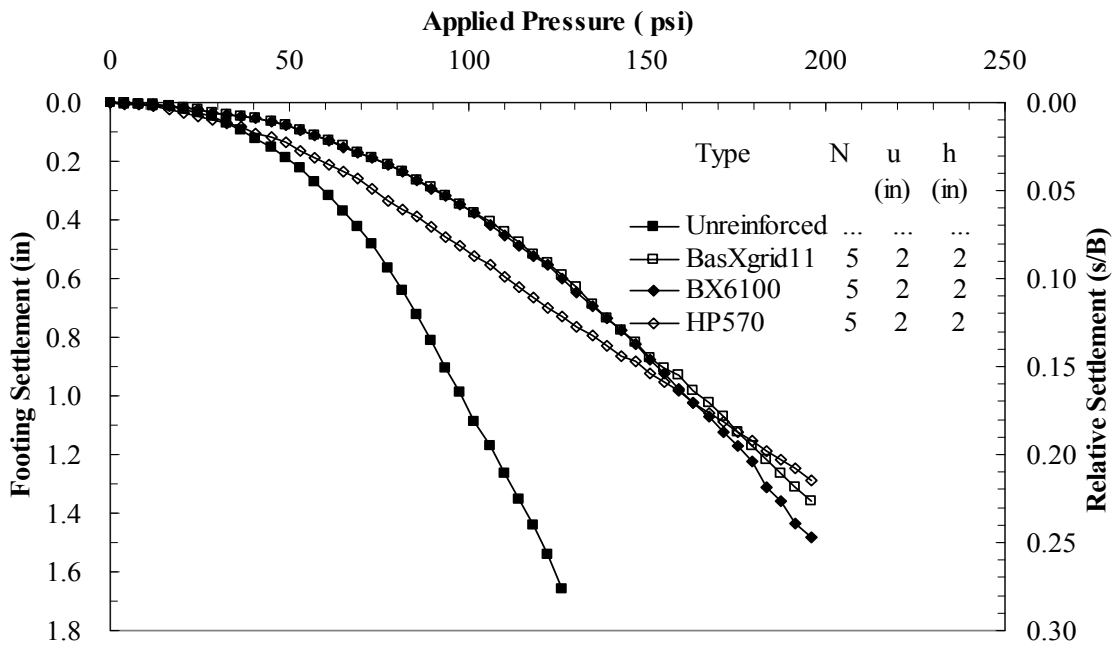

Figure B. 8
Pressure-settlement curves for model footing test with two layers of different types of reinforcements (B×L: 6 in. × 6 in.)
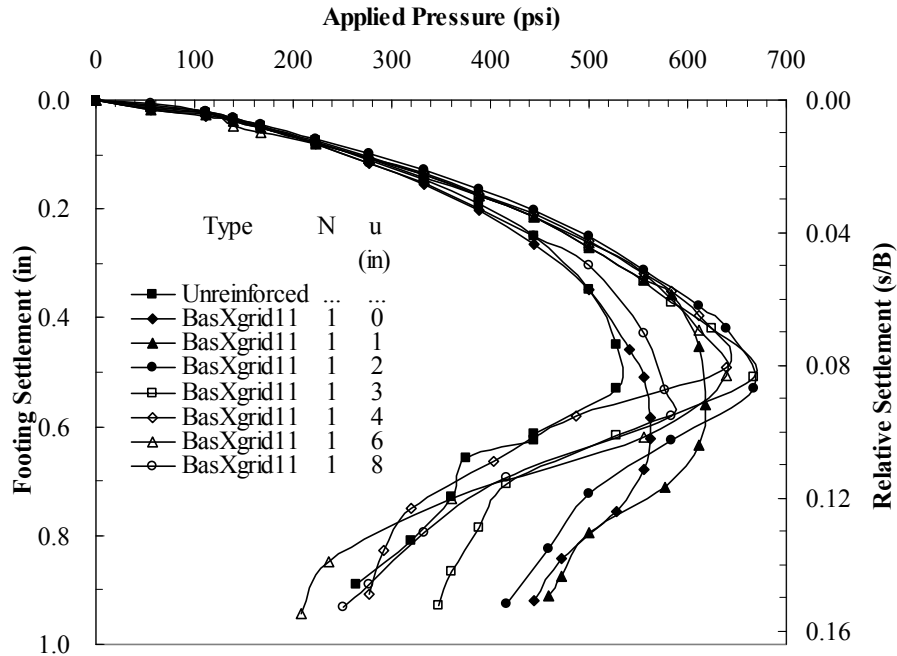
Figure B. 9
Pressure-settlement curves for model footing test with three layers of different types of reinforcements (B×L: 6 in. × 6 in.)

Figure B. 10
Pressure-settlement curves for model footing test with four layers of different types of reinforcements (B×L: 6 in. × 6 in.)
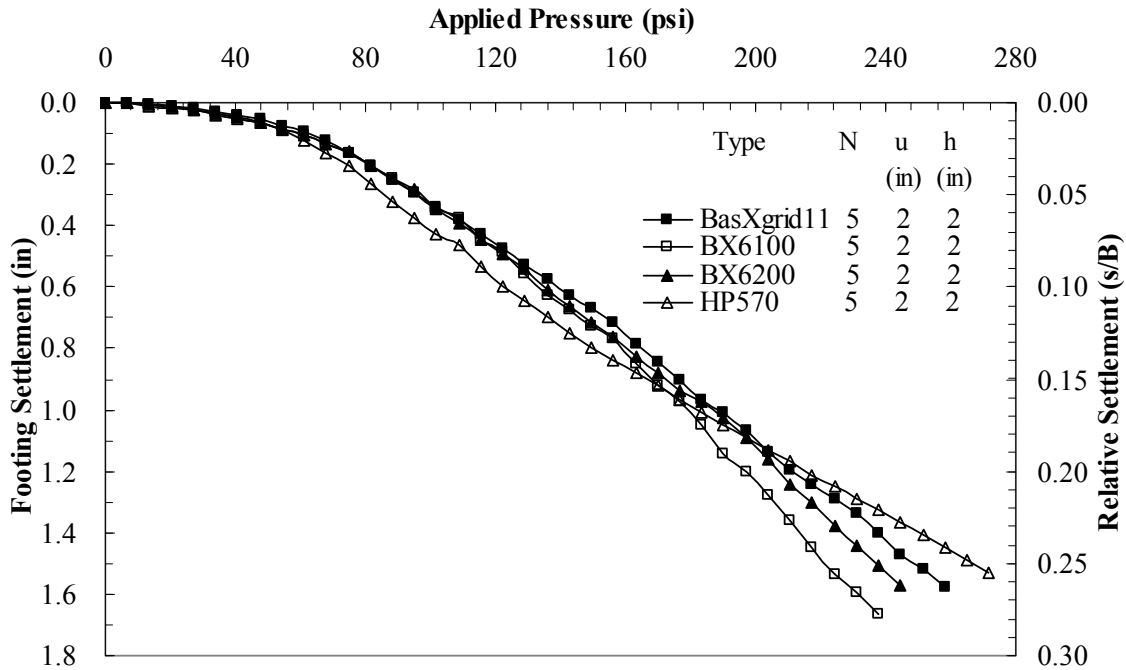
Figure B. 11
Pressure-settlement curves for model footing test with five layers of different types of reinforcements (B×L: 6 in. × 6 in.)


Figure B. 12
Pressure-settlement curves for model footing test with five layers of different types of reinforcements (B×L: 6 in. × 10 in.)

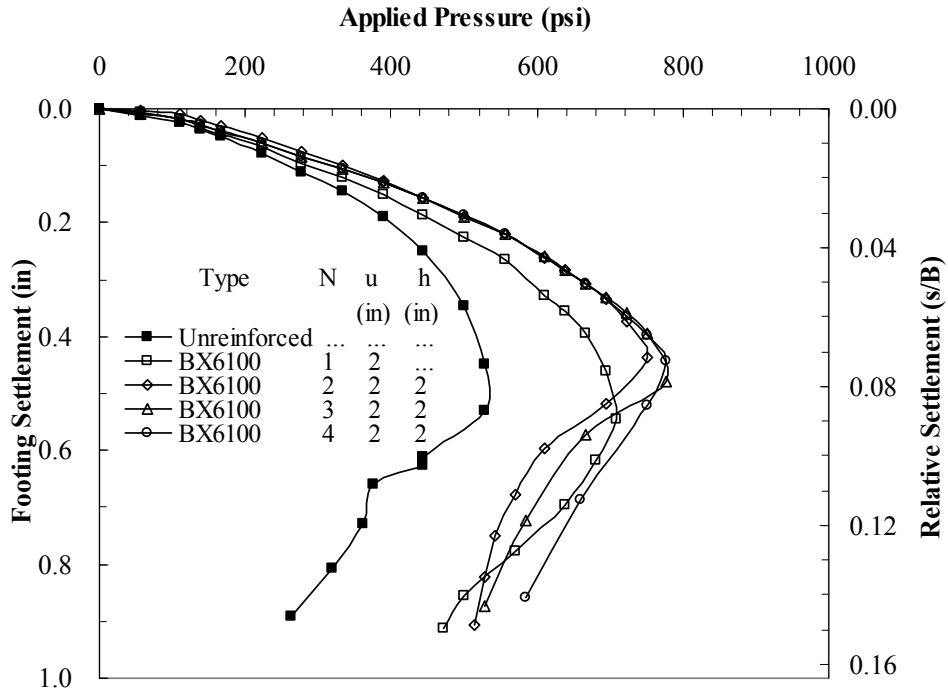# APPENDIX C PRESSURE-SETTLEMENT CURVES FOR SMALL-SCALE LABORATORY MODEL TESTS ON SAND

Figure C. 1
Pressure-settlement curves for model footing tests with single layer of BasXgrid11 placed at different top layer spacing (B×L: 6 in. × 6 in.; D_f/B: 1.0)
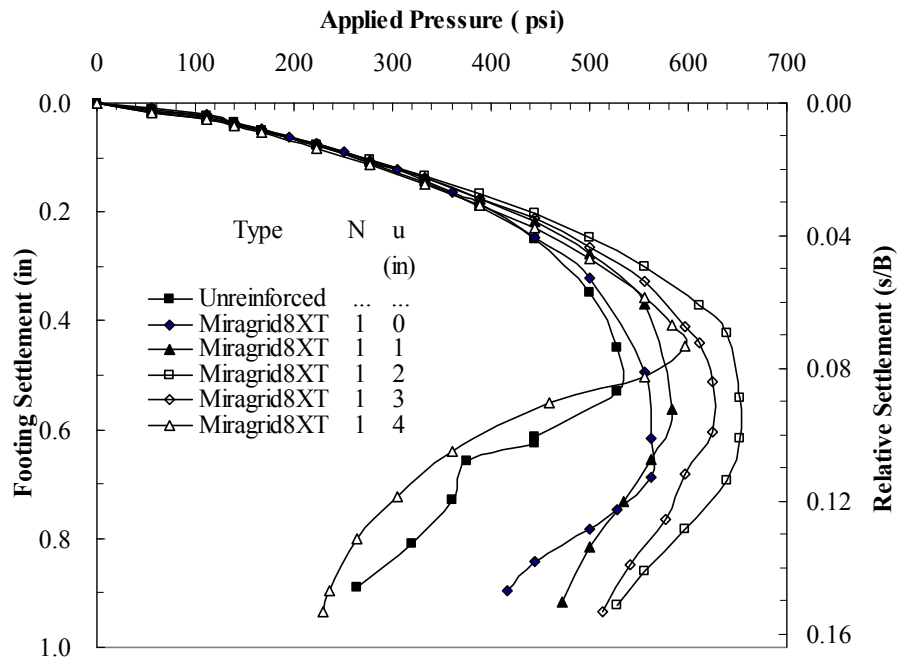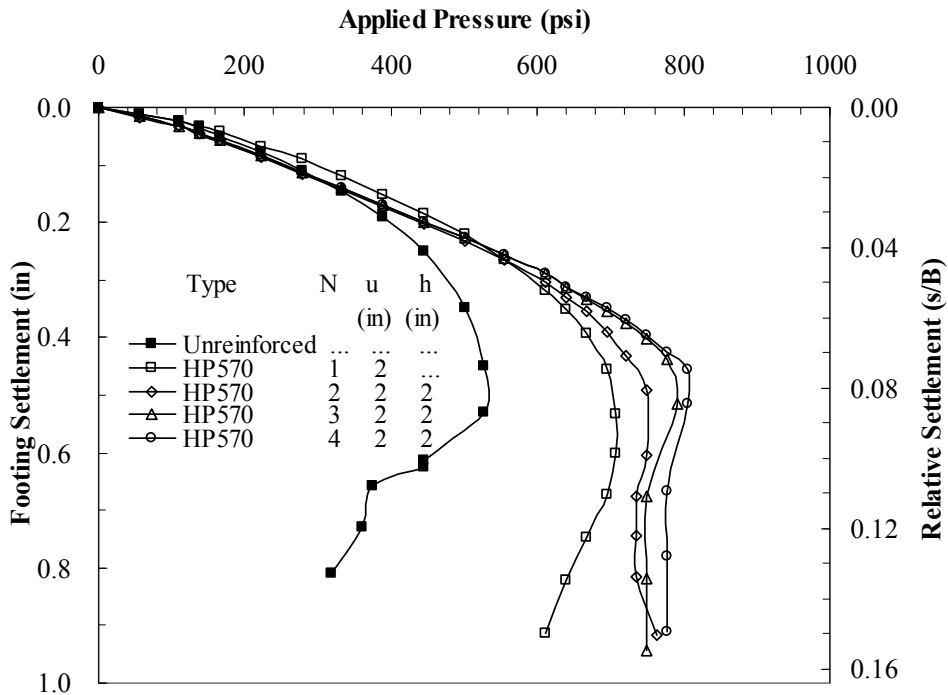

Figure C. 2
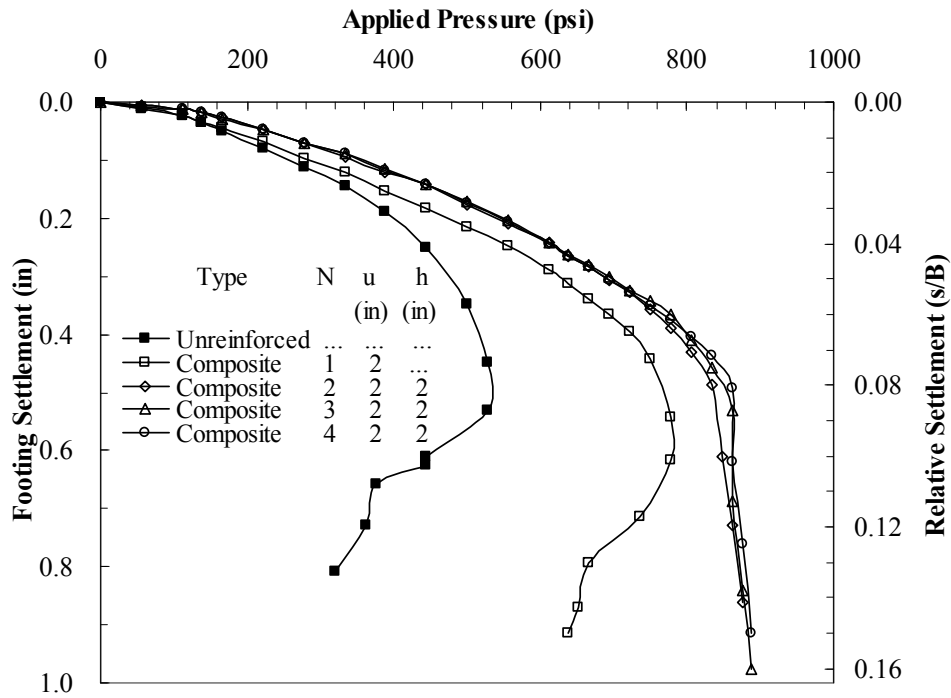**Pressure-settlement curves for model footing tests with single layer of Miragrid 8XT placed at different top layer spacing (B×L: 6 in. × 6 in.; D_f/B: 1.0)**
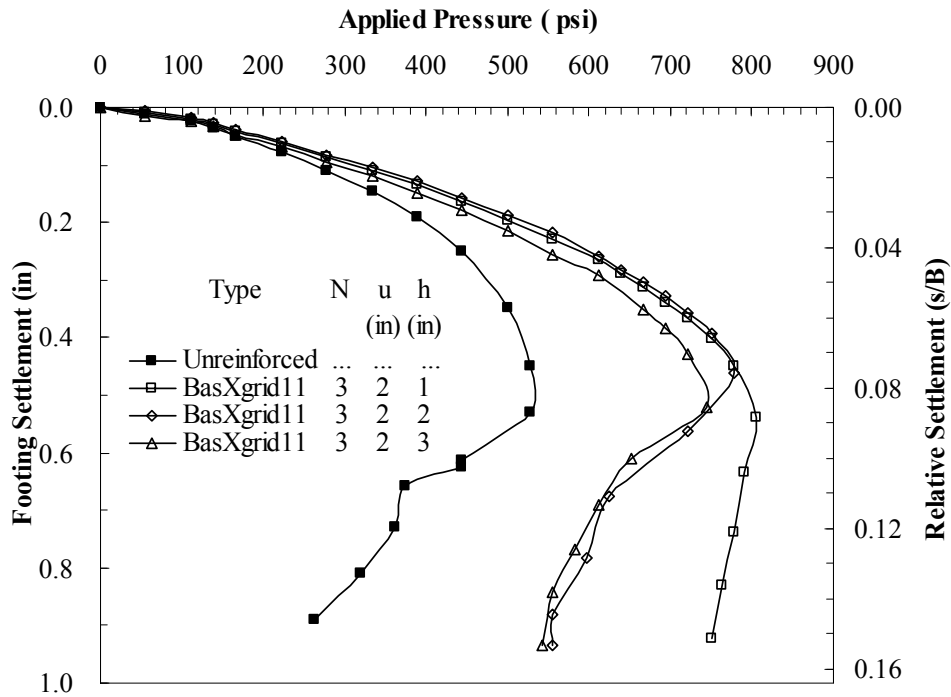
Figure C. 3
Pressure-settlement curves for model footing tests with different number of layers of BX6100 geogrid (B×L: 6 in. × 6 in.; D_f/B: 1.0)

Figure C. 4
Pressure-settlement curves for model footing tests with different number of layers of HP570 geotextile (B×L: 6 in. × 6 in.; D_f/B: 1.0)

Figure C. 5
Pressure-settlement curves for model footing tests with different number of layers of Composite (B×L: 6 in. × 6 in.; D_f / B: 1.0)

Figure C. 6
Pressure-settlement curves for model footing test with three layers of BasXgrid11 placed at different vertical spacing (B×L: 6 in. × 6 in.; D_f / B: 1.0)
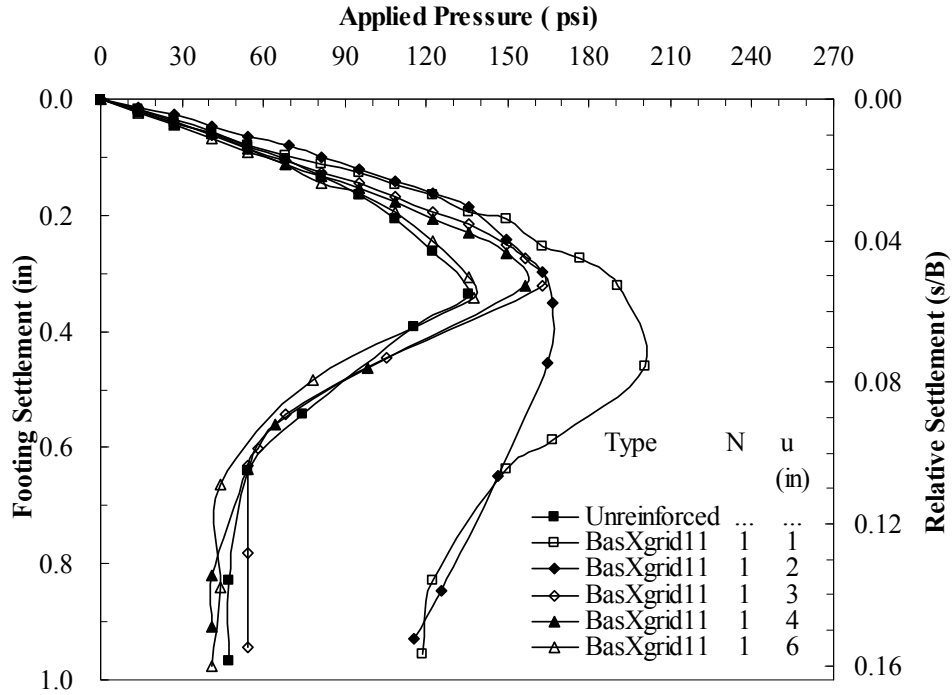
Figure C. 7
Pressure-settlement curves for model footing tests with single layer of BasXgrid11 placed at different top layer spacing (B×L: 6 in. × 6 in.; D_f/B: 0.0)
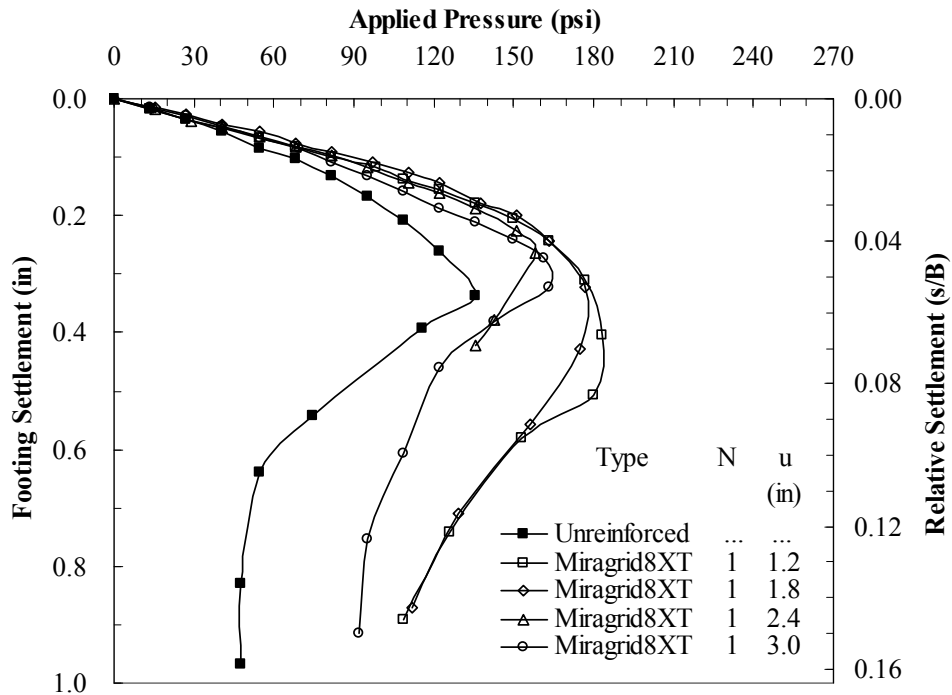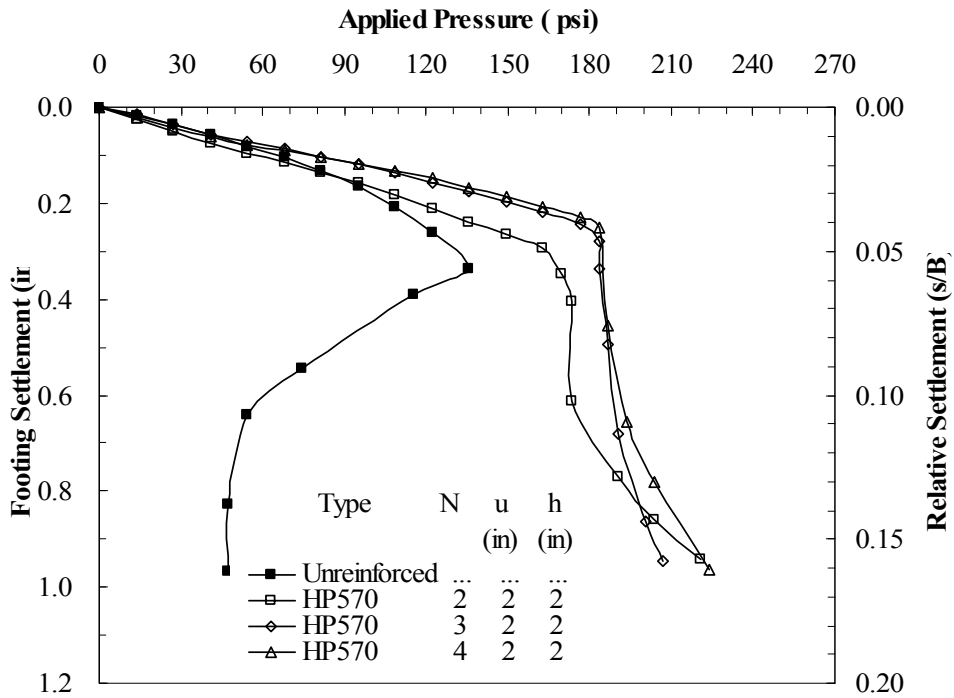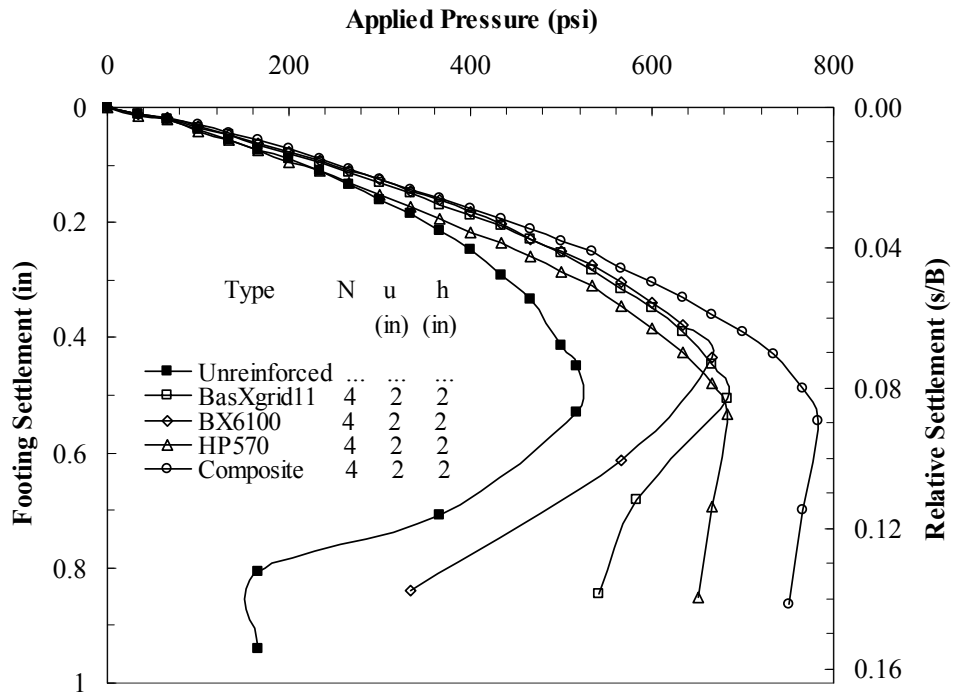

Figure C. 8
Pressure-settlement curves for model footing tests with single layer of Miragrid 8XT placed at different top layer spacing (B×L: 6 in. × 6 in.; D_f/B: 0.0)

180

Figure C. 9

Pressure-settlement curves for model footing tests with different number of layers of HP570 geotextile (B×L: 6 in. × 6 in.; D_f/B: 0.0)

Figure C. 10

Pressure settlement curves for model footing test with four layers of different types of reinforcements (B×L: 6 in. × 10 in.; D_f/B: 1.0)
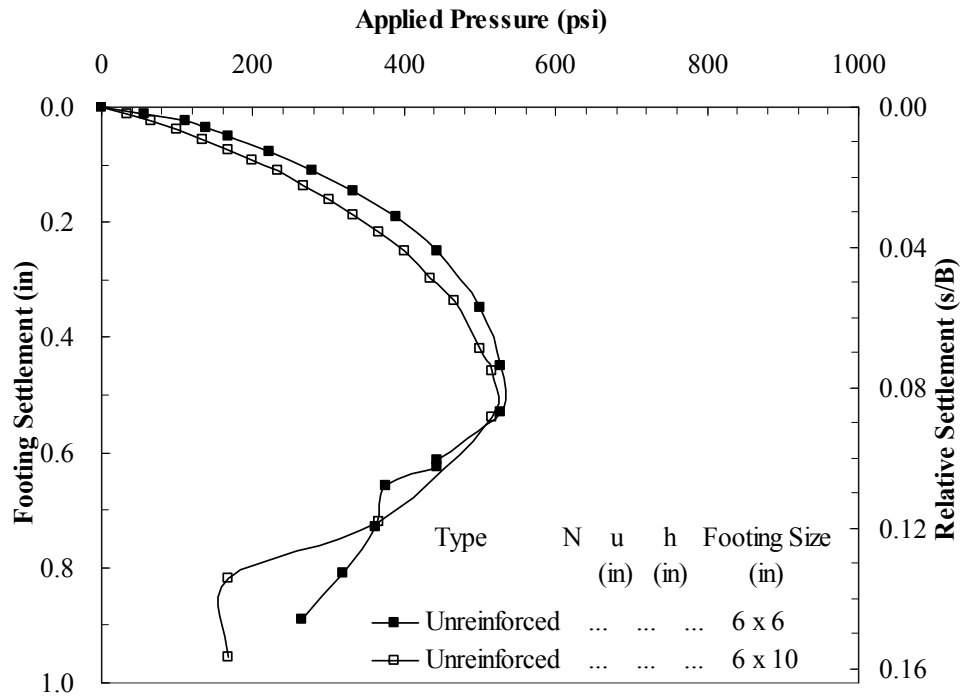
Figure C. 11
Pressure-settlement curves for model footing tests on unreinforced sand with different footing shape
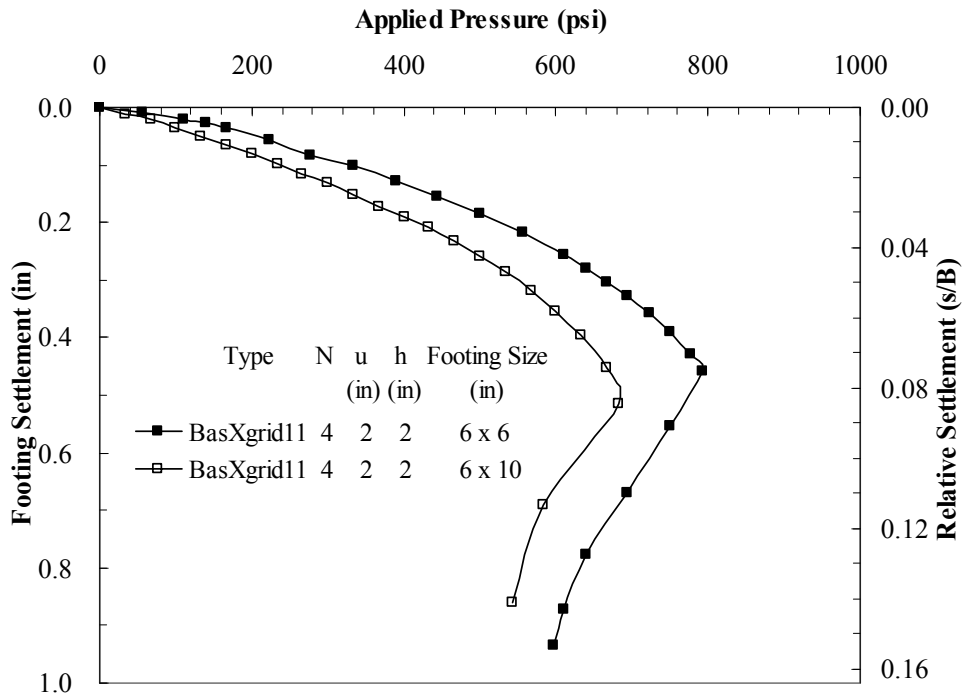
Figure C. 12
Pressure-settlement curves for model footing tests with four layers of BasXgrid11 geogrid and different shape footing

Figure C. 13
Pressure-settlement curves for model footing tests with four layers of BX6100 geogrid and different shape footing
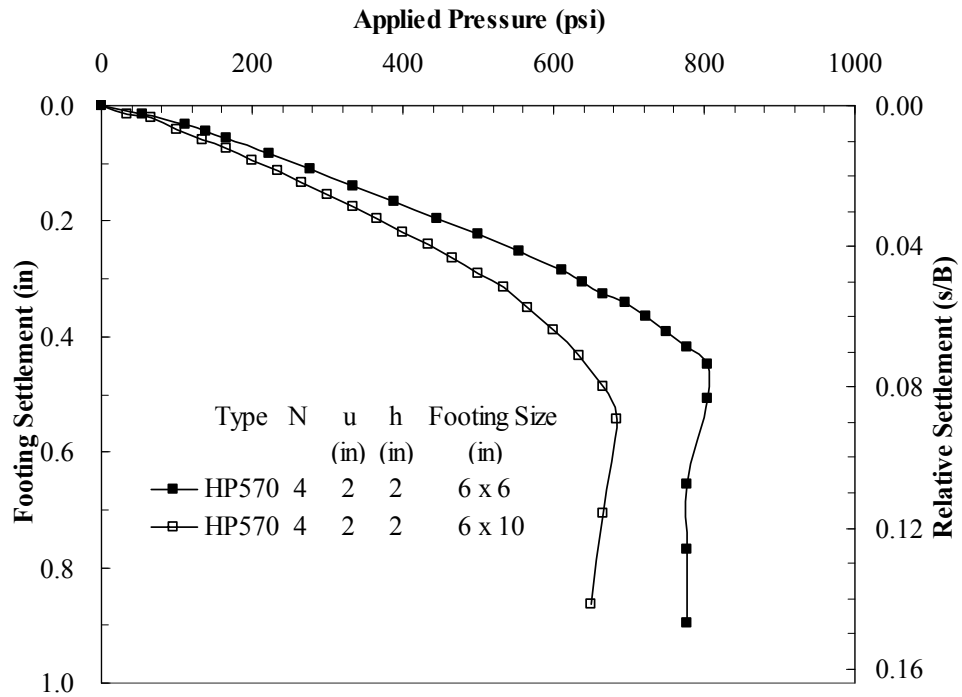
Figure C. 14
Pressure-settlement curves for model footing tests with five layers of HP570 geotextile and different shape footing
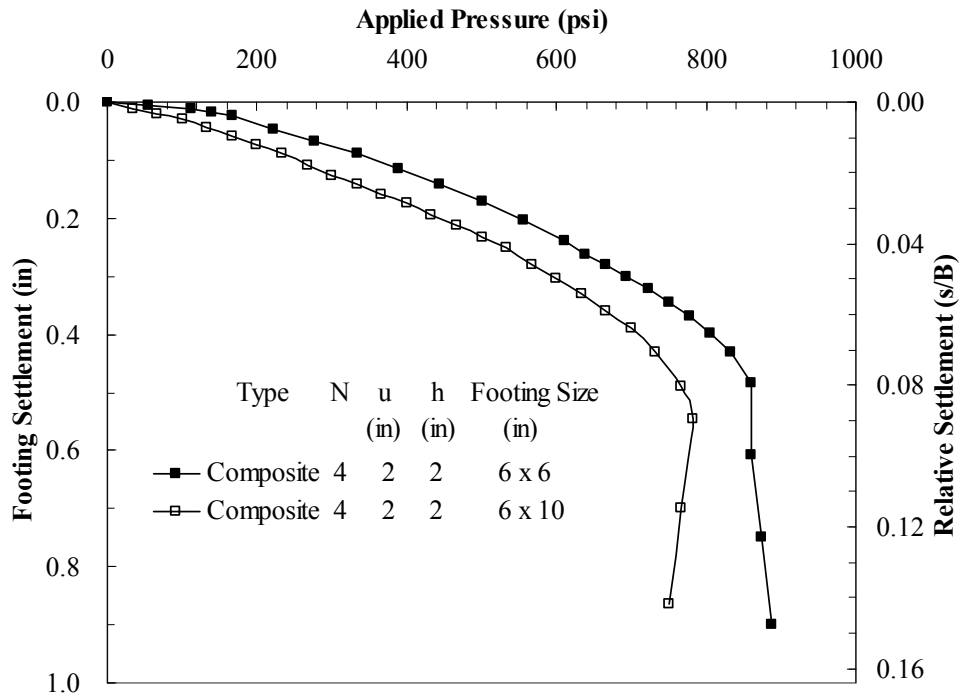
Figure C. 15
Pressure-settlement curves for model footing tests with five layers of Composite and different shape footing
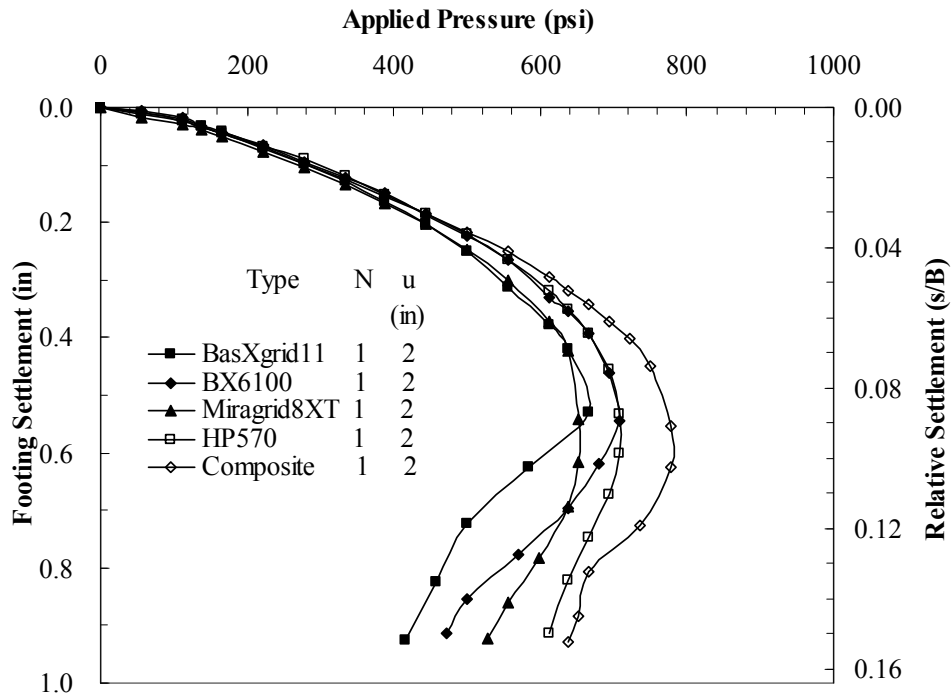
Figure C. 16
Pressure-settlement curves for model footing test with one layer of different types of reinforcements (B×L: 6 in. × 6 in.; $D_f / B = 1.0$)
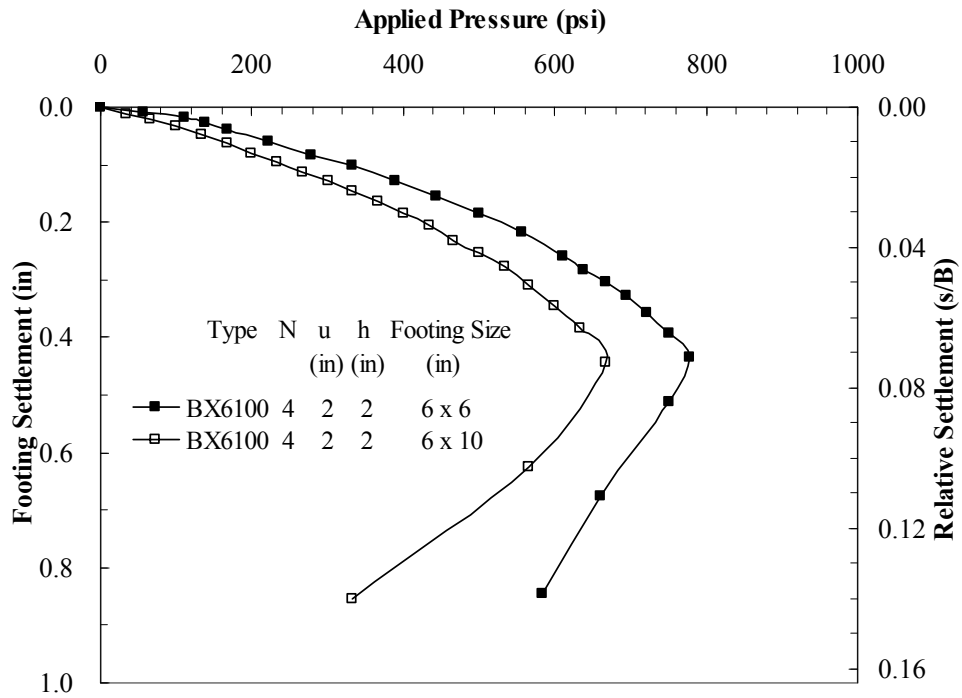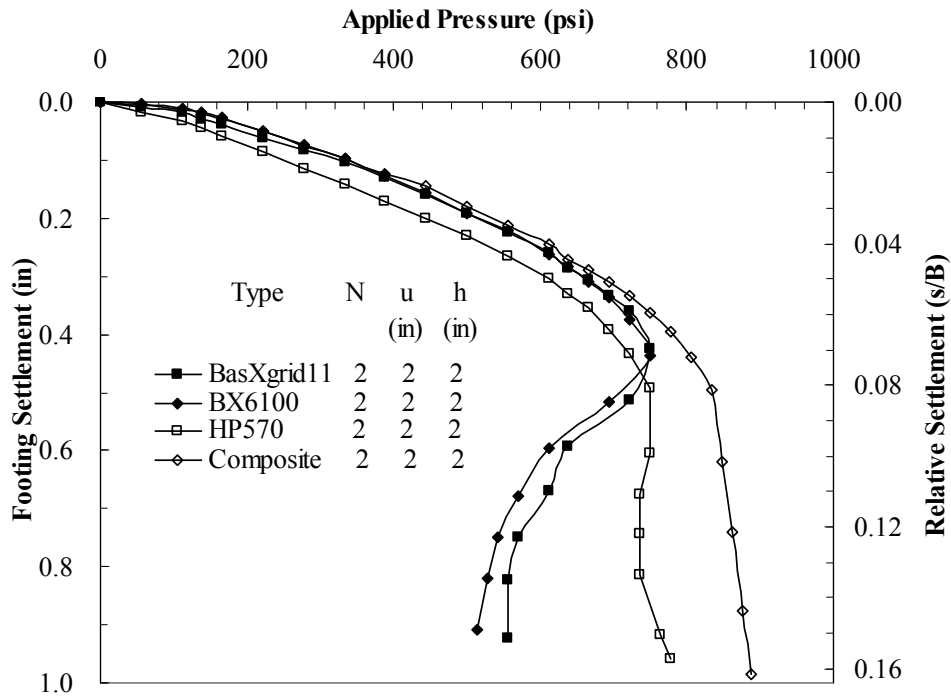
Figure C. 17
Pressure-settlement curves for model footing test with two layers of different types of reinforcements (B×L: 6 in. × 6 in.; $D_f / B = 1.0$)
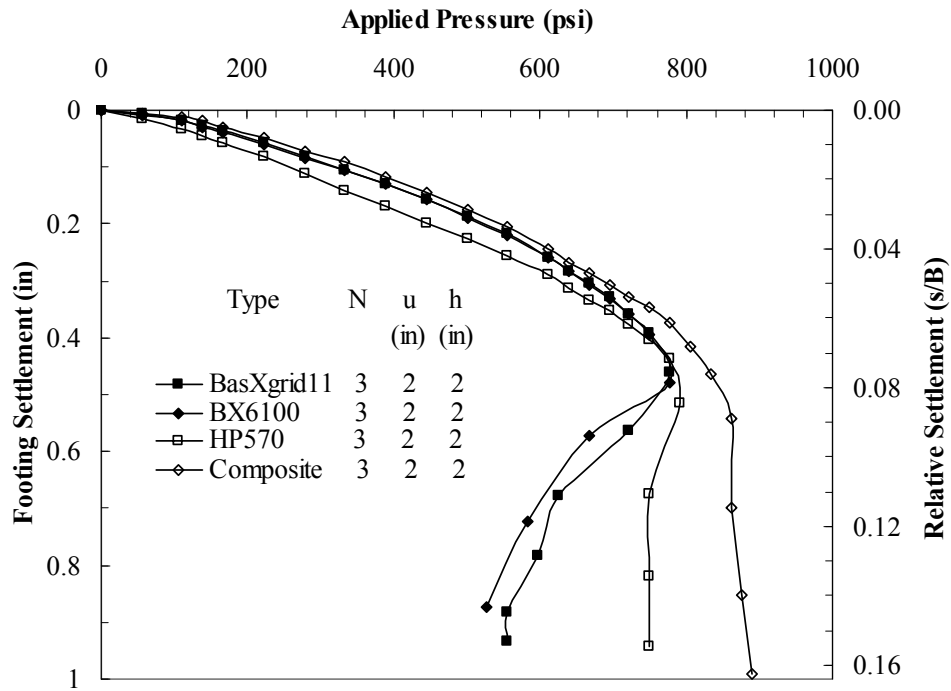
Figure C. 18
Pressure-settlement curves for model footing test with three layers of different types of reinforcements (B×L: 6 in. × 6 in.; $D_f / B = 1.0$)

Figure C. 19
Pressure-settlement curves for model footing test with four layers of different types of reinforcements (B×L: 6 in. × 6 in.; $D_f / B = 1.0$)
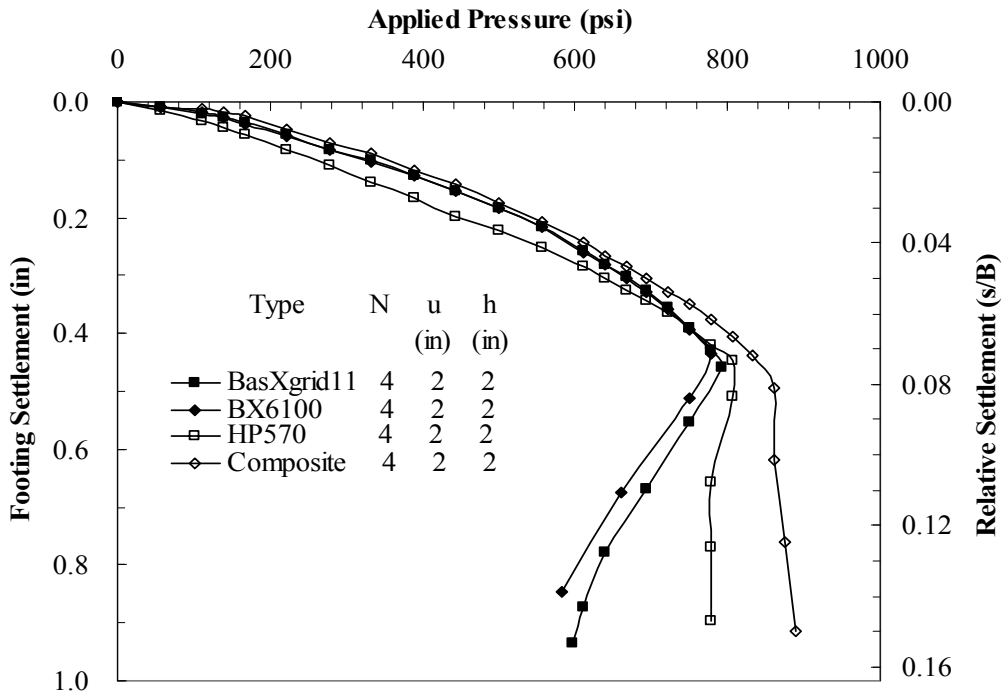
APPENDIX D VERIFICATION OF REGRESSION MODELS

Table D. 1
Verification of regression models for reinforced embankment soil

No.	h (in.)	X1	X2	X3	X4	X5	BCR (FEM)	BCR (Reg)	Abs (Err) (%)
1	12	0.25	1.16	0.5	0.00	1.0	1.62	1.61	0.16
2	12	0.25	1.16	0.7	0.00	1.0	1.69	1.73	2.13
3	12	0.25	2.42	0.5	0.00	1.0	1.78	1.77	0.48
4	12	0.25	3.50	0.7	0.00	1.0	1.99	2.01	1.01
5	24	0.50	1.45	0.7	0.00	1.0	1.32	1.26	4.79
6	24	0.50	2.71	0.7	0.00	1.0	1.45	1.41	2.98
7	12	0.25	2.71	0.7	0.00	1.0	1.84	1.92	4.22
8	6	0.13	1.45	0.7	0.00	1.0	2.05	2.01	1.62
9	6	0.13	2.71	0.7	0.00	1.0	2.23	2.17	2.63
10	18	0.38	1.16	0.7	0.00	1.0	1.50	1.47	1.80
11	9	0.19	1.16	0.7	0.00	1.0	1.79	1.85	3.49
12	18	0.38	2.42	0.7	0.00	1.0	1.63	1.63	0.20
13	9	0.19	2.42	0.7	0.00	1.0	1.98	2.01	1.41
14	18	0.38	3.50	0.7	0.00	1.0	1.72	1.76	2.41
15	9	0.19	3.50	0.7	0.00	1.0	2.08	2.14	2.93
16	24	0.50	2.42	0.7	0.25	1.0	1.42	1.37	3.20
17	18	0.38	2.42	0.7	0.25	1.0	1.61	1.62	0.86
18	12	0.25	2.42	0.7	0.25	1.3	1.82	1.88	2.92
19	24	0.50	2.42	0.7	0.75	1.3	1.39	1.36	1.97
20	18	0.38	2.42	0.7	0.75	1.3	1.56	1.61	3.63

Table D. 2
Verification of regression models reinforced crushed Limestone

| No.	X1	X2	X3	X4	FEM Result	Regression Result	Absolute Error (%)
1	0.375	0.100	0.00	1.00	1.3770	1.4101	2.402
2	0.375	0.148	0.00	1.00	1.4032	1.4146	0.816
3	0.375	0.442	0.00	1.00	1.4614	1.4427	1.279
4	0.375	0.884	0.00	1.00	1.4871	1.4849	0.150
5	0.375	1.325	0.00	1.00	1.4968	1.5270	2.017
6	0.375	0.148	0.25	1.00	1.3452	1.3640	1.396
7	0.375	0.148	0.50	1.00	1.3028	1.3133	0.807
8	0.375	0.148	0.75	1.00	1.2523	1.2626	0.826
9	0.375	0.148	1.00	1.00	1.2240	1.2120	0.982
10	0.375	0.148	0.00	0.75	1.5161	1.5017	0.949
11	0.375	0.148	0.00	1.25	1.3130	1.3275	1.109
12	0.375	0.148	0.00	1.50	1.2415	1.2404	0.083
13	0.1875	0.050	0.00	1.00	1.4243	1.4792	3.856
14	0.1875	0.100	0.00	1.00	1.4738	1.4840	0.689
15	0.1875	0.442	0.00	1.00	1.5568	1.5166	2.584
16	0.1875	0.663	0.00	1.00	1.5674	1.5376	1.896
17	0.1875	0.147	0.00	1.00	1.4996	1.4885	0.743
18	0.1875	0.147	0.25	1.00	1.4225	1.4378	1.075
19	0.1875	0.147	0.50	1.00	1.3741	1.3872	0.951
20	0.1875	0.147	0.75	1.00	1.3140	1.3365	1.717
21	0.1875	0.147	1.00	1.00	1.2816	1.2859	0.330
22	0.1875	0.147	0.00	0.75	1.6218	1.5756	2.848
23	0.1875	0.147	0.00	1.25	1.3977	1.4014	0.263
24	0.1875	0.147	0.00	1.50	1.3215	1.3143	0.545

Table D. 3
Verification of expanded regression models for reinforced embankment soil

| No.	X1	X2	X3	X4	X5	X6	X7	BCR (fem)	BCR (Reg)	Abs (Err) (%)
1	0.2500	1.16	0.5	0.00	1.0	1.00	1.00	1.62	1.61	0.16
2	0.2500	1.16	0.7	0.00	1.0	1.00	1.00	1.69	1.73	2.13
3	0.2500	2.42	0.5	0.00	1.0	1.00	1.00	1.78	1.77	0.48
4	0.2500	3.50	0.7	0.00	1.0	1.00	1.00	1.99	2.01	1.01
5	0.5000	1.45	0.7	0.00	1.0	1.00	1.00	1.32	1.26	4.79
6	0.5000	2.71	0.7	0.00	1.0	1.00	1.00	1.45	1.41	2.98
7	0.2500	2.71	0.7	0.00	1.0	1.00	1.00	1.84	1.92	4.22
8	0.1250	1.45	0.7	0.00	1.0	1.00	1.00	2.05	2.01	1.62
9	0.1250	2.71	0.7	0.00	1.0	1.00	1.00	2.23	2.17	2.63
10	0.3750	1.16	0.7	0.00	1.0	1.00	1.00	1.50	1.47	1.80
11	0.1875	1.16	0.7	0.00	1.0	1.00	1.00	1.79	1.85	3.49
12	0.3750	2.42	0.7	0.00	1.0	1.00	1.00	1.63	1.63	0.20
13	0.1875	2.42	0.7	0.00	1.0	1.00	1.00	1.98	2.01	1.41
14	0.3750	3.50	0.7	0.00	1.0	1.00	1.00	1.72	1.76	2.41
15	0.1875	3.50	0.7	0.00	1.0	1.00	1.00	2.08	2.14	2.93
16	0.5000	2.42	0.7	0.25	1.0	1.00	1.00	1.42	1.37	3.20
17	0.3750	2.42	0.7	0.25	1.0	1.00	1.00	1.61	1.62	0.86
18	0.2500	2.42	0.7	0.25	1.3	1.00	1.00	1.82	1.88	2.92
19	0.5000	2.42	0.7	0.75	1.3	1.00	1.00	1.39	1.36	1.97
20	0.3750	2.42	0.7	0.75	1.3	1.00	1.00	1.56	1.61	3.63
21	0.3750	2.42	0.7	0.00	1.0	0.83	1.00	1.81	1.85	2.35
22	0.1875	2.42	0.7	0.00	1.0	0.83	1.00	2.13	2.23	4.47
23	0.3750	2.42	0.7	0.00	1.0	1.17	1.00	1.40	1.42	1.54
24	0.1875	2.42	0.7	0.00	1.0	1.17	1.00	1.73	1.79	3.65
25	0.3750	2.42	0.7	0.00	1.0	1.00	0.78	1.89	1.82	4.08
26	0.1875	2.42	0.7	0.00	1.0	1.00	0.78	2.13	2.19	2.78
27	0.3750	2.42	0.7	0.00	1.0	1.00	1.22	1.51	1.46	3.87
28	0.1875	2.42	0.7	0.00	1.0	1.00	1.22	1.80	1.83	1.43

Table D. 4
Verification of expanded regression models for reinforced crushed Limestone

| No.	X1	X2	X3	X4	X5	X6	FEM Result	Regression Result	Absolute Error
1	0.3750	0.100	0.00	1.00	1.0000	1.0000	1.3770	1.4202	3.135
2	0.3750	0.148	0.00	1.00	1.0000	1.0000	1.4032	1.4239	1.481
3	0.3750	0.442	0.00	1.00	1.0000	1.0000	1.4614	1.4474	0.963
4	0.3750	0.884	0.00	1.00	1.0000	1.0000	1.4871	1.4825	0.314
5	0.3750	1.325	0.00	1.00	1.0000	1.0000	1.4968	1.5175	1.384
6	0.3750	0.148	0.25	1.00	1.0000	1.0000	1.3452	1.3694	1.800
7	0.3750	0.148	0.50	1.00	1.0000	1.0000	1.3028	1.3149	0.927
8	0.3750	0.148	0.75	1.00	1.0000	1.0000	1.2523	1.2603	0.640
9	0.3750	0.148	1.00	1.00	1.0000	1.0000	1.2240	1.2058	1.490
10	0.3750	0.148	0.00	0.75	1.0000	1.0000	1.5161	1.5172	0.072
11	0.3750	0.148	0.00	1.25	1.0000	1.0000	1.3130	1.3307	1.351
12	0.3750	0.148	0.00	1.50	1.0000	1.0000	1.2415	1.2375	0.323
13	0.1875	0.050	0.00	1.00	1.0000	1.0000	1.4243	1.4936	4.869
14	0.1875	0.100	0.00	1.00	1.0000	1.0000	1.4738	1.4976	1.613
15	0.1875	0.442	0.00	1.00	1.0000	1.0000	1.5568	1.5248	2.060
16	0.1875	0.663	0.00	1.00	1.0000	1.0000	1.5674	1.5423	1.600
17	0.1875	0.148	0.00	1.00	1.0000	1.0000	1.4996	1.5013	0.114
18	0.1875	0.148	0.25	1.00	1.0000	1.0000	1.4225	1.4468	1.706
19	0.1875	0.148	0.50	1.00	1.0000	1.0000	1.3741	1.3923	1.322
20	0.1875	0.148	0.75	1.00	1.0000	1.0000	1.3140	1.3377	1.809
21	0.1875	0.148	1.00	1.00	1.0000	1.0000	1.2816	1.2832	0.120
22	0.1875	0.148	0.00	0.75	1.0000	1.0000	1.6218	1.5946	1.676
23	0.1875	0.148	0.00	1.25	1.0000	1.0000	1.3977	1.4081	0.743
24	0.1875	0.148	0.00	1.50	1.0000	1.0000	1.3215	1.3149	0.502
25	0.3750	0.148	0.00	1.00	1.0000	0.8333	1.32367	1.3543	2.318
26	0.3750	0.148	0.00	1.00	1.0000	1.1667	1.479073	1.4935	0.979
27	0.3750	0.148	0.00	1.00	1.0417	0.8333	1.276591	1.2853	0.687
28	0.3750	0.148	0.00	1.00	1.0417	1.0000	1.339167	1.3549	1.178
29	0.3750	0.148	0.00	1.00	1.0417	1.1667	1.398148	1.4245	1.893
30	0.3750	0.148	0.00	1.00	1.0833	0.8333	1.231901	1.2163	1.261
31	0.3750	0.148	0.00	1.00	1.0833	1.0000	1.289694	1.2859	0.290
32	0.3750	0.148	0.00	1.00	1.0833	1.1667	1.339389	1.3555	1.206
33	0.1875	0.148	0.00	1.00	1.0000	0.8333	1.4103	1.4318	1.522
34	0.1875	0.148	0.00	1.00	1.0000	1.1667	1.5857	1.5709	0.933
35	0.1875	0.148	0.00	1.00	1.0417	0.8333	1.3457	1.3627	1.268
36	0.1875	0.148	0.00	1.00	1.0417	1.0000	1.4199	1.4323	0.876
37	0.1875	0.148	0.00	1.00	1.0417	1.1667	1.4856	1.5019	1.102
38	0.1875	0.148	0.00	1.00	1.0833	0.8333	1.2895	1.2937	0.327
39	0.1875	0.148	0.00	1.00	1.0833	1.0000	1.3528	1.3633	0.777
40	0.1875	0.148	0.00	1.00	1.0833	1.1667	1.4145	1.4329	1.303

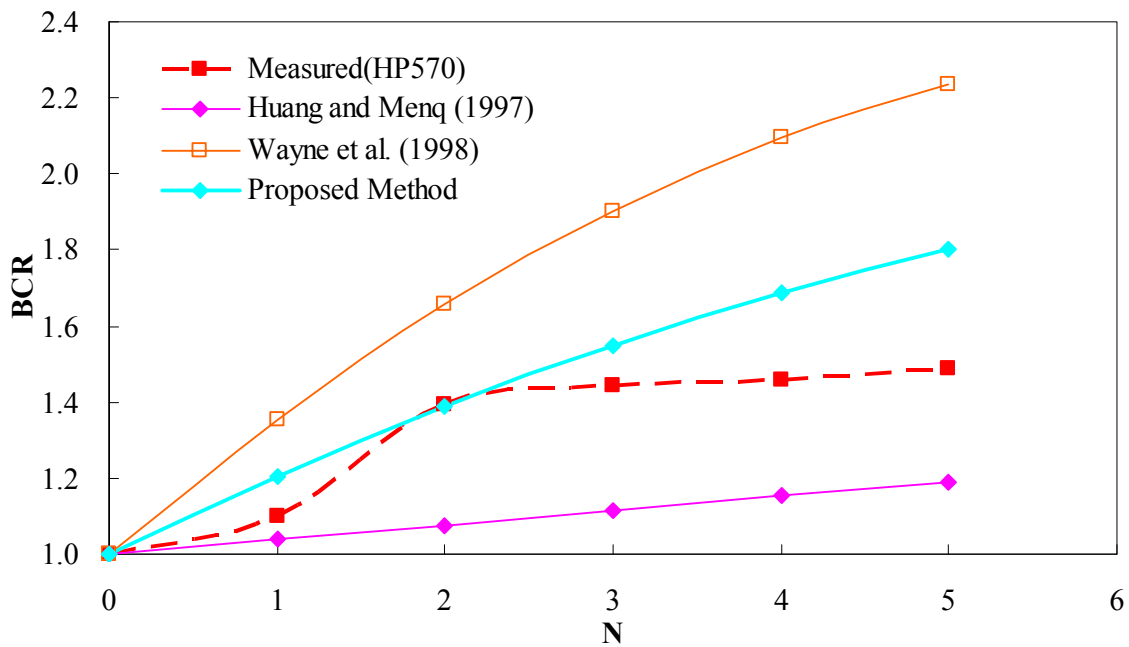# APPENDIX E COMPARISON OF ANALYTICAL SOLUTIONS WITH LABORATORY MODEL TEST RESULTS
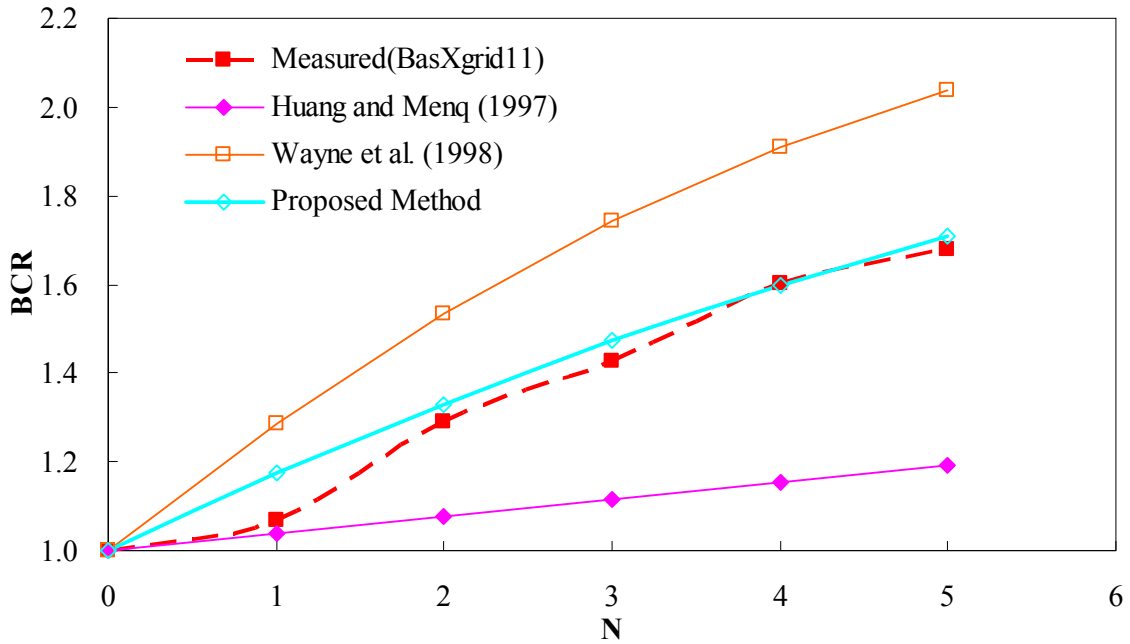
Figure E. 1

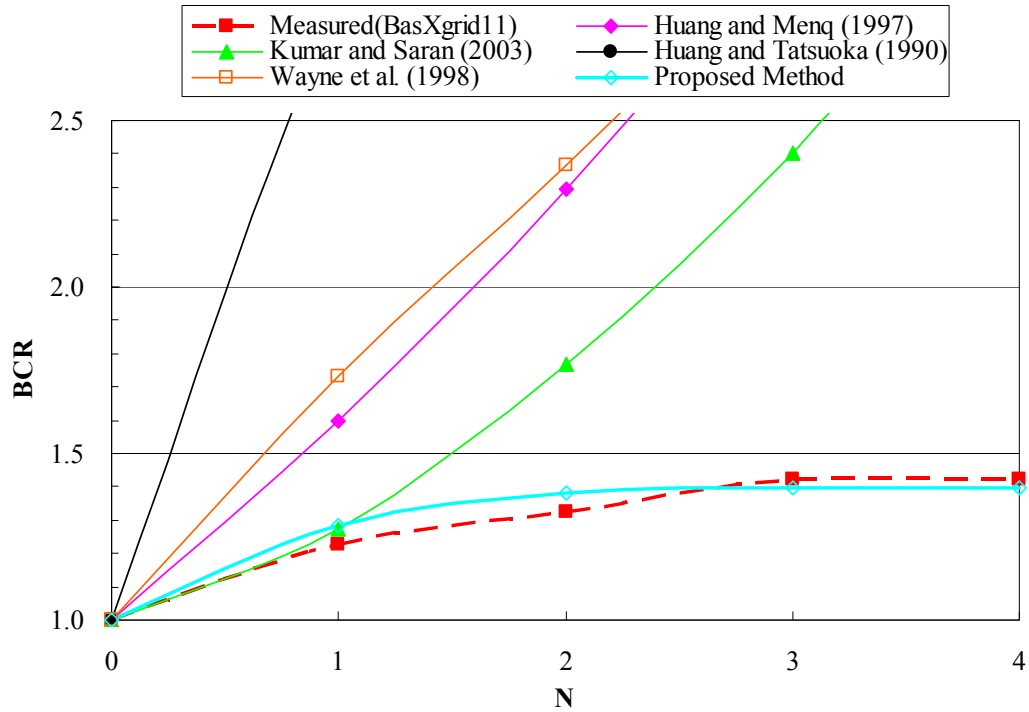**BCR vs. number of layers (N) for reinforced silty clay with BasXgrid11 geogrid**
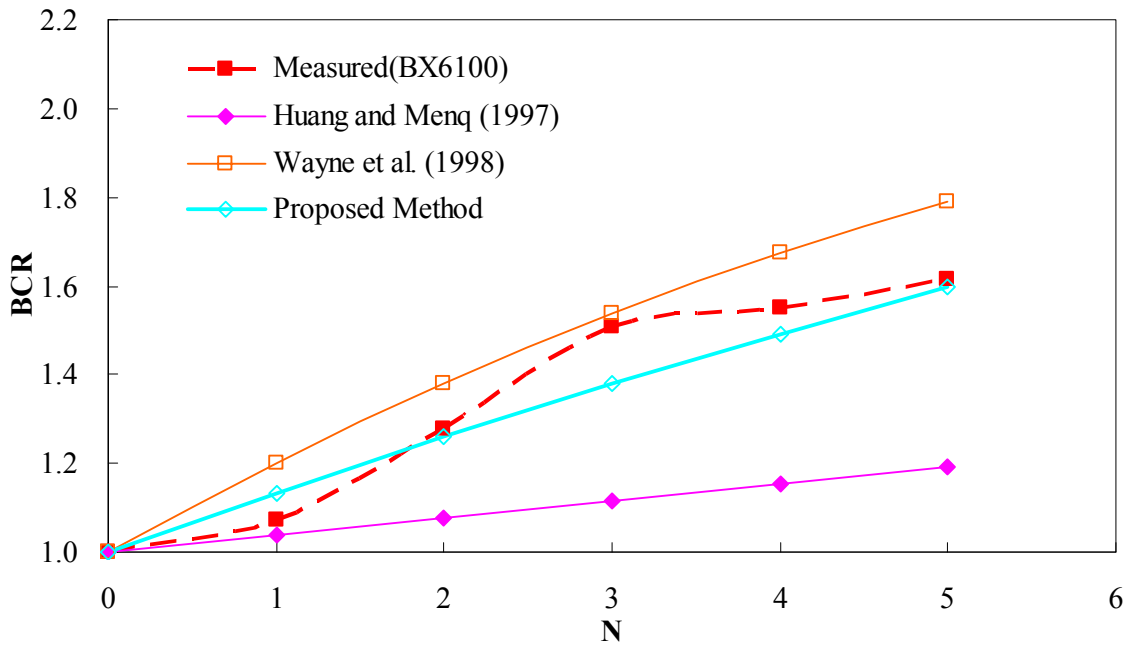
Figure E. 2

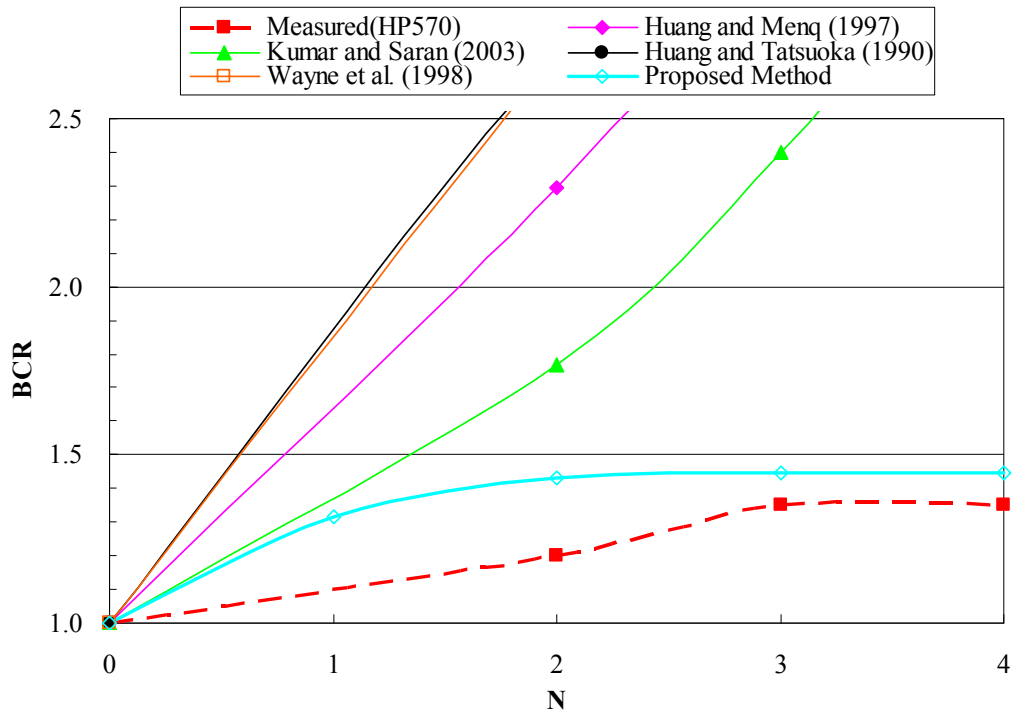**BCR vs. number of layers (N) for reinforced silty clay with BX6100 geogrid**
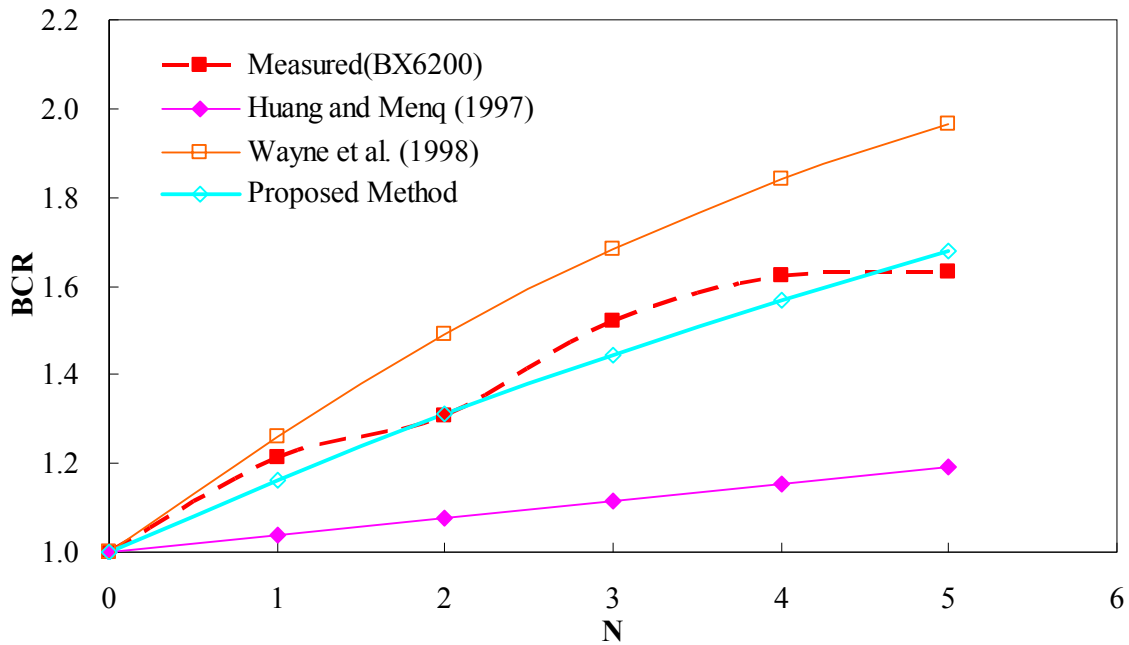
Figure E. 3
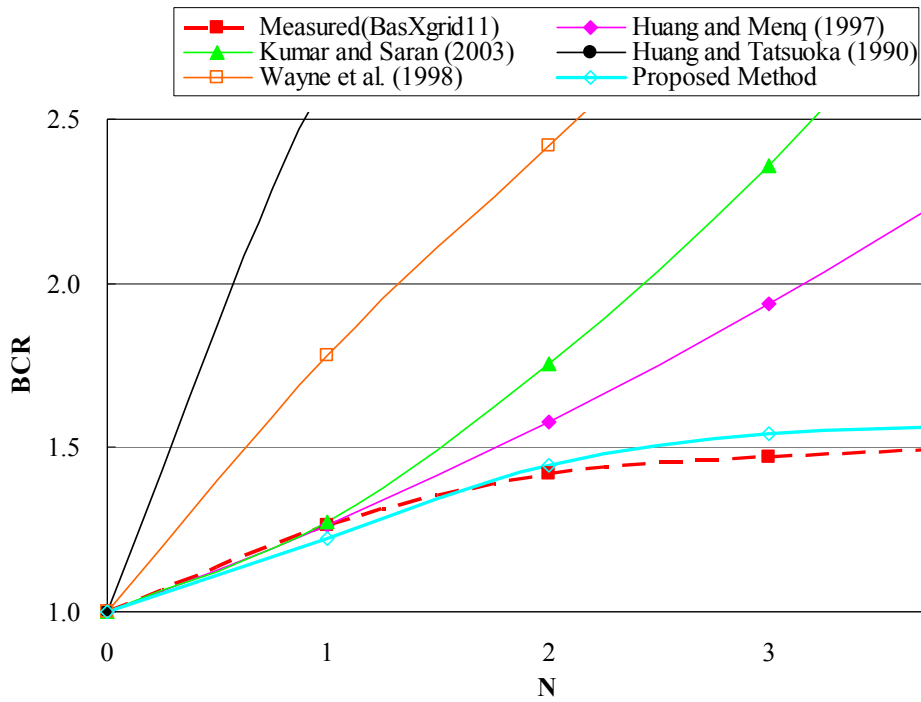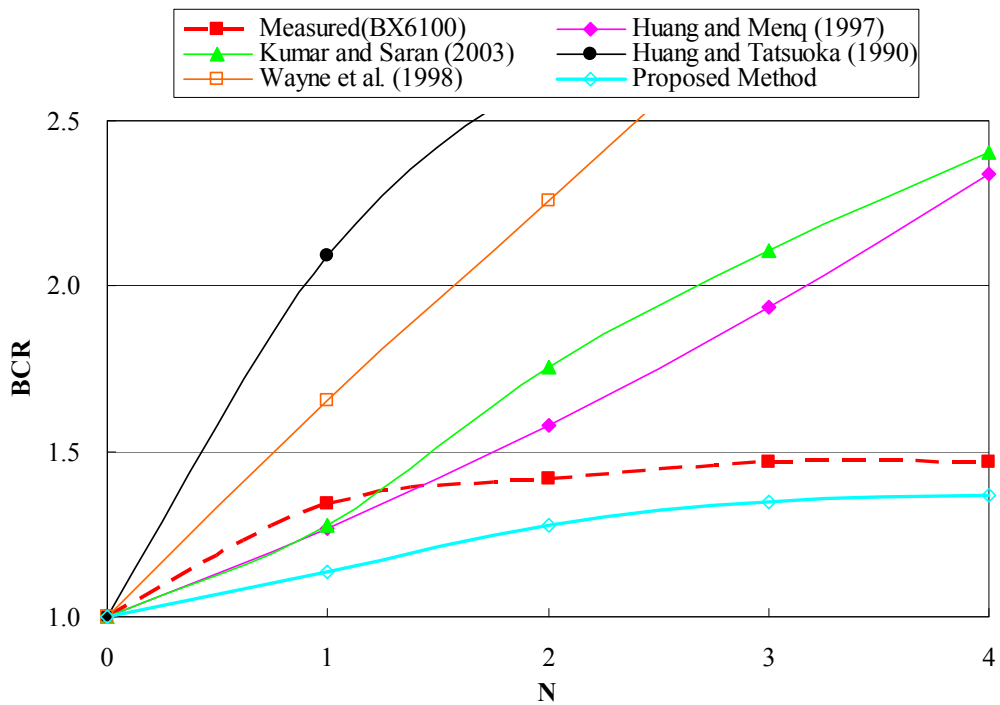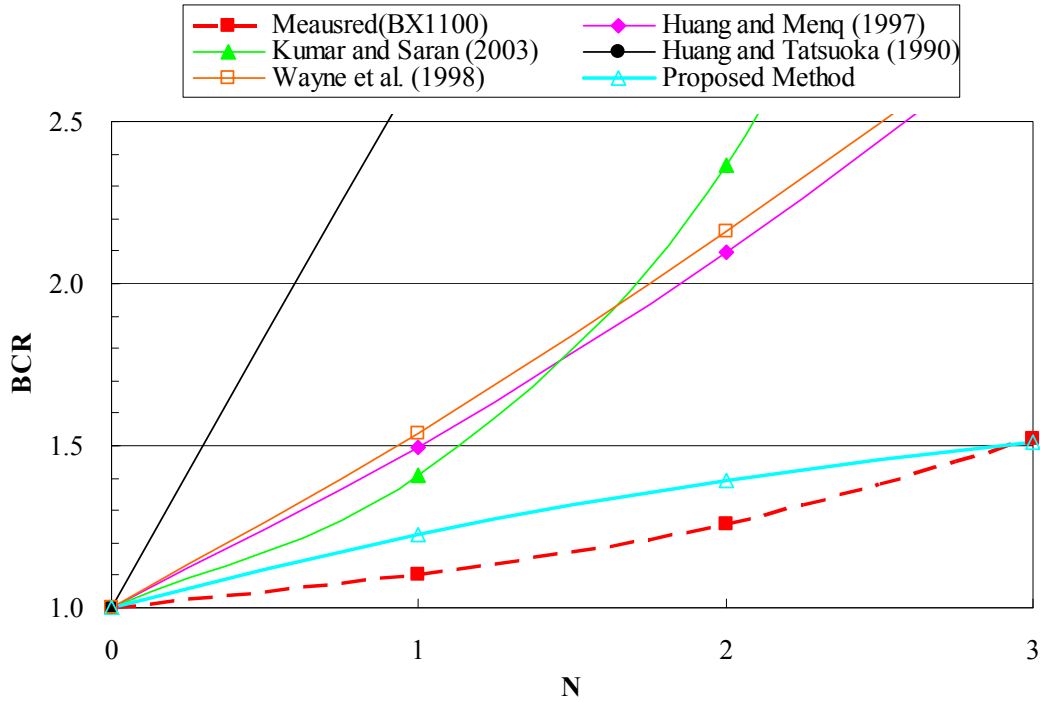**BCR vs. number of layers (N) for reinforced silty clay with BX6200 geogrid**

Figure E. 4
BCR vs. number of layers (N) for reinforced silty clay with HP570 geotextile

Figure E. 5
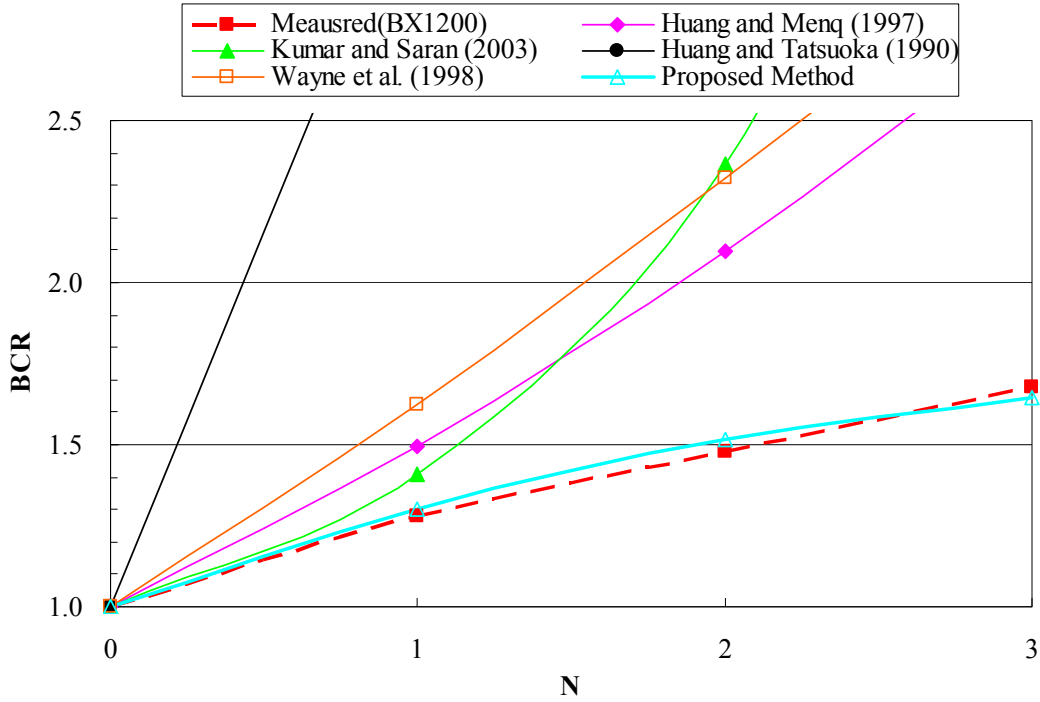**BCR vs. number of layers (N) for reinforced sand with BasXgrid11 geogrid ($D_f/B = 0.0$)**

Figure E. 6
BCR vs. number of layers (N) for reinforced sand with HP570 geotexitle ($D_f/B = 0.0$)

Figure E. 7
BCR vs. number of layers (N) for reinforced sand with BasXgrid11 geogrid ($D_f/B = 1.0$)

Figure E. 8
BCR vs. number of layers (N) for reinforced sand with BX6100 geogrid ($D_f/B = 1.0$)
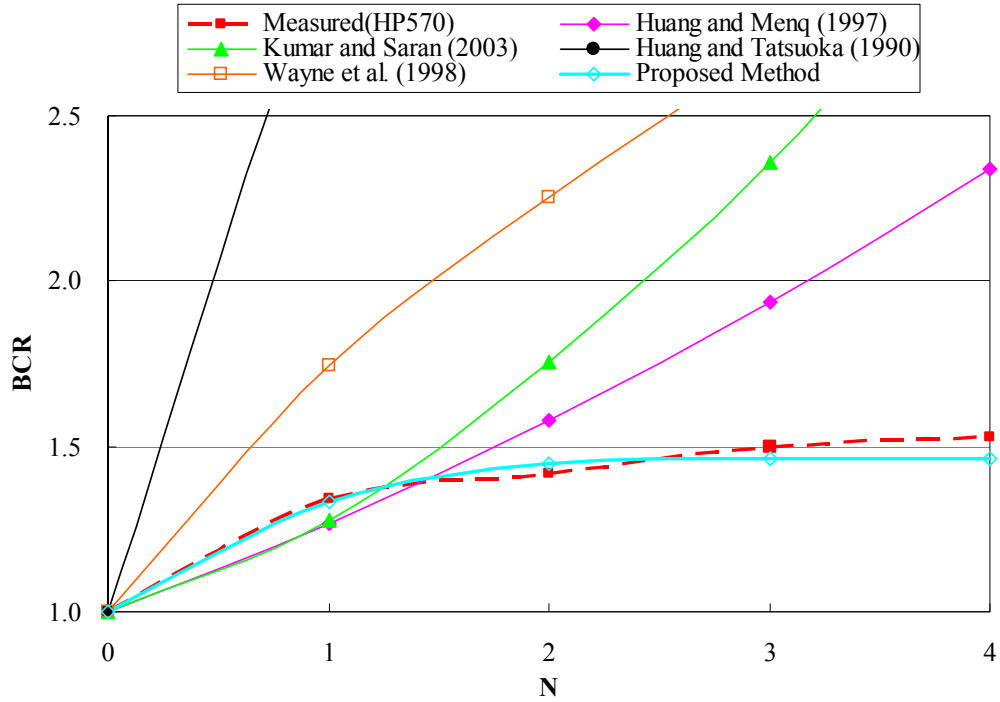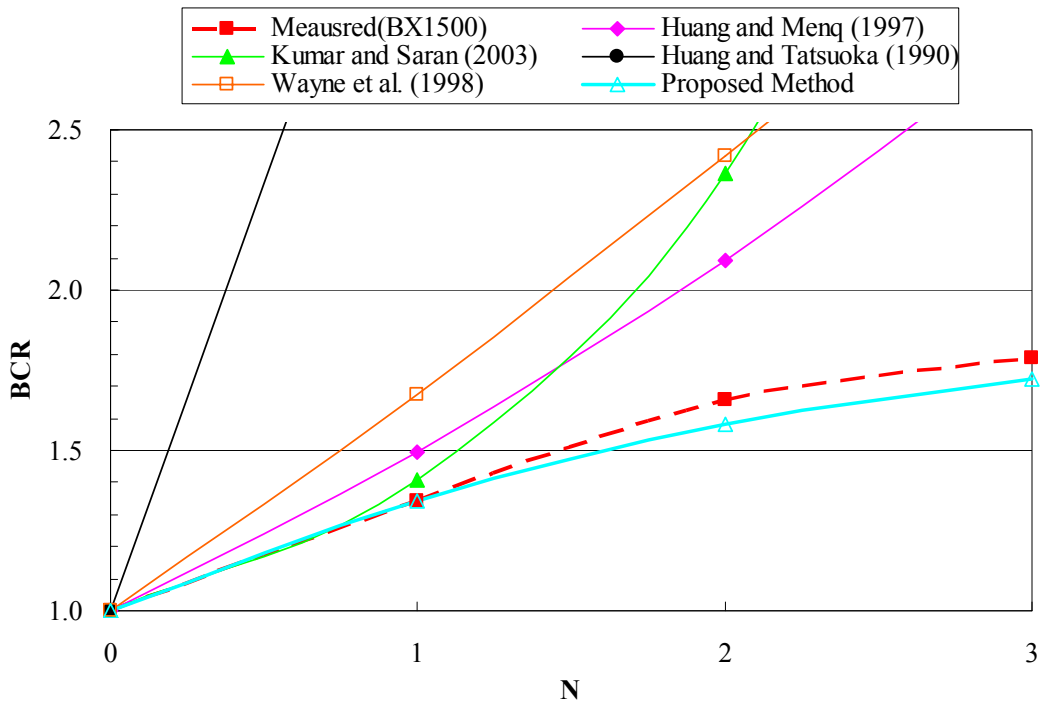
Figure E. 9
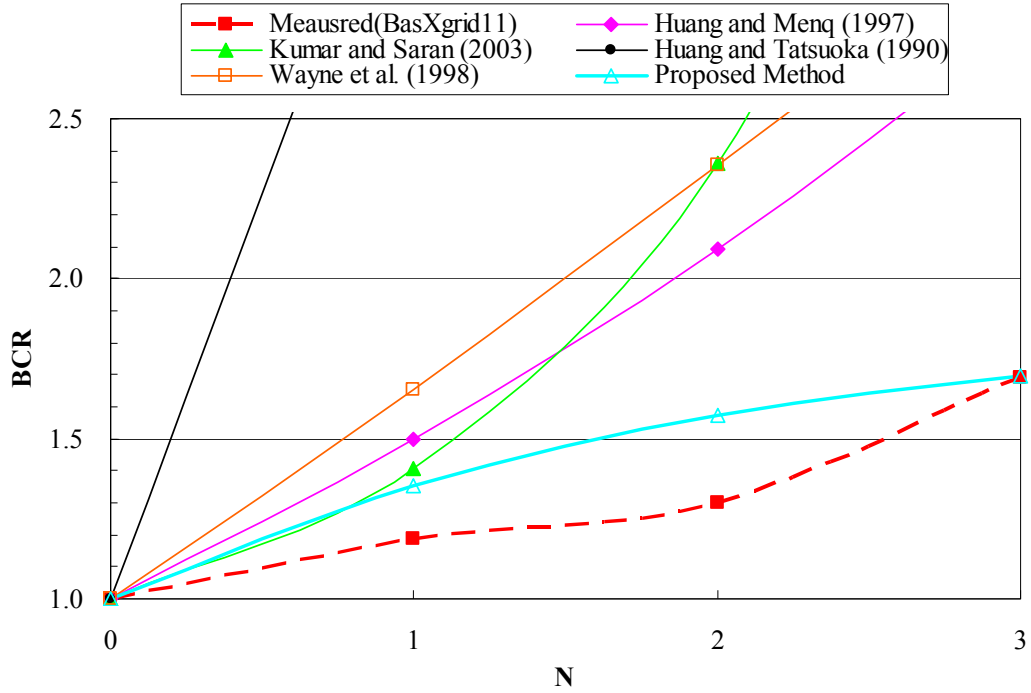**BCR vs. number of layers (N) for reinforced sand with HP570 geotextile (D_f/B = 1.0)**

Figure E. 10
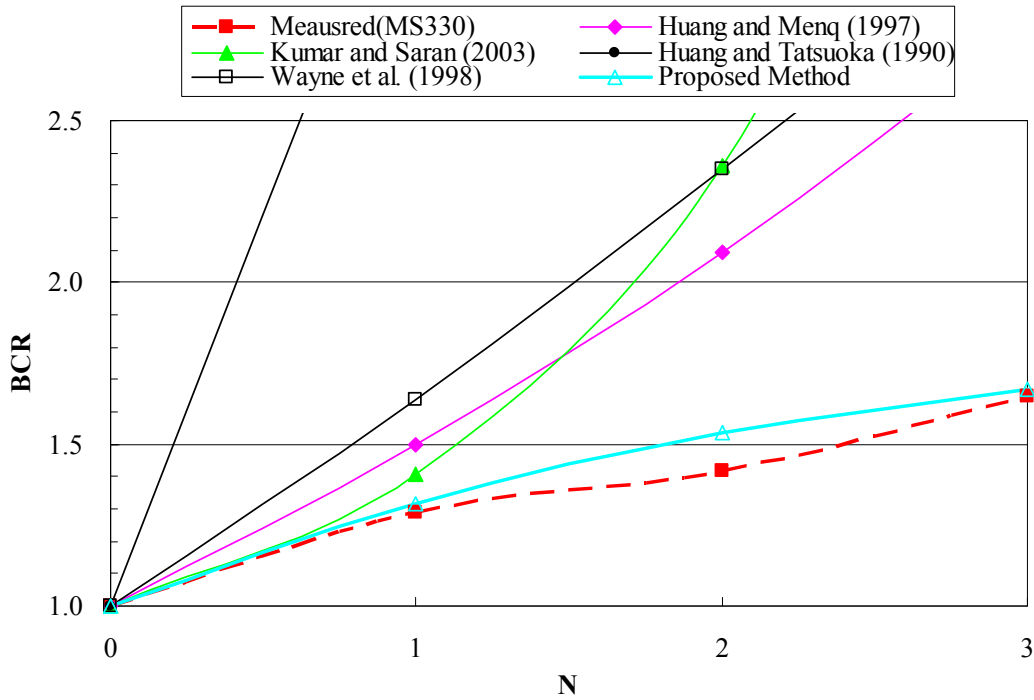**BCR vs. number of layers (N) for reinforced crushed limestone with BX1100 geogrid**

Figure E. 11
BCR vs. number of layers (N) for reinforced crushed limestone with BX1200 geogrid
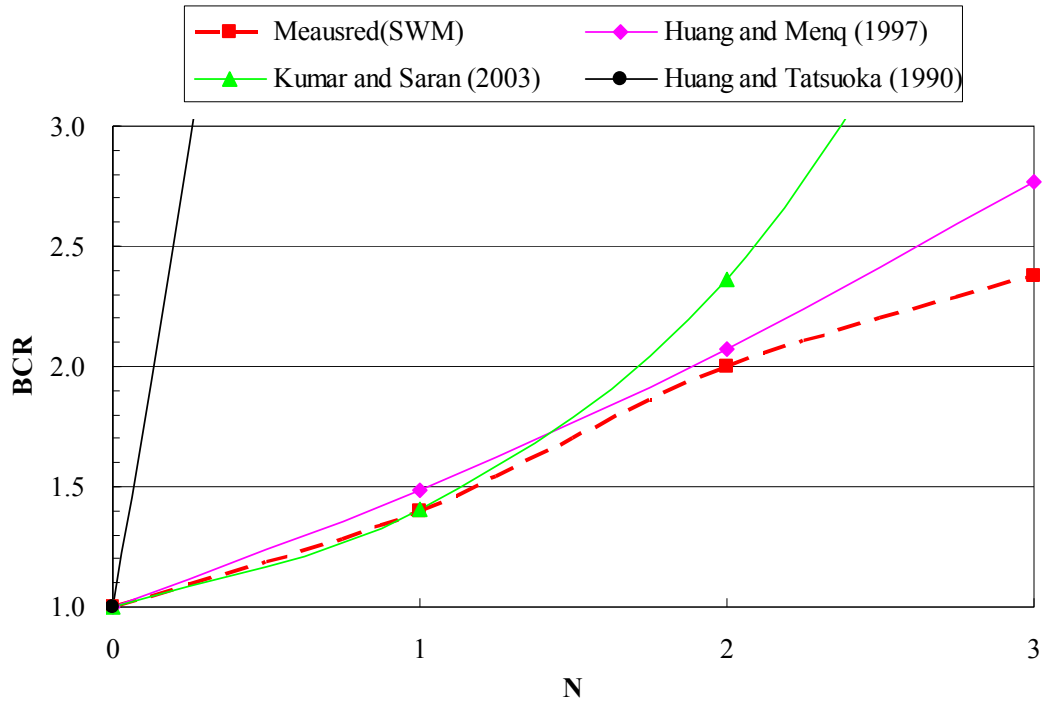

Figure E. 12
BCR vs. number of layers (N) for reinforced crushed limestone with BX1500 geogrid
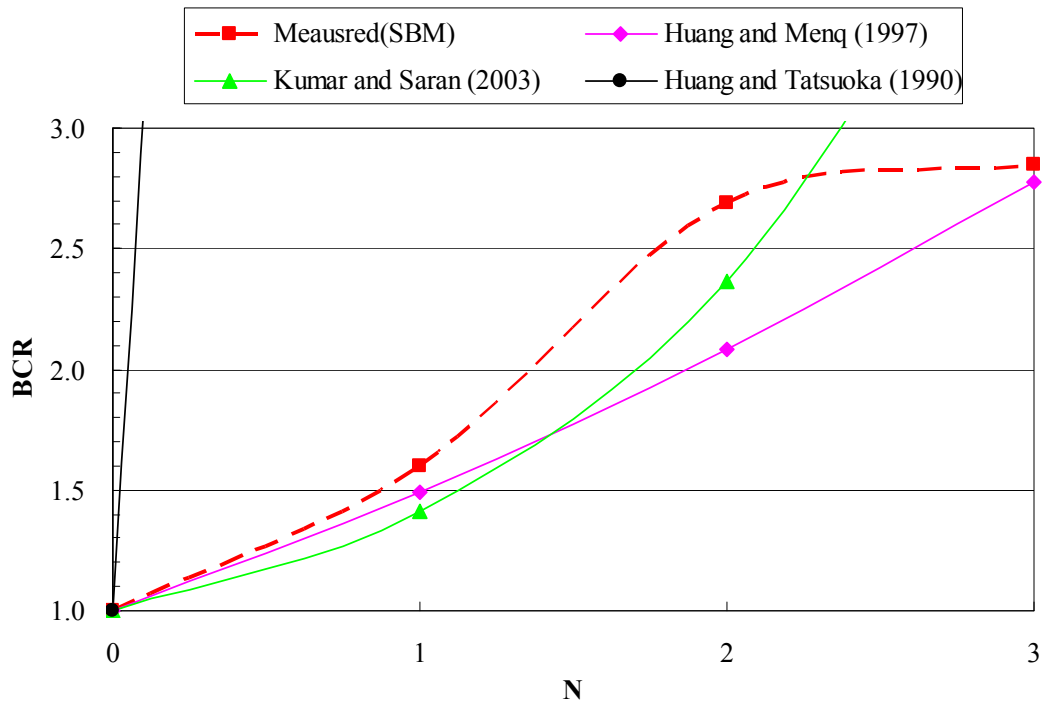
Figure E. 13
BCR vs. number of layers (N) for reinforced crushed limestone
with BasXgrid11 geogrid

Figure E. 14
BCR vs. number of layers (N) for reinforced crushed limestone with MS330 geogrid

Figure E. 15
BCR vs. number of layers (N) for reinforced crushed limestone with steel wire mesh

Figure E. 16
BCR vs. number of layers (N) for reinforced crushed limestone with steel bar mesh